Methodology for developing flexible, controllable and cost-effective heat exchanger network

Rupu Yang

PSL
UNIVERSITÉ PARIS

THÈSE DE DOCTORAT
DE L'UNIVERSITÉ PSL

Préparée à MINES ParisTech

Methodology for developing flexible, controllable and cost-effective heat exchanger network

Méthodologie pour développer un réseau d'échangeurs de chaleur flexible, contrôlable et rentable

Soutenue par

Rupu YANG

Le 18 September 2020

Ecole doctorale n° 621

Ingénierie des Systèmes, Matériaux, Mécanique, Énergetique

Spécialité

Énergétique et Procédés

Composition du jury :

Jean-Michel Reneaume Professeur, UPPA	*Président*
Raphaële Théry Hétreux Maître de conférence HDR, INPT	*Rapporteur*
Mahmoud M. El-Halwagi Professeur, Texas A&M University	*Rapporteur*
Assaad ZOUGHAIB Professeur, PSL-Mines ParisTech	*Directeur de thèse*
Cong-Toan TRAN Ingénieur de recherche, CES-Mines ParisTech	*Maître de thèse*

MINES ParisTech | PSL

Acknowledgements

Three years past, and it comes to the time to defend my doctoral degree, with many thanks to my supervisors, family, friends, to a certain period of memory we shared together. The first gratitude ought to give Assaad and Toan. They helped me to win the chance to be a Ph.D. candidate three years ago. And during the three years, unaccountable discussions with them enable me to find a good pathway to carry out the research work. Assaad has never missed any important things related to me, and even he gets a full calendar to manage. And he can always propose suggestive feedbacks when I stuck in the thesis progress with Toan. Most importantly, the most critical thing I learned from him is a positive attitude, which I believe will be the most significant wealth in my future life. My subject was directed by two supervisors, and Toan is responsible more for the research work's progress. Toan never lost his patience in the past three years, and even I made some somewhat naïve mistakes. Sometimes he even tried to write the preliminary model to help me start the work more quickly and also check errors, which I believe is really beyond his job. Assaad and Toan created a very relaxed, equality, and respectful working environment for me. We ever tried to make some academic results after obtaining some results during the thesis work. Even though the papers get rejected several times, they are still trying to encourage me to keep going and improve it. At the same, great appreciate owes to the China Scholarship Council that founds my doctoral thesis.

During the thesis work, friends and colleagues in the lab played a rather role. We talked about the thesis work, shared the opinion on the social issues, envisioned future life, etc.. Marc and Miza; we met each other in 2016 when we did our internship there. You are great guys, wish your thesis defense in the coming months will be successful. Rasha, Christelle, Christina, Joe, Etienne, Haytham, Rami, I can see the kindness from your eyes, and you are nice people. Phillip helped me deal with the PC problem many times, and your insistency to say hello in the Chinese way is harmony. Our lab atmosphere is amicable, and Maroun (director of the lab) even provided support to have a Chinese new year party in the lab in January 2019. My previous Chinese supervisor was there at that time. With the help of many friends from Palaiseau, we made it a great time that day. Here, I want to show my gratitude to Chuang, Jun, Heng, Huan, Hao, five master students, etc. Your friendship is very precious, and it will be a great wealth in my life. And Long, we both come from Wuhan and started the thesis almost at the same time, your passions toward the sport and envisions in investment inspired me quite a lot, thank you. I want to thank Dr. Feng, who provided me a great chance to continue to work in anti-atmosphere pollution after the thesis work. I will do my best to meet your trust. Great thanks for those 'answers' from stack overflow and google group, they helped to solve most of the coding problems in python.

Hui, my girlfriend, we get to know each other in October of 2018. We have many common points toward life, work, and relationship that make us cherish each other very much. You had always been very patient and inspiring when I got stuck either in the research or life and provided great comfort during the COVID-19 confinement period. Even though I am good at cooking, but sometimes the dishes taste bad,

and you never complain about that, and can always find the highlight of the work. Your presence and coming is a gift for me, and I will cherish the chance very carefully.

I get a small but adorable family, my father, my mother, and me. Father always work very hard in a public department, and he wants to deliver to me the honor to be an industrial person, he had ever noticed me that the great happiness in life is to work in your best effort. Mother lost her job very early in 2002, but she tried many ways to bring income to the family through different temporary jobs. She is an intelligent person and a great mentor and always reminds me to be cautious about future development and the competitive environment I will enter. I was lucky enough to make them visit France in February 2019, and it was their first time to take the plane, wish I can have more chance to bring them more happiness.

Great appreciate to those whoever gave a hand during these years, sorry I cannot count your name one by one, but your help and kindness affect me deeply. I will learn from you and pass on those good qualities in my life.

General introduction

Heat exchanger network (HEN) has been applied widely in the industrial process to reduce utility consumption and relieve the stress of corresponding greenhouse gas emissions. This thesis pioneers to consider the time response in the HEN design stage and provide methodologies to synthesize a flexible, controllable, and cost-effective HEN. We have defined an indicator which termed as the transition time (TT) to measure the dynamic controllability when HEN gets an operational period changeover. The core problem is how to carry out the multi-period HEN synthesis that the economic cost is the objective function and TT acts as a constraint. The difficulty locates in two aspects. One is how to estimate the TT that suits to be integrated into the design stage. The other one is to provide an appropriate HEN synthesis approach that can consider the TT.

To tackle the first point, we choose to follow a simplified analytical modeling approach to describe the dynamic performances of HEN, instead of numerical simulation or experimental approaches considering the great number of potential structures to test. However, there is no available HEN dynamic model to measure the TT fast and efficient. We built the HEN dynamic model by starting from a basic model of single heat exchanger relied on the Laplace transform and some simplifications. The HEN dynamic model proposed in chapter 3 is a basic one and might fail to work when HEN becomes complex due to the limitations of the inverse procedure of Laplace transform. An improved HEN dynamic model developed in an analytical way has been introduced in chapter 4 to avoid the numerical difficulty, and it applied quite well in medium-large scale HEN problems.

The second difficult point is the development of synthesis strategy. We have to follow a sequential approach to iterate various structures and obtain cost-optimized structures at first since the TT calculation requires the complete information of a HEN. We proposed two methodologies according to the problem scales. For a small scale problem, we suggested the most basic method to iterate all the potential structures (BINLP) with discarding those isomorphic structures and the structures with a loop as putting in Chapter 3. The effectiveness of BINLP has been validated against the traditional mixed-integer nonlinear programming (MINLP) synthesis method through four case studies. To deal with the medium-large scale synthesis problem, we provided an improved synthesis strategy (IINLP) in chapter 4. It originated from the HEN synthesis process characters, driven by the idea of reaching an excellent optimal total annual cost (TAC) design by manipulating the heat load distribution between the process heat exchangers and utilities. IINLP has been compared with simulated annealing (SA) in three medium-large scale problems, and IINLP shows more competitive designs with lower TAC, and it illustrates an average performance compared with SA (repeated three times for each case) in TAC-TT trade-off results.

The IINLP and improved HEN dynamic model have been applied in a distillation preheating system in chapter 5. Many structures that have close TAC, but their TT varies quite a lot (within 1.83% deviation of TAC, TT differs 85.26 %), and many structures with the same TT result but differ hugely in the TAC aspect (57.74 %) have been identified. Integrating the TT into the design stage can help engineers predict the potential time response of the various HENs. Due to the made assumptions, there might be some deviation compared with the real results by following our TT calculation model, and the deviation can be rather high in specific parameter conditions. However, as shown in Chapter 3, the relation between various designs predicted by the model still hold compared with the detailed simulation. The methods

proposed in this thesis can work as a pre-selection tool to estimate the time response when operational period change occurs and help designers to select the best design under a specific constraint on dynamic performance.

Contents

Nomenclature

Abbreviations

ACO	Ant Colony Optimization
AMTD	Arithmetic mean temperature difference, K or ℃
BINLP	Basic iteration nonlinear programming
CC	Composite curve
CLDG	Closed-loop disturbance gain
CN	Condition number
CV	Controlled variable
DCN	Disturbance condition number
DE	Differential evolution
GA	Genetic algorithms
GCOPs	Generalized Critical Operating Points
GHG	Greenhouse gas
GMTD	Geometric mean temperature difference, K or ℃
HE	Heat exchanger
HEN	Heat exchanger network
IEA	International Energy Agency
IINLP	Improved iteration nonlinear programming
IPCC	Intergovernmental Panel on Climate Change
LGO	Light diesel
LMTD	Logarithmic mean temperature difference, K or ℃
LP	Linear programming
MAE	Mean average error
MAPE	Mean average percent error
MER	Maximum energy recovery
MGO	Medium diesel
MILP	Mixed-integer linear programming
MIMO	Multi-input multi-output
MINLP	Mixed-integer nonlinear programming
MPA	Middle Pump-Around
MV	Manipulated variable
NLP	Nonlinear programming
ORC	Organic Rankine Cycle

PI	Process integration
PRGA	Performance relative gain array
PSO	Particle Swarm Optimization
RFO	Rocket Fire Optimization
RGA	Relative gain array
RHP-zeros	Right half plane-zeros
SA	Simulated annealing
ST	Stages of HEN superstructure
STEP	Stream Temperature vs. Enthalpy Plot
SWS	Stage-wise superstructure
TAC	Total annualized cost
TPA	Top Pump-Around
TT	Transition time
ΔT	Temperature difference, K or ℃

Greek letters

α	Temperature attenuation factor
β	Parameter of the heat exchanger
ε	Annualized factor
λ	Mass flow rate of bypass, kg/s
σ	Area cost coefficient
ϕ	Variable in the example of HEN dynamic model
φ	Period duration ratio

Roman letters

A	Heat transfer area, m^2
a	Variable in the example of HEN dynamic model
B	Binary variable/parameter to describe the existence of the heat exchanger in HEN
b	Variable in the example of HEN dynamic model
C	The set of cold utilities
CA	Area cost coefficient, $\$/m^2$
CaC	Capital cost, $
CCU	Cold utility operational cost, $/(kW•year)
CF	Fixed cost of a heat exchanger, $
CHU	Hot utility operational cost, $/(kW•year)

cp	Specific heat capacity, J/(K•kg)
G	Function in Laplace domain
H	The set of hot utilities
h	Heat transfer coefficient of the stream, W/(m^2•K)
I	The set of hot streams
J	The set of cold streams
K	Kelvin degree
m	Mass flow rate of stream in heat exchanger, kg/s
mf	Mass flow rate of parent stream, kg/s
n	Number of points to calculate the error in dynamic validation part
OC	Operational cost, $/year
p	Operational period
Q	Heat load, W
r	Parameter of the heat exchanger
s	Laplace variable
T	Temperature, K or ℃
t	Time
U	General heat transfer coefficient, W/(m^2•K)
v	Parameter of the inlet signal
w	Parameter of the inlet signal
x	Parameter of the heat exchanger
y	Temperature values in dynamic validation part
z	Parameter of the heat exchanger

Subscripts

c	Cold side
cu	Cold utility
h	Hot side
hu	Hot utility
i	Hot stream
in	Inlet
j	Cold stream
min	Minimum
out	Outlet
p	Operational period

st	Stage in the HEN structure
wall	Heat exchanger metal wall

Superscripts

c	Cold stream side
h	Hot stream side

List of Figures

List of Tables

Résumé du chapitre 1

Les émissions de GHG constituent déjà un problème mondial que nous devons résoudre ensemble. Le secteur industriel y contribue le plus, mais il a également les plus grandes potentialités de réduire les émissions. Parmi les différentes solutions potentielles dans le secteur industriel, le réseau d'échangeurs de chaleur est la technologie la plus couramment choisie pour récupérer l'énergie et réduire la consommation des services publics. Pour rendre la conception du réseau d'échangeurs de chaleur plus proche de la condition réelle, nous visons à explorer une méthodologie qui nous permet de considérer la flexibilité et la contrôlabilité dans le scénario d'optimisation rentable. Nous avons défini le temps de transition (TT) comme l'indicateur pour mesurer la performance dynamique de diverses conceptions HEN au niveau de la contrôlabilité, et la flexibilité sera gérée par la synthèse multi-période. Le travail de chaque chapitre a également été décrit.

Chapter 1 – Introduction

1.1 Background

The world witnessed considerable technology breakthrough during the past three hundred years, many countries accomplished the transition from an agriculture-based economy to the industrialization-based society, and even go future to the service-based system. The social welfare has achieved massive progress, and the lifestyle has been largely enriched. On the other side of the coin, we also made a significant impact on the environment and ecology system. Global warming has already been a severe problem for all human beings as one of the results of anthropogenic activities. Many countries have been devoted to fighting global warming, either through their efforts or cooperation, and leading to a well-known organization: Intergovernmental Panel on Climate Change (IPCC). According to the report (IPCC, 2014), the cumulative greenhouse gas (GHG) emissions from the last half-century accounts for more than 50% of accumulated emissions from 1750. People had already realized that fast accumulated GHG emissions could be irreversible and potentially massive damage to the environment if the world develops in the unaltered condition.

Fig 1.1 provides the GHG emissions compositions, CO_2 accounts for 76% in the total emission of GHG in 2010. From 1970 to 2010, the average increasing rate is about 1.5%, it was 1.3% in the first 30 years, and increased to 2.2% in the decade between 2000 – 2010. The GHG emissions exhibit a clear increasing trend in recent years. It will pose an enormous threat to the earth's ecological system if we care merely about economic growth, considering the potential climate change effects. The other important message we can read from Fig 1.1 is that fossil fuel consumption and industrial production contribute to the most substantial part of GHG emissions, reached up to 65% in 2010.

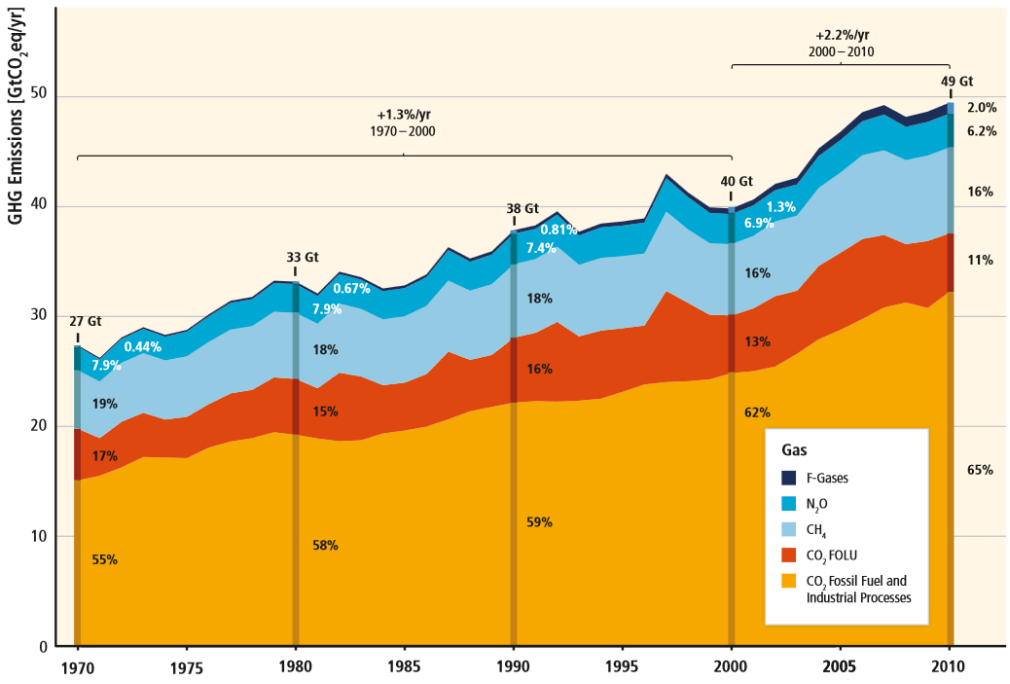

Fig 1.1. Total Annual Anthropogenic GHG Emissions by Groups of Gases 1970 – 2010 (IPCC, 2014)

The GHG emission does not only come from industrial production, but also from the residential, transportation, and other social sectors. Fig 1.2 shows the breakdown of GHG emissions over economic sectors, the electricity and heat production part corresponds to the most significant part. When considering both the direct and indirect ways, the industry sector came to the first place.

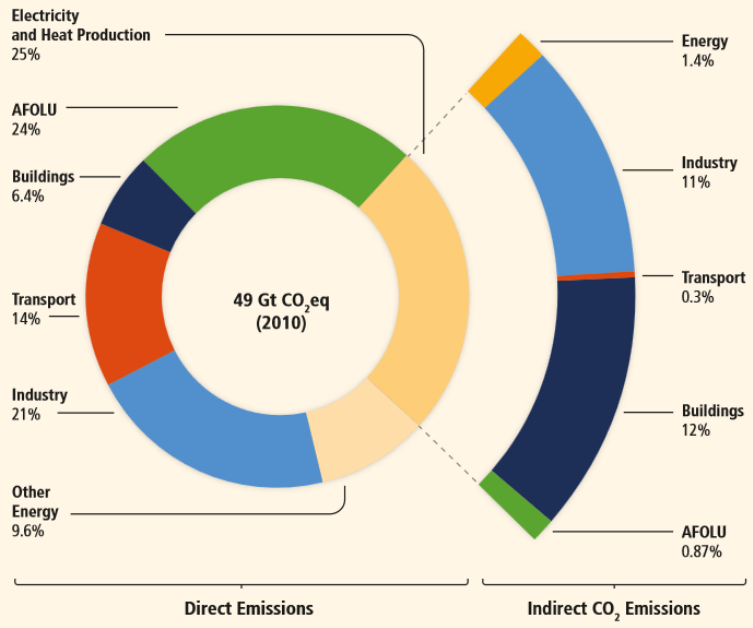

Fig 1.2. Total GHG Emissions by Economic Sectors (IPCC, 2014)

International Energy Agency (IEA) predicted the CO_2 emissions until 2030 by sectors, as illustrated in Fig 1.3, industry sector takes the first place. The industry sector has tremendous potential to improve to curb GHG emissions, and the pathway is to reduce industrial energy consumption by improving energy efficiency. The energy efficiency gets various definitions in different conditions. In a strictly technical definition, energy efficiency means the useful energy output over energy input for the energy conversion process. In passive systems such as buildings where useful energy is degraded to low-grade heat in return for thermal comfort (heating or cooling). Moreover, the mention of energy efficiency here covers both the above two definitions. Due to the improvements in energy efficiency in 2000, it is estimated to help to reduce 20% of energy use in the industry and service sectors and reduced a considerable amount of GHG. In terms of the potential for energy efficiency in industry, the study result from the University of Cambridge (Cullen et al., 2011) found that 73% of energy consumption can be avoided by applying current techniques.

The IEA asserts that 'energy efficiency improvements in buildings, appliances, transport, industry, and power generation represent the largest and least costly savings.' Moreover, energy efficiency plays a significant role in different scenarios to control climate change in 2060, as the study shows by (IEA, 2017). IEA estimated the potential CO_2 reduction in the coming years by advancing the technology to control the temperature increasing well below 2C° compared to the pre-industrial levels. The analysis result is given in Fig 1.4. Efficiency improvement is expected to contribute 40% and plays the most role among the other selections (renewable energies, CCS, Fuel switching, and Nuclear). The energy efficiency has also been set as one of the actions to achieve a sustainable society by the European

Commission, which set targets to improve energy efficiency at 32.5% in 2030 compared to 2005 (The European Commission: 2030 climate & energy framework | Climate Action).

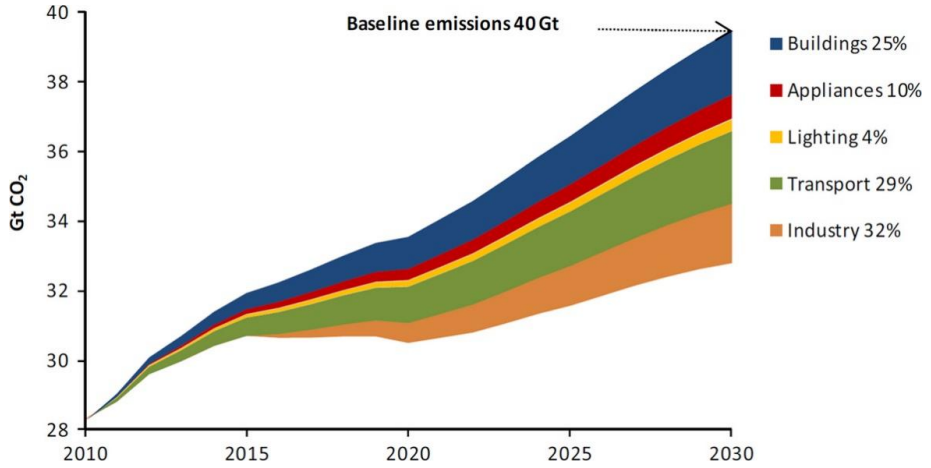

Fig 1.3. The global potential of different sectors for CO_2 mitigation by 2030 (IEA, 2011).

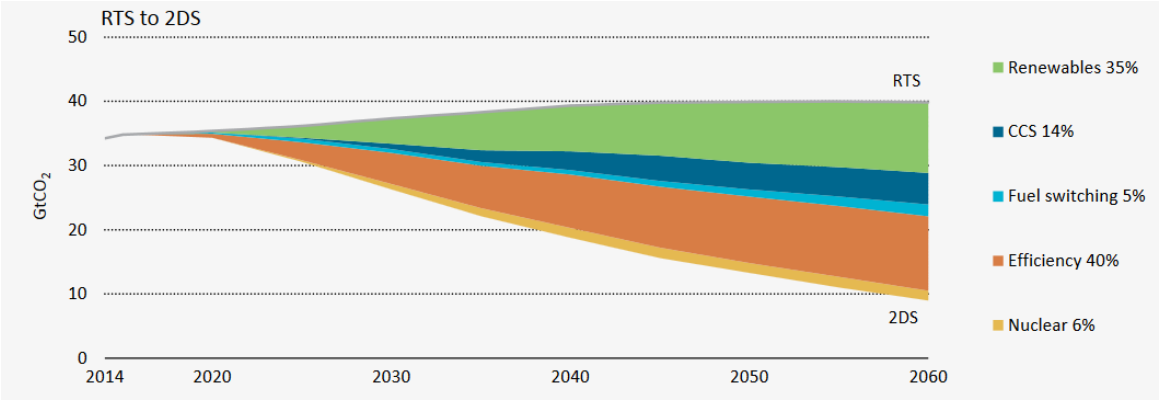

Fig 1.4. Sector contribution to emissions reduction (IEA, 2017).

The energy efficiency achievement in the industrial sector always relies on process integration (PI), which we will be described in detail in the following part.

1.2 Methods for improving energy efficiency

To explore pathways to improve industrial energy efficiency, we need to know the industry system's common points. Fig 1.5 provides a diagram to illustrate the mass and energy flow of a typical factory across borders. It consists of processes to produce products by consuming raw materials, resources, and energy. The output streams are usually regarded as waste products, such as waste heat and waste solid materials. The system does not merely consume energy, but also generates electricity, heating, and fuels. There are many strategies to improve the energy efficiency in different levels based on the classification in the doctoral thesis (Bühler, 2018):

i. Single process level.
   A single process can be updated, retrofitted, or replaced by other advanced equipment. It attracts heavy research focus, and many researchers try to explore more efficient furnace, mill, reactors,

and advanced control/operating strategies to perform better, which can also be interpreted as the technological progress in the specific field.

ii. Factory level.

The factory level aims to manage energy consumption by optimizing the process configuration. Since there are processes requiring to release heat, some processes need to consume heat, which gives the chance to balance the energy demand by internal heat recovery. The chance can also be extended to the mass, water, and power consumption aspects. The strategy also termed as PI and plays a rather significant role in improving energy efficiency currently. The energy crisis in the 1970s triggered the PI, and it is still a strong incentive until the present that helps to reduce energy consumption and leads to the reduction of emissions. According to the IEA definitions, PI is *'Systematic and general methods for designing integrated production systems ranging from individual Processes to Total Sites and with special emphasis on the efficient use of energy and reducing environmental effects.'*

iii. Site level.

PI inside the single factory cannot always reach the most energy recovery status, and the residual waste hot streams and cold waste streams are inevitable. However, the different factories might utilize the waste energy in other plants, and the site level integration has also been a hot topic in these years.

We are focusing on the Factory level in this thesis, on the heat exchanger network (HEN) design, to be more specific and contribute to the energy recovery field

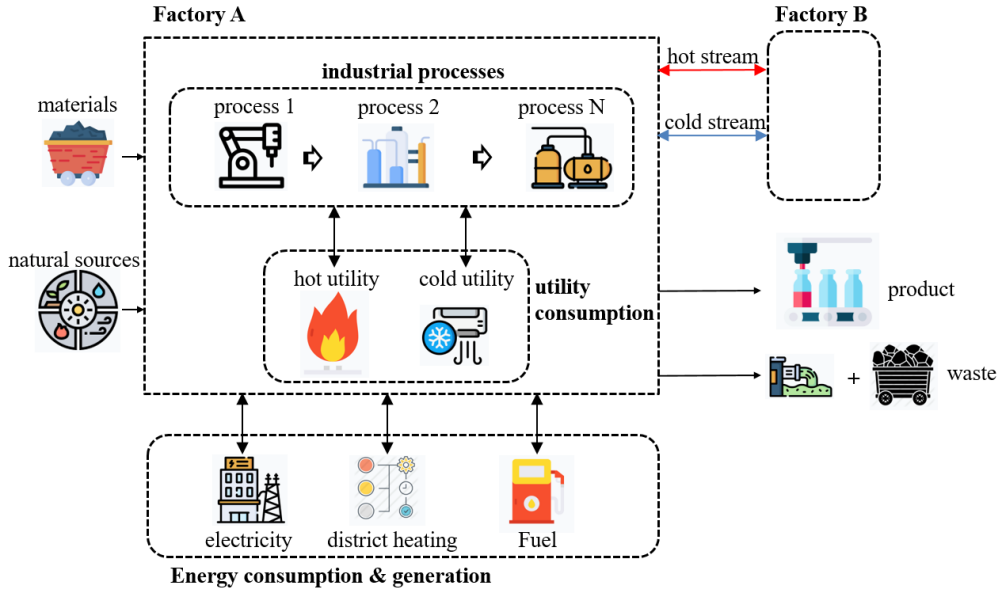

Fig 1.5. Diagram of the factory with energy and mass flow across borders

1.3 The role of heat exchanger network

The PI includes various kinds of technologies, and the most direct way to improve energy efficiency is through the HEN. The role of the HEN in the factory level is revealed in Fig 1.6, the famous 'Onion model'. The first layer is the reactor, which plays a critical role in a system, followed by the separation and recycling system, and the third level comes to the HEN.

HEN design was first in the direction to achieve maximum energy recovery (MER), and the most applied method is the Pinch Technology proposed by (Linnhoff and Flower, 1978). It is a graphical based method that employs the Temperature – Enthalpy diagram to differentiate the hot stream curves and cold stream curves into the upper Pinch and lower Pinch design regions. The MER design usually gets various HEN structures that depend on the experience of the users. It matters because the various structure will lead to various economic costs. Then, the research target become to achieve the optimal cost design, and the target variable is termed as total annual cost (TAC), many efforts have been devoted to the mathematical programming approach. The work of (Yee and Grossmann, 1990) acted as a milestone in the history of PI, in which they provided a stage-wise-superstructure idea to describe the HEN synthesis as a mixed-integer nonlinear programming problem. After that, the mathematical models have been widely extended to be closer to real conditions and have achieved much progress in the solving approaches. Besides the endeavor to find lower TAC design, the operating issues have also been studied.

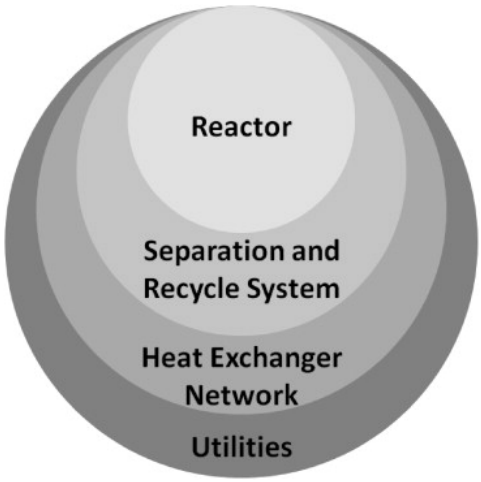

Fig 1.6. The "onion model" of process design (Smith and Linnhoff, 1988)

1.4 Motivation

In real operations, HEN can hardly work in a single operating point, and it requires to be flexible due to either the unexpected disturbance or pre-assumed changeover. The corresponding flexibility issue has been well studied, and to guarantee the designed HEN can operate feasibly in various points from a static point of view. When there is an operational changeover for HEN, the dynamic aspect (termed as controllability) has also been explored. The published research paid much attention to deciding the control structure, and most of them transferred to the study of bypass selection or control strategy (Knut W. Mathisen, 1992; Yan et al., 2001; Escobar and Trierweiler, 2011; Sun et al., 2018). There are efforts trying to compare the time response when choosing the control structure, but based on static criteria that require validation with dynamic studies (Lin et al., 2013; Rathjens et al., 2016). Multi-period synthesis as an approach of solving the flexible HEN design considers explicitly different operational points (Aaltola, 2002; Ahmad et al., 2012), but there is rarely research to care about the time response when the changeover happens. The importance of the HEN time response has already been recognized in the literature. Liu et al. (2019) mentioned that the time response in the evolution of flexibility study has to be settled. Jogwar et al. (2007) also argued the importance of enabling the HEN to achieve fast transient response. The previous work in our group (Fricker et al., 2013) showed that the economic optimal heat integrated system illustrates evident long transition time when the load of the HEN changes from the

nominal one to 50% of load, since the design relies on the Pinch technology that can only consider static performance. In a recent work in the domain of HEN design (Payet, 2018), the author studied a real case problem where the system ran in two operating conditions, and the transition duration between them could be about 2.5 hours to 3.5 hours, corresponding roughly to 30% of the working period. Knowing that during the transition phase the system's products may miss the requirement specifications, it might represent a loss for the production. Thus, it is crucial to explore the time response performance when there is an operational changeover of HEN since the design stage, to guarantee an excellent dynamic performance. The challenge is hence determining the dynamic performance of HEN in the design stage.

We define the transition period of HEN when there is an operational period changeover as the transition time (TT) in our thesis. The TT describes the time duration from the time the operating conditions change and the time to reach a new steady state. The system is considered in steady state when its variables (such as the outlet temperature) reach the final stable values, within a specific tolerance range (see Fig 1.6). It is a bit different from the 'setting time' as in the control theory field. The latter describes the system facing an ideal step change condition. In this thesis, we do not limit the change form of the inlet variables.

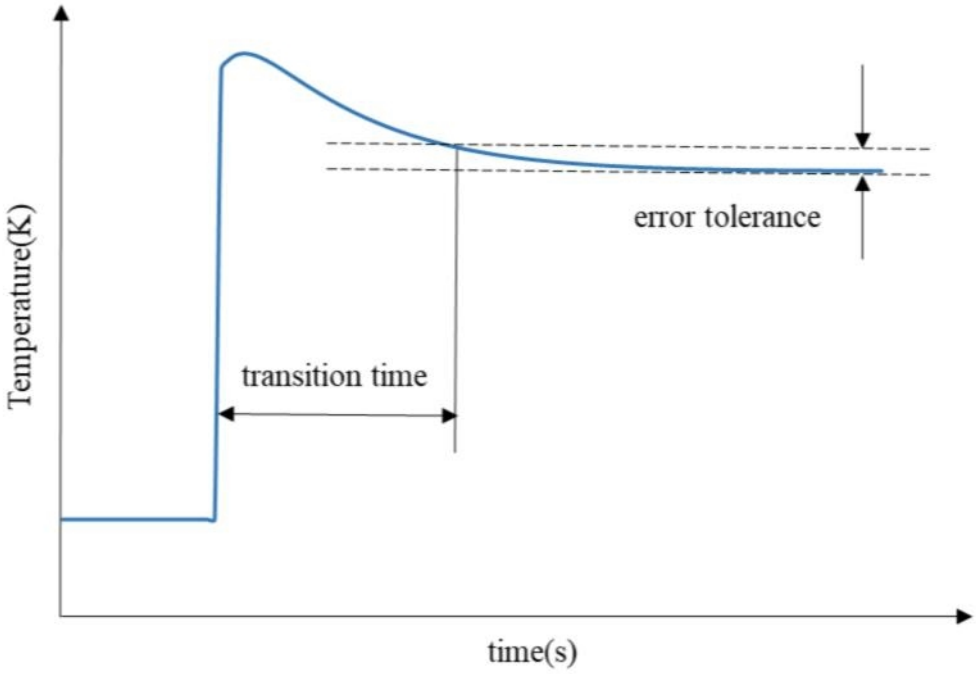

Fig 1.7. The transition time between operational periods

1.4 Objectives

The thesis aims to explore a method to synthesize HEN that can be flexible, controllable, and cost-effective. HEN synthesis primary concern is its economic performance. The synthesis seeks to design a flexible HEN feasible in different operating conditions, but the thesis's core problem is the controllability issue with the time response aspect that has rarely been studied in the design stage. To integrate these aspects into the study, we plan to utilize a multi-period synthesis to stand for the flexibility, the TT

between the operational periods represents the controllability aspect, and the economic performance is the primary objective function to optimize. Although the multi-period synthesis has been widely studied in the literature, it lacks a synthesis strategy to consider all these aspects (cost, flexibility, and controllability). Therefore, we have the following objectives to fulfill the thesis target:

- To find a method that can help to measure the TT during the HEN synthesis stage. The model is expected to deal with the HEN operational period change; in other words, the inlet parameters variation can be a simultaneous and significant change.
- To explore a HEN multi-period synthesis strategy that can consider the TT in the same time, the synthesis method is supposed to be work effectively regardless of the problem scale.

1.5 Thesis structure

The thesis report is structured in six chapters.

This chapter presents the background of the research topic to describe the global view of the research work.

Chapter 2 reviews HEN synthesis achievements, including the flexibility aspect, multi-period design, and controllability.

Chapter 3 provides the preliminary method to obtain TT of HEN through some simplifications and a basic iteration strategy to synthesis the multi-period HEN.

Chapter 4 gives the improved model to obtain the TT free of numerical difficulty concerns. Moreover, an improved iterative strategy to synthesize HEN that originated from the Pinch technology will be developed. These improvements allow the method to deal with large-scale problems.

Chapter 5 tests the proposed method in a real case problem.

Chapter 6 concludes the work of the thesis and discusses perspectives.

Résumé du chapitre 2

Dans ce chapitre, nous avons examiné la synthèse du HEN. Au début, nous avons fourni quelques chiffres principaux pour montrer la tendance de la recherche au cours des dernières années en nous référant aux travaux trouvés sur Google Scholar et Elsevier, et nous avons généré des nuages de mots pour illustrer les objets de la recherche focalisés au cours du dernier demi-siècle. Et l'examen détaillé a été effectué dans les aspects de la méthode de conception, de la flexibilité, de la multi-période et de la contrôlabilité. Pour chaque sous-partie, nous avons fourni un calendrier pour illustrer le travail important au cours du développement. Dans la sous-partie de la méthode de conception, nous avons suivi la méthode de résolution pour discuter de la progression et exploré les réalisations de l'extension du HEN combinées avec d'autres sujets. Les principales méthodes de synthèse ont été proposées en flexibilité et en revue pluriannuelle. Dans la partie de contrôlabilité, tous les indicateurs correspondants et la discussion de la performance dynamique réelle ont été fournis. Après avoir examiné les références pertinentes, nous avons constaté que la réponse temporelle dans la conception a rarement été explorée et de nombreux chercheurs ont déjà reconnu l'importance de la réalisation de l'étude.

Chapter 2 – Heat Integration: State-of-the-Art

2.1 Introduction

The heat exchanger network (HEN) design problem was firstly provided in an open journal by Ten Broeck (1944), and it was first rigorously defined by Masso and Rudd (1969). The HEN synthesis is formally defined as follows.

Given:

- a set H of hot process streams to be cooled,
- a set C of cold process streams to be heated,
- supply and target temperatures, heat capacities, flow rates and heat transfer coefficients of the hot and cold process streams,
- a set of hot and cold utilities available,
- temperatures or temperature ranges, costs and heat transfer coefficients of the utilities,
- heat exchanger cost data,

Develop:

- a network of HEs with minimum Total Annual Cost (TAC), where TAC is the sum of the annualized investment and operating costs.

The earliest method traced back from the doctoral thesis (Hohmann, 1971), in which the T-H (temperature-enthalpy) analysis was the first time introduced. The effect of heat load distribution over the heat transfer area and the relationship between the cost and the minimum temperature difference were also investigated. His work built the foundation for Pinch Technology (PT). However, his contribution received quite a little attention at that time. Since then, there are two significant publications in the HEN synthesis field and got cited almost in every HEN synthesis paper. The first one is the Pinch technology formalized by (Linnhoff and Flower, 1978) that represents the graphic-based solving method. The second one is the stage-wise superstructure (SWS) based simultaneous synthesis model suggested by (Yee and Grossmann, 1990) that stands for the mathematical solving method. There are four significant review works in the HEN synthesis study. Gundersen and Naess (1988) provided the first review of HEN synthesis work. The second one came from (Jezowski, 1994a; Jezowski, 1994b). In 2002, Furman and Sahinidis (2002) presented a critical review based on the previous review work and introduced a timeline to show the leading innovation and discovery in the HEN synthesis history until 2000. They also described the milestones in the development and discussed separately 461 of HEN synthesis work. The works they selected are either in English version or with an English abstract. Morar and Agachi (2010) gave the most recent review work, which covered the work published from 1975 to 2008. In which, they employed CiteSpace - II to illustrate the relationships between domains, authors, and journals.

The HEN synthesis started from the single period scenario and has achieved much progress. In actual operating conditions, the HEN can hardly keep working in the designed nominal status because of the environmental fluctuation or facing disturbances. Thus the HEN flexibility analysis and flexible HEN synthesis attracted the research focus, the research are mainly about the disturbance rejection and multi-period synthesis, and they are more in the steady-state discussion. Controllability, as the other aspect of the operating issues, reflected the short time dynamic response and was also studied. However, the HEN

synthesis considers the dynamic performance, especially time-related responses, are quite scarce. The review work (Morar and Agachi, 2010) confirmed that only a few studies treat the dynamic performance of HEN with a dynamic state point of view.

In this chapter, some numbers will be provided in terms of the HEN synthesis research development at first, followed by a time-line to illustrate the critical works based on the review work (Furman and Sahinidis, 2002; Morar and Agachi, 2010). Then comes the discussion about the progress of the HEN synthesis method, in which our review works are based on the journal papers, conference proceedings, and Ph.D. thesis written in English. After that, the HEN flexibility study and HEN multi-period synthesis contributions will be reviewed individually. The HEN controllability will be reviewed in the last part to discuss the achievements of the dynamic performance considerations in the HEN synthesis.

2.2 HEN synthesis

2.2.1 Main numbers

Fig 2.1 illustrates the trend of the number of publications over the year. The review sources come from Elsevier and Google scholar with HEN synthesis as the keyword, and each work counted precisely dealt with the HEN synthesis problem, not the retrofit scenario. There is a total of 442 papers that studied the HEN synthesis until the end of 2019. The trend of the publication increased before 2017 and peaked there with 42 publications. Looking at the journal source contributions as provided in Fig 2.2, Computers and Chemical Engineering accounts for 25% followed by Applied Thermal Engineering, then comes the Energy and Computer Aided Chemical Engineering, which is close to the distribution results presented by (Morar and Agachi, 2010) and (Anantharaman, 2011). Word clouds is generated to highlight the main concerns of the research by extracting the Keywords from these publications, as depicted in Fig 2.3. HEN, heat, integration, optimization, mixed-integer nonlinear programming (MINLP), and Pinch revealed the basic idea and approach of HEN synthesis. The keywords like uncertainty, Rankine, CO_2, and environmental represent the operational and environmental considerations in these years. The word cloud reveals the priority concerns and utilized tools of those works, detailed information is necessary for us to grasp the achievement of the field.

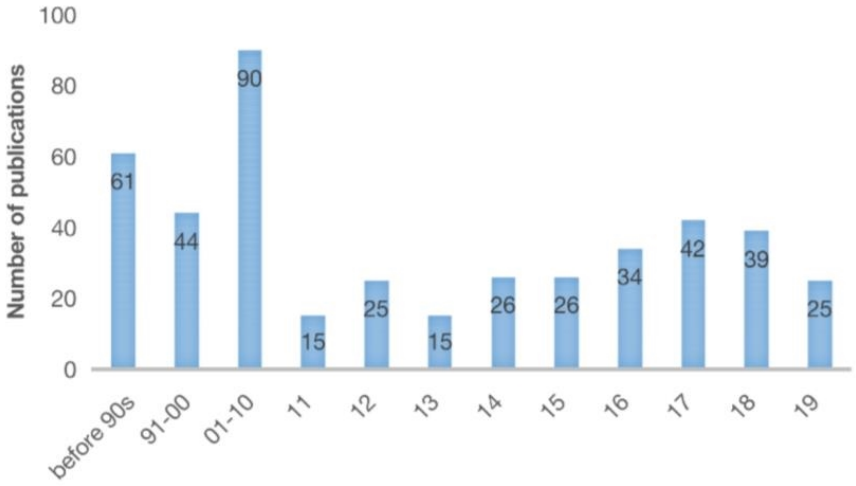

Fig 2.1. Number of publications that deal with HEN synthesis over the year

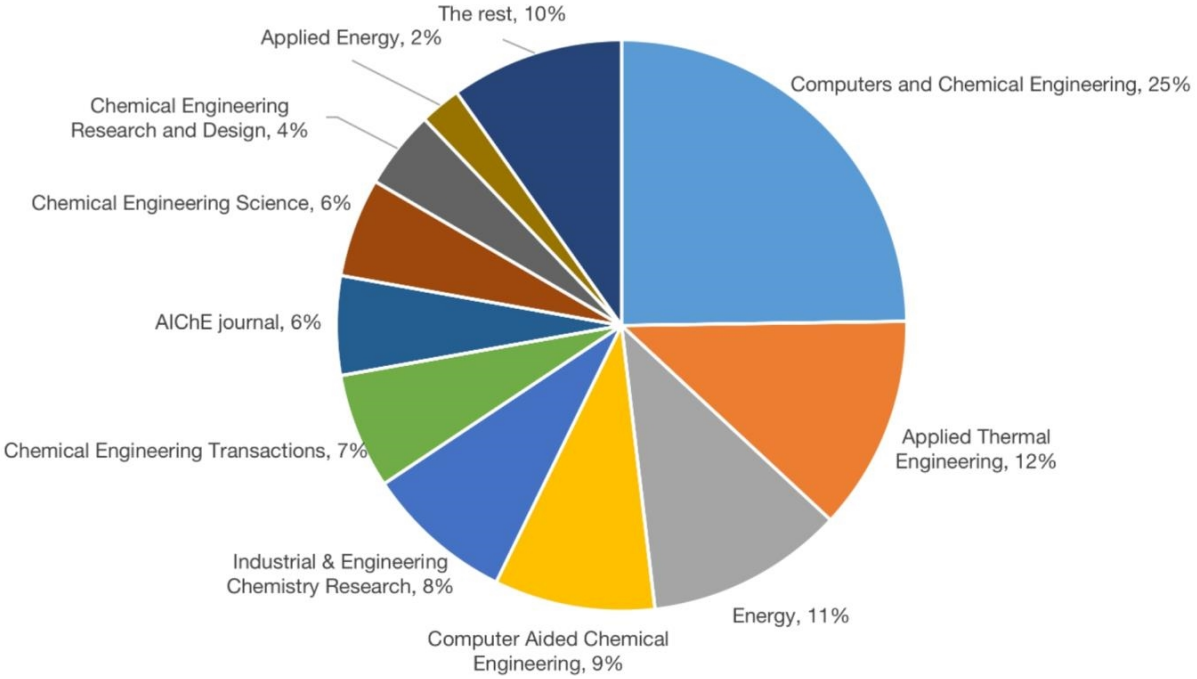

Fig 2.2. Publications over various journals

Fig 2.3. Word clouds extracted from the key words of these publications

2.2.2 Milestones in the HEN synthesis history

The list of milestones is based on (Furman and Sahinidis, 2002) and (Anantharaman, 2011), but with some adjustments, since we focus only on the grassroots design, not retrofit problem, and extend the time period to the end of 2019.

- 1964, first HEN related paper (Broeck, 1944).
- 1965, first grassroots design and superstructure (Hwa, 1965).
- 1969, first formal definition of HEN synthesis problem (Masso and Rudd, 1969).
- 1971, first T-H diagram analysis method for HENs, foundation for Pinch (Hohmann, 1971).
- 1978, formal introduction of pinch point (Linnhoff and Flower, 1978).
- 1978, first deterministic method for global optimization of HEN synthesis (Westerberg and Shah, 1978).
- 1983, Pinch design method is provided (Linnhoff and Hindmarsh, 1983).
- 1983, Transshipment model to minimize utilities and minimize the number of matches (Papoulias and Grossmann, 1983).
- 1984, Patterson's approximation for logarithmic mean temperature difference (LMTD) (Paterson, 1984).
- 1986, Multi-period transshipment model (Floudas and Grossmann, 1986).
- 1986, linear programming (LP) – mixed-integer linear programming (MILP) – nonlinear programming (NLP) sequential synthesis approach (Floudas et al., 1986).
- 1987, Chen's approximation for logarithmic mean temperature difference (LMTD) (Chen, 1987).
- 1989, first time to utilize meta-heuristic method, simulated annealing (SA) to synthesize HEN (Dolan et al., 1989).
- 1989, simultaneous HEN synthesis model (Yuan et al., 1989).
- 1990, stage-wise superstructure (Yee and Grossmann, 1990).
- 1990, first hybrid synthesis method, Pinch-NLP (Linnhoff and S.Ahmad, 1990).
- 2001, HEN synthesis proven to be N-P hard problem (Furman and Sahinidis, 2001).
- 2010, temperature interval based MILP model for HEN synthesis (Isafiade and Fraser, 2010).
- 2012, LMTD reformulation and comparison of various approximations (Huang et al., 2012).
- 2013, comparison of various mathematical models and solvers, large scale problem up to 39 streams (Escobar and Trierweiler, 2013).
- 2015, HEN multi-objective design to consider the CO_2 emissions (Kang et al., 2015)

2.2.3 Synthesis methods

Research in the early 60s were mainly on rules-of-thumb to locate the best structure, and the limitation in the computational technique lead to the methods originated from the thermodynamics in the 70s. The mathematical optimization method came to the research focus thanks to the advances in computation in the 80s and 90s, and sequential synthesis approaches are gradually replaced by the simultaneous way.

Furman and Sahinidis (2001) had proved that the HEN synthesis problem is an N-P hard problem. In other words, global optimal result is not expected to be reached within acceptable calculation time. After realizing the numerical difficulty to solve the MINLP model in large scale problems, the meta-heuristics method came to the research focus and exhibited quite a strong search ability, and the hybrid method had also been explored.

There are mainly two types of classification about HEN synthesis, as shown in Fig 2.4. The first one is to classify by the solving order as the simultaneous way and sequential way. The other one is differentiated by the solving approaches, which are deterministic, graphic-based, meta-heuristics based, and hybrid methods. The two different definitions get overlap parts, like the deterministic approach and meta-heuristics methods can be implemented in both simultaneous and sequential way, but the hybrid method and graphic-based methods are reported mostly in a sequential way. We are following the solving method to proceed with the HEN synthesis discussion.

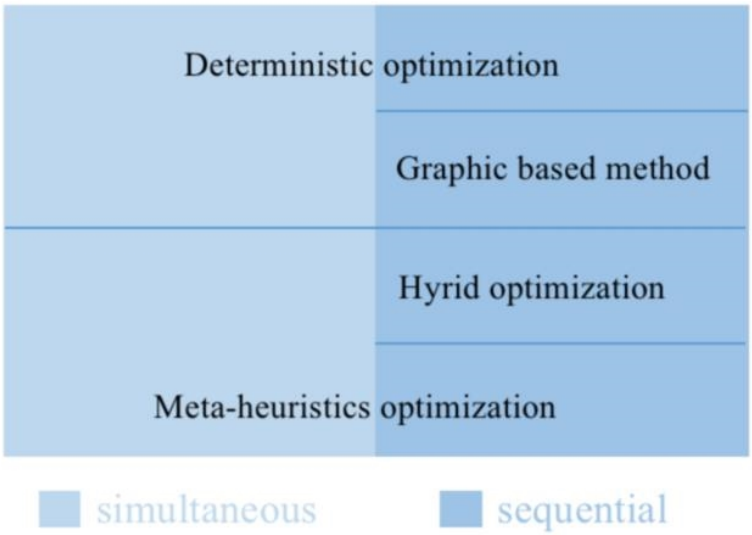

Fig 2.4. Two types of classification of HEN synthesis method

As the pioneers of the graphic-based method, Pinch technology proposed by (Linnhoff and Flower, 1978) provided a fast and efficient way to design the HEN. It is based on the laws of thermodynamics, and employs the Composite Curves (CC) to achieve energy integration. The CC is depicted in Fig 2.5. The hot streams and cold streams form two curves under the Temperature-Enthalpy graph. The graph can help decide, for a given minimum temperature difference, minimum cold and hot utility consumption, representing the maximum energy recovery (MER) design of the system. The Pinch technology provides a list of rules-of-thumb to design the system but the final HEN network depends on the experience of engineers because there are generally many structures that can reach the MER condition. Since utility costs contribute a significant part to the TAC of HEN, networks designed by the Pinch method are often with relatively low TAC even it is not optimal, and this is the reason why the resulting quality is still competitive compared to the result generated by the latest mathematical approaches (Aguitoni et al., 2019).

There are also other graphic tools that originate from the Pinch technology, as provides in Table 2.1. To overcome the limitations of CCs (because it cannot lead to an exact match between hot and cold streams), Alwi and A.Manan (2010) provided a new graphical tool named as STEP (Stream Temperature vs.

Enthalpy Plot) for simultaneous utility targeting and design of HEN. In the first step, stream temperatures are transferred into shifted temperatures by letting the hot stream temperature minus half of the ΔT_{min}, and the cold stream temperature adds half of the assumed ΔT_{min}. The second step is to construct a continuous hot and cold STEP, and each stream is manipulated sequentially. The idea is close to the CCs, but only keep the hot stream with the largest heat capacity flow rate in each temperature intervals, and more than one pair of CCs will be built. The third step is to identify the ΔT_{min} and the minimum utility targets.

Wang et al. (2014) suggested a heat duty-time diagram to synthesis HEN featuring batch streams. The method is based mainly on a combination of Gantt chart and CCs used in Pinch analysis. It calculates the heat load of each stream at first, followed by ranking all the streams in ascending order of supply temperature, then to plot Q-T diagram using the heat duty value and time interval by the order built in the first step.

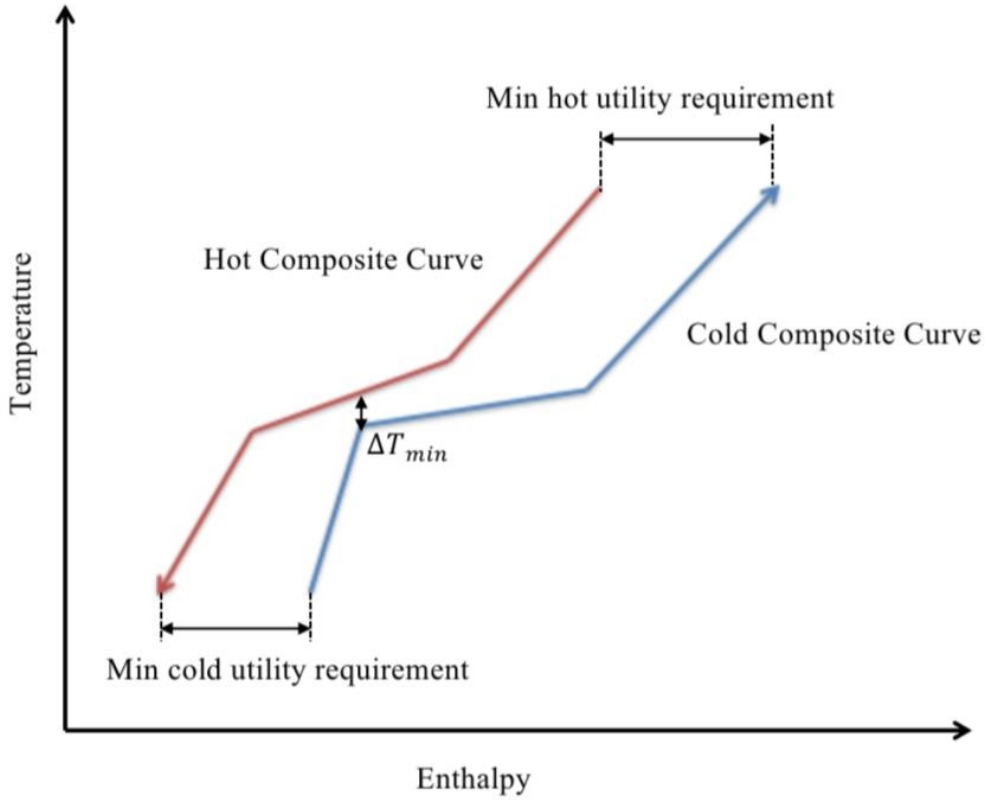

Fig 2.5. Composite Curves of Pinch analysis

Table 2.1. Graphic synthesis methods

Temperature - Enthalpy diagram	(Hohmann, 1971)
Pinch technology	(Linnhoff and Flower, 1978)
Stream Temperature vs. Enthalpy plot	(Wan Alwi et al., 2012)

Mathematical programming methods for the HEN synthesis followed closely to the Pinch technology. Papoulias and Grossmann (1983) framed the synthesis problem as an LP model to find the MER design,

and a MILP model to predict the minimum number of units. The most important work came from the SWS model proposed by (Yee and Grossmann, 1990), the model enables us to describe the HEN synthesis problem with an MINLP model to optimize the TAC directly, and it usually termed as SYNHEAT model. The SYNHEAT model includes all the potential matches with a given stage. The model considers no bypass, no crossflow, each split stream allows maximum one HE, and assumed isothermal mixing for split streams. These assumptions and simplifications make the corresponding MINLP less complicated to solve. Based on SYNHEAT model, efforts had been made to consider non-isothermal mixing (Björk and Westerlund, 2002), crossflow (Floudas et al., 1986), utility implementation in the stages (Ponce-Ortega et al., 2010), phase change (Hasan et al., 2010), etc., the synthesis model had been largely expanded.

Analyzing the complexity of the MINLP model, the trade-off among heat transfer area cost, utility cost, and number of matches take the most important responsibility. Looking at the math equations, the LMTD to describe the heat transfer performance contributes hugely to the nonlinearity. Approximations have been adapted to avoid LMTD numerical difficulty. The most commonly selected approximations are Chen's approximation (Chen, 1987), Paterson's approximation (Paterson, 1984), arithmetic mean temperature difference (AMTD) (Zamora and Grossmann, 1998) and geometric mean temperature difference (GMTD) (Pettersson, 2008). Pettersson (2008) compared the accuracy of these four expressions with real LMTD by varying the temperature difference and found that Chen's approximation gets the best accuracy, the AMTD and GMTD can also have excellent accuracy when temperature differences in both sides of HE are close.

The mathematical programming methods can be further divided as the deterministic way and the meta-heuristics based way according to the solving approach. Deterministic approaches take advantage of the analytical formulation of the problem to generate a sequence of points that tries to converge to a global optimal solution (Lin et al., 2012). For the simultaneous deterministic way, the prescribed MINLP model usually solved with Branch-Bound based algorithms, efforts have been made in improving Branch-Bound searching ability (Adjiman et al., 1997), bound contraction methods (Faria et al., 2015), reformulation of LMTD expression (Huang et al., 2012), etc.. But the binary variables (to describe the existence of HEs) in the MINLP model bring considerable convergence difficulty in the solving process. The difficulty increases massively with the scale of the problem. On the other hand, the sequential synthesis approach can be solved relatively with less burden. The representative sequential approach was provided by (Floudas et al., 1986), they utilized a LP model to achieve the minimum utility cost result, then a MILP model to reach the minimum number of HEs design, ended up with the NLP model to optimize the TAC. Anantharaman (2010) decomposed the synthesis problem into a MILP and a NLP sequential tasks to minimize the number of units. Isafiade and Fraser (2010) transformed the MINLP model into MILP by dividing the supply and target temperatures of streams into small intervals. Escobar and Trierweiler (2013) compared the deterministic models from the simultaneous way and sequential way with various solvers through small case studies to a 39 stream case. They found that the sequential method is easy to implement and requires less computational effort, but the optimized results are not competitive. The deterministic way is rather powerful if the problem is just LP or NLP. The deterministic sequential way allows us to reach a good design, but the potential better design might have been discarded during the decomposition process. The deterministic simultaneous way cannot handle the large scale problem due to the convergence failure.

The solving difficulty of the MINLP problem had been figured out very early in the 90s, and meta-heuristics based method has been proposed correspondingly. Currently, the meta-heuristic methods have displayed quite a strong ability in HEN synthesis (Aguitoni et al., 2019; Bao et al., 2018; Pavão et al., 2016). Some well-known algorithms are Genetic Algorithms (GA), SA (Kirkpatrick et al., 1983), Particle Swarm Optimization (PSO) (Kennedy and Eberhart, 1995), Ant Colony Optimization (ACO) (Dorigo and Di Caro, 1999). The implementation of meta-heuristics in HEN optimization are summarized in Table 2.2. The meta-heuristic based method includes two types of implementation. The first one is the two-level approach adopted by most studies (Pavão et al., 2016; Aguitoni et al., 2019). The upper level is designed to optimize the HEN structure and decide the binary variables, the lower level, to optimize the NLP model. The second type is the one level approach, where the HEN synthesis problem was optimized by a single algorithm (Lewin, 1998; Yerramsetty and Murty, 2008).

Taking the work by Aguitoni et al. (2019) as an example to explain the two-level approach, they utilized SA in the upper level to generate the structure and employed differential evolution (DE) algorithm in the lower level to optimize the NLP model. The SA is proposed in (Kirkpatrick et al., 1983), which mimics the metal annealing process. The annealing process aims to minimize the internal energy by figuring out the best atomic configuration, and the solid temperature always decreases slowly. There exists a similarity between the annealing process and HEN synthesis, considering the HEN synthesis process is to find the best place of HE that can minimize the TAC from scratch. A random structure was generated from the start, and corresponding TAC was obtained by DE. Then the structure will add or remove randomly several HEs. The structure will get updated when the TAC can decrease. The structure with poor TAC still gets a chance to be accepted by comparing the acceptance criteria with a random value within 0 and 1. SA gets three parameters to set for the optimization process. They are the annealing temperature, progress of TAC, decreasing coefficient of temperature. DE is an evolutionary algorithm that can select the heat load, heat transfer area, and stream split fractions as decision variables. It includes the initialization, mutation, cross, and selection processes to update the population by each generation and return the best result among the group until reaching the maximum generation. There are also stochastic mechanisms both in the mutation and cross processes. Like the work of (Lewin, 1998), the one-level approach utilized the algorithm, such as GA, to optimize both the binary and continuous variables.

Table 2.2. Meta-heuristics applied in HEN synthesis

GA	(Luo et al., 2009) (Li et al., 2012)
SA	(Dolan et al., 1989) (Ciric and Floudas, 1991)
SA- Rocket Fire Optimization (RFO)	(Pavão et al., 2018)
Chaotic Ant Swarm	(Zhang et al., 2016)
Random Walking and Compulsory Evolution	(Zhang et al., 2017)
PSO	(Silva et al., 2010)
SA-PSO	(Pavão et al., 2016)
Tabu search	(Chen et al., 2008)
Harmony search	(Khorasany and Fesanghary, 2009)

The stochastic mechanism inside the meta-heuristics algorithms can avoid the convergence difficulty that occurs in a deterministic simultaneous way, and can enable to escape from local optimal points by increasing iteration steps. Under such a case, LTMD can be settled directly without necessity to employ approximate expressions. However, it cannot guarantee a competitive solution within a reasonable calculation time, and the parameter setting is also an intricate part due to the lack of a uniform method. Moreover, these proposed solving algorithms are brought from other fields of optimization work, their core mechanisms are quite similar, and we cannot tell which one is more suitable for the HEN synthesis problem. Their application contributes a lot to obtain large scale synthesis results, but they cannot help to understand further about the synthesis problem. Not every algorithm is suitable to optimize both the binary and continuous variables, which can be interpreted as a part of the adaption in the HEN problem. Moreover, they are not specifically designed for HEN synthesis, and there does not exist a single algorithm that performs well enough for all kinds of HEN synthesis problems.

The combination of Pinch based method and mathematical programming provided another pathway to solve the HEN synthesis problem, which is also termed as the hybrid approach, as illustrated in Table 2.3. The idea is to locate suitable structures or to reduce the search region by Pinch related method and then implement mathematical optimization. Inspired by the thermal circuit law, Chen et al. (2015) introduced a thermal circuit based HEN synthesis method based on the concept of entransy-dissipation-based thermal resistance. Angsutorn et al. (2014) combined the Pinch technology and MINLP model, in which the Pinch analysis divides the synthesis problem into upper-Pinch and lower Pinch parts, and utilizes MINLP to optimize them separately. Linnoff and Ahmad (1990) repeated the Pinch design many times over various minimum temperature differences to obtain the lowest TAC design. Then the structure was optimized by an NLP model to obtain the best TAC design. The case study results in their work are still competitive compared to the current meta-heuristics based result. Ma et al. (2008) adopted a similar idea to carry out the design work by selecting the HEN structure through the proposed temperature – enthalpy (T-H) diagram, and then the continuous parameters are improved by a combined method of GA and SA. The method can be seen as a hybrid method based on the T-H diagram and meta-heuristic algorithms. It seems that the strategy to find the structure by Pinch related method and then optimize the continuous variables with the NLP model is promising. Since the structure is found by understanding HEN synthesis, which can be regarded as a deterministic approach when fixing the selection criteria. The NLP optimization can also be completed by the deterministic solver, and the convergence burden is largely reduced due to the removal of binary variables compared with MINLP model. Therefore, such a method can provide a solution free of the parameter tuning problem posed in a meta-heuristics way.

Table 2.3. Hybrid methods for HEN synthesis

Pinch - NLP	(Linnhoff and S.Ahmad, 1990)
Pinch - MINLP	(Angsutorn et al., 2014)
T-H diagram - GA/SA	(Ma et al., 2008)

2.2.4 Detailed considerations

Except for the efforts to reduce assumptions and simplifications in the preliminary model (Yee and Grossmann, 1990), many endeavors have been devoted to considering more aspects as detailed in Table 2.4. As the work to consider the environmental impacts, measure the system reliability, investigate the

phase change scenario, accounts for the costs of piping and pumping cost, study the condition that thermodynamic parameters are temperature dependent, or even integrate the HE design into the HEN design work.

Table 2.4. HEN synthesis detailed considerations

Environmental effects	(Kang et al., 2015; Isafiade and Short, 2016; L. V Pavão et al., 2017)
System reliability – economic performance	(Lv et al., 2017)
Non-isothermal phase change	(Hasan et al., 2010)
Piping and pumping cost (pressure drop)	(Akbarnia et al., 2009;, Serna-González et al., 2010; Chang et al., 2017)
Temperature dependent parameters	(Huang and Chang, 2012; Lou and Wang, 2013; Tan et al., 2014; Wu et al., 2015),
HE design	(Silva et al., 2008; Jin et al., 2008; Akbari et al., 2008; Allen et al., 2009; Navia et al., 2010; Short et al., 2016; Xu et al., 2017)
Fouling	(Azad et al., 2011; Liu et al., 2015)
Batch operation	(Liu et al., 2011; Wang et al., 2014; P. Yang et al., 2014)
Lifetime consideration	(Nemet et al., 2012; Luo et al., 2013; Abuhalima et al., 2016)
Inherent safety	(Chan et al., 2014)

2.2.5 Extension of HEN synthesis and application in industrial systems

The HEN synthesis is not constrained in the heat integration field, and it has already been widely applied in the field like heat-water nexus, heat-water-pressure networks. As an essential energy recovery tool, many attempts have been made to integrate into various renewable systems such as the biogas plant, fuel cell system, Organic Rankine Cycle (ORC) system, etc. Even in a traditional coal-fired power plant, researchers expected to combine it with sustainable technology like super-critical CO_2 power cycle and CO_2 capture system. There are also many other industrial implementations of HEN, as shown in Table 2.5, which revealed the promising role of HEN in the way to reach a more economical and ecological industrial world.

The efforts to find more economic HEN design are enormous. However, it is vital to accept that HEN synthesis is not just about the economic optimization, it must also empower the operability to achieve the economic performance in a practical operating environment (Escobar et al., 2013a). The operability is more about the flexibility and controllability issues that are rather important to be considered in the design stage. Otherwise, the performance can deviate very far even equipped with an advanced control strategy. These two points are to be discussed in the following parts.

Table 2.5. HEN synthesis applications

Oil refinery process	(Bulasara et al., 2009; Lai et al., 2011)
Heat-integrated water networks	(Bogataj and Bagajewicz, 2008; Leewongtanawit and Kim, 2008; Kim et al., 2009; Ahmetović and Kravanja, 2013; Gabriel et al., 2016)
Integrated heat, mass and pressure networks	(Dong et al., 2014; Onishi et al., 2014)
Coal-fired power plant	(Leng et al., 2010; Wan Alwi et al., 2013; Hanak et al., 2014; Wan Alwi and Manan, 2016; Zhao et al., 2018)
Renewable energy integrated systems	(Arteaga-Perez et al., 2009; Oliva et al., 2011; Drobež et al., 2012; Chen et al., 2014; Luo et al., 2016; Isafiade and Short, 2017; Abikoye et al., 2019; Choomwattana et al., 2016; Shemfe et al., 2016; Shemfe et al., 2016; Francesconi et al., 2017)
Membrane Distillation System	(Lu and Chen, 2012)
Heat pump integration	(M. Yang et al., 2014; A. Yang et al., 2019)
Refrigeration system	(Anastasovski, 2014; Lira-Barragán et al., 2014)
Ammonia-water absorption	(Chen et al., 2017)
Cu-Cl cycle	(Ozbilen et al., 2014)

2.3 Literature review on flexible HEN synthesis

The HEN can hardly stay in a single operating condition. It gets chances to vary with time mainly due to two reasons: the first one is the unplanned operational fluctuations are inevitable; the second one goes for the designed periodic variations to meet the production requirement. For example, the reacting operation temperature in hydrotreating and hydrocracking in refineries can be changed for catalyst deactivation (Ahmad et al., 2012). The fluctuating operating condition forms the basis as the requirement for flexible HEN design, and in some cases, extend to the multi-period scenario. Swaney and Grossmann (1985) defined flexibility as the problem of ensuring feasible steady-state operation over various of operating conditions. Grossmann and Halemane (1982) classified the design of flexible chemical plants into two categories. The first type is the deterministic multi-period problem, in which the operational periods are specified. Such as refineries that handle various types of crudes, or pharmaceutical plants with multi-products. The second type deals with some parameters facing significant uncertainty variations, such as the transfer coefficients, physical properties, or cost data. The flexibility study should be incorporated into the synthesis study for both types. While multi-period synthesis will be discussed in detail in the next section, we focus on the second type of problem in this section.

2.3.1 Flexibility studies

Main timeline for flexibility study

- 1972, first HEN sensitivity study (McGalliard and Westerberg, 1972).
- 1978, first flexibility discussion (Grossmann and Sargent, 1978).
- 1982, HEN resilience issue (Marselle et al., 1982).
- 1985, resilience index (Saboo et al., 1985).
- 1985, flexibility index (Swaney and Grossmann, 1985).
- 1987, MILP/MINLP flexibility study model (Grossmann and Floudas, 1987).
- 1995, dynamic flexibility (Dimitriads and Pistikopoulos, 1995).

McGalliard & Westerberg (1972) pioneered the flexibility study in the sensitivity aspect under the HEN synthesis regime through a three-step method: sensitivity analysis to examine the disturbance propagation over-controlled variables and process modifications to keep the controlled variables within the expected range and performance evaluation, sequentially. Marselle et al. (1982) studied the resilience of HEN in terms of tolerance over uncertainties in temperatures and flowrates. Moreover, the method requires manual work toward a group of designs over various extreme operation conditions, limiting the implementation in large scale problems. The HEN flexibility study started from the early 70s as in the work of (Grossmann and Sargent, 1978), and then it gradually got enriched by the works of Grossmann and co-workers (Grossmann and Morari, 1983; Grossmann and Halemane, 1982; Papoulias and Grossmann, 1983), until (Swaney and Grossmann, 1985) gave the flexibility index to measure the maximum deviation of an uncertain parameter while keeping the outlet temperature in the feasible region. Since flexibility issues usually occur in the extreme conditions of disturbance variables, the flexibility problem had been transferred into the flexibility test problem and flexibility index problem. The corresponding MILP/MINLP model proposed by (Grossmann and Floudas, 1987) had become the commonly utilized method until nowadays, and the flexibility study always follows the sequential way.

2.3.2 Flexible HEN synthesis

The flexible HEN synthesis always follows a two-stage synthesis, mainly dominated by flexibility measuring step, as Fig 2.6 illustrates. With the design information, a multi-period HEN is generated to satisfy some specific operating conditions. It is followed by the flexibility checking process toward the identified critical operating conditions. If the design can pass the checking process, the synthesis process terminates. Otherwise, the multi-period design requires to repeat again by adding the operational points failed in the flexibility checking procedure. There are also some researchers trying to find new approaches.

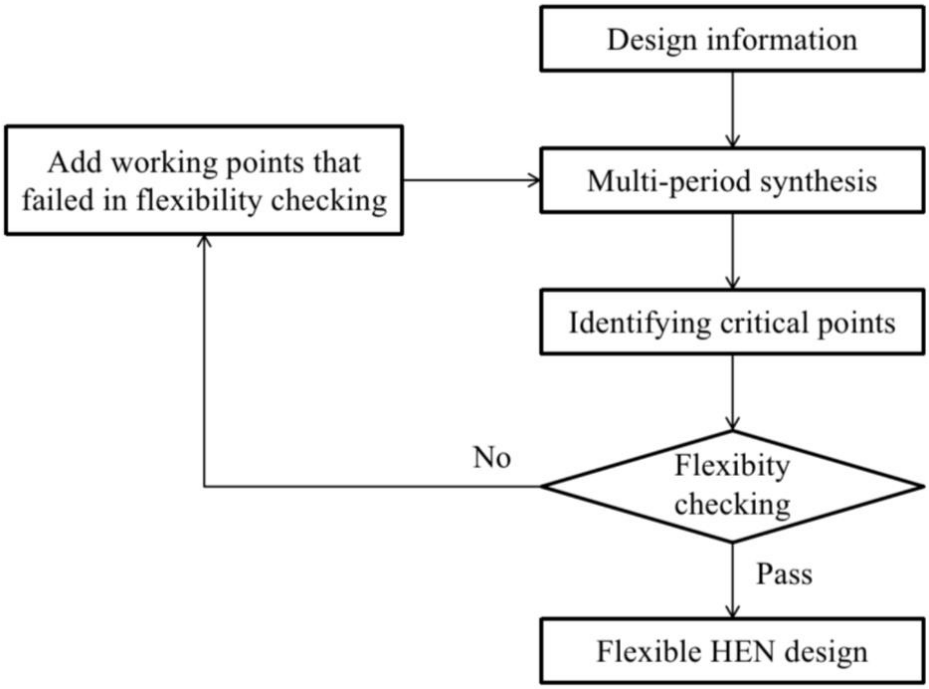

Fig 2.6. Commonly applied flexible HEN synthesis method

Following the above-described approach, Chen and Hung (2004) utilized the integer cuts in the iteration of multi-period synthesis to reduce the search region. Pintarič and Kravanja (2015) extended their two-stage approach (Pintarič and Kravanja, 2004) to have a large number of uncertain parameters to reduce the potentially enormous number of scenarios. Their strategy was to optimize the reduced multi-scenario model, and the obtained optimal design is then tested by stochastic Monte Carlo optimization. Li et al. (2014) presented a two-step sequential method. The HEN synthesis starts with the nominal operating point and updated by critical points. An iterative approach was then utilized to optimize heat transfer area based on the effect of areas on flexibility index and TAC.

Besides the problem with the given region of uncertainty, the stochastic uncertain conditions have also been investigated, and most of them relied on the probability distribution functions. The earliest work was provided by (Pistikopoulos and Mazzuchi, 1990), they introduced a stochastic flexibility index by employing the Gaussian distribution model for the parameter uncertainty and assuming the linear model for HEN synthesis. Moreover, the index reflects the probability that a given HEN is feasible to operate by explicitly considering the operating degree of freedom. Pintarič and Kravanja (2004) coped the problem with a two-stage method. In the first stage, HEN was optimized in over-sized conditions to guarantee flexibility. In the second stage, additional manipulated variables (MVs) and structural alternatives are included to increase the degree of freedom. Then they suggested a strategy to determine a minimal set of critical points of the HEN toward stochastic uncertainties (Pintarič and Kravanja, 2005). The NLP model was solved for each variable to exclude unfavorable critical points after transforming stochastic uncertainty parameters into continuous variables. Pavão et al. (2017) studied the financial risks by assuming the utility cost as stochastic uncertainty parameters and synthesize HEN with meta-heuristics based methods. The utility prices distributions were reached by the Monte Carlo simulation. Liu et al. (2019) considered the gradually accumulating fouling effect in designing flexible HEN problems and provided a three-step method. The first step is to optimize HEN, with the second step to carry out all-cycle flexibility analysis, and the last step to improve the network with an MINLP model to compromise

the flexibility and TAC at the same time. Bai et al. (2017) also studied the flexible HEN synthesis considering fouling problems. Kang and Liu (2019) provided a detailed review of the flexible HEN synthesis development, and they discussed the flexible study through four aspects: sensitivity, resilience, flexibility, and multi-period synthesis. They also illustrated the history and milestones of these four aspects through a timeline.

The above steady-state based flexibility analysis does not consider time-varying disturbances, and it might lead to significant deviation even though the system is equipped with an advanced control system when facing dynamic disturbances. In pure flexibility study, the dynamic flexibility over time-varying disturbances are deeply investigated (Dimitriads and Pistikopoulos, 1995; Huang et al., 2017; Adi and Chang, 2013; Adi et al., 2016), but the works focused only on the flexibility of a given HEN. The dynamic flexibility study works directly for the HEN synthesis was seldom reported. Until recently, Gu et al. (2019) provided an optimization-based HEN synthesis strategy to consider dynamic flexibility. Their work differentiated from the commonly selected over-design HENs to cope with disturbance and flexibility issues, and they targeted to explore the trade-off between dynamic flexibility and TAC. They proposed to use the Generalized Critical Operating Points (GCOPs) to locate the bottleneck of dynamic flexibility toward multiple disturbances. Then the HEN retrofit is carried out for each GCOP to accommodate the stochastic and time-varying disturbances.

The multi-period synthesis as a solution to deal with flexible HEN design with explicit operating parameters accounts for a significant part of the research, and we will discuss it in detail in the next section. It should be noted that the main objective of this type of problem is not only to guarantee the feasibility of the network in any pre-defined operating condition but also optimizes the TAC of the HEN considering all operating periods.

2.3.3 HEN multi-period synthesis

Main timeline for multi-period studies:

- 1986, Multi-period transshipment model (Floudas and Grossmann, 1986).
- 2002, Multi-period SWS model (Aaltola, 2002).
- 2008, Graphic combined with a meta-heuristics method to solve multi-period HEN synthesis (Ma et al., 2008) .
- 2012, Time-sharing mechanism (Sadeli and Chang, 2012).
- 2012, Meta-heuristic method to synthesize multi-period HEN (Ahmad et al., 2012).
- 2013, Lagrangean based decomposition approach (Escobar et al., 2013b)

The earliest synthesis work to deal with the multi-period synthesis was proposed by (Floudas and Grossmann, 1986), and they defined the problem with specified changes in flow rates, inlet temperatures, and outlet temperatures in a finite sequence of periods. Finally, the synthesis problem was converted into a multi-period synthesis work. A MILP transshipment model was employed to minimize the utility cost for each operational period and target the minimum number of units. After that, they suggested a sequential way to carry out the synthesis by utilizing the NLP model to optimize pre-selected HEN configurations (Floudas and Grossmann, 1987). Papalexandri and Pistikopoulos (1994a; 1994b) sought alternatives in an MINLP problem, and the strategy is limited to small scale problems. Aaltola (2002)

provided an MINLP-NLP approach to optimize the design variables simultaneously, in which the MINLP model removed the bypass, assumed isothermal mixing, and reconsidered in the NLP model to improve the optimized result by MINLP model. Reminding that MINLP even for single period HEN synthesis can pose serious convergence difficulty due to the model complexity, the multi-period condition will increase severe the difficulty. Simplification can help reach a preferable design, as Isafiade and Fraser (2010) extended their interval-based method into the multi-period condition with the MINLP model. Futhermore, researchers tried to follow the sequential synthesis way with heuristics or employ the meta-heuristics based method.

The sequential approach is the most common way to avoid solving difficulty due to the largely increased complexity of the problem. Verheyen and Zhang (2006) provided a sequential solution based on the outer-approximation/equality-relaxation algorithm. Escobar et al. (2013b) proposed a sequential method based on the Lagrange decomposition approach to solve large scale problems. Miranda et al. (2016) followed the three-step sequential method by decomposing the optimization target into sub-targets that have been implemented in single period synthesis work (Floudas et al., 1986). Firstly, an LP model was utilized to decide the utility parameters, followed by the MILP model to optimize the structure and end up with the NLP model to optimize all the continuous parameters. Kang et al. (2016) suggested a two-step synthesis method for multi-period HEN synthesis by considering the features of sub-periods. In which the longest duration period is taken as the representative one and HEN structure is optimized toward such a single period, and operational parameters are optimized to meet other non-representative sub-periods. Kang and Liu (2018) proposed a three-stage method to achieve flexible HEN. Firstly, an initial HEN was obtained from the synthesis result of single period information. Secondly, the obtained structure will be modified and optimized by considering both the multi-period operational characteristics and the sub-period operational flexibilities. In the third stage, examine the flexibility of all the sub-periods and improve them by solving a sub-period debottlenecking model.

The efforts to explore the heuristics based on Pinch analysis also worked very well. Ma et al. (2008) employed a hybrid optimization method by combing the graphic method and stochastic optimization to synthesize multi-period HEN. In which the HEN is designed by the temperature – enthalpy (T-H) diagram, and then improved by a combined method of GA and SA.

As the meta-heuristics based methods have illustrated successful implementations in HEN single period synthesis, the application in multi-period condition have also been studied, and the effectiveness in large scale problem is also impressive. Ahmad et al. (2012) employed SA to optimize the MINLP model of the multi-period HEN synthesis problem. Pavão et al. (2018) employed the meta-heuristics two-level method to carry out the synthesis work. In the upper-level, SA was utilized to generate new structures. In the lower-level, continuous SA optimize the given structure first, followed by the RFO to optimize the continuous variables. In addition, a post-optimization (PO) has also been applied to improve the final results.

Apart from the efforts to find more efficient heuristics and solving methods, Sadeli and Chang (2012) suggested the timesharing schemes in the multi-period HEN synthesis scenario, expected to achieve lower TAC design, which the HEs can be shared by different streams in different periods. The timesharing mechanism was also studied by Jiang and Chang (2013) and Miranda et al. (2016). However, their research did not take the corresponding piping cost into the calculation, and the compatibility between

HEs and various streams have not been addressed, which may represent an essential part of the cost in the sharing condition.

Multi-period synthesis as an approach to deal with the flexible HEN design has been utilized in many studies, and the achievement is also considerable. However, it can only reflect the static feasibility to operate the HEN in different operation points, the dynamic performance during the transition phase between two operation points is also deserved to be cautious in the design stage. Next section, the controllability that describes the dynamic response of the HEN operating performance will be discussed.

2.4 HEN controllability studies

Controllability is a significant vocabulary in many fields, such as electrical engineering and computer science. There are many descriptions about the controllability, leading to various analysis methodologies (Swaney and Grossmann, 1985; Lin, 1974; Skogestad, 1996). Nowadays, the input-output controllability is a more widely chosen definition in the HEN controllability analysis (Yuan et al., 2011; Westphalen et al., 2003; Lin et al., 2013). To distinguish from flexibility, Mathisen (1991) regard the controllability of HEN as the performance to reject dynamic disturbance within a short time and refer to the long term operation point change as flexibility. The shifting of different operating points always relies on the change of MVs or input parameters quickly. Thus, it also deserved to be studied as controllability, as Aguilera and Marchetti (1998) argued. Most of the controllability studies focused on selecting the parings of MVs and controlled variables (CVs), and especially the interactions among various combinations of MVs-CVs. Many works confirmed that the controllability is strongly affected by the HEN synthesis, and it is necessary to integrate the controllability study into the HEN design stage. In the next section, we will review the HEN controllability studies.

2.4.1 Controllability study

The controllability and flexibility are both operable issues. The flexibility focuses more on the long-term performance, and the controllability cares more about the short-time response. The current controllability studies rely heavily on various indicators, and the HEN synthesis considering the controllability issue always follows the sequential way since the indicators can hardly be integrated into the synthesis model. Here we are going to provide a timeline to demonstrate the development of involved indexes.

- 1973, Relative gain array (RGA) (Nisenfeld, 1973).
- 1990, Singular value decomposition (Grosdidier, 1990), closed-loop disturbance gain (Skogestad and Hovd, 1990).
- 1992, Performance RGA (Erik A.Wolf, Sigurd Skogestad, 1992).
- 1996, RGA-number (Skogestad and Postlethwaite, 1996).
- 2003, Condition number (CN) (Westphalen et al., 2003).
- 2006, Partial disturbance gain (PDG), disturbance condition number (DCN) (Tellez et al., 2006).

Many efforts devoted to exploring the causes of HEN controllability limitation (Knut W. Mathisen, 1994), and to propose easier and explicit indicators to quantify the controllability (Knut W. Mathisen, 1991; Tellez et al., 2006; Miranda et al., 2017). Those indicators have been integrated into the HEN design

stage (via a sequential approach) (Yan et al., 2001; Masoud et al., 2016; Rathjens et al., 2016) to avoid poor control performance. The HEN controllability problem is a part of the MIMO (multi-input multi-output) problem, and thus many methods originated from the MIMO control field. The earlier works were based on frequency analysis (Erik A.Wolf, Sigurd Skogestad, 1992; Knut W. Mathisen, 1991; Knut W. Mathisen, 1994), and came up with the indicators like RGA (Nisenfeld, 1973), performance relative gain array (PRGA) (Erik A.Wolf, Sigurd Skogestad, 1992), closed-loop disturbance gain (CLDG) (Tellez et al., 2006) and set-point tracking (Erik A.Wolf, Sigurd Skogestad, 1992).

Looking deep into these indexes. RGA is mainly utilized to decide pairings of MV and CV based on steady state system gain matrix (Bristol, 1966), it is well accepted as a useful tool in interaction analysis, and almost present in every work trying to discuss the HEN controllability. Nevertheless, RGA measures mainly the diagonal element of the gain matrix, thus coming to the RGA-number to measure the effect of the non-diagonal element (Skogestad and Postlethwaite, 2005). There are some efforts tried to propose new indicators, Westphalen et al. (2003) utilized the CN as an indicator, by arguing that the closer the CN to 1, the better the controllability, and a large amount of study also employed CN as the HEN controllability indicator (Rathjens et al., 2016; Escobar et al., 2013a; Masoud et al., 2016). On the contrary, Skogestad and Postlethwaite (2005) were cautious about employing CN, and they stated that the small CN means the system is less sensitive to the variance of input information but large CN does not necessarily indicate the system become sensitive, the interpretation of CN result can hardly inform on the HEN controllability. Since the HEN control study usually goes with the system disturbance rejection, disturbance related indicators have also been explored, such as the DCN and closed-loop disturbance gain (CLDG). Reminding that these indicators are based on the steady-state analysis, the derived results often ought to be validated through dynamic simulation results.

Most of the published papers related with HENs controllability problems are trying to find a relatively better bypass placement structure by analyzing the interactions of different control loops and disturbance, by considering only final state (Knut W. Mathisen, 1992; Yan et al., 2001; Westphalen et al., 2003; Hernández et al., 2010; Lin et al., 2013; Rathjens et al., 2016), and lead to many works to decide the bypass placement and preferable control structures (Knut W. Mathisen, 1992; Yan et al., 2001; Escobar and Trierweiler, 2011; Sun et al., 2018). Mathisen (1994) tried to explain the performance limitations with the physical structure in much detailed information based on MIMO theory, and they pointed out several critical physical status that would lead to controllability limitations. They identified the existence of right half plane-zeros (RHP-zeros) is one of the essential problems in HEN control since it will cause the inverse response, which might delay the decentralized control time response. However, they did not analyze the possible methods to diminish the inverse response result by providing corresponding suggestions. The RHP-zeros is based on the frequency study (Skogestad and Postlethwaite, 2005), and requires the system transfer function. It is difficult to calculate the RHP-zeros directly for HEN, considering the complexity to manipulate. When we use the inverse response to detect the RHP-zeros, it will be much easier. In HEN, the inverse response will happen when MV affects the CVs in different downstream pathways with contrary effects. Thus it can be identified through structural and parametric study, which has been applied (R. Yang et al., 2019). Lersbamrungsuk and Srinophakun (2009) proposed to follow the structural way to measure the HEN controllability with three indicators to select preferable control structures. Nevertheless, they did not discuss any clues to handle the potential inverse response, let alone the real dynamic performance.

It is a pity that the dynamic point of response has rarely been discussed, such as the time response when we need to change operating conditions, while it is also a critical aspect in HEN design. The time-related performance has been discussed by (Escobar et al., 2013a) to consider the operability in their HEN synthesis work. They utilized the rising time as one of the criteria to decide the control structure by using a proportional–integral control structure. The dynamic performance, especially the time response of HEN throughout periods changeover can be a problem (Liu et al., 2019) also mentioned that the time response in the evolution of flexibility study has to be settled. Taking the coal-fired power plant as an example where HEN is often integrated (Leng et al., 2010), the plant heat load is required to change regularly to meet the grid demand, and the integrated HEN is also expected to shift the operational period within a particular time considering the embedded catalyst require specific temperature level to keep the activity. Jogwar et al.(2007) also argued the importance of enabling the HEN to achieve fast transient.

Looking from the control performance point of view. The HEN control problem has almost been transformed as the control structure decision problem and the bypass selection to be more precise. It means that the available methods to analyze the HEN controllability can be used only when the HEN is known (structures, HE areas, …). The measuring criteria include the potential interaction among each control loop and the corresponding dynamic performance which is usually about avoiding large overshoot and get a fast response. Fast response has always been regarded as a key point in many HEN control studies (Hernández et al., 2010; Sun et al., 2017;). The HEN multi-period operation is also one of the control strategies that is termed as an open loop, in which bypass, stream split, and utility execute the optimized parameters and wait for the outlet temperature to reach the design status. The time response is also a crucial criterion to measure the goodness of a given HEN multi-period design. Checking the measuring temperatures of the real plant in (Payet, 2018) doctoral thesis, the transition of the working conditions takes 2.5h to 3.5h even in a low heat integration condition. It can be imagined that the time duration will be rather significant in a high heat integration status if efforts have not been devoted to the design stage. Reviewing the HEN multi-period flexible studies, the available indicators are static aspects of research, and they are not enough to reflect the real dynamic performance of HEN. There is no available approach to consider the time response in the design stage to reflect the controllability, and it will be challenging work to cope with such a problem.

2.5 Conclusion

HEN as an efficient tool to recover energy in the industrial process has been widely explored. The solving methods witnessed the transition from graphic based methods to mathematical programming, and the solving ability has been considerably extended by meta-heuristics based approach. However, there is still no uniform solving approach that can handle all the conditions, and the pinch based method can still lead to competitive results in some cases. The synthesis model had been largely extended to make it closer to the real condition or finding a lower cost. The efforts include using the simultaneous model, considering non-isothermal mixing, exploring the phase-change condition, assuming the temperature dependent parameters, etc.. The more critical aspect might be the operating issues since HEN can hardly work in single point and usually faces disturbance or pre-defined fluctuating conditions. Thus the HEN is required to be flexible in various operable regions. The corresponding flexible HEN design had also been deeply investigated with two approaches based on the inlet parameters change information. The first one is the inlet parameters change in a region without explicit points, it usually follows the sequential approach by

measuring the flexibility index iteratively. The other is the condition that the inlet variation is explicit and divided in a number of operational periods, thus multi-period synthesis is carried out to optimize the HEN. The other aspect related to the operability issues is the controllability, which drive the attention to the dynamic performance when HEN changes operational condition. The current research deals with the controllability as the problem to select the pairings of MVs-CVs and most of the indexes are only able to reflect the static characteristics. The dynamic point of performance, such as the time response, has rarely been studied, with some researchers showed the concern of lack of works. Despite the prosperous endeavors in the HEN synthesis, the synthesis that considers dynamic response is a challenging work. In the next chapter, we will build the dynamic model of the HEN to measure the transition time when HEN operational period changes, together with a basic synthesis strategy to integrate the dynamic study into the design stage. Then, chapter four will try to improve both the dynamic model and synthesis method to enable it to be applicable in medium-large scale HEN synthesis problems.

Résumé du chapitre 3

Dans ce chapitre, nous avons proposé le modèle préliminaire pour synthétiser le HEN multi-période qui peut mesurer TT au stade de la conception par la méthode d'itération la plus basique de manière séquentielle, qui est également appelée le modèle BINLP. Le modèle BINLP a été comparé à l'approche MINLP dans quatre petits cas, avec le processus d'élimination des structures isomorphes et des structures avec boucle, et le BINLP prend plus de temps de calcul que MINLP, mais il est capable de trouver une meilleure conception de TAC dans la plupart des cas. Quant à la mesure de TT, nous avons tenté de construire un modèle dynamique HEN en partant d'un modèle dynamique de HE reposant sur la transformation de Laplace. Pour faciliter l'analyse, nous avons utilisé la force motrice de la température moyenne arithmétique pour décrire le processus de transfert de chaleur dans HE. Associé à une méthode d'itération un par un, le modèle dynamique de HE peut être étendu au HEN et obtenir la température de sortie du HEN dans le domaine de Laplace. Ensuite, TT peut être calculé après avoir effectué le processus de Laplace inverse pour atteindre la fonction dans le domaine temporel.

La méthodologie a été appliquée avec succès dans un cas avec quatre flux sous trois périodes opérationnelles, ce qui prend 8min28s pour terminer le processus d'optimisation HEN et 5min56s pour obtenir le résultat TT. Le TAC optimisé est compétitif par rapport à d'autres études, le TT varie beaucoup pour divers modèles, allant de 100 à 2500, et la structure de conception de TAC la plus basse nécessite environ 703. La méthodologie proposée s'est avérée efficace, et l'étude de cas a également confirmé la nécessité d'étudier le TT au stade de la conception, car divers modèles présentent une grande différence dans l'aspect de la réponse temporelle.

Chapter 3 – HEN Synthesis with Consideration of Transition Time: Preliminary Methodology

3.1 Introduction

In this chapter, we aim to provide the preliminary method to reach the thesis target, expecting to find an efficient way to estimate the TT that can be integrated into the HEN design stage, then come up with a synthesis methodology as the start of the work. Except for the HEN parameters to affect the TT when changing the operational period, the control strategy also impacts. There are two types of control strategy: The first type, the open-loop control in which the manipulated variables (MVs) will be fixed according to the condition of each period, and the method do not consider any feedback control effects; The second type, the closed-loop control in which the feedback information is considered. The first method is easier to model than the second. Boyaci et al. (1996) compared the time-dependent open-loop control and the temperature-dependent closed-loop control of the HEN dynamic performance and found that neither solution could dominate the other one. The HEN multi-period synthesis problem usually follows the open-loop way, in which bypass, stream split ratio, and utilities act as MVs. Thus in the thesis, we focus only on the open-loop control method. The main objective of the thesis is to explore the possibility of integrating the consideration of TT into the HEN multi-period synthesis, not to select the best control strategy in the synthesis stage.

The calculation of TT cannot be formulated as an analytic expression in a synthesis model like MINLP (for more information, refer to part 3.3). It can only be reached when obtaining all the information about one specific HEN (structure and other variables like flowrates, utilities). Therefore, the synthesis strategy should separate the TAC optimization and the TT calculation process while keeping the economic performance as the chief target. In the beginning, we plan to follow the most basic iteration approach (BINLP) to solve the problem, as shown in Fig 3.1. We aim to iterate all the potential structures except unfavorable structures identified by pre-selection strategies to reduce iterations. For each structure, the NLP model will be optimized to reach the lowest TAC design, and TT can be calculated correspondingly afterward. Finally, we can reach a TAC-TT trade-off result to select an optimal design by following the TT criteria. Thus, our approach transfers an MINLP problem into a series of NLP problems, and by consequence, the solving convergence difficulty is supposed to decrease drastically.

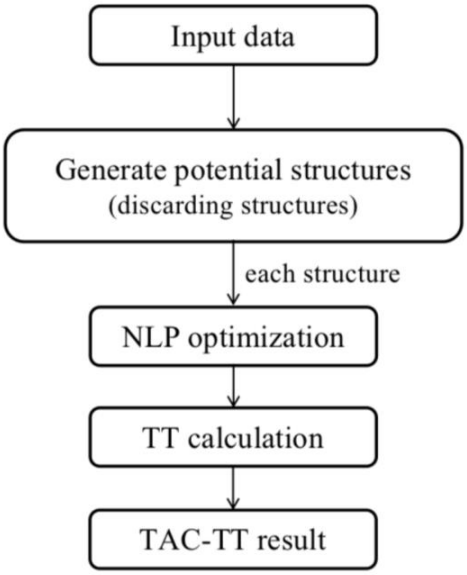

Fig 3.1. BINLP Method for HEN multi-period synthesis considering TAC and TT

In this chapter, we introduce the cost optimization model at first, which includes the NLP model and a method to generate potential structures and discard, if necessary, unfavorable ones. Since loop tends to exist during the iteration of structures and does not lead to excellent economic performance based on pinch technology, we compared the iteration results with loops and without loops. Additionally, a comparison of our BINLP model and commonly used MINLP model will also be provided through four case studies. In part 3.3, we will develop a dynamic model of HEN to reach the TT after providing the corresponding review work. The dynamic model will be tested through a comparison with a numerical simulation method. A four-streams case with three working periods will be employed to test the whole method. The limitations of the method will be discussed, allowing us to figure out the aspects in which the method needs to be improved.

3.2 Cost optimization model: BINLP

The cost optimization model is based on the idea of SWS by (Yee and Grossmann, 1990), which is a common choice in the HEN synthesis study, and iterating all the potential structures is the most basic option. Here, the NLP model will be presented at first, followed by the structural screening processes. The iteration to consider or not the HEN with a loop will be discussed by comparing case studies. A comparison of our BINLP method and an MINLP based method will be used to check the feasibility of our approach.

3.2.1 NLP model

The NLP model is extended from the single-period model proposed by (Huang et al., 2012), which originated from the SWS introduced by (Yee and Grossmann, 1990). The structure is shown as in Fig 3.2, as the problem is composed of I hot streams ($i \in HP, I = |HP|$), J cold streams ($j \in CP, I = |CP|$), ST process stages ($st \in [1, ST]$), C cold utilities($CU_i \in CU, C = |CU|$) , H hot utilities ($HU_j \in HU, H = |HU|$), and P different operational periods ($p \in [1, P]$). Each hot stream will be split into J sub-streams and a bypass at each stage, and each cold stream will also be split into I sub-streams and a bypass at each stage, enables the potential HE (i, st, j) among every hot stream i and cold stream j at each stage st to exist. Because the placement of a HE is defined by three indexes: hot stream i, stage st and cold stream j, a binary parameter $B_{i,st,j}$ is utilized to represent the existence of a HE. Every hot stream is assumed to

end up with a cold utility at stage ST + 1, and the same for every cold stream with a hot utility at stage 0 by assuming a counter-current flow in the HEN. The model tries to find the minimum heat transfer areas, and corresponding utility parameters aims to reach the lowest TAC. Note that the final heat transfer areas are set to be the same value throughout various operational periods. The following assumptions build the basis of the problem:

- Inlet stream mass flow rate, heat capacity, heat transfer coefficient of all the involved fluids, period operating time, cost functions, inlet, and outlet temperature of utility are known and are constant in a specific operational period.
- The stream mixing process can be non-isothermal.
- The heat flow is strictly limited from a hot stream i (which needs to be cooled down) to a cold stream j (which needs to be heated up).
- The minimum HE temperature difference is a given constant.

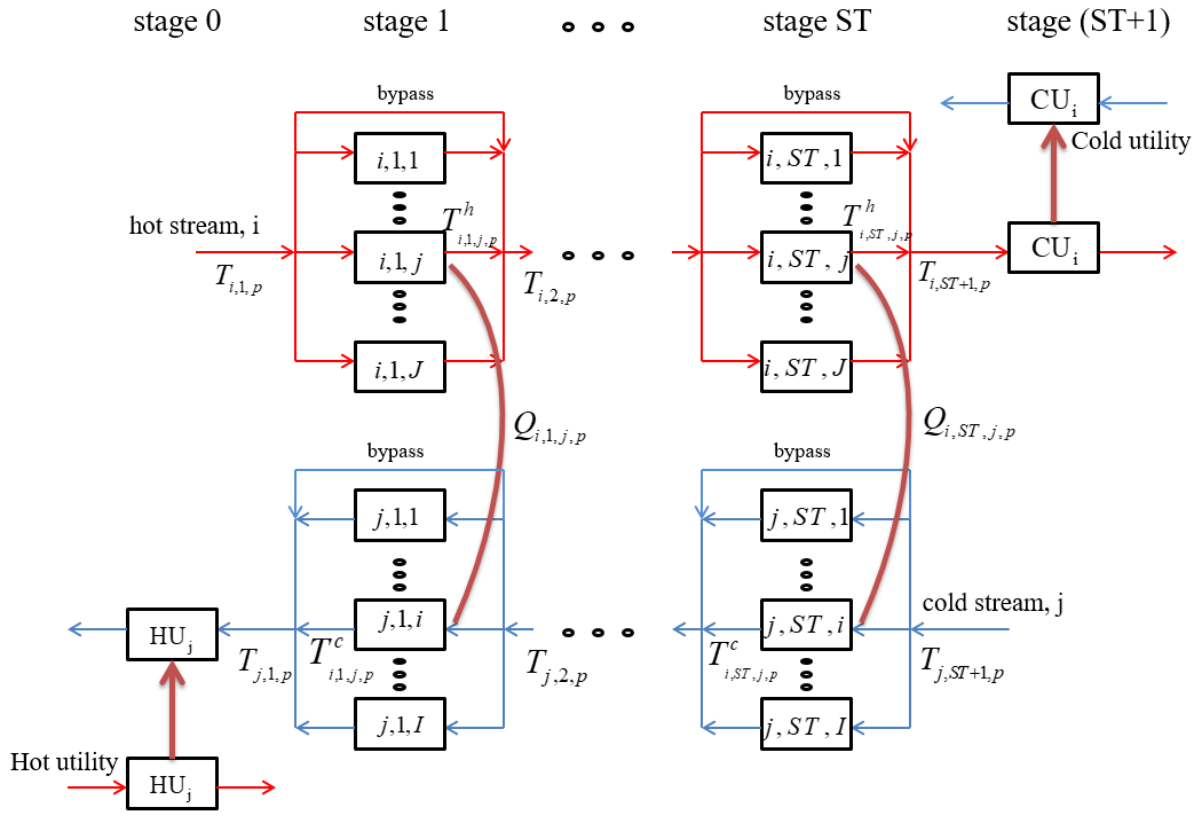

Fig 3.2. SWS for HEN with bypass for each potential HE

In what follows, the equations are applied for all hot process streams i ∈ HP, all cold process streams j ∈ CP, all periods p ∈ [1, P] and all stages st ∈ [1, ST], except contrary indication. The mass flow rate variables were utilized to describe the stream mixing process. $m^{h}_{i,st,j,p}$ and $m^{c}_{i,st,j,p}$ represent the mass flow rate of hot stream and cold stream that go through one HE, $\lambda_{i,st,p}$ and $\lambda_{j,st,p}$ are the mass flow rate for bypass in hot stream and cold stream, $mf_{i,p}$ and $mf_{j,p}$ are the mass flow rate for parent streams.

$$mf_{i,p} \cdot T_{i,st+1,p} = \sum_{j \in CP} m^{h}_{i,st,j,p} \cdot T^{h}_{i,s,j,p} + \lambda_{i,st,p} \cdot T_{i,s,p} \tag{3-1}$$

$$mf_{i,p} = \sum_{j \in CP} m_{i,st,j,p} + \lambda_{i,st,p} \tag{3-2}$$

$$mf_{j,p} \bullet T_{j,st,p} = \sum_{i \in HP} m^{c}_{i,st,j,p} \bullet T^{c}_{i,st,j,p} + \lambda_{j,st,p} \bullet T_{j,st+1,p} \tag{3-3}$$

$$mf_{j,p} = \sum_{i \in HP} m^{c}_{i,st,j,p} + \lambda_{j,st,p} \tag{3-4}$$

Equations (3-1) and (3-3) represent the energy balance of split streams in the mixing process, (3-2) and (3-4) describe the mass balance during the splitting process. Where $T_{i,st,p}$ and $T_{j,st,p}$ stand for the hot and cold stream temperature at stage st of period p, $T^{h}_{i,st,j,p}$ and $T^{c}_{i,st,j,p}$ are hot, and cold split stream temperatures after heat transfer.

The heat transfer coefficient is obtained from individual streams. The general heat transfer coefficients for process HE, hot utility, and cold utility are formulated in equations (3-5) ~ (3-7), respectively.

$$U_{i,j,p} = \frac{1}{\frac{1}{h_{i,p}} + \frac{1}{h_{j,p}}} \tag{3-5}$$

$$U_{i,p} = \frac{1}{\frac{1}{h_{i,p}} + \frac{1}{h_{cu}}} \tag{3-6}$$

$$U_{j,p} = \frac{1}{\frac{1}{h_{j,p}} + \frac{1}{h_{hu}}} \tag{3-7}$$

Where $h_{i,p}$ and $h_{j,p}$ are heat transfer coefficients of the hot and cold stream at period p, h_{cu} and h_{hu} are the heat transfer coefficients for cold and hot utility which keep constant during all operational period.

Our approach aims to iterate all potential HEN structures, the binary parameter $B_{i,st,j}$ will be used to do the iteration through the combination of 0/1 values. For each potential structure, $B_{i,st,j} = 0$ means no HE between hot stream i and cold stream j at stage st, and in that case, the following constraints are written to guarantee the mixing part (3-1)~(3-4) function normally. When $B_{i,st,j} = 0$:

$$m^{h}_{i,st,j,p} = 0 \tag{3-8}$$

$$m^{c}_{i,st,j,p} = 0 \tag{3-9}$$

When $B_{i,st,j} = 1$, the energy balance of the heat transfer process is described with equations (3-10) ~ (3-12). $A_{i,st,j}$ is the transfer area, which is a variable, but has the same value throughout all the operational periods, and to be optimized as well as mass flow rate and temperatures, $cp_{i,p}$ and $cp_{j,p}$ are specific heat capacities.

$$Q_{i,st,j,p} = U_{i,j,p} \bullet A_{i,st,j} \bullet LMTD_{i,st,j,p} \tag{3-10}$$

$$Q_{i,st,j,p} = m^{h}_{i,st,j,p} \bullet cp_{i,p} \bullet \left(T_{i,st,p} - T^{h}_{i,st,j,p} \right) \tag{3-11}$$

$$Q_{i,st,j,p} = m^{c}_{i,st,j,p} \bullet cp_{j,p} \bullet \left(T^{c}_{i,st,j,p} - T_{j,st+1,p} \right) \tag{3-12}$$

The LMTD was expressed in the formulations (3-13) and (3-14) as suggested by (Huang et al., 2012) to help the solver to deal with the condition that the temperature differences in two sides of a HE $\Delta T^{h}_{i,st,j,p}$ and $\Delta T^{c}_{i,st,j,p}$ are close. When this condition occurs, equation (3-13) can easily lead to a wrong value of LMTD due to numerical issues. Thus, constraint expression (3-14) has to be applied to avoid such a problem. Since the arithmetic mean value is always larger than the logarithmic average value, inequality (3-14) can set the upper bound for LMTD, then to improve the convergence of the model.

When $B_{i,st,j} = 1$:

$$\Delta T^{h}_{i,st,j,p} = \Delta T^{c}_{i,st,j,p} + LMTD_{i,st,j,p} \bullet \ln \frac{\Delta T^{h}_{i,st,j,p}}{\Delta T^{c}_{i,st,j,p}} \tag{3-13}$$

$$LMTD_{i,st,j,p} \le \frac{\Delta T^{h}_{i,st,j,p} + \Delta T^{c}_{i,st,j,p}}{2} \tag{3-14}$$

$$\Delta T^{h}_{i,st,j,p} = T^{h}_{i,st,p} - T^{c}_{i,st,j,p} \tag{3-15}$$

$$\Delta T^{c}_{i,st,j,p} = T^{h}_{i,st,j,p} - T^{c}_{j,st+1,p} \tag{3-16}$$

The utility heat transfer process is described similarly, but no bypass will be implemented for the utility stage for both the hot and cold stream. Equations (3-17) ~ (3-22) are implemented for cold utility, assuming the utility inlet and outlet temperatures are known, and the same way for hot utility with equations (3-23) ~ (3-28).

For cold utilities: $\forall i \in HP, \forall p \in P$

$$Q_{i,p} = g_{i,p} \bullet cp_{i,p} \bullet \left(T_{i,ST+1,p} - T_{i,ST+2,p} \right) \tag{3-17}$$

$$\Delta T^{h}_{i,p} = \Delta T^{c}_{i,p} + LMTD_{i,p} \bullet \ln \frac{\Delta T^{h}_{i,p}}{\Delta T^{c}_{i,p}} \tag{3-18}$$

$$LMTD_{i,p} \le \frac{\Delta T^{h}_{i,p} + \Delta T^{c}_{i,p}}{2} \tag{3-19}$$

$$Q_{i,p} \le \frac{A_i \bullet LMTD_{i,p}}{U_{i,p}} \tag{3-20}$$

$$\Delta T^{h}_{i,p} = T_{i,ST+1,p} - T_{cu,out,p} \tag{3-21}$$

$$\Delta T^{c}_{i,p} = T_{i,ST+2,p} - T_{cu,in,p} \tag{3-22}$$

For hot utilities: $\forall j \in CP, \forall p \in P$

$$Q_{j,p} = g_{j,p} \bullet cp_{j,p} \bullet \left(T_{j,0,p} - T_{j,1,p} \right) \tag{3-23}$$

$$\Delta T^{h}_{j,p} = \Delta T^{c}_{j,p} + LMTD_{j,p} \bullet \ln \frac{\Delta T^{h}_{j,p}}{\Delta T^{c}_{j,p}} \tag{3-24}$$

$$LMTD_{j,p} \le \frac{\Delta T^{h}_{j,p} + \Delta T^{c}_{j,p}}{2} \tag{3-25}$$

$$Q_{j,p} \le \frac{A_j \bullet LMTD_{j,p}}{U_{j,p}} \tag{3-26}$$

$$\Delta T_{j,p}^{h} = T_{huj,in,p} - T_{j,0,p} \tag{3-27}$$

$$\Delta T_{j,p}^{c} = T_{huj,out,p} - T_{j,1,p} \tag{3-28}$$

For expressions (3-20) and (3-26), inequality equations are utilized to describe the heat transfer of the utilities throughout various operational periods. The inlet and outlet temperature of utility are fixed as an assumption of the model. However, in practice, when operating conditions change, the constant area of HE leads to a change in the outlet temperature, which adapts to the duty. Therefore, using equality equations will systematically result in an infeasible problem. In practice, these inequalities will allow the real outlet temperature of the utility to deviate from the expected value.

The minimum temperature difference ΔT_{min} is also set as constraints for the model with equations (3-29) ~ (3-32) to keep the heat transfer feasibility.

$$\Delta T_{i,st,j,p}^{h} \geq \Delta T_{min} \tag{3-29}$$

$$\Delta T_{i.st,j,p}^{c} \geq \Delta T_{min} \tag{3-30}$$

$$\Delta T_{i,p}^{h} \geq \Delta T_{min} \tag{3-31}$$

$$\Delta T_{j,p}^{h} \geq \Delta T_{min} \tag{3-32}$$

Feasibility constraints are set to guarantee the heat flow comes from hot stream to cold stream. Hot stream temperature should decrease over the stage st as in equation (3-33), and cold stream temperature is also lower in higher stage st as in equation (3-34).

$$T_{i,st,p} \geq T_{i,st+1,p} \tag{3-33}$$

$$T_{j,st,p} \geq T_{j,st+1,p} \tag{3-34}$$

HEN is a typical non-convex nonlinear problem, bounds setting for variables is critical to helping the solver reach a solution. All the HE and utility power variables will be set with upper bounds that are the maximum heat load of the stream in equations (3-35) ~ (3-37). The temperature bound is set according to the stream minimum or maximum temperature throughout the periods and minimum temperature difference in equations (3-38) ~ (3-41).

$$Q_{i,st,j,p} \in [0, max\{g_{i,p} gcp_{i,p} g(T_{i,1,p} - T_{i,ST+2,p}), m_{j,p} gcp_{j,p} g(T_{j,0,p} - T_{j,ST+1,p})\}] \tag{3-35}$$

$$Q_{i,p} \in [0, g_{i,p} \bullet cp_{i,p} \bullet (T_{i,1,p} - T_{i,ST+2,p})] \tag{3-36}$$

$$Q_{j,p} \in [0, m_{j,p} \bullet cp_{j,p} \bullet (T_{j,0,p} - T_{j,ST+1,p})] \tag{3-37}$$

$$T_{i,st,p}, T_{i,st,j,p}^{h} \in [min\{T_{j,ST+2,p} + \Delta T_{min}, \forall j \in J, \forall p \in P\}, max\{T_{i,1,p}, \forall i \in I, \forall p \in P\}] \tag{3-38}$$

$$T_{j,st,p}, T_{i,st,j,p}^{c} \in [min\{T_{j,ST+2,p}, \forall j \in J, \forall p \in P\}, max\{T_{i,1,p} - \Delta T_{min}, \forall i \in I, \forall p \in P\}] \tag{3-39}$$

$$m_{i,st,j,p}^{h}, f_{i,st,p} \in [0, g_{i,p}] \tag{3-40}$$

$$m_{i,st,j,p}^{c}, f_{j,st,p} \in [0, g_{j,p}] \tag{3-41}$$

In the end, the main objective to synthesize HEN is to minimize the TAC which is given as:

$$TAC = \varepsilon \bullet CA \bullet (\sum_i \sum_s \sum_j A_{i,st,j}^{\sigma} + \sum_i A_i^{\sigma} + \sum_j A_j^{\sigma}) + \varepsilon \bullet CF \bullet N_{exh} + CCU \bullet \sum_i \sum_p \varphi_p \bullet Q_{i,p} + CHU \bullet \sum_j \sum_p \varphi_p \bullet Q_{j,p} \quad (3\text{-}42)$$

The first term is the investment cost, which depends only on the HE area (CA and σ are coefficients). The second term is a fixed cost, which depends on the existence of a HE (CF is a coefficient), N_{exh} is the number of HEs including process HEs and utilities. Finally, the last two terms are operational cost where CCU and CHU are costs for cold utility and hot utility for a unit of energy consumption, ε is the annualized actualization factor to transform the fixed cost and area cost into yearly cost, φ refers to the period duration.

Relaxed model for initialization

The NLP model is still difficult to solve without suitable initial values due to the non-convex character. It is not just about the global optimization result but also whether they can converge or not. A relaxed model is developed by converting some complex constraints to simpler equations, and it is employed to provide an initial value for the NLP model. To do so, the LMTD is replaced by arithmetic average temperature, and area cost function has also been simplified. Therefore (3-43) takes over (3-13) and (3-14), (3-44) takes over (3-19) and (3-20), (3-45) takes over (3-24) and (3-25), and the objective equation (3-46) replaced by (3-42).

$$LMTD_{i,st,j,p} = \frac{\Delta T_{i,st,j,p}^{h} + \Delta T_{i,st,j,p}^{c}}{2} \quad (3\text{-}43)$$

$$LMTD_{i,p} = \frac{\Delta T_{i,p}^{h} + \Delta T_{i,p}^{c}}{2} \quad (3\text{-}44)$$

$$LMTD_{j,p} = \frac{\Delta T_{j,p}^{h} + \Delta T_{j,p}^{c}}{2} \quad (3\text{-}45)$$

$$TAC = \varepsilon \bullet CA \bullet (\sum_i \sum_s \sum_j A_{i,st,j} + \sum_i A_i + \sum_j A_j) + \varepsilon \bullet CF \bullet N_{exh} + CCU \bullet \sum_i \sum_p \varphi_p \bullet Q_{i,p} + CHU \bullet \sum_j \sum_p \varphi_p \bullet Q_{j,p} \quad (3\text{-}46)$$

3.2.2 Structural screening

It is unnecessary to iterate exactly all structures since some structures are equivalent, leading to the same cost and dynamic performance. Indeed, Fig 3.3 illustrates an example where all four structures are different in point of view of SWS, but they are the same network. Therefore, we propose a graph-based method to discard those equivalent structures by finding isomorphic structures, to decrease the calculation burden.

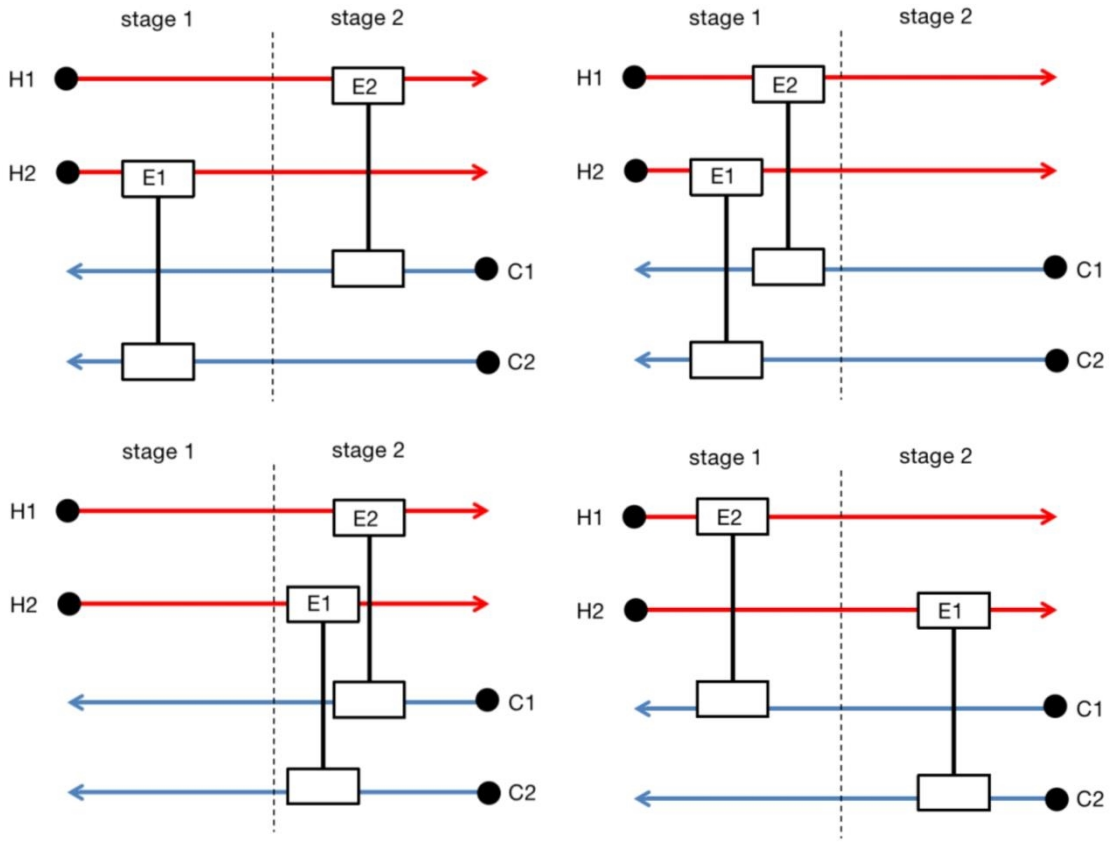

Fig 3.3. Example of equivalent HEN structures in different iterations

The graph is about node and directed edge for HEN, which is built from a HE basis as shown in Fig 3.4. For a hot stream i and cold stream j connected by a HE at stage st, with a bypass at the hot stream side. It includes six nodes of two types, one type is the stream stage node $(\mathrm{I}, \mathrm{st}), (\mathrm{I}, \mathrm{st}+1), (\mathrm{j}, \mathrm{st}), (\mathrm{j}, \mathrm{st}+1)$ and the other one is the HE node $(\mathrm{i}, \mathrm{st}, \mathrm{j}), (\mathrm{j}, \mathrm{st}, \mathrm{i})$ (represented by rectangles). In this example, all the declared edges are $<h_{i,st}, h_{i,st,j}>$, $<h_{i,st,j}, h_{i,st+1}>$, $<h_{i,st}, h_{i,st+1}>$, $<h_{i,st,j}, c_{i,st,j}>$, $<c_{i,st,j}, h_{i,st,j}>$, $<c_{j,st+1}, c_{i,st,j}>$, $<c_{i,st,j}, c_{j,st}>$ (represented by lines), where h and c stand for hot and cold nodes. After declaring all the nodes and directed edges for HEs, the directed graph of a specific HEN can be obtained.

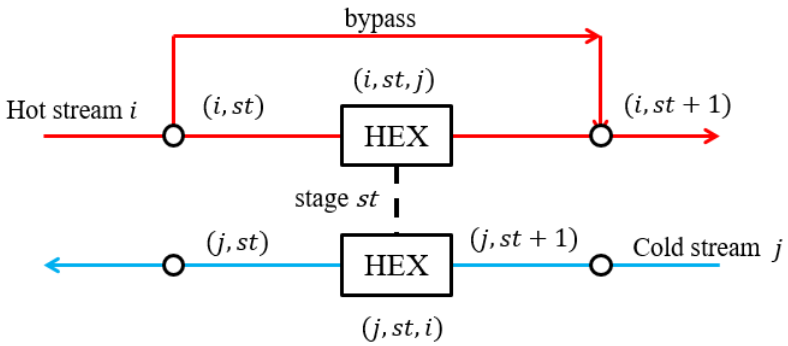

Fig 3.4. Graph representation for HE

The equivalent HEN structures are found by searching the isomorphic graphs. According to the definition of (Chartrand, 1984): *'when two graphs differ only in the way they are drawn and/or labeled, they are said to be isomorphic.'* The method to find the isomorphic structure from defined HEN graphs is based

on the VF2 algorithm. VF2 finds all the feasible mappings between two given graphs provided by (Cordella et al., 2001).

Before optimizing the NLP model of potential structures, each group of isomorphic structures will be found by the VF2 algorithm and keep the single structure for each group. Here, the group means those HENs contain the same number of HEs but connect different pairing of hot and cold streams.

3.2.3 Comparison of iterations with and without loop

Apart from screening out the isomorphic structures, there is another potential chance to discard a considerable part that structures with a loop. A loop is a cyclic path in a HEN that allows heat load shift among exchangers forming the cyclic path while maintaining an overall stream's enthalpy balance (Wan Alwi and Manan, 2010). Taking the HEN in Fig 3.5 as an example, E1, E3 form a loop where they are both exchanging heat with C1 but having E2 in between.

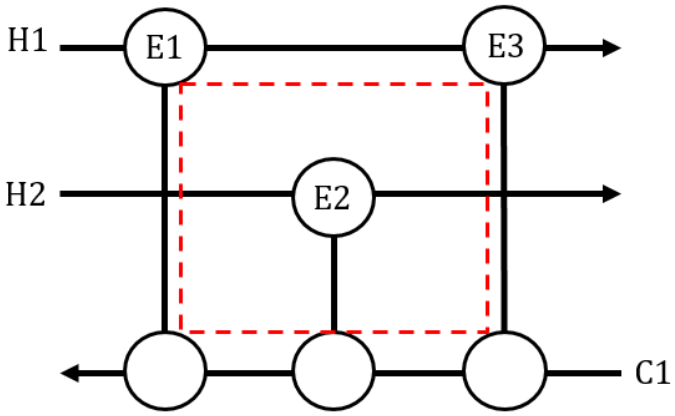

Fig 3.5. Example of HEN with loop

In the Pinch based HEN synthesis method, loop breaking is one of the many heuristics to reduce the number of HEs and lead to good economic performance (Bochenek and Je, 2001). In our context, loops are present in a high frequency during the iterations and correspond to a considerable part of computational time. After rejecting HENs with a loop, we have a high chance to reduce the iteration time but keep good economic performance at the same time. We will compare the iterative strategy by discarding HENs with a loop, and the one where these are not discarded.

It is easy to observe HENs with a loop manually, but we need a specific method to find it automatically during the iteration. The main idea is to check whether a node can find a pathway back to itself by following directed edges. The searching algorithm is provided by (Johnson, 2005) that aims to find all the elementary circuits of a directed graph within a limited time.

For comparing two strategies (with and without a loop), four small cases are used, and problem parameters are provided in Table 3.1. Even though the thesis focuses on multi-period HEN design, we plan to use both single and multiple period problems because that allows us to have a full picture of the comparison.

Table 3.1. Case study parameters

Stream	T_{in}(K)	T_{out}(K)	CP(kW/K)	h (kW/m^2•K)
Case 1				
H1	533	433	3.0	0.4
H2	523	403	1.5	0.4
C1	393	508	2.0	0.4
C2	453	513	4.0	0.4
HU	553	552	-	0.4
CU	303	353	-	0.4
Exchanger cost ($) = 300A$^{0.5}$ for all matches, CHU = 110 $/(kW•year), CCU = 12.2 $/(kW•year), $\varepsilon = 1$, $\Delta T_{min} = 1K$				
Case 2				
H1	423	323	200	0.2
H2	443	313	100	0.2
C1	323	398	300	0.2
C2	353	383	500	0.2
HU	453	453	-	0.2
CU	293	313	-	0.2
Exchanger cost ($) = 9094 + 211A$^{0.81}$ for all matches. CHU = 110 $/(kW•year), CCU = 10 $/(kW•year), $\varepsilon = 1$, $\Delta T_{min} = 1K$				
Case 3				
H1	428	303	8	2
H2	353	313	15	2
H3	473	313	15	2
C1	293	433	20	2
C2	293	373	15	2
HU	493	493	-	2
CU	303	353	-	2
Exchanger cost ($) = 6000 + 600A$^{0.85}$ for all matches. CHU = 120 $/(kW•year), CCU = 20 $/(kW•year), $\varepsilon = 1$, $\Delta T_{min} = 1K$				
Case 4				
Period 1				
H1	650	370	10	1
H2	590	370	20	1
C1	410	640	15	1
C2	350	500	13	1
Period 2				
H1	630	380	10.2	1.03
H2	570	340	20.5	1.04
C1	390	630	15	1.02
C2	340	520	13.5	1.05
Period 3				
H1	645	350	10	1.01
H2	600	350	20.3	1.04
C1	420	660	14.3	1.05
C2	320	540	13	1.03
HU	680	680	-	5
CU	300	320	-	1
Exchanger cost ($) = 4333A$^{0.6}$ for all matches. CHU = 150.163$/(kW•year), CCU = 53.064$/(kW•year), $\varepsilon = 1$, $\Delta T_{min} = 1K$				

We use the same optimization procedure based on the NLP model and method of discarding equivalent structures. The only difference between both iterations is to discard the structures with a loop or not. Case 1 (Khorasany and Fesanghary, 2009), case 2 (Aguitoni et al., 2018), and case 3 are single-period conditions (in our NLP model, the period parameter p is just set to 1 for these case studies). Case 4 is a typical two hot streams and two cold streams multi-period case, which has also been studied by (Da Jiang and Chuei-Tin Chang, 2013; Pavão et al., 2018; Miranda et al., 2016). All these cases are assumed to have two stages in the NLP model. The computer employed for the calculation is equipped with Intel Xeon (R) CPU 3.5GHz 32Gb. The NLP model is built under the Python environment with the pyomo package (Hart et al., 2011), and Baron 19.3.24 (Kılınç and Sahinidis, 2018) is taken as solvers.

In the following, the iterative NLP strategies with loop and without loop are termed as BINLP -1 and BINLP -2. For the optimization of the NLP model, we have set two termination constraints in the solving process to limit the whole calculation time. The first termination constraint is to stop the searching process when finding the first local optimum result. The second constraint is to terminate the searching process at 30s for each iteration even if the first local optimum result has not been found yet, and in that case we keep the best solution found. The comparison results are provided in Table 3.2, the optimal HENs of case 1, case 2, and case3 are provided in Fig 3.6 (a), (b) and (c), the optimal HEN of case 4 will be discussed in section 3.5. CPU time and TAC have been compared, and the deviation of the optimal TAC by the two approaches has been quantified. BINLP -1 and BINLP -2 reached to the same optimal TAC result with the same HEN design in case 2, case 3 and case 4 with less than half of the computational time after discarding the HENs with loop. In case 1, BINLP -2 exhibits 1.05% larger TAC than the result by BINLP -1 but also with much less calculation time (38.07%). Throughout these four cases, discarding the structures with a loop can help save the iteration time significantly but keep excellent TAC performance. This is the reason why the loop screening will be employed as a structure pre-selection strategy in our work. Therefore, BINLP -2 become the synthesis method that will be discussed in the followings, and termed as BINLP in the context.

Table 3.2. Comparison of BINLP -1 (iteration consider loop) and BINLP -2 (iteration without loop)

Case	Method	CPU time	TAC ($/year)
1	BINLP -1	662 s	11,832
	BINLP -2	252 s	11,956
	Difference	-61.93%	1.05%
2	BINLP -1	2,252 s	1,803,521
	BINLP -2	896 s	1,803,521
	Difference	-60.21%	0
3	BINLP -1	39,988 s	262,046
	BINLP -2	19,605 s	262,046
	Difference	-50.97%	0
4	BINLP -1	508 s	206,164
	BINLP -2	178 s	206,164
	Difference	-64.96%	0

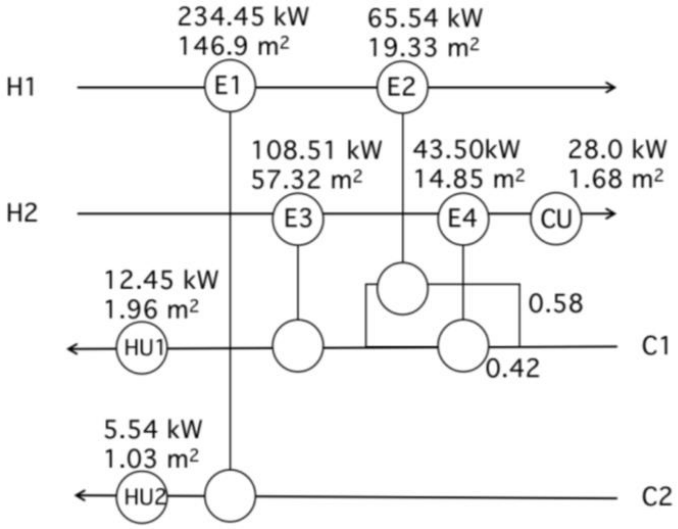

(a) case 1

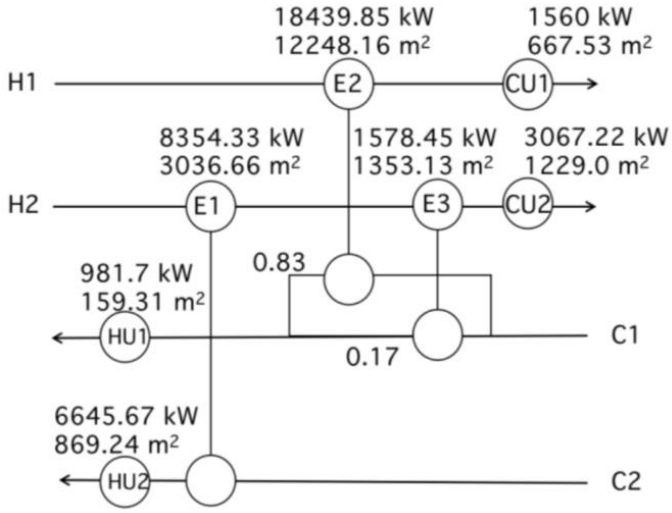

(b) case 2

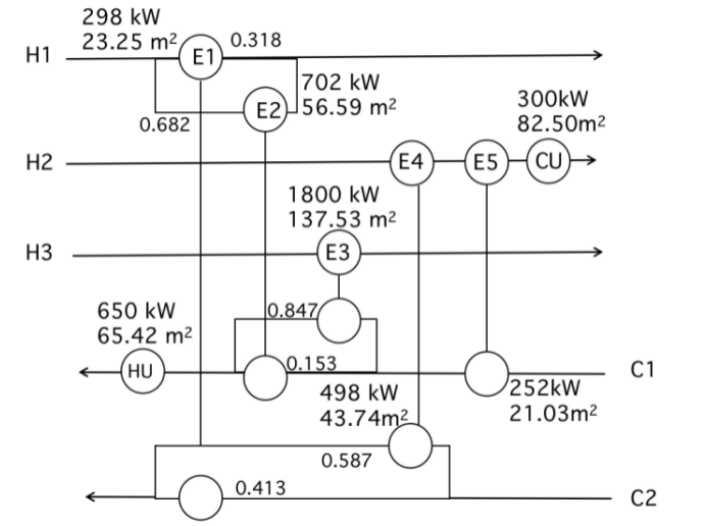

(c) case 3

Fig 3.6. The HENs with the lowest TAC of the comparison study (obtained by BINLP-1)

3.2.4 Comparison of MINLP and BINLP

BINLP aims to iterate all the potential structures with a screening procedure to discarding the equivalent structures and those with loops, while the MINLP approach has been a common solution to the HEN synthesis problem. However, the privilege of MINLP over iterative NLP strategy has not been confirmed in the literature yet. Carrying out a comparison study enables us to understand more clearly the pros and cons of different approaches.

In MINLP approach, $B_{i,st,j}$ is not a parameter (like in the NLP model) but a variable to be optimized. The MINLP model has most of the equations of the NLP model, and multiply the mass flow rate variables with (i, st, j, p) as indexes by the binary variable $B_{i,st,j}$ in corresponding equations (such as the equation (3-1) and (3-3)). Finally, the MINLP model is initialized in the same way as the NLP model does.

We employ the same case studies as in the above part, and the solving process of the NLP model keeps the same termination settings. The MINLP model solving process gets two scenarios: to stop at the 1st local optimal result for scenario 1, and stop at the same calculation time as BINLP method does for scenario 2. The results are summarized in Table 3.3. Comparing the BINLP and the MINLP scenario 1, we observe that the BINLP can find a better design with lower TAC in all case studies (the deviations range between 53 % and 165 %), but it takes longer calculation time. The MINLP scenario 1 performs poorly in these cases due to the used solving constraints, which stops the solver from finding more than one locally optimal solution, while the BINLP model gives more chance to reach a global optimal one by optimizing many different structures. Scenario 2 can help improving the performance of the MINLP approach, which is what we have observed in cases 2 and 4. However, the improvement is quite small in case 1, and in case 3, the two scenarios have provided the same solution despite a very high difference in calculation times. Compared to the BINLP, the MINLP scenario 2 has provided worse solutions in most cases (deviations ranging between 53 % and 154 %), except the case 4 where the found solution is slightly better (deviation of 2.12 %).

Table 3.3. Comparison of MINLP and BINLP approaches

Case	Method	CPU time	TAC ($/year)	Deviation (from the lowest TAC)
1	MINLP (1)	88 s	31,324	162 %
	MINLP (2)	252 s	30,071	152 %
	BINLP	252 s	11,956	0
2	MINLP (1)	13 s	4,052,345	125 %
	MINLP (2)	856 s	2,929,750	62 %
	BINLP	856 s	1,803,521	0
3	MINLP (1)	21 s	401,112	53 %
	MINLP (2)	19,605 s	401,112	53 %
	BINLP	19,605 s	262,046	0
4	MINLP (1)	37 s	536,639	165 %
	MINLP (2)	178 s	201,893	0
	BINLP	178 s	206,164	2.12 %

* The results correspond to scenario (1) "1st local optimal result" or feasible result within a given time, scenario (2) optimal result within the same time as the NLP approach

In section 3.2, we described the BINLP to synthesis HEN, which includes a structure pre-selection strategy to discard those unfavorable structures. The iterations that consider the HENs with a loop that has been compared with those discarding HENs with a loop through four case studies, and results show that the found optimized TAC are almost the same, but the calculation time saving is about 30%. Therefore, discarding HEN with a loop also serves as the structure pre-selection strategy and rejecting isomorphic structures. The BINLP method has been compared with the MINLP model based on the same four case studies as before, in which the BINLP method found the lower TAC design in three cases out of four, but also with quite longer iteration time. From these comparisons, it is concluded that the BINLP shows an excellent performance in terms of TAC and can be a way to be used in the synthesis work and future study. However, for a larger case study (more streams in the process), the current BINLP model may be not appropriate to be used because of the calculation time aspect, and this limitation will be discussed at the end of this chapter.

3.3 Transition time and HEN dynamic model

The synthesis strategy proposed in Fig 3.1 in section 3.2 provides a group of cost-optimized HENs, of which we get adequate information to calculate TT for these structures. This section will focus on the method to estimate TT for a given HEN. The TT calculation depends on the way to construct the dynamic model of HEN, and we need to select a proper approach that can be integrated into a design method or, in other words, an efficient and fast approach. At first, a review will be provided to decide how to build the HEN dynamic model, followed by the model description and validation.

3.3.1 Review of the study about HEN & HE dynamic performance

There are many efforts devoted to exploring HEN dynamic performance. In general, it can be classified in two ways: numerical simulation or analytical models. In the simulation approach, the objective is to use available numerical methods or simulation tools to solve the governing equations of the problem (mass and energy balances), while in the analytical approach the different variables of a HEN can be expressed by a function of the known parameters (such as heat transfer areas…) and the inlet information of the HEN (inlet flowrates and temperatures).

Papastratos et al. (1993) followed the simulation approach by utilizing the SpeedUp dynamic process simulator. Mathisen and Morari (1994) proposed the HEN dynamic model based on the lumped model for HE, with the main focus on the discussion about the model features for HE and HEN. As for the dynamic performance, their target is to avoid the control difficulty caused by the inverse response, and the dynamic result is obtained through MATLAB/Simulink. In their model, the number of cells describing the HE dynamic model determines the accuracy, and they provided a range to select this number. Their approach does not fit complex HEN structures because of the complexity, computational speed, and numerical stability, as argued by (Chen et al., 2018). Boyaci et al. (1996) constructed a HEN dynamic model based on a distributed-parameter model of multi-tubes, single-pass for HEs. They mainly focused on comparing HEN dynamic response under the scenarios of open-loop bypass control and closed-loop bypass control, and they employed the LSODES to solve their dynamic models. Similar researches to study HEN dynamic response under the effect of bypasses through the simulation are reported in (Hernández et al., 2010; Rathjens et al., 2016).

Until recently, Chen et al. (2018) provided an analytic method to study the transient behavior of HEN facing disturbance, which can be a promising method to achieve better control performance of HEN. In their work, the HE model was described with a first-order model, and the model enables engineers to obtain transfer function between any two nodes of HEN, which is a relatively convenient method to study HEN dynamic behavior. Nevertheless, their method aims to predict the system transient behavior facing quite small disturbances, which is not suitable for studying the operational change case.

Table 3.4 summarizes the comparison between the numerical simulation and analytical ways to reach the HEN dynamic performance. The numerical simulation approach can function well for most HEN conditions, but the high computational cost will be impractical to be applied in the design stage where the simulation is required for each of the potential structures. Indeed, the simulation of a specific change between certain operational periods requires a corresponding initial value setting (to help the numerical method converge). Such a setting will be required for all the iterative structures and throughout all the working periods. Comparatively, the analytical method might be a more promising way to study the dynamic performance of the HEN in the design problem. Developing an analytical solution may take time, but the computational cost to get the numerical results is expected to be lower than the simulation approach when the solution is known. Therefore, the TT calculation problem is transferred to the construction of the HEN dynamic model to obtain the outlet temperature function when there is an operational changeover. Besides, the HEN dynamic model ought to handle simultaneous temperature and mass flow change.

Table 3.4. Comparison of HEN dynamic model types

	Numerical simulation	Analytic
Pros	Complexity can be controlled by choosing the discretized cells number	Fast calculation without convergence problem
Cons	Convergence difficulty, initial value setting	Complex expression

The current available analytical method is not sufficient to undertake substantial inlet parameter change of a HEN. We can dig out the chance through the available analytical models of a single HE, the fundamental element of the HEN. Traditional analytical methods deal with Laplace transform over energy balance governing equations and end up with a rather complicated result just for HE (Gvozdenac, 2012), and it can hardly be extended to obtain the HEN outlet temperature. The main advantage of the traditional method is the capability to explore the temperature distribution inside the HE. Many authors adopted such a point to simplify the model by selecting the first-order model to approach the dynamic performance of the HE, and such choice originated from the observation of experimental results. But most studies only reported the single inlet parameter change condition (Lachi et al., 1997; Romie, 1999; Roetzel and Xuan, 1992), without discussing the possibility to explore the simultaneous change scenario. Yin and Jensen (2003) suggested the integral approach which extends from the work by (Reynolds and Dolton, 1959). They assumed that the first-order model could describe transient temperature, and stable temperature decided by the NTU method, without showing the potential to handle simultaneous parameter change scenario. The analytic model suggested by (Roetzel W. et al., 2002) is able to deal with arbitrary temperature change, the mass flow rate dependent parameters conditions, and the temperature distributions. However, their lumped HE dynamic model requires experimental or numerical simulations results to calibrate the corresponding parameters, which cannot be acceptable. Chen et al. (2018) tried to

study the simultaneous disturbance effect on outlet temperature by deriving potential gain and time constant toward various types of small disturbances based on the first-order transfer function originated from (Romie, 1984).

The comparison of HE analytical methods to study the dynamic performance is provided in Table 3.5. The targeted HE analytic model is expected to deal with simultaneous changes that can be both small and significant and be appropriate for any form of change in HE inlet. Laplace transform might be the most suitable approach to construct the HE dynamic model in our context, and we can try to explore a simplified method by ignoring the temperature distribution inside the HE.

Table 3.5. Summary of HE analytical models

	Method	Temperature distribution	Simultaneous changes	Minor or significant change	Parameter calibration
(Roetzel and Xuan, 1992)	First order transfer function	Yes	Yes	Minor	None
(Lachi et al., 1997)	Empirical exponential expression	No	No	Both	None
(Roetzel W. et al., 2002)	Laplace Transform	No	Yes	Both	Experimental /simulation
(Yin and Jensen, 2003)	Integral	Yes	No	Both	None

In what follows, we will introduce a simplified HE dynamic model at first, then provide the strategy to reach the HEN dynamic model.

3.3.2 HE dynamic model

Several assumptions are added to the assumptions made in part 3.1.2, which aim to simplify the dynamic model and apply it to all the discussed cases as follow:

- When there is an inlet variation, stream mass flow rate changes instantly (in other words, the change is in the form of the step function), and there is no time delay from the inlet port to the outlet port of the network because the fluid is supposed to be incompressible. The variation of the inlet temperature can take any form.
- Stream heat transfer coefficients keep constant during the transient phase.
- The temperature of the heat exchanger metal wall is uniform.

The HE model (depicted in Fig 3.7) is the basis to develop the HEN model. Here we assume the HE is counter-current flow configuration, which is coherent with most actual industry cases. The energy balance equations can be formulated as in equations (3-47) to (3-49) where the indexes h, c, wall, in, and

o stand for the hot stream, cold stream, HE metal wall, inlet, and outlet, respectively. M, c, CP, h and A stand for mass, heat capacity, heat capacity flow, heat transfer coefficient, and heat transfer area. It should be noted that the heat transfer is calculated via the arithmetic mean temperature difference (AMTD), which is an acceptable choice to simplify the model. GIREI (2015) also adopted the AMTD to study the operating issues of HEN in his doctoral thesis. This model provides the exact solution when the HE size is small enough. For a large HE, the error caused by the average temperature assumption will be quantified at the end of the section.

$$CP_h \bullet \left(T_{h,in}(t) - T_{h,o}(t)\right) = A_h \bullet h_h \bullet \left(\frac{T_{h,in}(t) + T_{h,o}(t)}{2} - T_{wall}(t)\right) \tag{3-47}$$

$$CP_c \bullet \left(T_{c,o}(t) - T_{c,in}(t)\right) = A_c \bullet h_c \bullet \left(T_{wall}(t) - \frac{T_{c,in}(t) + T_{c,o}(t)}{2}\right) \tag{3-48}$$

$$CP_h \bullet \left(T_{h,in}(t) - T_{h,o}(t)\right) = CP_c \bullet \left(T_{c,o}(t) - T_{c,in}(t)\right) + M_{wall} c_{wall} \bullet \frac{dT_{wall}(t)}{dt} \tag{3-49}$$

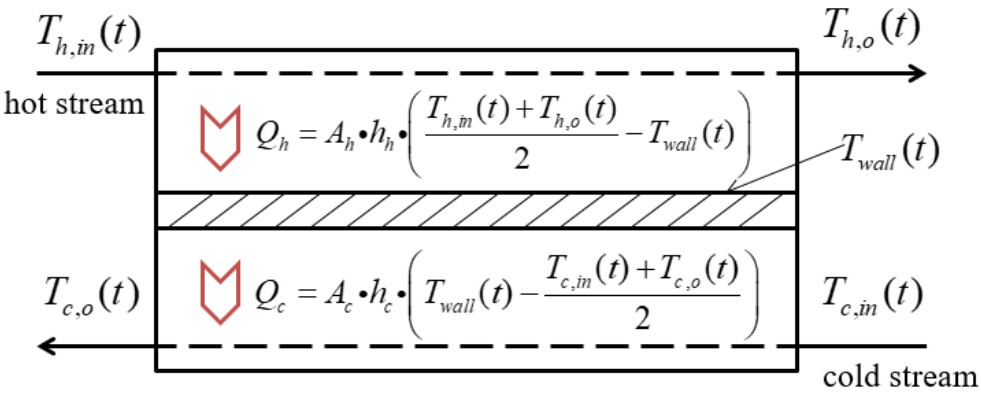

Fig 3.7. Simplified HE dynamic model

Expressing $T_{h,o}(t)$ and $T_{c,o}(t)$ with $T_{wall}(t)$, $T_{h,in}(t)$ and $T_{c,in}(t)$ by reformulating (3-47) and (3-48) we have:

$$T_{c,o}(t) = \frac{h_c \bullet A_c}{CP_c + \frac{h_c \bullet A_c}{2}} \bullet T_{wall}(t) + \frac{CP_c - \frac{h_c \bullet A_c}{2}}{CP_c + \frac{h_c \bullet A_c}{2}} \bullet T_{c,in}(t) \tag{3-50}$$

$$T_{h,o}(t) = \frac{h_h \bullet A_h}{CP_h + \frac{h_h \bullet A_h}{2}} \bullet T_{wall}(t) + \frac{CP_h - \frac{h_h \bullet A_h}{2}}{CP_h + \frac{h_h \bullet A_h}{2}} \bullet T_{h,in}(t) \tag{3-51}$$

Take (3-50) and (3-51) into (3-49) by seeking the relationship between $T_{wall}(t)$, $T_{h,in}(t)$ and $T_{c,in}(t)$, we can reach:

$$M_{wall}c_{wall}\bullet\frac{dT_{wall}(t)}{dt}+\frac{CP_h\bullet h_h\bullet A_h}{CP_h+\frac{h_h\bullet A_h}{2}}\bullet T_{wall}(t)+\frac{CP_c\bullet h_c\bullet A_c}{CP_c+\frac{h_c\bullet A_c}{2}}\bullet T_{wall}(t)$$
$$=\frac{CP_h\bullet h_h\bullet A_h}{CP_h+\frac{h_h\bullet A_h}{2}}\bullet T_{h,in}(t)+\frac{CP_c\bullet h_c\bullet A_c}{CP_c+\frac{h_c\bullet A_c}{2}}\bullet T_{c,in}(t) \quad (3\text{-}52)$$

The HE is expected to operate under various operational periods, heat capacity flow and inlet temperature will change at the period change time. When we look at the time after the period change, while the temperatures vary with time, the heat capacity flow rates can be regarded as constant because their variation follows the step functions. Taking Laplace transform over equation (3-52) just after the operation period change from period 1 to period 2, and we can have:

$$T_{wall}(s)=\frac{r_h\bullet T_{h,in}(s)+r_c\bullet T_{c,in}(s)+M_{wall}c_{wall}\bullet T_{wall}(0)}{M_{wall}c_{wall}\bullet s+r_h+r_c} \quad (3\text{-}53)$$

Where $r_h=\frac{CP_h\bullet h_h\bullet A_h}{CP_h+\frac{h_h\bullet A_h}{2}}$, $r_c=\frac{CP_c\bullet h_c\bullet A_c}{CP_c+\frac{h_c\bullet A_c}{2}}$, and all these parameters correspond to period 2. $T_{wall}(0)$ is the wall temperature at the time 0, and it is determined by the heat transfer coefficients together with the stream temperature before the operation period change (i.e. in the period 1, *p1*), and described as:

$$T_{wall}(0)=\left.\frac{h_h\bullet A_h\bullet(T_{h,in}(0)+T_{h,o}(0))+h_c\bullet A_c\bullet(T_{c,in}(0)+T_{c,o}(0))}{2(h_h\bullet A_h+h_c\bullet A_c)}\right|_{p1} \quad (3\text{-}54)$$

Taking Laplace transform over equations (3-50) and (3-51):

$$T_{c,o}(s)=x_c\bullet T_{wall}(s)+z_c\bullet T_{c,in}(s) \quad (3\text{-}55)$$

$$T_{h,o}(s)=x_h\bullet T_{wall}(s)+z_h\bullet T_{h,in}(s) \quad (3\text{-}56)$$

where, $x_h=\frac{h_h\bullet A_h}{CP_h+\frac{h_h\bullet A_h}{2}}$, $x_c=\frac{h_c\bullet A_c}{CP_c+\frac{h_c\bullet A_c}{2}}$, $z_c=\frac{CP_c-\frac{h_c\times A_c}{2}}{CP_c+\frac{h_c\times A_c}{2}}$ and $z_h=\frac{CP_h-\frac{h_h\bullet A_h}{2}}{CP_h+\frac{h_h\bullet A_h}{2}}$.

Finally taking (3-53) to (3-55) and (3-56), the outlet temperatures of the cold and hot streams can be obtained in Laplace form:

$$T_{c,o}(s)=(\beta_c\bullet r_c+z_c)\bullet T_{c,in}(s)+\beta_c\bullet r_h\bullet T_{h,in}(s)+\beta_c\bullet M_{wall}c_{wall}\bullet T_{wall}(0) \quad (3\text{-}57)$$

$$\beta_c=\frac{x_c}{M_{wall}c_{wall}\bullet s+r_h+r_c}$$

$$T_{h,o}(s)=(\beta_h\bullet r_h+z_h)\bullet T_{h,in}(s)+\beta_h\bullet r_c\bullet T_{c,in}(s)+\beta_h\bullet M_{wall}c_{wall}\bullet T_{wall}(0) \quad (3\text{-}58)$$

$$\beta_h=\frac{x_h}{M_{wall}c_{wall}\bullet s+r_h+r_c}$$

From equations (3-57) and (3-58), both the outlet temperatures of hot and cold sides are composed of hot and cold inlet temperatures and metal wall temperature with different coefficients. In the next section,

we will use the single HE model to get the outlet temperatures of a HEN in Laplace form, allowing afterward to get solutions in the time domain.

3.3.3 HEN dynamic model

When the system operation period changes, three types of inlet data will change: inlet temperature, inlet mass flow rate, and bypass ratio. Our objective is to calculate the outlets (temperature and mass flow rate) of the network as a function of the inlets, knowing the other parameters of HEN (for example, HE areas).

It is necessary to decompose the network into several components to obtain the HEN dynamic model. For simplification, in our HEN dynamic model, the pipe (in-between two components) is ignored (because its residence time is generally short compared to the temperature propagation time of the network). Hence, there are three common components to take into account.

1. Heat transfer happens in a HE between hot and cold streams;
2. Stream split when there is one (or more) HE and bypass for a stream in a specific stage;
3. Stream mixing after a stream split happens.

We need to identify the transfer functions of these processes. For the HE, it was already done in the previous section 3.3.2. For the stream split process, the temperatures of the sub-streams are considered the same as the parent stream, and when there is a change in the working period, the flowrates can reach to the desired values without delay.

To deal with the stream mix, take Fig 3.8 as an example when two branches of stream H1 are mixed. The mixing is adiabatic, equation (3-59) describes the energy balance, where m_1 and m_2 stand for mass flow ratio of two split streams.

$$T_{H1,mix}(t) = m_1(t) \bullet T_{H1,1}(t) + m_2(t) \bullet T_{H1,2}(t) \tag{3-59}$$

While the temperature of each split stream is a continuous function over time, the mass flow rate ratio of each split stream is a step function, and can be considered constant after the operation change (in other words, just after the change m_1 and m_2 do not depend on time). For these reasons, equation (3-59) can be transferred to (3-60) in Laplace form when the operation changes from period 1 to period 2. A Similar equation can be used when more than two streams mix.

$$T_{H1,mix}(s) = m_1 \bullet T_{H1,1}(s) + m_2 \bullet T_{H1,2}(s) \tag{3-60}$$

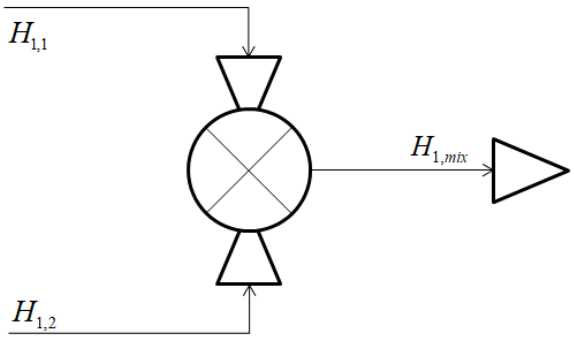

Fig 3.8. Stream mix in HEN

Following the presented component models (mixing, splitting, and HE), it is possible to determine the HEN outlets as a function of the inlet information and other parameters of the network. Indeed, the outlet

mass flow rate can be easily calculated because it is always equal to the inlet mass flow rate of the same stream. However, the outlet temperature calculation requires a specific method.

Because of the thermal propagation through the network, the inlet of a HE corresponds to the outlet of another HEs. In other words, to obtain the HEN outlet temperature, it is the consequence of the outlet temperature of all the relevant HEs calculation. Here, a method termed as one-by-one iteration is provided to obtain the outlet temperature of corresponding HEs and finally reach to target HEN outlet temperature.

One-by-one iteration

An example shown in Fig 3.9 is employed to illustrate the process to obtain the target HEN outlet temperature by obtaining the outlet temperature of corresponding HEs step by step, in which the outlet temperature of C2 is the target variable. Reminding the outlet temperature of a HE as in equations (3-57) and (3-58), it composes of three sources: the hot inlet stream, cold inlet stream, and thermal inertia part of the metal wall. The iteration goal is to find all the sources which affect the target variable. We start searching from the target variable as the procedure shown in Fig 3.10. The information to calculate the target $T_{c2,out}$ is incomplete since $T_{c2,2}$ is unknown, and $T_{c2,2}$ cannot be obtained directly because of $T_{h2,2}$ is an unknown variable, which is the hot outlet temperature of E1. The inlet information of E1 is also inadequate as $T_{c1,2}$ is to be calculated, $T_{c1,2}$ corresponds to the cold outlet temperature of E3 of which the inlet information is complete. Black rectangles represent all the sources that affect the target variable in Fig 3.10.

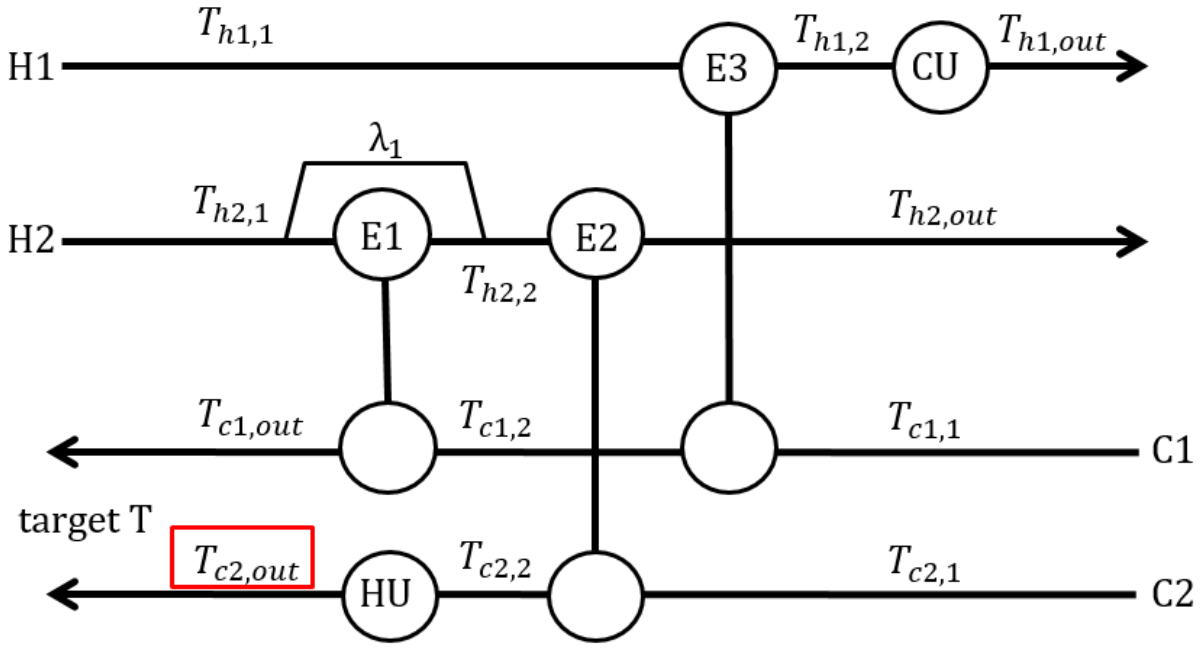

Fig 3.9. HEN example to obtain the outlet temperature function

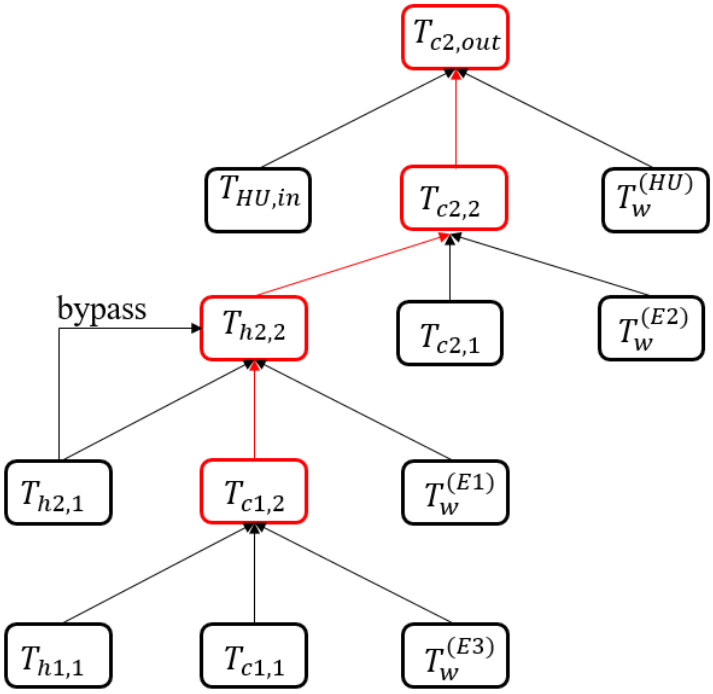

Fig 3.10. One-by-one iteration order to obtain the target variable

Analyzing the calculation steps in the Laplace domain, to get the analytic expression of the target variable, the calculation starts from the bottom of the diagram (Fig. 3.10). The starting step is to obtain the $T_{c1,2}$ as in the equation (3-61) by following the cold stream outlet temperature function as in (3-57). Then we can reach the $T_{h2,2}$ as in the equation (3-62) by following the hot stream outlet temperature function as in (3-58), and take care that there is a bypass from $T_{h2,1}$ to $T_{h2,2}$. Next, $T_{c2,2}$ can be calculated by following the cold stream outlet temperature function as in (3-57), and finally $T_{c2,out}$ can be reached as in the equation (3-64). The full expressions for corresponding variables are provided in the following equations.

$$T_{c1,2}(s)=(\beta_c\bullet r_c+z_c)_{E3}\bullet T_{c1,1}(s)+(\beta_c\bullet r_h)_{E3}\bullet T_{h1,1}(s)+(\beta_c\bullet M_{wall}c_{wall}\bullet T_{wall}(0))_{E3} \tag{3-61}$$

$$T_{h2,2}(s)=(\beta_h\bullet r_h+z_h)_{E1}\bullet(1-\lambda_1)\bullet T_{h2,1}(s)+\lambda_1\bullet T_{h2,1}(s)+(\beta_h\bullet r_c)_{E1}\bullet T_{c1,2}(s)+(\beta_h\bullet M_{wall}c_{wall}\bullet T_{wall}(0))_{E2} \tag{3-62}$$

$$=(\beta_h\bullet r_c)_{E1}\bullet\left((\beta_c\bullet r_c+y_c)_{E3}\bullet T_{c1,1}(s)+(\beta_c\bullet r_h)_{E3}\bullet T_{h1,1}(s)+\left(\beta_c\bullet M_{wall}c_{wall}\bullet T_{wall}(0)\right)_{E3}\right)$$

$$+(\beta_h\bullet r_h+z_h)_{E1}\bullet(1-\lambda_1)\bullet T_{h2,1}(s)+\lambda_1\bullet T_{h2,1}(s)+(\beta_h\bullet M_{wall}c_{wall}\bullet T_{wall}(0))_{E2}$$

$$T_{c2,2}(s)=(\beta_c\bullet r_c+y_c)_{E1}\bullet T_{c2,1}(s)+(\beta_c\bullet r_h)_{E1}\bullet T_{h2,2}(s)+(\beta_c\bullet M_{wall}c_{wall}\bullet T_{wall}(0))_{E1} \tag{3-63}$$

$$=(\beta_c\bullet r_c+z_h)_{E1}\bullet T_{c2,1}(s)+(\beta_c\bullet M_{wall}c_{wall}\bullet T_{wall}(0))_{E1}+$$

$$(\beta_c\bullet r_h)_{E1}\bullet\begin{pmatrix}(\beta_h\bullet r_c)_{E1}\bullet\left((\beta_c\bullet r_c+z_c)_{E3}\bullet T_{c1,1}(s)+(\beta_c\bullet r_h)_{E3}\bullet T_{h1,1}(s)+\left(\beta_c\bullet M_{wall}c_{wall}\bullet T_{wall}(0)\right)_{E3}\right)\\+(\beta_h\bullet r_h+z_h)_{E1}\bullet(1-\lambda_1)\bullet T_{h2,1}(s)+\lambda_1\bullet T_{h2,1}(s)+(\beta_h\bullet M_{wall}c_{wall}\bullet T_{wall}(0))_{E2}\end{pmatrix}$$

$$T_{c2,out}(s)=(\beta_c\bullet r_c+z_c)_{HU}\bullet T_{c2,2}(s)+(\beta_c\bullet r_h)_{HU}\bullet T_{HU,in}(s)+(\beta_c\bullet M_{wall}c_{wall}\bullet T_{wall}(0))_{HU} \tag{3-64}$$

$$=(\beta_c\bullet r_h)_{HU}\bullet T_{HU,in}(s)+(\beta_c\bullet M_{wall}c_{wall}\bullet T_{wall}(0))_{HU}+$$

$$(\beta_c\bullet r_h)_{HU}\bullet\begin{pmatrix}(\beta_c\bullet r_c+y_c)_{E1}\bullet T_{c2,1}(s)+(\beta_c\bullet M_{wall}c_{wall}\bullet T_{wall}(0))_{E1}+\\(\beta_c\bullet r_h)_{E1}\bullet\begin{pmatrix}(\beta_h\bullet r_c)_{E1}\bullet\left((\beta_c\bullet r_c+y_c)_{E3}\bullet T_{c1,1}(s)+(\beta_c\bullet r_h)_{E3}\bullet T_{h1,1}(s)+\left(\beta_c\bullet M_{wall}c_{wall}\bullet T_{wall}(0)\right)_{E3}\right)\\+(\beta_h\bullet r_h+y_h)_{E1}\bullet(1-\lambda_1)\bullet T_{h2,1}(s)+\lambda_1\bullet T_{h2,1}(s)+(\beta_h\bullet M_{wall}c_{wall}\bullet T_{wall}(0))_{E2}\end{pmatrix}\end{pmatrix}$$

Carrying out the calculation sequentially allows us to get the outlet temperatures of the HEN in the Laplace domain. The final HEN outlet temperature in time function requires carrying out the inverse Laplace transform. It should be noted that the one-by-one iteration method can be used only in the case where the network does not have a loop. In the case with loop, solving a system of linear equations is necessary to get the expression of the target variable, but it is out of concern of the thesis because we do not consider HEN with loop in our method of design (see part 3.2.3).

3.3.4 Validation of the HEN dynamic model

3.3.4.1 Validation of the solving method based on Laplace transform

Dymola is employed to validate the dynamic HEN model. It is based on the Modelica language, which is quite a commonly used tool in energy system modeling (Arce et al., 2018). To build the reference model in Dymola, we apply the equations (3-47) ~ (3-49) to model the HE and use the Modelica standard library for the other components (splitting and mixing processes). The dynamic HEN model is implemented in Python, and the inverse Laplace transform is done through the sympy module in Python.

A structure from case 4 in part 3.2.3 is taken as an example, illustrated in Fig 3.11. H1 outlet temperature is the target variable, and three conditions will be tested: inlet temperature change, mass flow rate change, and simultaneous change (full data provided in Table 3.6).

Carrying out the calculation by following the above described HEN dynamic model, we can reach the HEN outlet temperature function in three change conditions as given in equations (3-65) ~ (3-67), t stands for the time with seconds as a unit.

only inlet temperature change:

$$T_{h1,out}(t) = 355.5359 + 49.4715e^{(-0.0131t)} + 53.1702e^{(-0.0060t)} - 101.0873e^{(-0.0099t)} + 6.8577e^{(-0.0379t)} \quad (3\text{-}65)$$

only inlet mass flowrate change:

$$T_{h1,out}(t) = 382.8465 - 3.8568e^{(-0.0130t)} - 22.9203e^{(-0.0060t)} + 13.5898e^{(-0.0098t)} - 5.7113e^{(-0.0384t)} \quad (3\text{-}66)$$

simultaneous change:

$$T_{h1,out}(t) = 348.8855 + 87.9754e^{(-0.0130t)} + 90.7794e^{(-0.0060t)} - 176.1995e^{(-0.0098t)} + 12.5071e^{(-0.0384t)} \quad (3\text{-}67)$$

The dynamic response comparison results toward the inlet parameters change are illustrated in Fig 3.12. The solid lines represent the outlet temperature of H1 facing inlet temperature changes as with time, and the dashed lines depict the difference between the dynamic model result and the Dymola simulation result. The differences are rather small, which are within 0.008K throughout all three conditions. The differences are caused by the selected significant numbers. Thus, we believe that the HEN dynamic model is correctly implemented. The proposed solving method based on Laplace transform runs well, both for single change and simultaneous change.

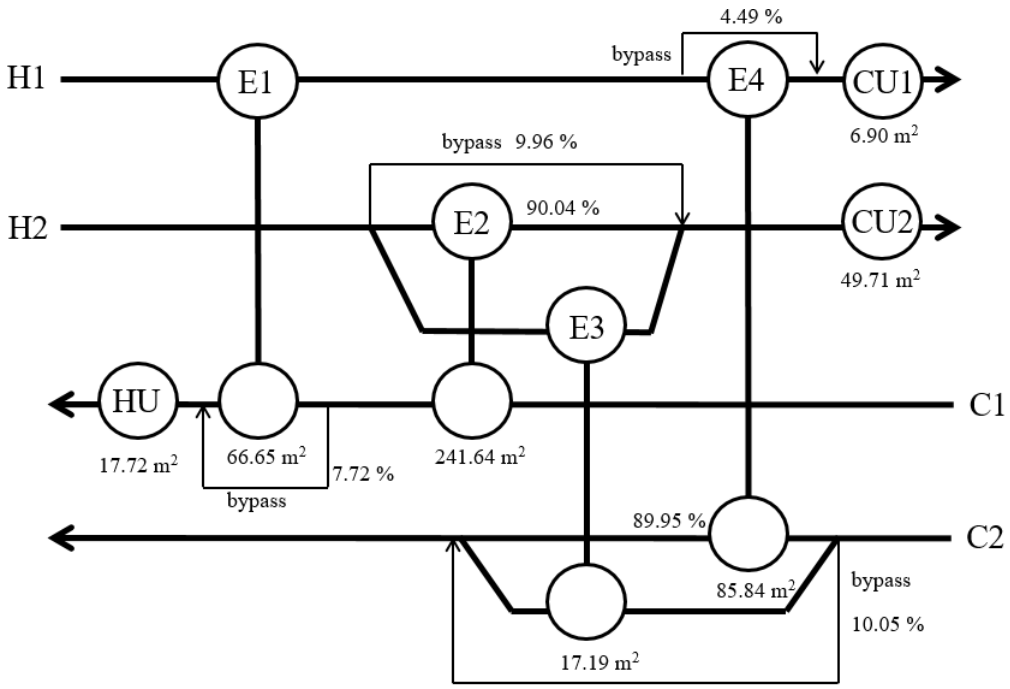

Fig 3.11. HEN example to validate the dynamic model

Table 3.6. Conditions to validate the implementation of the dynamic model

	Value	Signal
Inlet temperature change	H1:650K to 630K H2: 590K to 570K C1: 410K to 390K C2: 350K to 340K	Step
Mass flow rate change (or heat capacity flow)	H1: 10 kW/K to 11 kW/K H2: 20 kW/K to 22 kW/K C1: 15 kW/K to 13.5 kW/K C2: 13 kW/K to 11.7 kW/K	Step
Simultaneous change	Temperature & mass changes at the same time as above data	Step

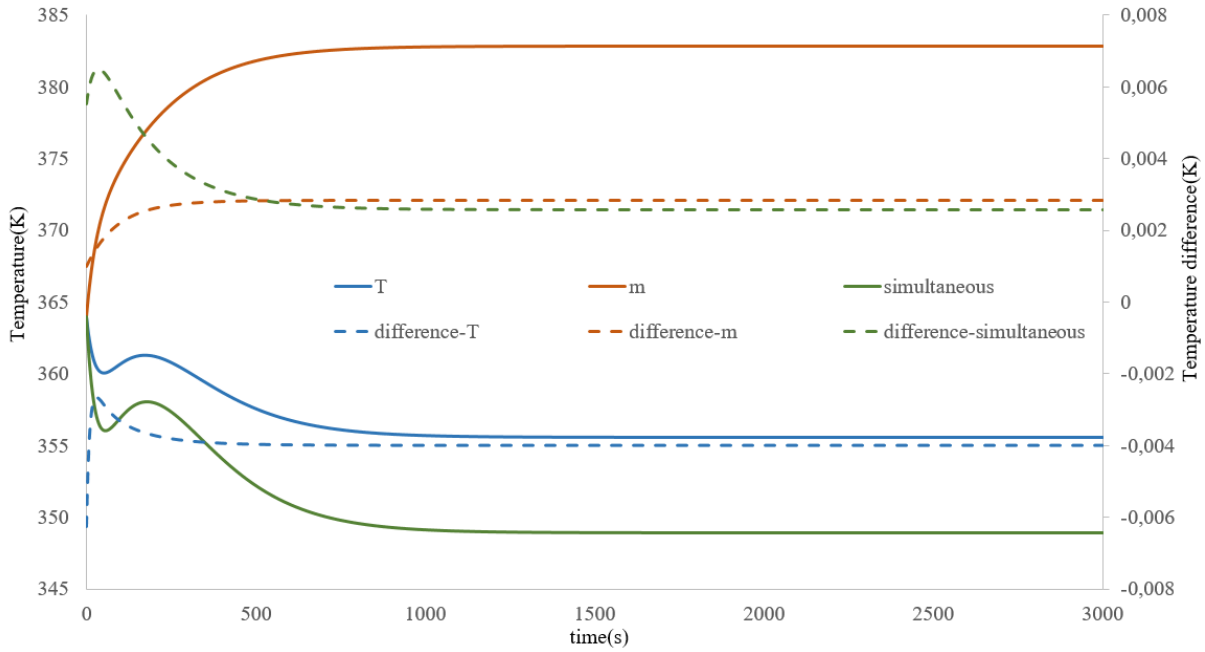

Fig 3.12. The H1 outlet temperature response toward various inlet change

3.3.4.2 Errors of the dynamic models

Reminding that we employed the arithmetic average temperature to describe the heat transfer process, it is an acceptable strategy to simplify the model as an approach in the dynamic study (GIREI, 2015). However, it will cause a certain error, which depends on the parameters. Therefore, we need to check the error level by comparing it with the real result. HE is the basis of HEN, the accuracy of the HE decides the accuracy of the HEN. In this section, we will test the error of the model in two levels: the HE and the HEN separately, and select an appropriate number of cells to discretize the HE to approach the real results that can be utilized in further validation work.

Validation of the HE model

It should be noted that, for the sake of simplification, the model bases on the AMTD to describe the heat transfer process, which causes some errors compared to the LMTD formulation in the steady-state condition. The error is quantified in Fig 3.13 as a function of the temperature differences at two sides of HE. Delta_T_left and Delta_T_right describe the temperature differences of the hot and cold streams in the two sides of the HE separately. The error is small when the two temperature differences are close, while it can be up to 20% when the difference between Delta_T_left and Delta_T_right is about 50K, and increase rapidly as the difference goes up.

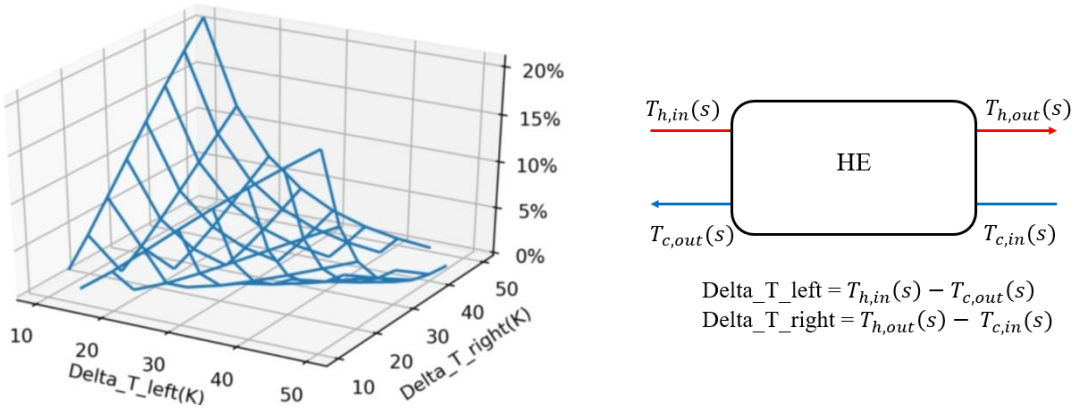

Fig 3.13. The difference between AMTD and LMTD

Discretizing the HE into many small cells is a common method to approach the real condition. The larger the number of the cells, the closer to the real condition. Implementing the HEN dynamic model will be rather inconvenient when having a large number to discretize the HE, so we can choose a reasonable number by increasing it gradually and comparing the progress. It is difficult to quantify the dynamic performance error generally, but we can know the degree of the deviation through a case study. The HE E1 in Fig 3.11 is selected as an example to quantify the error, the heat exchanger area, heat transfer coefficients, and capacity flow, all of which are the same as in the above case study, except there is no bypass in the cold side of the HEN, and corresponding parameters are provided in Table 3.7. We select 1, 2, 4, 8, 16, and 32 different numbers of cells to discretize the HE, expecting to obtain two objectives. The first one is to quantify the bias of HE dynamic model by comparing it with the near real result. The other is to check the progress of the accuracy and choose a suitable number to construct the HEN model in Dymola to act as the reference to quantify the error of HEN dynamic model.

The dynamic responses of H1 outlet temperature are depicted in Fig 3.14. From the observation, all these six curves evolve in the same trend. In terms of the temperature difference, 2 cells based model made substantial progress than 1 cell, and a step further with 4 cells based model. However, the progress from 8 cells is quite little, and the lines of 16 cells and 32 cells almost overlap. The temperature difference can be quantified with mean average error (MAE) and mean average percent error (MAPE) as described in equations (3-68) and (3-69), in which 32 cells based results can be taken as reference. Where y_i is the current value, y_i^o is the reference value, and n stands for the total number of points within the duration of TT.

$$MAE = \frac{\sum_{i}^{n} \left| y_i - y_i^o \right|}{n} \tag{3-68}$$

$$MAPE = \frac{\sum_{i}^{n} \left| y_i - y_i^o \right| / y_i}{n} * 100\% \tag{3-69}$$

The error of MAE and MAPE is essential to understand the potential error, but the dynamic response difference is quantified by the TT. Using the obtained outlet temperature function in the time domain, or simulation result. The TT is calculated by following the idea shown in Fig 1.7 in Chapter 1 with the

tolerance of 0.1% of the final stable value (in K). Therefore, TT, together with MAE and MAPE, are provided in Table 3.8. Compared with the 32 cells based model, the MAE shows about 5 K error of the HE dynamic model in this case study, and MAPE corresponds to about 1.18%. In terms of time response, TT gets about 25.80% error, which can be acceptable in this study, and we will discuss it in detail in HEN dynamic result validation part. Checking the accuracy progress when increasing the number of cells for the model, 4 cells based model exhibits quite small error (<0.7%) both in MAPE and TT, we will take it to build HEN dynamic model in Dymola to obtain the reference result.

Table 3.7. HE parameters to validate the accuracy

	Inlet temperature (K)	Heat capacity flow (kW/K)	Heat transfer coefficient (kW/m^2•K)
H1	650 to 630	10	1
C1	410 to 390	15	1

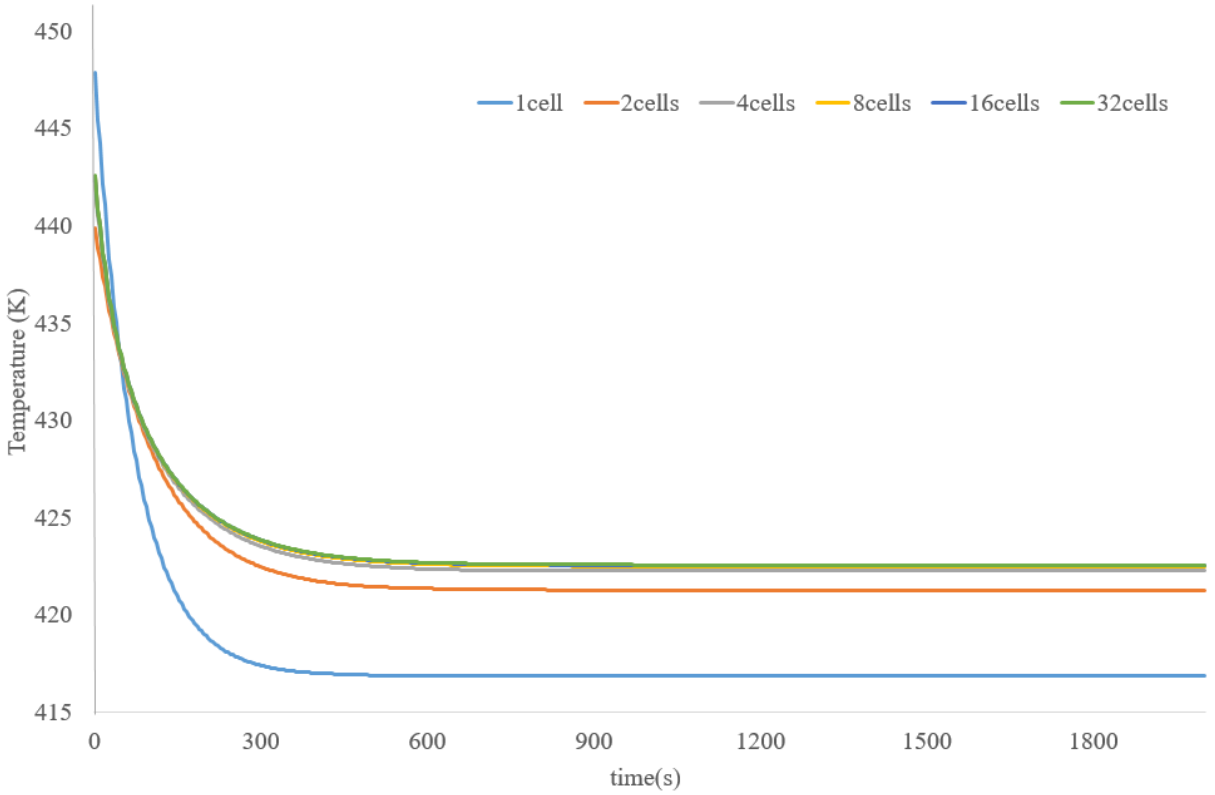

Fig 3.14. Dynamic response of hot outlet temperature under various number of cells

Table 3.8. Comparisons of various number of cells models

	MAE (K)	MAPE	TT(s)
1 cell	4.729	1.11%	325
2 cells	1.365	0.32%	410
4 cells	0.248	0.06%	435
8 cells	0.058	0.01%	438
16 cells	0.013	0	438
32 cells	-	-	438

Validation of HEN model

The HEN in Fig 3.11 is also used as an example here to compare HEN's dynamic performance by following the dynamic model and the real dynamic performance. The inlet parameter changing scenario is the same as in Table 3.6, inlet temperature and inlet mass flow rate is expected to change individually and simultaneously. The simulated dynamic performance will be obtained through Dymola simulation, in which the HEs are discretized into four cells by keeping the same governing equations for each cell, the heat transfer area and metal wall are divided into four parts evenly. Three parameter-changing scenarios will be compared: only temperature change, only mass flow rate change, and simultaneously change of temperature and mass flow. The comparison of dynamic response results, as provided in Fig 3.15. The solid lines represent the model-based result, and the dashed lines stand for the simulation result. We also utilize MAE, MAPE, and TT (0.1% tolerance as criteria, of final table value in K) to quantify the error, and the results are listed in Table 3.9.

The absolute difference is relatively small as MAE shows, and MAPE is under 0.6%, which is also acceptable. The most crucial criterion is TT's deviation, as we can observe obvious TT's difference between the model-based result and the real result. Under the inlet temperature change condition, the TT deviates about 13.61%, the simultaneous change condition deviates more with about 33%. Such deviation is acceptable in our context to compare the TT of various HENs in the design stage since the aim is to give a relative estimate of the TT change with configuration. This preliminary estimate should provide a ranking of the solutions for the TT criteria. We can increase the dynamic performance accuracy by discretizing the HE, but that will lead to a quite heavy dynamic model, which leads to significant numerical difficulty in obtaining the final result and cannot work effectively in the design stage. The dynamic model proposed in part 3.3.3 is based on a bold assumption that leads to a certain degree of error, but the error is within the tolerance range to complete the research target. It can be implemented in the HEN synthesis stage to measure the time response of various structures.

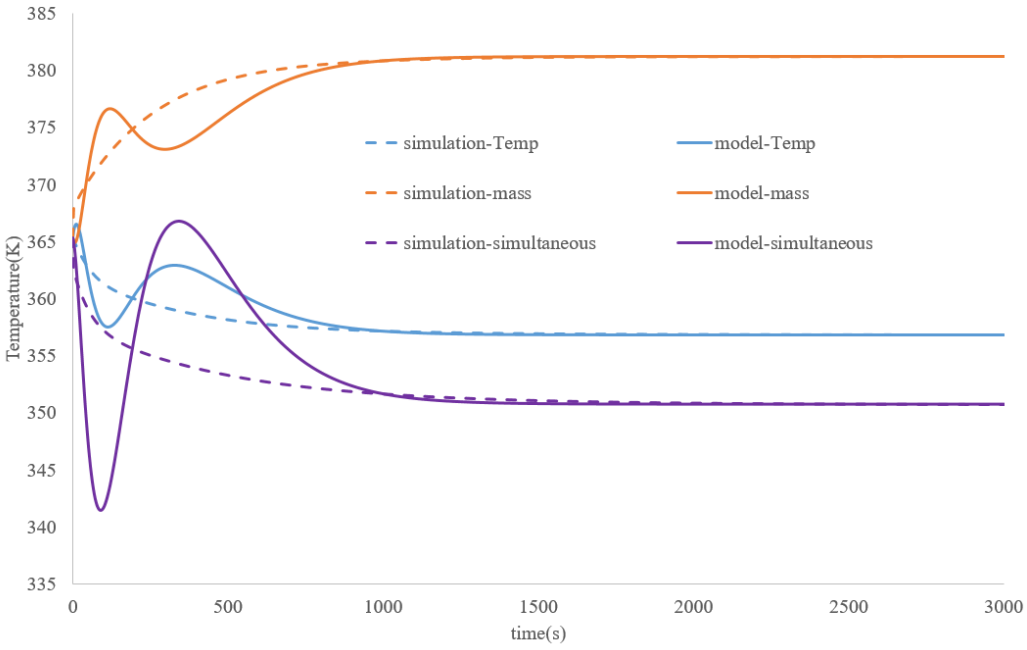

Fig 3.15. Validation of dynamic response by comparing the model result and simulation result

Table 3.9. Errors between the model result and simulation result

		MAE (K)	MAPE	TT(s)	Deviation of TT
Temperature change	Model	1.11	0.31%	838	13.61%
	Simulation	-	-	970	-
Mass flow rate change	Model	2.28	0.60%	692	30.94%
	Simulation	-	-	1002	-
Simultaneous change	Model	1.97	0.56%	949	33.07%
	Simulation	-	-	1418	-

In part 3.3, we built the HEN dynamic model based on the Laplace transform over the governing equations for HE and the proposed 'one-by-one' iteration strategy, in which the HE dynamic model assumed the arithmetic average temperature driving force to describe the heat transfer. The way to obtain the HEN dynamic model has been validated with the simulation result through a case study by testing the inlet temperature change, inlet mass flow rate change, and simultaneous change. The validation result illustrates quite good coherence. The accuracy of the dynamic model has been studied in both HE and HEN levels. The TT results get up to about 33% error compared with the simulation result (by discretizing the HE into small cells) when using the 0.1% deviation tolerance (of final stable value in K).

3.4 Case study for HEN synthesis considering transition time

To follow the synthesis methodology provided in Fig 3.1. The first process is to decide the potential structures to be optimized, then implementing the NLP optimizing process toward all the selected structures and then calculate the corresponding TT. Finally, the TAC-TT trade-offs result can be obtained. Case 4, in part 3.2.3, is employed as an example to test the synthesis method. The models were implemented in Python 3.6, the computer and solver information is given in part 3.2.3.

3.4.1 Optimal TAC design

For the lowest TAC, the algorithm finally reached a HEN with a capital cost of 206,164 $/year and equipped with four process HEs and three utilities with 499.06 m^2 heat transfer area in total. The final optimized HEN, together with operational parameters, is illustrated in Fig 3.16. All the streams are connected by process HEs, bypasses are installed in all the process HEs, and stream split exists in H2 and C2 in stage 2.

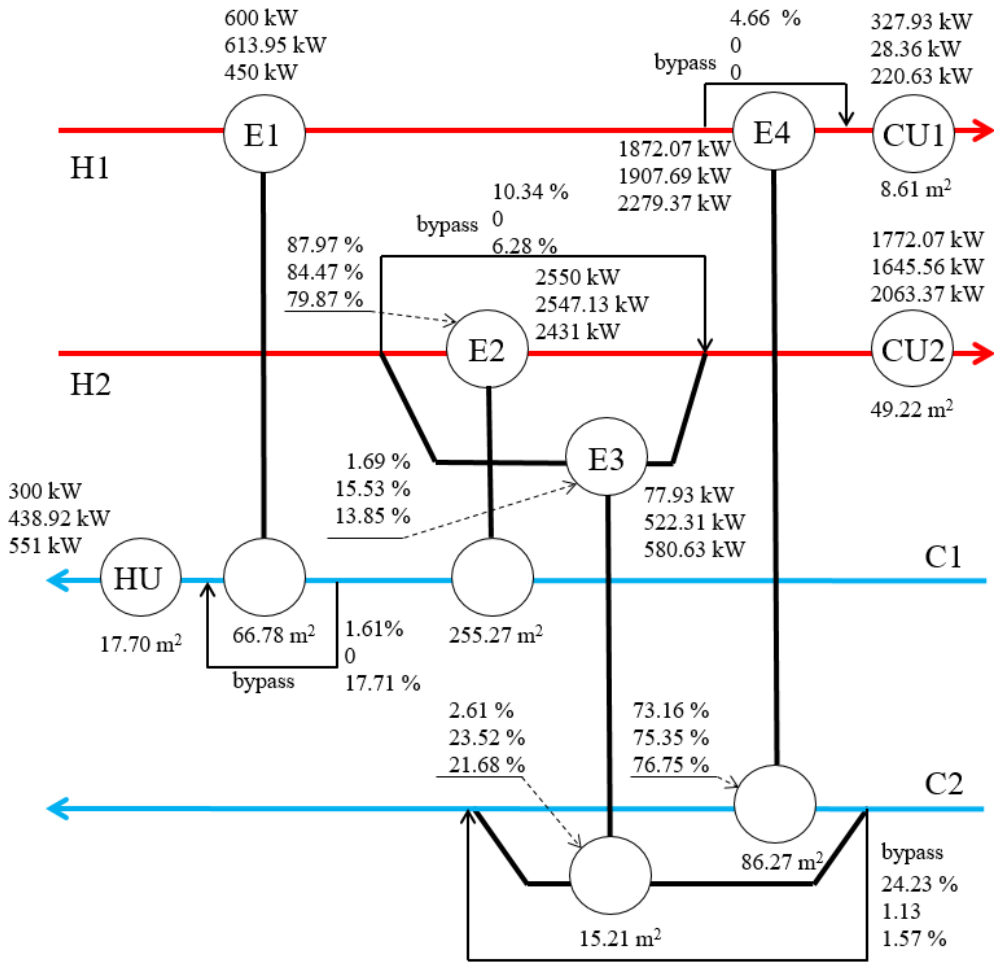

Fig 3.16. Optimized multi-period HEN with the best economic result (values for each period)

The comparison of the results from the literature is given in Table 3.10. Da Jiang and Chuei-Tin Chang (2013) studied the case with time-sharing mechanism and reached a final design with TAC as 205,283$/year. However, their result requires to be updated, because of violating the Second Law of Thermodynamics with the outlet temperature of hot stream 1 (472.6 K) is lower than the inlet temperature of cold stream 1 (560.0 K) for the HE (1,1,1). The other error is the ignorance of the stream mix in HE (2,2,2,), and the calculated area is not consistent with their given temperatures. These two aspects have also been pointed out by (Camila B Miranda et al., 2016). After revising their heat transfer area of HE (2,2,2) from 14.6 m^2 to 118.3 m^2, their final TAC should be 210,714 $/s, which is not as good as the solution found by our approach. Miranda et al. (2016) extended the time-sharing mechanism (Da Jiang and Chuei-Tin Chang, 2013) by adding heat transfer direction constraints and non-isothermal mixing with an MINLP model to design each period separately and then select the largest area. They reached quite a good result, but their strategy to replace the LMTD with Chen's approximation might make the final TAC not so accurate, it can be up to 7% error compared with LMTD as discussed in (Huang et al., 2012), so a post-optimization method is required for evaluating their solution. Then Pavão et al. (2018) proposed an MINLP model with a meta-heuristics method that deals with LMTD directly, and the same case study revealed much better TAC improvement. It seems that they utilized a smaller minimum temperature difference constraint which might contribute mainly to the TAC improvement. From Table 3.2 of their paper, one can deduce that the minimum temperature difference of the HE (p,1,1,1) is 1.6 K,

1.8 K, and 1.4 K respectively in 3 periods. Setting the minimum temperature difference to 1.8 K, the method of our work can provide a far much better solution. Our method can achieve lower TAC design because the method iterated all the potential structures and synthesis all operational periods simultaneously, which gets a higher chance to reach a global optimal point.

Table 3.10 also presents the calculation time for each method (the comparison must be treated with some caution because the values are directly reported from the original works with different processors and solvers). We can observe that the calculation time increases significantly when the LMTD formulation is used. In this case study, since the number of potential structures is not large, our method gives the optimal solution with a reasonable time. It should be noted that the iterated configurations are independent and defined clearly, which allows us to carry out the calculation in a parallel programming manner. Thus, calculation time can be largely cut down according to the number of cores and capability of computers.

Table 3.10. Results comparison (the values are reported from the original works)*

	Heat transfer	Units	Area (m^2)	CaC ($/year)	OC ($/year)	TAC ($/year)	CPU time
$\Delta T_{\min} = 10K$							
(Da Jiang and Chuei-Tin Chang, 2013)	Approximate	6	521	33,627	171,656	205,283	1 min 41s *
Corrected Jiang and Chang	Approximate	6	624	39, 058	171,656	210,714	-
(Camila B Miranda et al., 2016)	Approximate	6	498	33,202	171,656	204,858	< 1s *
This work	LMTD	7	499	33,983	171,656	206,164	8min 28s
$\Delta T_{\min} = 1.8K$							
(Pavão et al., 2018)	LMTD	7	738	45,937	147,988	193,925	3h49min *
This work	LMTD	7	584	38,254	147,082	185,336	2 min 11s

3.4.2 TAC-TT trade-off result

The dynamic model calculation requires information about the heat capacity of the HE metal wall, and we utilize the equation (3-70) to determine it. Even though it is a simplified correlation, it is acceptable for research purposes. (L. V Pavão et al., 2017) also adopted a similar equation.

$$M_{wall} c_{wall} = 40A \text{ (kW/K)} \tag{3-70}$$

The case study gets three operational periods, we choose to study the TT of all the hot streams when the system changes from period 3 to period1, there might be other operational changeovers, and the selection depends on the users or the operational requirements. The HEN TT takes the maximum TT among the sub-TT of H1 and H2, and the criteria to calculate TT is 0.1% of the final stable value in K. The method takes 8min28s to complete the HEN optimizing process and 5min56s to obtain the TT toward the optimized structures. The results of optimized cost and TT between operational periods are shown in Fig 3.17. It can be observed that the design with similar TAC can have a vast difference in TT performance. TT varies in a broad range, from 100s to 2,500s. Under such a considerable variation, the TT calculation model can still distinguish the structures that respond faster even though there is deviation compared with the real value shown in the validation part. From the results, we can also find that the sacrifice of TAC cannot guarantee a shorter TT, giving the chance to reach a HEN to meet economic and

time response requirements. The number of HEs does not reveal a clear relation with the time response in the resulting graph.

A pseudo-Pareto front can be fitted through the frontier of cost and TT dots as black line presents, and three representative HENs in the Pareto front are provided in Fig 3.18. HEN1 is the optimal TAC design that requires the largest TT (703s) among the three structures, it gets the same number of HEs as with HEN2, but the structure is more complex as we can see from the graph. There is no stream split happening in HEN2, and one more utility added compared with HEN1. HEN3 is free of process HE and only equipped with utilities, and it gets the fastest response throughout all the structures. By implementing the TT requirement, preferable design can be decided from the potential structures in the Pareto-front and trying to achieve a compromise between TAC and TT. For engineers working in the HEN synthesis field, the proposed method provides a trade-off choice to select preferable HEN design according to either cost or time response criteria.

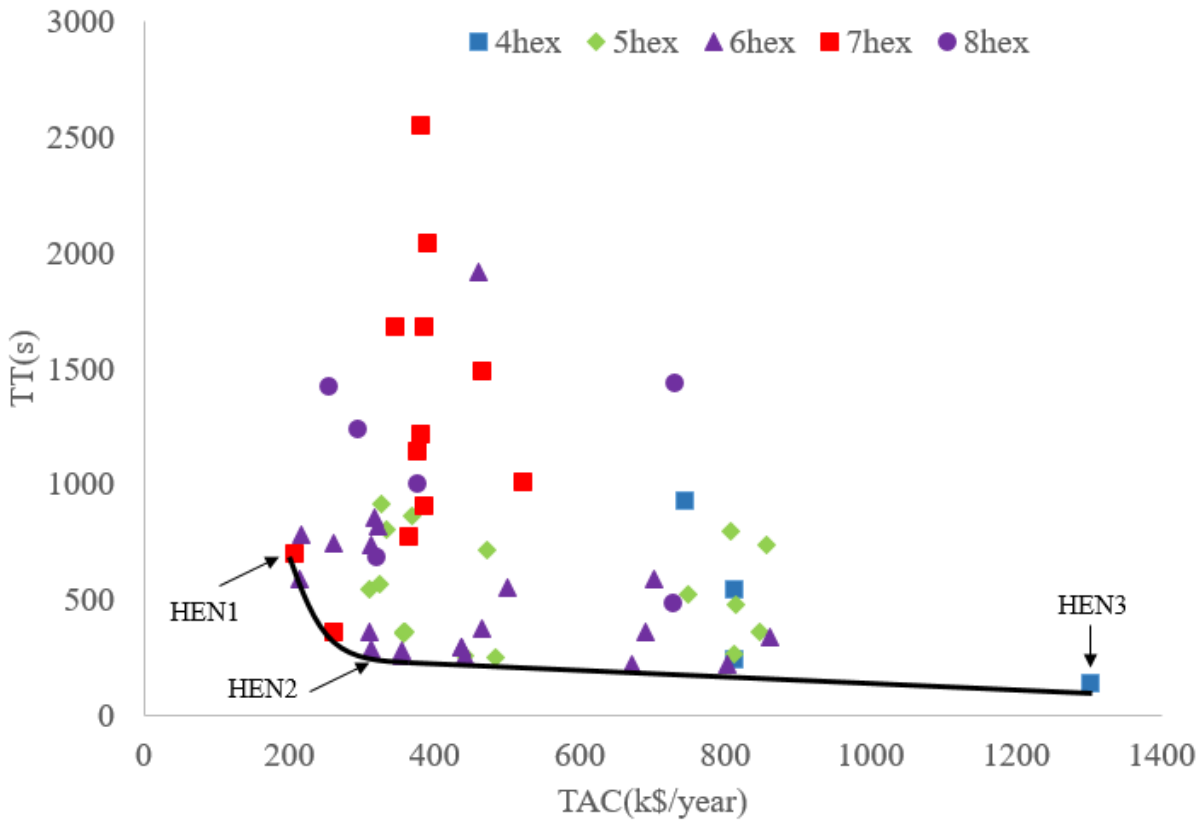

Fig 3.17. TAC-TT trade-off result

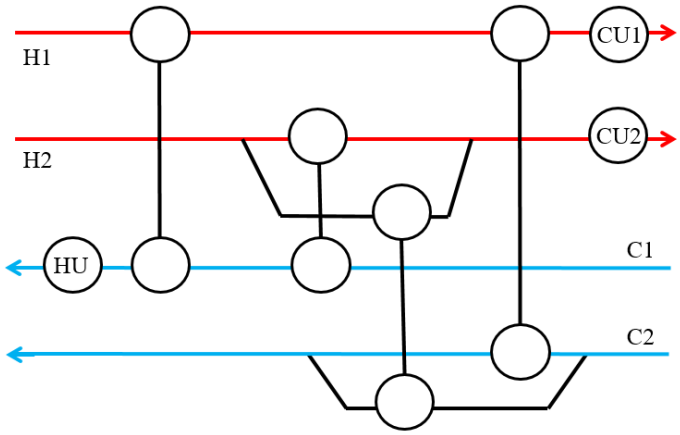

Cost = 206,164 $/year, TT = 703 s

(a) HEN1 (optimal TAC)

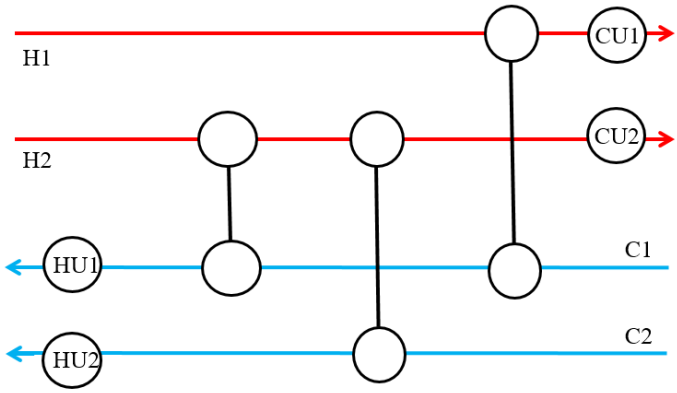

Cost = 313,658 $/year, TT = 290 s

(b) HEN2

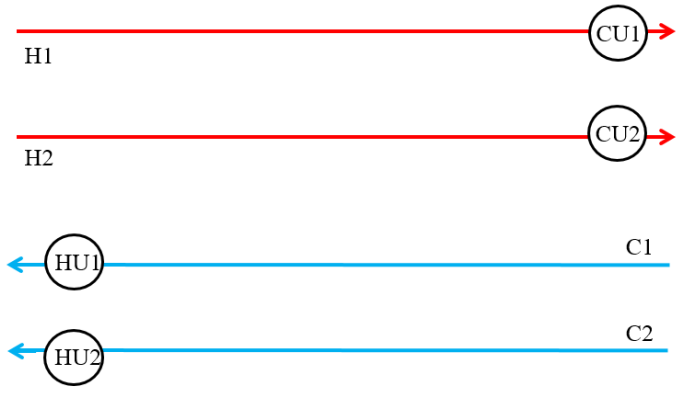

Cost = 1301,106 $/year, TT = 136 s

(c) HEN3

Fig 3.18. HEN designs in Pareto-front of the TAC-TT trade-off result (see Fig. 3.17)

3.4.3 Validation of the TT ranking

Since the TT calculation model described in part 3.3.3 gets a certain degree of deviation from the real result due to the simplification of the heat transfer model, it is better to validate the TT ranking predicted by the model for various HENs. Utilizing the same approach provided in part 3.3.4.2 enables us to obtain

a more precise simualted dynamic performance through discretizing the HE into small cells. We carried out the simulation in Dymola over the HEN1, HEN2, and HEN3 that are given in Fig 3.18, to obtain the outlet temperature of H1 and H2 when the HEN change from period 3 to period 1. The dynamic response of hot streams of these HENs is depicted in Fig 3.19. Applying 0.1% deviation (of final stable value in K) as the criteria to calculate the TT, the simulated TT result of these three HENs are provided in Table 3.11. Even though the deviation of the TT obtained by the model is evident compared to the simulated result, but the TT ranking it helps to define is still correct. HEN1 requires a longer time than HEN2 and HEN3 to transfer from period 3 to period 1, HEN3 is the fastest one. This confirms the effectiveness of the TT model, that it can act as a pre-selection tool in the design stage to help designers select those structures that can change faster. We also observe that the deviation of TT between the model result and the simulation result of HEN3 is larger than other structures. Which might be because HEN3 gets no process HE, all the heat transfer relies on the utility, and the heat capacity flow of the streams in the utility makes larger difference and magnify the error caused by the average temperature difference assumption.

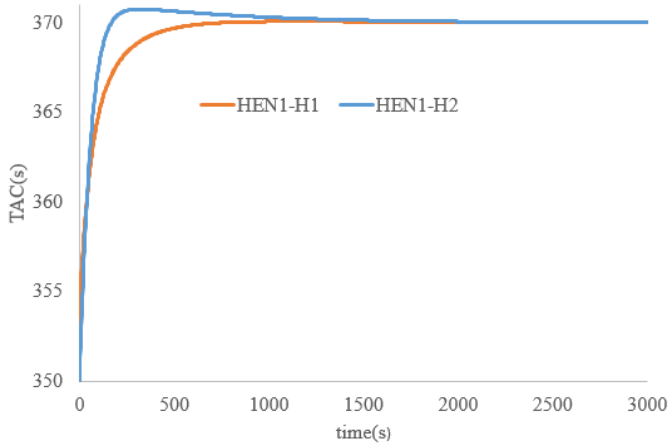

(a) HEN1

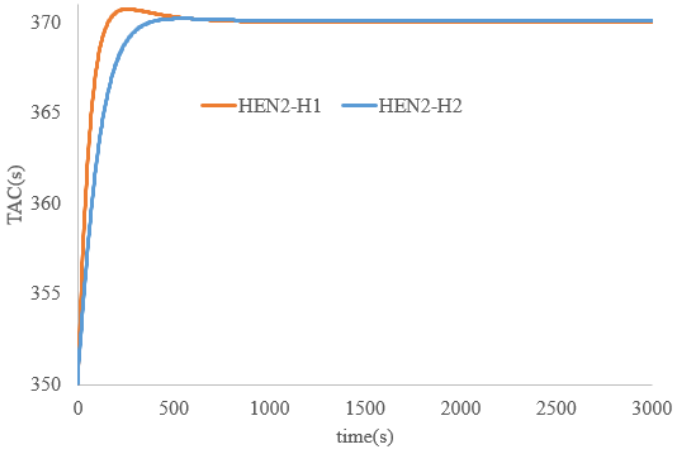

(b) HEN2

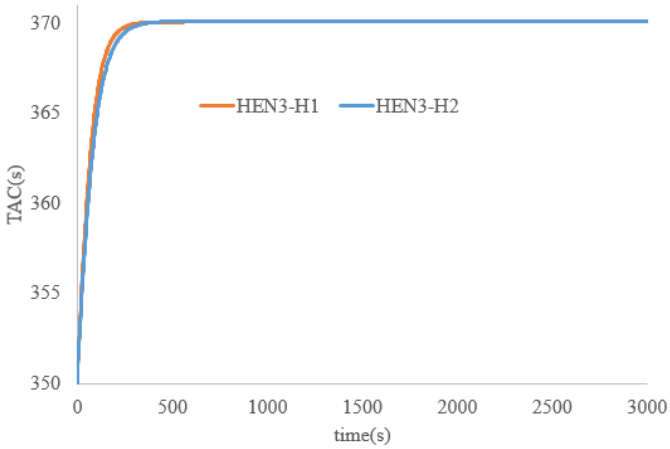

(c) HEN3

Fig 3.19. Dynamic response of HEN1, HEN2 and HEN3 with Dymola

Table 3.11. Simulated TT result of HEN1, HEN2 and HEN3

HEN	TT(simulated)	TT(model)
HEN1	688s	703s
HEN2	358s	290s
HEN3	61s	136s

3.5 Conclusion

In this chapter, we proposed the preliminary model to synthesize multi-period HEN that can consider TT in the design stage by the most basic iteration method in a sequential way, since the calculation of TT cannot be integrated into the commonly used synthesis models (such as MINLP). The synthesis model aims to iterate all the potential structures after discarding the isomorphic ones and structures with a loop, and the usual MINLP synthesis has been transformed into a series of NLP optimization problem. The proposed synthesis strategy is also termed as BINLP model. The iteration result that includes structures with a loop has been compared with the one without a loop, and it is found that the optimized TAC are the same for three out of the four cases and giving a very close result for the fourth case. The BINLP model has been compared with the MINLP approach in four small cases, with the process to discard isomorphic structures and structures with loop, the BINLP takes longer calculation time than MINLP, but is able to find a better TAC design in most of the case.

After validating the effectiveness of the BINLP synthesis approach in small problems, we moved to the core problem of the work to find a method to obtain the TT of each optimized HEN in the synthesis step. The simulation approach seems unsuitable for the design stage due to the extensive parameter setting work toward potential HENs. We tried to explore the chance by utilizing a HEN dynamic model, with the expectation that the dynamic model shall deal with simultaneous inlet information change and be appropriate for big variations in the working condition of the network. After reviewing the HEN dynamic studies, we found that there is no available model to be utilized efficiently, and we proposed to utilize an analytical approach to obtain the HEN outlet temperature and then calculate TT. We start from the development of a dynamic model of HE by employing the Laplace transform. To facilitate the analysis, we utilized the arithmetic average temperature driving force to describe the heat transfer process in HE.

Together with a one-by-one iteration method, the dynamic model of HE can be extended to HEN and obtain the HEN outlet temperature in the Laplace domain. Then TT can be calculated after carrying out the inverse Laplace process to reach the function in the time domain.

The methodology has been applied successfully in a case with four streams under three operational periods, which takes 8min28s to complete the HEN optimizing process and 5min56s to obtain the TT result. The optimized TAC is competitive compared with other studies, the TT varies a lot for various designs, ranging from 100s to 2,500s, and the lowest TAC design structure requires about 703s. The proposed methodology is proved to be efficient, and the case study also confirmed the necessity to study the TT in the design stage since various designs exhibit a vast difference in the time response aspect.

However, the method still gets some aspects to improve. The potential number of HEN structures increase exponentially as the synthesis problem scales up, and the corresponding iterations will be a huge number that cannot be acceptable even with pre-defined structure discarding processes. A more efficient iterative strategy is required to carry out the medium-large scale synthesis problem, and we are going to investigate the heuristics-based strategy. Another point to be handled in the following work is the TT calculation that relies on the inverse Laplace transform process. Indeed, the tools to carry out inverse Laplace transform might not work well, such as through MATLAB or the python package, since they can easily fail to reach a result with heavy expressions. Moreover, the difficulty increases as with the HEN scale increases because the outlet temperature function will be more complex. New strategies are required to make the proposed methodology more applicable to significant scale problems. These two points will be addressed in the next chapter.

Résumé du chapitre 4

Ce chapitre a amélioré deux points de la méthode préliminaire proposée au chapitre 3. Le premier est de fournir un modèle dynamique amélioré pour obtenir directement la température de sortie du HEN dans le domaine temporel sans se soucier de la transformation de Laplace inverse. Le second est une stratégie itérative de structure améliorée pour réduire le nombre d'itérations. Ces deux méthodes permettent à la méthodologie de conception proposée d'être réalisable dans des problèmes de synthèse à moyenne et grande échelle.

L'amélioration du modèle dynamique vise à décomposer la fonction de température cible en expressions simples dans le domaine de Laplace afin que leur fonction dans le domaine temporel puisse être obtenue directement en référençant la table de transformation de Laplace. Le modèle dynamique amélioré a été appliqué avec succès dans un HEN à 10 flux de la littérature qui fait face aux signaux d'entrée dans les conditions de signal de pas et de signal de rampe. Pour l'IINLP, il est né de l'idée Pinch, qui vise à trouver une conception rentable en manipulant la répartition de la charge thermique entre l'échangeur de chaleur de processus et les services publics. La stratégie a été validée contre SA dans trois problèmes de taille moyenne et grande. L'IINLP a pu trouver de meilleures conceptions de TAC dans les trois cas (TAC inférieur entre 0,03% et 42,8%). Les résultats du TT vont de 150 à 4500 dans le cas 1, de 3 000 à 5 000 dans le cas 2 et de 100 à 4500 dans le cas 3. Nous avons comparé les pseudo-fronts Pareto de l'IINLP et SA en trois essais et avons atteint le pseudo-front Pareto intégré pour les trois études de cas, et nous avons constaté que l'IINLP y contribue (7/11, 1/11, 10/12 in trois cas individuellement). Ni l'IINLP ni la SA ne peuvent dominer l'autre, et IINLP illustre une performance moyenne de SA en trois exécutions. En général, la méthode améliorée de synthèse multi-période HEN qui prend en compte la réponse temporelle peut fonctionner avec succès dans des problèmes de moyenne à grande échelle.

Chapter 4 – Improved HEN Dynamic Model and Synthesis Strategy

4.1 Introduction

In the last chapter, we proposed a preliminary method to measure transition time (TT) and integrate it into the HEN multi-period synthesis stage through the most basic iteration strategy (BINLP). It has been applied successfully in a four-stream case study but gets difficulties in applying in large scale synthesis problems with mainly two deficiencies. The first one is the BINLP requires enormous computation time as with the increase of the problem scale. Thus, we need to explore a more suitable iterative strategy for large scale problems. The second point is that the TT calculation model might need massive computational effort or even failed to work when reaching complex expressions. The proposed model relies on the inverse Laplace transform process to obtain the target temperature function in the time domain and then to obtain TT. However, the inverse Laplace transform process might fail to work when the HEN outlet temperature function in the Laplace domain tends to be rather heavy for a complex HEN. The difficulty is located in the limitation of tools to carry out the inverse Laplace process.

There exist many methods to compute numerically inverse Laplace transform, such as the Fourier series method, Schapery's method, Talbot method, and others, that can be found in Kuhlman (2013) review on the topic. Most popular calculating tools, such as MATLAB, Wolfram, or Python packages, all are based on these methods. It should be noted that, for any numerical method, it is required to provide some information or parameters to work, and correct results can be expected only when the provided information is close to an analytical solution (Craig et al., 1994).

The required information varies with the methods but generally relates to the Laplace function's singularities or poles. The approach presented and used in chapter 3 does not provide any information, which may lead to computational problems. The numerical difficulty was not reached in chapter 3 because the function is not complex enough. Our experience while using the common computing tools confirms this numerical issue: when the Laplace function is complex, the numerical methods are hard to converge or even get a solution and the answer may be completely wrong. To make the TT calculation model applicable in medium-large scale HEN problems, we need to find a way to avoid such an obstacle of carrying out inverse Laplace transform.

In this chapter, we start with the improved TT calculation part, then the improved iteration strategy. Both of the two improved parts are validated through three case studies, and then the TAC-TT trade-off result will be discussed in the end.

4.2 Improved HEN dynamic analytical model

Reminding the expressions of (3-64) in Chapter 3 as the outlet temperature function of cold stream C2 in the Laplace domain, it is rather complicated even when the HEN is equipped with only four streams and three process HEs. The expression can be much more complicated when the number of HEs increases and leads to massive numerical difficulty when carrying out inverse Laplace transform to obtain the expression in the time domain. To avoid such numerical problems and guarantee the successful application of the HEN dynamic model, we propose a method to directly reach the HEN outlet temperature by decomposing the target temperature function in a combination of simple expressions. The difference of this part compared with the method in Chapter 3 locates how to construct the HEN outlet

temperature function from the same heat exchanger (HE) dynamic model. First of all, we will reformulate the HE dynamic model, as shown in the next section.

4.2.1 Heat exchanger dynamic model: reformulation

We use the same HE dynamic model as provided in Part 3.3.2, and the equations (3-58), (3-57) are reformulated into (4-1), (4-6), where coefficient functions f and g are functions in Laplace domain. Such transformation aims to decompose the outlet temperature function into small parts of which the coefficients can share the same form that facilitates further analysis in the HEN level. After the reformulation, the outlet temperature function is composed of four parts. The coefficient functions are all in the form of $\frac{b}{s+a}$ or $const$ (where a, b and $const$ are known parameters), which are detailed in equations (4-2) to (4-5) and equations (4-7) to (4-10).

$$T_{h,o}(s) = f_{11} \bullet T_{h,in}(s) + f_{12} \bullet T_{h,in}(s) + f_2 \bullet T_{c,in}(s) + f_3 \bullet T_{wall}(0) \tag{4-1}$$

$$f_{11} = \frac{\dfrac{CP_h \bullet h_h \bullet A_h}{CP_h + \dfrac{h_h \bullet A_h}{2}} \bullet \dfrac{h_h \bullet A_h}{CP_h + \dfrac{h_h \bullet A_h}{2}}}{M_{wall} c_{wall} \bullet s + \dfrac{CP_h \bullet h_h \bullet A_h}{CP_h + \dfrac{h_h \bullet A_h}{2}} + \dfrac{CP_c \bullet h_c \bullet A_c}{CP_c + \dfrac{h_c \bullet A_c}{2}}} \tag{4-2}$$

$$f_{12} = \frac{CP_h - \dfrac{h_h \bullet A_h}{2}}{CP_h + \dfrac{h_h \bullet A_h}{2}} \tag{4-3}$$

$$f_2 = \frac{\dfrac{CP_c \bullet h_c \bullet A_c}{CP_c + \dfrac{h_c \bullet A_c}{2}} \bullet \dfrac{h_h \bullet A_h}{CP_h + \dfrac{h_h \bullet A_h}{2}}}{M_{wall} c_{wall} \bullet s + \dfrac{CP_h \bullet h_h \bullet A_h}{CP_h + \dfrac{h_h \bullet A_h}{2}} + \dfrac{CP_c \bullet h_c \bullet A_c}{CP_c + \dfrac{h_c \bullet A_c}{2}}} \tag{4-4}$$

$$f_3 = \frac{M_{wall} c_{wall} \bullet \dfrac{h_h \bullet A_h}{CP_h + \dfrac{h_h \bullet A_h}{2}}}{M_{wall} c_{wall} \bullet s + \dfrac{CP_h \bullet h_h \bullet A_h}{CP_h + \dfrac{h_h \bullet A_h}{2}} + \dfrac{CP_c \bullet h_c \bullet A_c}{CP_c + \dfrac{h_c \bullet A_c}{2}}} \tag{4-5}$$

$$T_{c,o}(s) = g_{11} \bullet T_{c,in}(s) + g_{12} \bullet T_{c,in}(s) + g_2 \bullet T_{h,in}(s) + g_3 \bullet T_{wall}(0) \tag{4-6}$$

$$g_{11} = \frac{\dfrac{CP_c \bullet h_c \bullet A_c}{CP_c + \dfrac{h_c \bullet A_c}{2}} \bullet \dfrac{h_c \bullet A_c}{CP_c + \dfrac{h_c \bullet A_c}{2}}}{M_{wall} c_{wall} \bullet s + \dfrac{CP_h \bullet h_h \bullet A_h}{CP_h + \dfrac{h_h \bullet A_h}{2}} + \dfrac{CP_c \bullet h_c \bullet A_c}{CP_c + \dfrac{h_c \bullet A_c}{2}}} \tag{4-7}$$

$$g_{12} = \frac{CP_c - \frac{h_c \times A_c}{2}}{CP_c + \frac{h_c \times A_c}{2}} \tag{4-8}$$

$$g_2 = \frac{\frac{CP_h \bullet h_h \bullet A_h}{CP_h + \frac{h_h \bullet A_h}{2}} \bullet \frac{h_c \bullet A_c}{CP_c + \frac{h_c \bullet A_c}{2}}}{M_{wall} c_{wall} \bullet s + \frac{CP_h \bullet h_h \bullet A_h}{CP_h + \frac{h_h \bullet A_h}{2}} + \frac{CP_c \bullet h_c \bullet A_c}{CP_c + \frac{h_c \bullet A_c}{2}}} \tag{4-9}$$

$$g_3 = \frac{M_{wall} c_{wall} \bullet \frac{h_c \bullet A_c}{CP_c + \frac{h_c \bullet A_c}{2}}}{M_{wall} c_{wall} \bullet s + \frac{CP_h \bullet h_h \bullet A_h}{CP_h + \frac{h_h \bullet A_h}{2}} + \frac{CP_c \bullet h_c \bullet A_c}{CP_c + \frac{h_c \bullet A_c}{2}}} \tag{4-10}$$

We can also interpret that there are four pathways from the inlet source to the outlet target in a HE, the coefficient function corresponds to the transfer function of each pathway as shown in Fig 4.1 for the outlet temperature of a HE, and the outlet temperature function equals to the sum-up of the effect of each pathway.

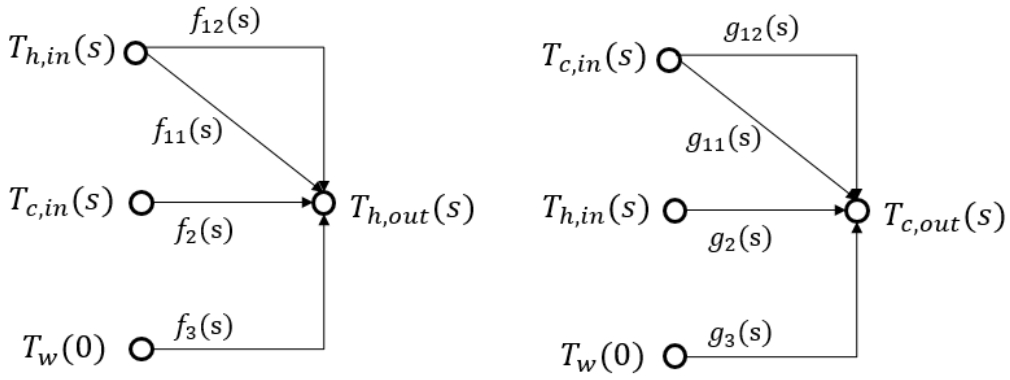

Fig 4.1. HE outlet temperature decomposition: pathway representation

4.2.2 HEN dynamic model

The pathway analysis of the whole network allows us to construct the function of the HEN outlet temperature. We need to take care of two processes that connect various HEs in a HEN, which is HEs in series and stream split. In the following analysis, we do not consider the HEN with a loop as explained in Chapter 3. In what follows, we will use two examples to illustrate the method.

In the first example, we analyze the condition when two HEs are in series, as shown in Fig 4.2, in which we expect to reach the H1 outlet temperature. H1 transfers heat with C1 in E1 to reach $T_{h1,2}(s)$ at first, and then transfers heat with C2 in E2 to reach the outlet temperature $T_{h1,out}(s)$. As explained before, every outlet temperature of a given HE comprises four pathways from the inlet sources to the outlet target, so there are two "steps" to reach $T_{h1,out}(s)$ from the inlet sources. The pathway analysis of this example is provided in Fig 4.3. There are total 10 pathways and the corresponding transfer function, as listed in

Table 4.1. The transfer function of each pathway is obtained through the multiplication of each involved sub-functions. Then, $T_{h1,out}(s)$ is equal to the sum of all these transfer functions. Note that we can analyze the pathways from the inlet to the outlet directly without the necessity to calculate the intermediate temperature $T_{h1,2}(s)$.

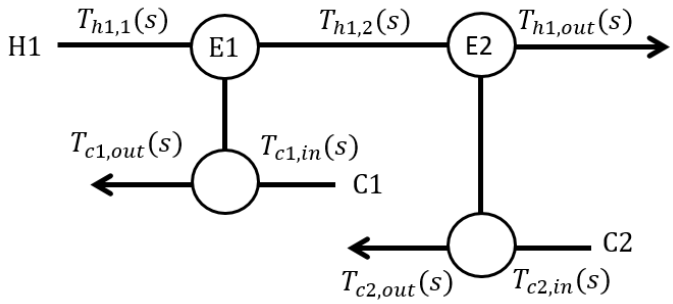

Fig 4.2. Example of HEs in-series

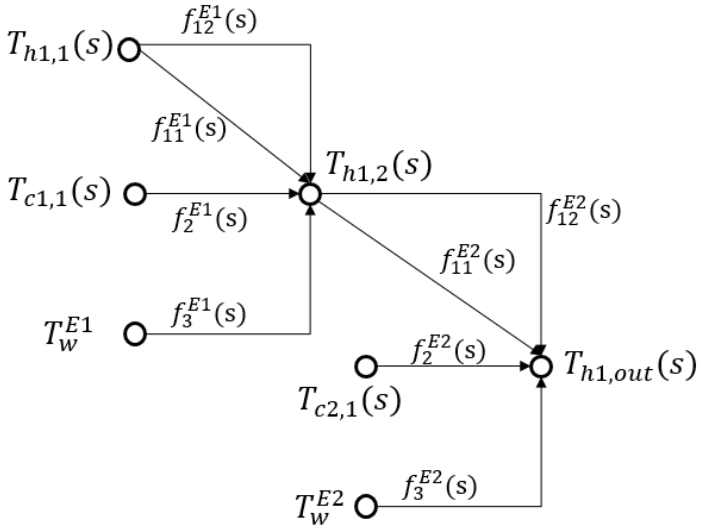

Fig 4.3. Pathway analysis of the HEs in series (example in Fig. 4.2)

Table 4.1. Pathway and corresponding function of the HEs in series (example in Fig. 4.2)

Pathway	Function
1	$T_{h1,1}(s) \bullet f_{12}^{E1}(s) \bullet f_{12}^{E2}(s)$
2	$T_{h1,1}(s) \bullet f_{11}^{E1}(s) \bullet f_{12}^{E2}(s)$
3	$T_{c1,1}(s) \bullet f_{2}^{E1}(s) \bullet f_{12}^{E2}(s)$
4	$T_{w}^{E1}(s) \bullet f_{2}^{E1}(s) \bullet f_{12}^{E2}(s)$
5	$T_{h1,1}(s) \bullet f_{12}^{E1}(s) \bullet f_{11}^{E2}(s)$
6	$T_{h1,1}(s) \bullet f_{11}^{E1}(s) \bullet f_{11}^{E2}(s)$
7	$T_{c1,1}(s) \bullet f_{2}^{E1}(s) \bullet f_{11}^{E2}(s)$
8	$T_{w}^{E1}(s) \bullet f_{3}^{E1}(s) \bullet f_{11}^{E2}(s)$
9	$T_{c2,1}(s) \bullet f_{2}^{E2}(s)$
10	$T_{w}^{E2}(s) \bullet f_{3}^{E2}(s)$

The stream split enlarges the number of pathways and gives specific split ratios to the corresponding downstream paths. Here, we use a second example (Fig 4.4) to show how to handle both HEs in-series and with split-mixing process (this example is taken from part 3.3.3). It is a four-stream problem, and the outlet temperature of C2 is the target variable to be obtained. The pathway analysis diagram can be constructed, as shown in Fig 4.5. We can observe five pathways to reach $T_{h2,2}$: four pathways coming from the HE E1, and the fifth one from the bypass. Calculating the transfer function of each pathway, we can obtain the results as provided in Table 4.2.

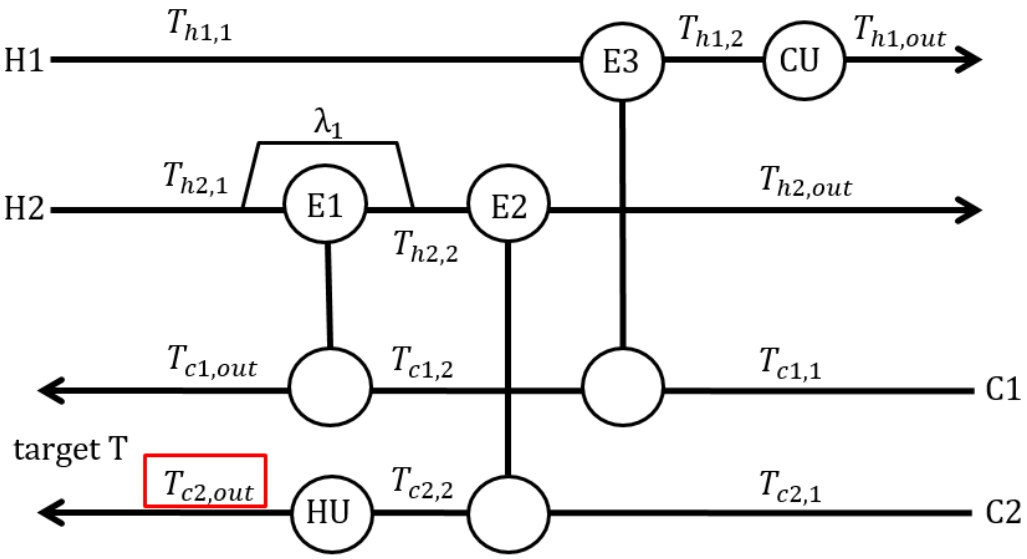

Fig 4.4. Example of HEN using HEs in-series and split

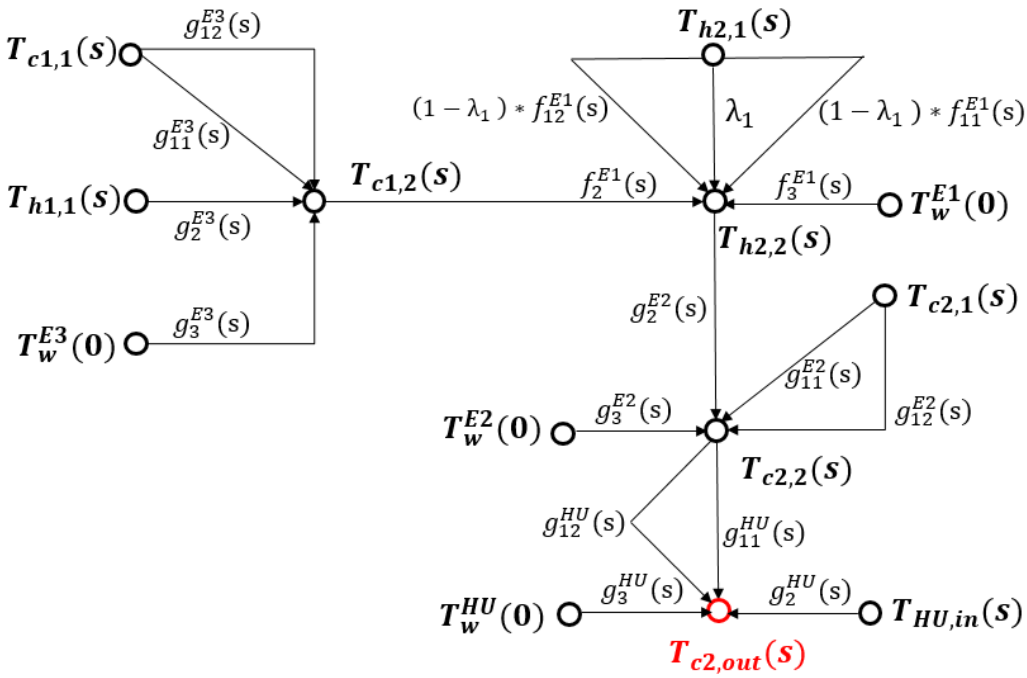

Fig 4.5. Pathway analysis toward the case example

Table 4.2. Pathway and corresponding transfer function of the HEs in series

Pathway	Sub-function
1	$T_{c1,1}(s) \bullet g_{12}^{E3}(s) \bullet f_{2}^{E1}(s) \bullet g_{2}^{E2}(s) \bullet g_{11}^{HU}(s)$
2	$T_{c1,1}(s) \bullet g_{12}^{E3}(s) \bullet f_{2}^{E1}(s) \bullet g_{2}^{E2}(s) \bullet g_{12}^{HU}(s)$
3	$T_{c1,1}(s) \bullet g_{11}^{E3}(s) \bullet f_{2}^{E1}(s) \bullet g_{2}^{E2}(s) \bullet g_{11}^{HU}(s)$
4	$T_{c1,1}(s) \bullet g_{11}^{E3}(s) \bullet f_{2}^{E1}(s) \bullet g_{2}^{E2}(s) \bullet g_{12}^{HU}(s)$
5	$T_{h1,1}(s) \bullet g_{2}^{E3}(s) \bullet f_{2}^{E1}(s) \bullet g_{2}^{E2}(s) \bullet g_{11}^{HU}(s)$
6	$T_{h1,1}(s) \bullet g_{2}^{E3}(s) \bullet f_{2}^{E1}(s) \bullet g_{2}^{E2}(s) \bullet g_{12}^{HU}(s)$
7	$T_{w}^{E3}(0) \bullet g_{3}^{E3}(s) \bullet f_{2}^{E1}(s) \bullet g_{2}^{E2}(s) \bullet g_{11}^{HU}(s)$
8	$T_{w}^{E3}(0) \bullet g_{3}^{E3}(s) \bullet f_{2}^{E1}(s) \bullet g_{2}^{E2}(s) \bullet g_{12}^{HU}(s)$
9	$T_{h2,1}(s) \bullet \lambda_1 \bullet g_{2}^{E2}(s) \bullet g_{11}^{HU}(s)$
10	$T_{h2,1}(s) \bullet \lambda_1 \bullet g_{2}^{E2}(s) \bullet g_{12}^{HU}(s)$
11	$T_{h2,1}(s) \bullet (1-\lambda_1) \bullet f_{12}^{E1}(s) \bullet g_{2}^{E2}(s) \bullet g_{11}^{HU}(s)$
12	$T_{h2,1}(s) \bullet (1-\lambda_1) \bullet f_{12}^{E1}(s) \bullet g_{2}^{E2}(s) \bullet g_{12}^{HU}(s)$
13	$T_{h2,1}(s) \bullet (1-\lambda_1) \bullet f_{11}^{E1}(s) \bullet g_{2}^{E2}(s) \bullet g_{11}^{HU}(s)$
14	$T_{h2,1}(s) \bullet (1-\lambda_1) \bullet f_{11}^{E1}(s) \bullet g_{2}^{E2}(s) \bullet g_{12}^{HU}(s)$
15	$T_{w}^{E1}(0) \bullet f_{3}^{E1}(s) \bullet g_{2}^{E2}(s) \bullet g_{11}^{HU}(s)$
16	$T_{w}^{E1}(0) \bullet f_{3}^{E1}(s) \bullet g_{2}^{E2}(s) \bullet g_{12}^{HU}(s)$
17	$T_{c2,1}(s) \bullet g_{12}^{E2}(s) \bullet g_{11}^{HU}(s)$
18	$T_{c2,1}(s) \bullet g_{11}^{E2}(s) \bullet g_{11}^{HU}(s)$
19	$T_{c2,1}(s) \bullet g_{12}^{E2}(s) \bullet g_{12}^{HU}(s)$
20	$T_{c2,1}(s) \bullet g_{11}^{E2}(s) \bullet g_{12}^{HU}(s)$
21	$T_{w}^{E2}(0) \bullet g_{3}^{E2}(s) \bullet g_{11}^{HU}(s)$
22	$T_{w}^{E2}(0) \bullet g_{3}^{E2}(s) \bullet g_{12}^{HU}(s)$
23	$T_{w}^{HU}(0) \bullet g_{3}^{HU}(s)$
24	$T_{hu,in}(s) \bullet g_{2}^{HU}(s)$

There are 24 pathways from various sources to affect the outlet temperature of C2, and the target temperature function equals the sum of all these sub-functions. The next step is to carry out the inverse Laplace transform to obtain the temperature function in the time domain. Knowing that the inverse Laplace transform of a sum is equal to the sum of inverse Laplace transforms (equation (4-11)), the main question is how to carry out efficiently inverse Laplace transform of each sub-function.

$$\ell^{-1}\{F_1(s)+F_1(s)\} = \ell^{-1}\{F_1(s)\} + \ell^{-1}\{F_1(s)\} \tag{4-11}$$

Observing the sub-functions in Table 4.2, each of them is a product of basic functions of f and g, which are in the form of $\frac{b}{s+a}$ or $const$ (a, b and $const$ are parameters depend on the specific HE and pathway). Applying the partial fraction decomposition makes it possible to decompose the sub-function as a sum of simple fractions. The advantage of implementing such decomposition is that the simple fractions function in standard form in which the inverse Laplace transform can be reached easily. To illustrate the method, we take the pathway 24 as an example, and we assume the inlet temperature change in the step signal. Thus, the function of pathway 24 ($G_{24}(s)$) in Table 4.2 can be expressed as the equation (4-12). $T_{hu,in}(0)$ is the temperature just after the step change which is a constant, a is the root of the expression which differentiates by HEs, b is the parameter that depends on both the specific HE and also corresponding

coefficients f and g. The equation (4-12) can be decomposed into the simple forms, as in the equation (4-13), with the help of equation (4-14).

Here, we can take the inverse Laplace transform table as the reference to obtain the function in time directly in equation (4-15) by following Table 4.3 as reference. Since all the pathways' equations are similar to equation (4-12), they can be decomposed into the simple forms as with equation (4-13) that can reach the function in the time domain without the concern of numerical difficulty. That is why we divide the outlet temperature function of HE, as shown in the equations (4-1) and (4-6), and propose to obtain the function by dealing with every pathway separately. Applying the similar decomposition method, we can obtain all the functions in the time domain for each pathway by assuming all the inlet temperature change in the step form, as listed in Table 4.4.

$$G_{24}(s) = \frac{T_{hu,in}(0)}{s} \bullet \frac{b_{g_2}^{HU}}{s + a^{HU}} \tag{4-12}$$

$$G_{24}(s) = \frac{T_{hu,in}(0) \bullet b_{g_2}^{HU}}{a^{HU}} \left(\frac{1}{s} - \frac{1}{s + a^{HU}} \right) \tag{4-13}$$

$$\frac{1}{s + a_1} \bullet \frac{1}{s + a_2} = \frac{1}{a_2 - a_1} \left(\frac{1}{s + a_1} - \frac{1}{s + a_2} \right), a_2 \neq a_1 \tag{4-14}$$

$$G_{24}(t) = \frac{T_{hu,in}(0) \bullet b_{g_2}^{HU}}{a^{HU}} \left(1 - e^{-a^{HU} t} \right) \tag{4-15}$$

Table 4.3. Part of inverse Laplace transform table

Function in Laplace domain	Function in time domain
$\frac{1}{s}$	1
$\frac{1}{s + a}$	e^{-at}
$\frac{n!}{s^{n+1}}$	t^n , n = 1, 2, 3…

Table 4.4. Inverse Laplace results for all the pathways in Fig 4.5

	Function in Laplace domain	Function in time domain
$G_1(s)$	$\frac{T_{c1,1}(0)}{s}\bullet b_{g_{12}}^{E3}\bullet\frac{b_{f_2}^{E1}}{s+a^{E1}}\bullet\frac{b_{g_2}^{E2}}{s+a^{E2}}\bullet\frac{b_{g_{11}}^{HU}}{s+a^{HU}}$	$\frac{T_{c1,1}(0)\bullet b_{g_{12}}^{E3}\bullet b_{g_2}^{E2}\bullet b_{g_2}^{E2}\bullet b_{g_{11}}^{HU}}{(a^{HU}-a^{E2})a^{E1}}\bullet$ $\left(\frac{1-e^{-a^{E2}t}}{a^{E2}}-\frac{1-e^{-a^{HU}t}}{a^{HU}}\right.$ $\left.-\frac{e^{-a^{E1}t}-e^{-a^{E2}t}}{a^{E2}-a^{E1}}+\frac{e^{-a^{E1}t}-e^{-a^{HU}t}}{a^{HU}-a^{E1}}\right)$
$G_2(s)$	$\frac{T_{c1,1}(0)}{s}\bullet b_{g_{12}}^{E3}\bullet\frac{b_{f_2}^{E1}}{s+a^{E1}}\bullet\frac{b_{g_2}^{E2}}{s+a^{E2}}\bullet b_{g_{12}}^{HU}$	$\frac{T_{c1,1}(0)\bullet b_{g_{12}}^{E3}\bullet b_{f_2}^{E1}\bullet b_{g_2}^{E2}\bullet b_{g_{12}}^{HU}}{a^{E1}-a^{E12}}\bullet$ $\left(\frac{1}{a^{E2}}(1-e^{-a^{E2}t})-\frac{1}{a^{E1}}(1-e^{-a^{E1}t})\right)$
$G_3(s)$	$\frac{T_{c1,1}(0)}{s}\bullet\frac{b_{g_{11}}^{E3}}{s+a^{E3}}\bullet\frac{b_{f_2}^{E1}}{s+a^{E1}}\bullet\frac{b_{g_2}^{E2}}{s+a^{E2}}\bullet\frac{b_{g_{11}}^{HU}}{s+a^{HU}}$	$\frac{T_{c1,1}(0)\bullet b_{g_{11}}^{E3}\bullet b_{f_2}^{E1}\bullet b_{g_2}^{E2}\bullet b_{g_{11}}^{HU}}{(a^{E1}-a^{E3})(a^{E2}-a^{HU})}\bullet$ $\left(\frac{1}{a^{HU}-a^{E3}}\left(\frac{1-e^{-a^{E3}t}}{a^{E3}}-\frac{1-e^{-a^{HU}t}}{a^{HU}}\right)\right.$ $-\frac{1}{a^{E2}-a^{E3}}\left(\frac{1-e^{-a^{E3}t}}{a^{E3}}-\frac{1-e^{-a^{2}t}}{a^{E2}}\right)$ $-\frac{1}{a^{HU}-a^{E1}}\left(\frac{1-e^{-a^{E1}t}}{a^{E1}}-\frac{1-e^{-a^{HU}t}}{a^{HU}}\right)$ $\left.+\frac{1}{a^{E2}-a^{E1}}\left(\frac{1-e^{-a^{E2}t}}{a^{E2}}-\frac{1-e^{-a^{E1}t}}{a^{E1}}\right)\right)$
$G_4(s)$	$\frac{T_{c1,1}(0)}{s}\bullet\frac{b_{g_{11}}^{E3}}{s+a^{E3}}\bullet\frac{b_{f_2}^{E1}}{s+a^{E1}}\bullet\frac{b_{g_2}^{E2}}{s+a^{E2}}\bullet b_{g_{12}}^{HU}$	$\frac{T_{c1,1}(0)\bullet b_{g_{11}}^{E3}\bullet b_{f_2}^{E1}\bullet b_{g_2}^{E2}\bullet b_{g_{12}}^{HU}}{(a^{E3}-a^{E2})a^{E1}}\bullet$ $\left(\frac{1-e^{-a^{E2}t}}{a^{E2}}-\frac{1-e^{-a^{E3}t}}{a^{E3}}-\right.$ $\left.\frac{e^{-a^{E1}t}-e^{-a^{E2}t}}{a^{E2}-a^{E1}}+\frac{e^{-a^{E1}t}-e^{-a^{HU}t}}{a^{E3}-a^{E1}}\right)$

	Function in Laplace domain	Function in time domain
$G_5(s)$	$\frac{T_{h1,1}(0)}{s}\bullet\frac{b_{g_2}^{E3}}{s+a^{E3}}\bullet\frac{b_{f_2}^{E1}}{s+a^{E1}}\bullet\frac{b_{g_2}^{E2}}{s+a^{E2}}\bullet\frac{b_{g_{11}}^{HU}}{s+a^{HU}}$	$\frac{T_{h1,1}(0)\bullet b_{g_2}^{E3}\bullet b_{f_2}^{E1}\bullet b_{g_2}^{E2}\bullet b_{g_{11}}^{HU}}{(a^{E1}-a^{E3})(a^{E2}-a^{HU})}\bullet$ $\left(\begin{array}{l}\frac{1}{a^{HU}-a^{E3}}\left(\frac{1-e^{-a^{E3}t}}{a^{E3}}-\frac{1-e^{-a^{HU}t}}{a^{HU}}\right)\\ -\frac{1}{a^{E2}-a^{E3}}\left(\frac{1-e^{-a^{E3}t}}{a^{E3}}-\frac{1-e^{-a^{2}t}}{a^{E2}}\right)\\ -\frac{1}{a^{HU}-a^{E1}}\left(\frac{1-e^{-a^{E1}t}}{a^{E1}}-\frac{1-e^{-a^{HU}t}}{a^{HU}}\right)\\ +\frac{1}{a^{E2}-a^{E1}}\left(\frac{1-e^{-a^{E2}t}}{a^{E2}}-\frac{1-e^{-a^{E1}t}}{a^{E1}}\right)\end{array}\right)$
$G_6(s)$	$\frac{T_{h1,1}(0)}{s}\bullet\frac{b_{g_2}^{E3}}{s+a^{E3}}\bullet\frac{b_{f_2}^{E1}}{s+a^{E1}}\bullet\frac{b_{g_2}^{E2}}{s+a^{E2}}\bullet b_{g_{12}}^{HU}$	$\frac{T_{h1,1}(0)\bullet b_{g_2}^{E3}\bullet b_{f_2}^{E1}\bullet b_{g_2}^{E2}\bullet b_{g_{12}}^{HU}}{(a^{E3}-a^{E2})a^{E1}}\bullet$ $\left(\begin{array}{l}\frac{1-e^{-a^{E2}t}}{a^{E2}}-\frac{1-e^{-a^{E3}t}}{a^{E3}}-\\ \frac{e^{-a^{E1}t}-e^{-a^{E2}t}}{a^{E2}-a^{E1}}+\frac{e^{-a^{E1}t}-e^{-a^{HU}t}}{a^{E3}-a^{E1}}\end{array}\right)$
$G_7(s)$	$T_w^{E3}(0)\bullet\frac{b_{g_3}^{E3}}{s+a^{E3}}\bullet\frac{b_{f_2}^{E1}}{s+a^{E1}}\bullet\frac{b_{g_2}^{E2}}{s+a^{E2}}\bullet\frac{b_{g_{11}}^{HU}}{s+a^{HU}}$	$\frac{T_w^{E3}(0)\bullet b_{g_3}^{E3}\bullet b_{f_2}^{E1}\bullet b_{g_2}^{E2}\bullet b_{g_{11}}^{HU}}{(a^{E1}-a^{E3})(a^{E2}-a^{HU})}\bullet$ $\left(\begin{array}{l}\frac{e^{-a^{E3}t}-e^{-a^{HU}t}}{a^{HU}-a^{E3}}-\frac{e^{-a^{E2}t}-e^{-a^{E3}t}}{a^{E2}-a^{E3}}\\ -\frac{e^{-a^{HU}t}-e^{-a^{E1}t}}{a^{HU}-a^{E1}}+\frac{e^{-a^{E2}t}-e^{-a^{E1}t}}{a^{E2}-a^{E1}}\end{array}\right)$
$G_8(s)$	$T_w^{E3}(0)\bullet\frac{b_{g_3}^{E3}}{s+a^{E3}}\bullet\frac{b_{f_2}^{E1}}{s+a^{E1}}\bullet\frac{b_{g_2}^{E2}}{s+a^{E2}}\bullet b_{g_{12}}^{HU}$	$\frac{T_w^{E3}(0)\bullet b_{g_{12}}^{HU}}{a^{E1}-a^{E2}}\left(\begin{array}{l}\frac{1}{a^{E2}-a^{E3}}(e^{-a^{E3}t}-e^{-a^{E2}t})\\ -\frac{1}{a^{E1}-a^{E3}}(e^{-a^{E3}t}-e^{-a^{E1}t})\end{array}\right)$
$G_9(s)$	$\frac{T_{h2,1}(0)\bullet\lambda_1}{s}\bullet\frac{b_{g_2}^{E2}}{s+a^{E2}}\bullet\frac{b_{g_{11}}^{HU}}{s+a^{HU}}$	$\frac{T_{h2,1}(0)\bullet\lambda_1\bullet b_{g_2}^{E2}\bullet b_{g_{11}}^{HU}}{a^{HU}-a^{E2}}\bullet$ $\left(\frac{1}{a^{E2}}(1-e^{-a^{E2}t})-\frac{1}{a^{HU}}(1-e^{-a^{HU}t})\right)$

	Function in Laplace domain	Function in time domain
$G_{10}(s)$	$\frac{T_{h2,1}(0)\bullet\lambda_1}{s}\bullet\frac{b_{g_2}^{E2}}{s+a^{E2}}\bullet b_{g_{12}}^{HU}$	$T_{h2,1}(0)\bullet\lambda_1\bullet\frac{b_{g_2}^{E2}\bullet b_{g_{12}}^{HU}}{a^{E2}}\bullet(1-e^{-a^{E2}t})$
$G_{11}(s)$	$\frac{T_{h2,1}(0)\bullet(1-\lambda_1)}{s}\bullet b_{f_{12}}^{E1}\bullet\frac{b_{g_2}^{E2}}{s+a^{E2}}\bullet\frac{b_{g_{11}}^{HU}}{s+a^{HU}}$	$\frac{T_{h2,1}(0)\bullet(1-\lambda_1)\bullet b_{f_{12}}^{E1}\bullet b_{g_2}^{E2}\bullet b_{g_{11}}^{HU}}{a^{HU}-a^{E2}}\bullet\left(\frac{1}{a^{E2}}(1-e^{-a^{E2}t})-\frac{1}{a^{HU}}(1-e^{-a^{HU}t})\right)$
$G_{12}(s)$	$\frac{T_{h2,1}(0)\bullet(1-\lambda_1)}{s}\bullet b_{f_{12}}^{E1}\bullet\frac{b_{g_2}^{E2}}{s+a^{E2}}\bullet b_{g_{12}}^{HU}$	$\frac{T_{h2,1}(0)\bullet(1-\lambda_1)\bullet b_{f_{12}}^{E1}\bullet b_{g_2}^{E2}\bullet b_{g_{12}}^{HU}}{a^{E2}}(1-e^{-a^{E2}t})$
$G_{13}(s)$	$\frac{T_{h2,1}(0)\bullet(1-\lambda_1)}{s}\bullet\frac{b_{f_{11}}^{E1}}{s+a^{E1}}\bullet\frac{b_{g_2}^{E2}}{s+a^{E2}}\bullet\frac{b_{g_{11}}^{HU}}{s+a^{HU}}$	$\frac{T_{h2,1}(0)\bullet(1-\lambda_1)\bullet b_{f_{11}}^{E1}\bullet b_{g_2}^{E2}\bullet b_{g_{11}}^{HU}}{(a^{HU}-a^{E2})a^{E1}}\bullet\left(\frac{1-e^{-a^{E2}t}}{a^{E2}}-\frac{1-e^{-a^{HU}t}}{a^{HU}}-\frac{e^{-a^{E1}t}-e^{-a^{E2}t}}{a^{E2}-a^{E1}}+\frac{e^{-a^{E1}t}-e^{-a^{HU}t}}{a^{HU}-a^{E1}}\right)$
$G_{14}(s)$	$\frac{T_{h2,1}(0)\bullet(1-\lambda_1)}{s}\bullet\frac{b_{f_{11}}^{E1}}{s+a^{E1}}\bullet\frac{b_{g_2}^{E2}}{s+a^{E2}}\bullet b_{g_{12}}^{HU}$	$\frac{T_{h2,1}(0)\bullet(1-\lambda_1)\bullet b_{f_{11}}^{E1}\bullet b_{g_2}^{E2}\bullet b_{g_{12}}^{HU}}{a^{E2}-a^{E1}}\bullet\left(\frac{1}{a^{E1}}(1-e^{-a^{E1}t})-\frac{1}{a^{E2}}(1-e^{-a^{E2}t})\right)$
$G_{15}(s)$	$T_w^{E1}(0)\bullet\frac{b_{f_3}^{E1}}{s+a^{E1}}\bullet b_{g_2}^{E2}\bullet\frac{b_{g_{11}}^{HU}}{s+a^{HU}}$	$T_w^{E1}(0)\bullet b_{f_3}^{E1}\bullet b_{g_2}^{E2}\bullet b_{g_{11}}^{HU}\bullet\frac{e^{a^{-E1}t}-e^{-a^{HU}t}}{a^{HU}-a^{E1}}$
$G_{16}(s)$	$T_w^{E1}(0)\bullet\frac{b_{f_3}^{E1}}{s+a^{E1}}\bullet b_{g_2}^{E2}\bullet b_{g_{12}}^{HU}$	$T_w^{E1}(0)\bullet b_{f_3}^{E1}\bullet b_{g_2}^{E2}\bullet b_{g_{12}}^{HU}\bullet e^{-a^{E1}t}$
$G_{17}(s)$	$\frac{T_{c2,1}(0)}{s}\bullet b_{g_{12}}^{E2}\bullet\frac{b_{g_{11}}^{HU}}{s+a^{HU}}$	$\frac{T_{c2,1}(0)\bullet b_{g_{12}}^{E2}\bullet b_{g_{11}}^{HU}}{a^{HU}}\left(1-e^{-a^{HU}t}\right)$
$G_{18}(s)$	$\frac{T_{c2,1}(0)}{s}\bullet\frac{b_{g_{11}}^{E2}}{s+a^{E2}}\bullet\frac{b_{g_{11}}^{HU}}{s+a^{HU}}$	$\frac{T_{c2,1}(0)\bullet b_{g_{11}}^{E2}\bullet b_{g_{11}}^{HU}}{a^{HU}-a^{E2}}\bullet(\frac{1-e^{-a^{E2}t}}{a^{E2}}-\frac{1-e^{-a^{HU}t}}{a^{HU}})$
$G_{19}(s)$	$\frac{T_{c2,1}(0)}{s}\bullet b_{g_{12}}^{E2}\bullet b_{g_{12}}^{HU}$	$T_{c2,1}(0)\bullet b_{g_{12}}^{E2}\bullet b_{g_{12}}^{HU}$

	Function in Laplace domain	Function in time domain
$G_{20}(s)$	$\frac{T_{c2,1}(0)}{s}\bullet\frac{b_{g_{11}}^{E2}}{s+a^{E2}}\bullet b_{g_{12}}^{HU}$	$\frac{T_{c2,1}(0)\bullet b_{g_{11}}^{E2}\bullet b_{g_{12}}^{HU}}{a^{E2}}\bullet(1-e^{-a^{E2}t})$
$G_{21}(s)$	$T_w^{E2}(0)\bullet\frac{b_{g_3}^{E2}}{s+a^{E2}}\bullet\frac{b_{g_{11}}^{HU}}{s+a^{HU}}$	$\frac{T_w^{E2}(0)\bullet b_{g_3}^{E2}\bullet b_{g_{11}}^{HU}}{a^{HU}-a^{E2}}\bullet(e^{-a^{E2}t}-e^{-a^{HU}t})$
$G_{22}(s)$	$T_w^{E2}(0)\bullet\frac{b_{g_3}^{E2}}{s+a^{E2}}\bullet b_{g_{12}}^{HU}$	$T_w^{E2}(0)\bullet b_{g_3}^{E2}\bullet b_{g_{12}}^{HU}\bullet e^{-a^{E2}t}$
$G_{23}(s)$	$T_w^{HU}(0)\bullet\frac{b_{g_3}^{HU}}{s+a^{HU}}$	$T_w^{HU}(0)\bullet b_{g_3}^{HU}\bullet e^{-a^{HU}t}$
$G_{24}(s)$	$\frac{T_{hu,in}(0)}{s}\bullet\frac{b_{g_2}^{HU}}{s+a^{HU}}$	$\frac{T_{hu,in}(0)\bullet b_{g_2}^{HU}}{a^{HU}}\left(1-e^{-a^{HU}t}\right)$

Another advantage of the above method is the capability to deal with the inlet temperature change in the other forms without limiting the step signal since they can also follow the above-described decomposition approach, such as the ramp, exponential signal. By assuming the inlet temperature change as a ramp function as in equation (4-16), the inlet function in the Laplace domain is obtained in equation (4-17). Thus, $G_{24}(s)$ can be reached as in the equation (4-18) and function in the time domain, as shown in equation (4-19). When it changes with the exponential signal as in the equation (4-20), the same method can be applied to obtain the temperature function in time domain directly from equation (4-22) to equation (4-23). The method can deal with the inlet change that can be represented as the combinations of step, ramp, and exponential functions.

$$T_{hu,in}(t)=\begin{pmatrix} w+vt, 0\le t\le t_1; \\ w+vt_1, t>t_1 \end{pmatrix}, \text{ Ramp signal} \tag{4-16}$$

$$T_{hu,in}(s)=\begin{pmatrix} \frac{w}{s}+\frac{v}{s^2}, 0\le t\le t_1; \\ \frac{w+vt_1}{s}, t>t_1 \end{pmatrix} \tag{4-17}$$

$$G_{24}(s)=\begin{pmatrix} (\frac{w}{s}+\frac{v}{s^2})\bullet\frac{b_{g_2}^{HU}}{s+a^{HU}}, 0\le t\le t_1; \\ \frac{w+vt_1}{s}\bullet\frac{b_{g_2}^{HU}}{s+a^{HU}}, t>t_1 \end{pmatrix} \tag{4-18}$$

$$G_{24}(t)=\begin{pmatrix}\frac{w\bullet b_{g_2}^{HU}}{a^{HU}}\bullet(1-e^{-a^{HU}t})+\frac{v\bullet b_{g_2}^{HU}}{(a^{HU})^2}\bullet(e^{-a^{HU}t}-1+a^{HU}t), 0\le t\le t_1;\\ \frac{(w+vt_1)\bullet b_{g_2}^{HU}}{a^{HU}}\bullet(1-e^{-a^{HU}t}), t>t_1\end{pmatrix} \tag{4-19}$$

$$T_{hu,in}(t)=w+ve^{\phi t}\text{, Exponential signal} \tag{4-20}$$

$$T_{hu,in}(s)=\frac{w}{s}+\frac{v}{s-\phi} \tag{4-21}$$

$$G_{24}(s)=(\frac{w}{s}+\frac{v}{s-\phi})\bullet\frac{b_{g_2}^{HU}}{s+a^{HU}} \tag{4-22}$$

$$G_{24}(t)=\frac{w\bullet b_{g_2}^{HU}}{a^{HU}}\bullet(1-e^{-a^{HU}t})+\frac{v\bullet b_{g_2}^{HU}}{a^{HU}+\phi}\bullet(e^{-a^{HU}t}-e^{\phi t}) \tag{4-23}$$

However, the analytic model fits for the HEN without a loop, and the HEN with a loop requires further effort. In the thesis, we do not consider the HEN with a loop in the iteration, one of the reasons is that discarding HENs with a loop does not sacrifice the economic performance but saves a considerable part of calculation effort. The other reason is that the presence of a loop acts as the HEN's feedback control and gets a high chance to require a too long time to reach a stable status.

In this part, we have reformulated the expressions of the outlet temperature of the HE, to enable the coefficients of each subpart taking the same form. Then, we can obtain the HEN outlet temperature function through the pathway analysis, in which the function of each corresponding pathway is the product of the simple form function. The core step is to carry out the partial fraction decomposition toward each pathway's function to transfer it into the sum of simple functions, and the inverse Laplace transform of those simple functions can be obtained directly from the standard Laplace transform table. Moreover, we have illustrated methodology by changing the inlet temperature variation forms such as step signal, ramp signal, and exponential signal. In the next section, the validation of this new formulation is performed.

4.2.3 Validation of the HEN analytical model

The validation of the above described analytical model will be done through the comparison with Dymola simulation result by building the HE model following the same governing equations as in equations (3-47) to (3-49). The improved HEN dynamic model aims to solve a complicated HEN, and we select the optimized HEN of case 2 in work (Aguitoni et al., 2019) as an example to test the model. It is a 10 streams case problem, as shown in Fig 4.6 with HEN parameters listed in Table 4.5, and the outlet temperature of C1 is set as the target variable. The inlet temperatures are assumed to change in the form of step and ramp signal, and the inlet parameters are expected to change in three scenarios:

- scenario1 (S1): Inlet temperature change: the inlet temperature of all hot streams increase 20 K, and the cold stream decrease 20 K.
- scenario2 (S2): Mass flow change: hot stream mass flows increase 10%, and cold stream decrease 10%.

- scenario3 (S3): Simultaneous temperature and mass flow change: The streams temperature and mass flow change simultaneously as the same value as in the above two scenarios.

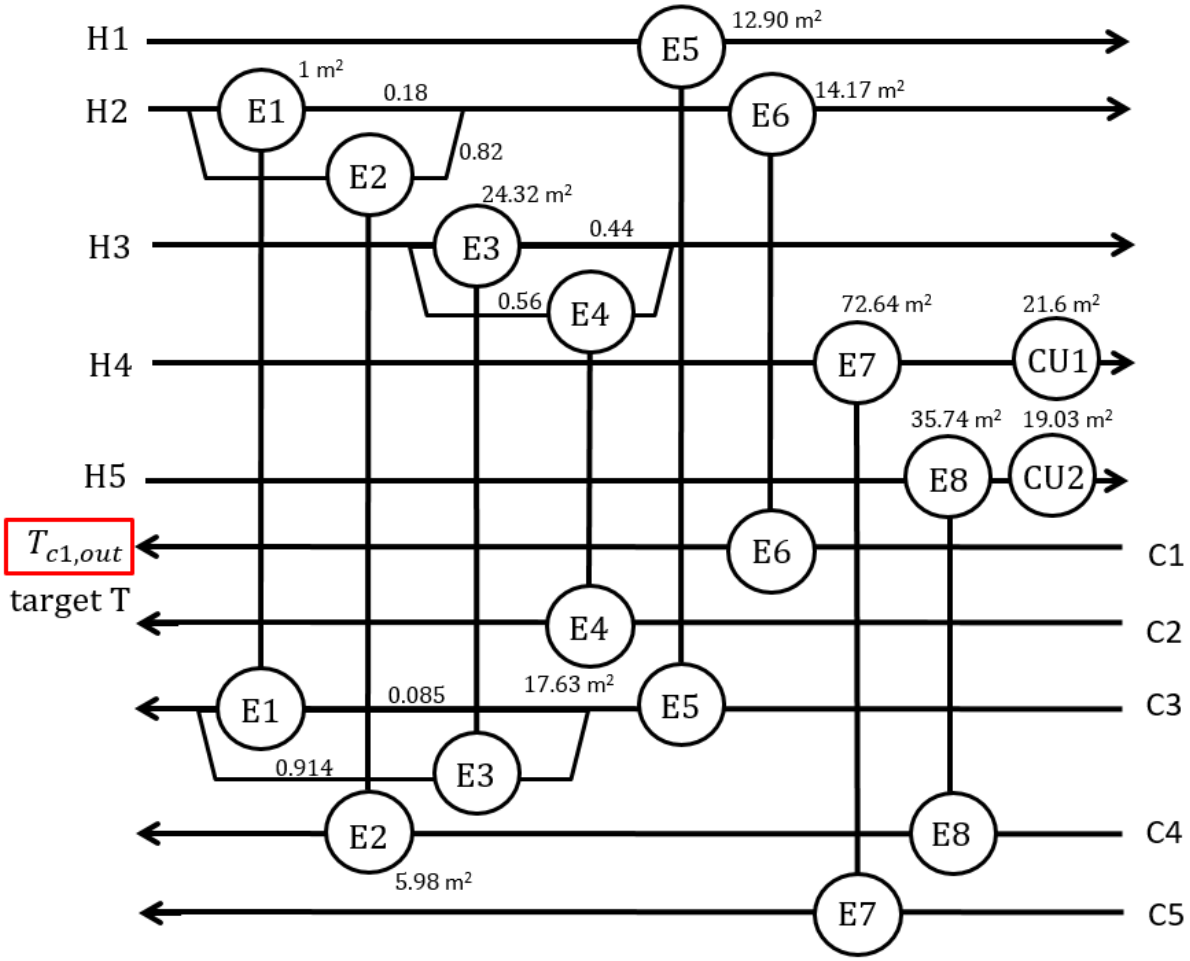

Fig 4.6. HEN example to validate the improved HEN dynamic model

Table 4.5. Parameters for the HEN example in Fig 4.6

Stream	T_{in}(K)	T_{out}(K)	CP(kW/K)	h (kW/m²•K)
H1	433.15	366.15	8.79	1.704
H2	522.15	411.15	10.55	1.704
H3	544.15	422.15	12.56	1.704
H4	500.15	339.15	14.77	1.704
H5	472.15	339.15	17.73	1.704
C1	333.15	433.15	7.62	1.704
C2	389.15	495.15	6.08	1.704
C3	311.15	494.15	8.44	1.704
C4	355.15	450.15	17.28	1.704
C5	366.15	478.15	13.9	1.704
HU	509.15	509.15	-	3.408
CU	311.15	355.15	-	3.408

Step signal

When the inlet parameters change with the step signal, the target temperature functions can be obtained by the above decomposition-based method and are provided as follows.

scenario1 only inlet temperature change:

$$T_{c1,out}(t) = 437.955 - 119.116e^{(-0.049t)} + 40.379e^{(-0.060t)} + 1121.244e^{(-0.037t)} - 1121.865e^{(-0.036t)} + 80.790e^{(-0.031t)} \quad (4\text{-}24)$$

scenario2 only inlet mass flowrate change:

$$T_{c1,out}(t) = 448.869 + 119.784e^{(-0.049t)} - 29.912e^{(-0.06t)} - 1130.072e^{(-0.037t)} + 1120.805e^{(-0.036t)} - 90.484e^{(-0.031t)} \quad (4\text{-}25)$$

scenario3 simultaneous change:

$$T_{c1,out}(t) = 455.139 - 43.213e^{(-0.049t)} + 21.138e^{(-0.060t)} + 355.711e^{(-0.037t)} - 338.629e^{(-0.036t)} - 5.671e^{(-0.031t)} \quad (4\text{-}26)$$

The comparison result by the above equations and the simulation from Dymola is provided in Fig 4.7, in which two approaches show quite good coherence, with a maximum 0.008K deviation, and it is caused by the selected significant numbers.

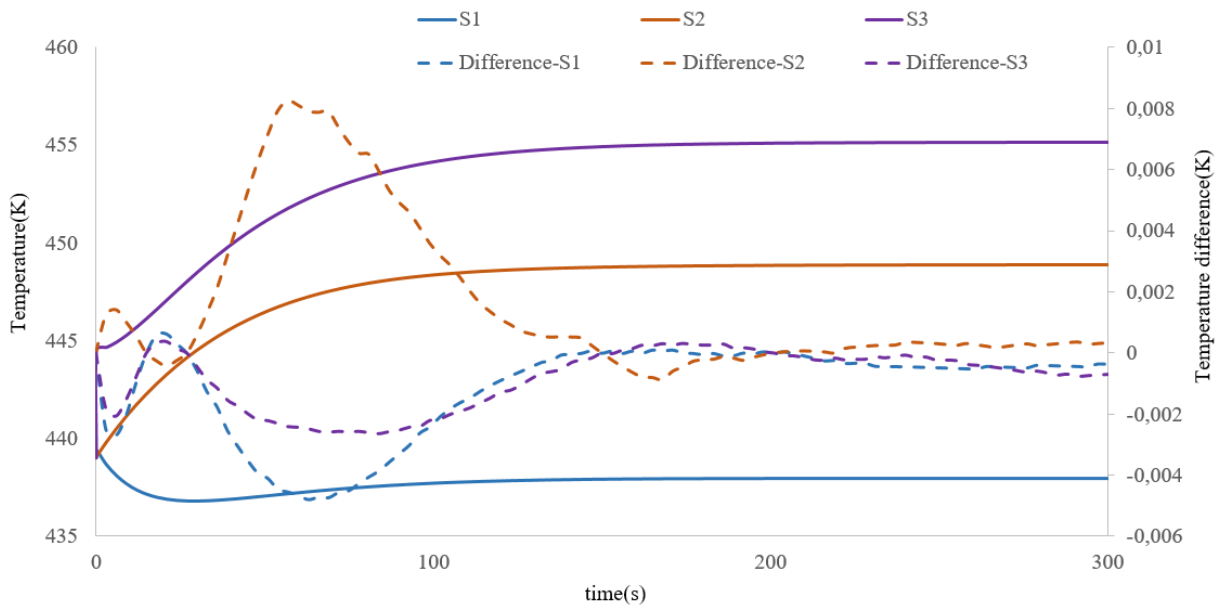

Fig 4.7. Validation of the improved HEN dynamic model: inlet parameters changes in the step signal

Ramp signal

When the inlet parameters change with the ramp signal, we assume the ramp signal's time duration is 20s. Since the mass flowrate can only evolve with the step signal as the model's assumption, we carry out the study toward the 2 conditions: inlet temperature ramp change and simultaneous inlet temperature change, and mass flowrate step change. The analytical solutions based on the above method are reached as follows.

only inlet temperature change:

$$\begin{aligned} T_{c1,out}(t) &= 456.510 + 2857.880e^{(-0.049t)} - 447.758e^{(-0.060t)} - 54953.342e^{(-0.037t)} \\ &+ 59099.900e^{(-0.036t)} - 6578.302e^{(-0.031t)} + 0.127t \end{aligned}, \quad 0 \le t \le 20\,s; \tag{4-27}$$

$$\begin{aligned} T_{c1,out}(t) &= 437.964 + 103.510e^{(-0.049t)} - 15.783e^{(-0.060t)} \\ &- 807.007e^{(-0.037t)} + 783.521e^{(-0.036t)} - 58.172e^{(-0.031t)} \end{aligned}, \quad t > 20\,s$$

Simultaneous change:

$$\begin{aligned} T_{c1,out}(t) &= 494.970 + 6703.799e^{(-0.049t)} - 980.838e^{(-0.060t)} - 13368.776e^{(-0.037t)} \\ &+ 143034.001e^{(-0.036t)} - 15132.167e^{(-0.031t)} + 0.266t \end{aligned}, \quad 0 \le t \le 20\,s; \tag{4-28}$$

$$\begin{aligned} T_{c1,out}(t) &= 455.135 + 81.610e^{(-0.049t)} - 7.816e^{(-0.060t)} \\ &- 635.437e^{(-0.037t)} + 622.990e^{(-0,036t)} - 67.747e^{(-0.031t)} \end{aligned}, \quad t > 20\,s$$

The reference results were obtained through the simulation in Dymola (an overview of the Dymola model is given in Annex), and the comparison result is depicted in Fig 4.8. We can observe rather exact coherence between the simulation result and analytic result with the above equations. The maximum error is about 0.02K, which can be regarded as the error caused by the selected significant numbers. We can also observe the corner of the outlet temperature function in Fig 4.8 for both the inlet temperature change and the simultaneous change in the 20s since ramp signal stops there.

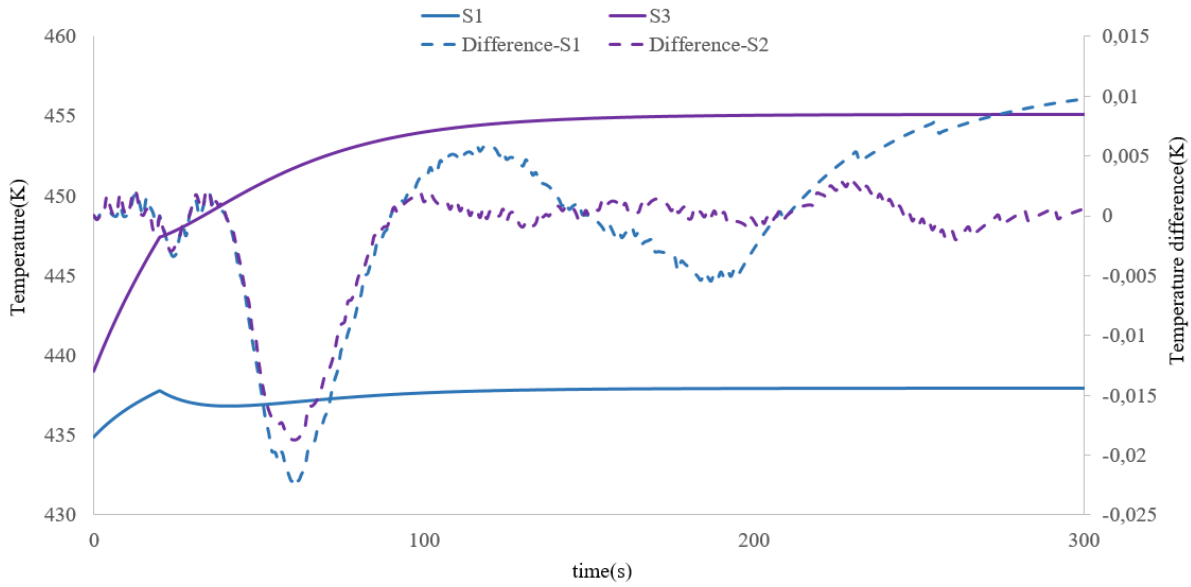

Fig 4.8. Validation of the improved HEN dynamic model: inlet temperature changes in the ramp signal

To make the TT calculation model applicable in medium-large scale problem, and avoid the inverse Laplace transform difficulty. We have provided a decomposition-based strategy that enabled us to obtain the HEN outlet temperature by the sum of simple functions. Then inverse Laplace transform process can be implemented easily to obtain the function in the time domain. The analytical method does not limit the change form of the inlet temperatures. We have illustrated the application when they change in step, ramp, and exponential signals. The method has been validated through the simulation result in Dymola via a 10 streams case study and exhibits quite good coherence to continue for further application.

In the next part we will discuss how to improve the HEN iterative strategy to enable the applicability in the medium-large scale cases.

4.3 Improved HEN iterative strategy

In this part, we provide an improved iteration NLP (IINLP) synthesis strategy that is based on the BINLP proposed in part 3.2. In other words, we try to find a smart way to iterate various HENs to find an optimal cost design without being obliged to iterate all the possible combinations. In parallel, a simulated annealing (SA) algorithm is implemented to optimize the HEN's configuration while in both cases the NLP model is used to optimize every proposed structure. Both methods are compared for several case studies to validate the effectiveness of the iterative strategy.

4.3.1 Description of improved iterative strategy: IINLP

Iterating the NLP toward all the potential structures can lead to the global optimal result, but it requires enormous amounts of computational efforts that cannot be accepted as a generic tool, it may be acceptable only for small cases as we have shown in our previous work (Yang et al., 2020). The basic iteration strategy can give some results within specific calculation time when facing large scale problems, but it is expected to be far from the optimal TAC design because the total number of iterations is enormous. By consequence, the final TAC - TT trade-off result might also be not promising. Our objective in this part is to provide an improved iteration strategy to reach better TAC-TT result when potential number of structures are enormous. The primary concern is still the optimized cost, and the problem becomes how to select potential structures. Here, we try to explore a hybrid method that combines the Pinch originated method and mathematical programming. The idea is to locate suitable structures or reduce search region by Pinch originated method, and then implement mathematical optimization. The combination of Pinch originated methods, and mathematical optimization models have already been tested in several works. Angsutorn et al. (2014) combined the Pinch technology and mixed-integer nonlinear programming (MINLP) model, in which the Pinch analysis divided the synthesis problem into upper-Pinch and lower Pinch parts, then they are optimized by the MINLP model separately. Linnhoff and S.Ahmad (1990) repeated the Pinch design many times over various minimum temperature differences and selected the lowest TAC design. The obtained structure was then been optimized by an NLP model to reach the best TAC design. The case study result reported in their work is still competitive compared to the current meta-heuristics based results. Ma et al. (2008) adopted a similar idea to carry out the design work by selecting the HEN structure through the proposed temperature – enthalpy (T-H) diagram, the continuous parameters are improved by a combined method of genetic algorithm (GA) and SA.

The strategy to find the structure by Pinch related method and then to optimize the continuous variables with the NLP model is promising. Compared with purely meta-heuristics based methods, the hybrid method is free of parameter settings and permitted to reach the deterministic result when implemented correctly. The hybrid method is similar to the deterministic sequential synthesis way, but the approach to generate the HEN structure might exhibit considerable difference by applying various Pinch based knowledge. However, the available algorithms seem inappropriate in our context, aiming to find an optimal TAC but under the specific constraint of TT. Indeed, the hybrid methods presented in (Angsutorn et al., 2014) and (Ma et al., 2008) fixed the HEN with a single structure, limiting the chance of improving the TT by changing the structure information. The approach by (Linnhoff and S.Ahmad, 1990) also shaped with a limited number of HENs and that limits to explore a better trade-off result between TAC and TT. Iterating a nonlinear programming (NLP) model over various structures seems to be a promising approach. However, to avoid massive iteration time, the objective is limited to finding a relatively good design result within acceptable iteration times using a structure evolution strategy that allows trying only part of the potential structures.

Analyzing the process of optimizing HEN in the view of heat load distribution, we can interpret it as the process to find the optimal ratio between process HEs and utilities' heat loads. The way to manipulate the ratio can be achieved by changing the heat transfer area, and stream split fractions or the number of HEs. The heat transfer area and stream split fractions are optimized by the NLP model toward a given HEN in the thesis, then the way to manipulate the ratio relies on manipulating the number of HEs, which leads to our HEN iterative strategy. We try to add HEs when the ratio requires increasing, and vice versa, remove one of the HEs in the current HEN when the ratio requires decreasing. Here, an example is provided to illustrate the ratio's evolving process in the effort to find optimal TAC design (Fig 4.9). In the beginning, the ratio starts from 0 without any process HE. Then TAC starts to decrease as energy has been recovered with the ratio increase, and the TAC improving process continues until reaching the local optima result 5. From 1 to 5, it is the process to add HEs, but no more progress can be made by increasing the ratio in point 5. Then it is time to decrease the ratio and reach a new point 6 to restart the searching process and finally reach the global optima result. In general, the HEN optimizing process composes of various combinations of increasing and decreasing ratio processes, in other words, to add or remove HEs. Then it is a problem to decide when to add or remove a HE.

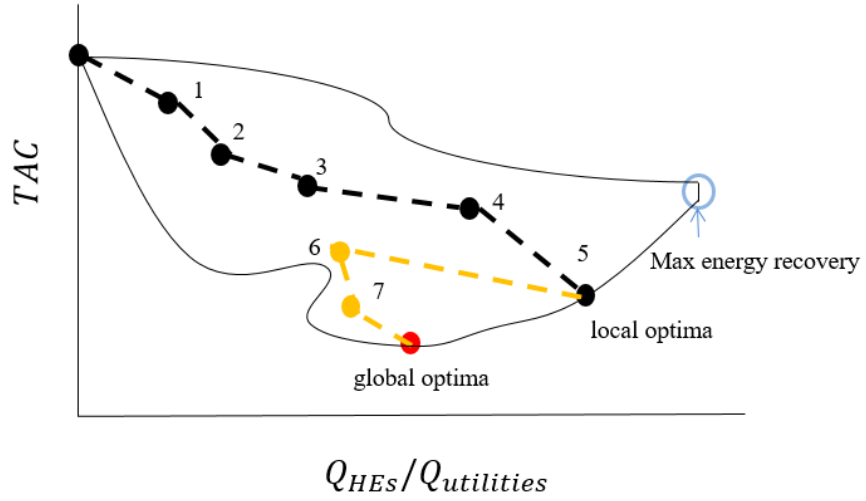

Fig 4.9. Evolutionary process of the heat load distribution during the HEN optimizing process

We propose the IINLP, as shown in Fig 4.10, to implement the methodology. From the starting point, HEN has no process HE, and the system is purely composed of utilities. The direction to decrease TAC is to reduce utility consumption, and the strategy is to add process HE as the shallow green part shows. For a given HEN, the algorithm will iterate all the potential structures having a HE that does not exist in the current HEN and update the HEN by selecting the structure that gets the lowest TAC. To do so, we follow the same method presented in part 3.2.1. For each structure, we optimize the NLP model and use the relaxed model to initiate the optimization. The HEN with a loop will be avoided during the iteration process. The adding process continues until no more progress can be achieved in TAC, and such a point means to increase heat load of process HEs does not allow better results for the given HEN, and reaches the 1st local optimal HEN.

Such a point may not be the global optimal point, a new trade-off point may exist, and it is highly possible that the heat load of process HEs needs to be decreased. The iteration will continue by shifting the direction to decrease the heat loads of process HE by removing one of the existing HEs. The deep green part presents the strategy to delete a HE, by keeping the sub-HENs with the lowest TAC. Therefore, a new start point presents, and the adding process can start again to search for a potential better design. When both the processes of removing and adding HEs cannot contribute to the design's progress, the iteration stops. The strategy does not aim to find the global optimal result, but adjusting the search direction can help escape several local optimal design results.

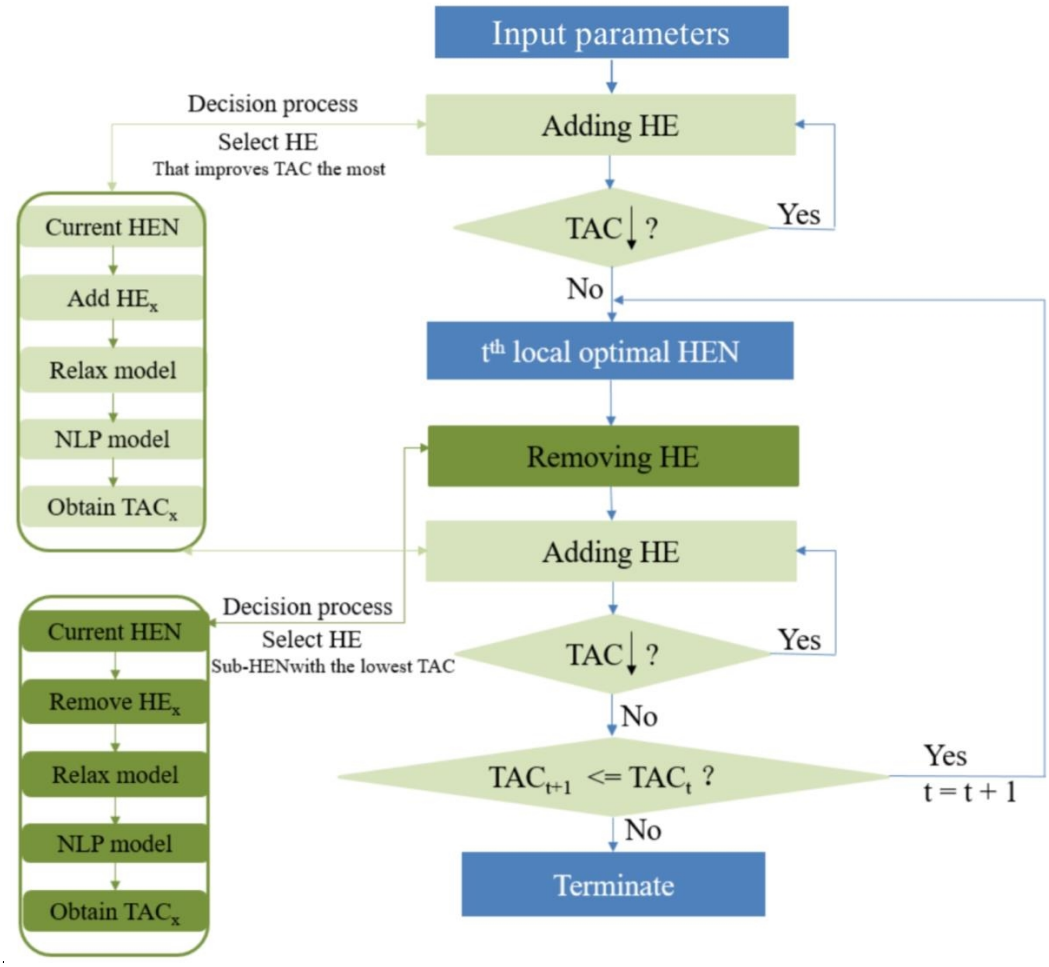

Fig 4.10. IINLP strategy to search the HEN optimal design

4.3.2 SA based strategy

The iteration strategy presented in Fig 4.10 is a heuristics way to select a group of HENs that might contain the optimal cost design structures. The idea is similar to the two-level meta-heuristics based methods, where the evolutionary mechanism is always employed to generate the structures. The difference locates in the way to update the structure during the iteration. The meta-heuristics based method relies on the stochastic mechanism, but our method derived from the HEN characteristics. Among the available meta-heuristic methods, SA is an efficient one for the HEN design problem, so we will use it as a reference to compare it with our iteration strategy.

SA is a multivariable combinatorial optimization algorithm that mimics the physical annealing of solids. SA utilizes the Monte Carlo sampling based on the Metropolis algorithm (Metropolis et al., 1953) to determine the equilibrium state of multi-atomic systems. The global optimal solution is expected to be found by SA only under an infinite time searching condition. In practice, the search time is limited, leading to a sub-optimal result by SA. Since the stochastic mechanism is embedded in the algorithm and shapes with unidirectional characteristics, different runs can generate sub-optimal results. SA has been successfully utilized in HEN synthesis (Athier et al., 1997; Nielsen et al., 1996; Luo et al., 2009; Pavão et al., 2018). The core idea of SA is to reach an optimal atomic configuration that minimizes the internal energy. To reach the optimal point, SA will generate a group of '*Move*'. A *Move* means the condition that a random move is carried out for a random molecule in a random direction with a random length facing with a structure. A new structure appears after each *Move*, and it will be accepted when internal energy decreases but also gets a chance to be accepted by measuring the acceptance function $e^{-\Delta E/T}$, which ΔE corresponds to the difference of internal energy of the structures, and T is the current system temperature. The system temperature T decreases gradually after each structure update, and it decreases gradually to the final stable value that corresponds to the optimal atomic configuration. Such a temperature decreasing process is called the annealing process. Applying the SA in HEN synthesis, ΔE becomes the difference of TAC, *Move* stands for adding/removing HEs in a HEN. The pseudo-code is as followings:

step 1. Generate an initial feasible HEN randomly.
step 2. Select the initial temperature T_{init}, the temperature attenuation factor α, maximum iterations Max_{ite} , and the number of HEs to change each time N_{he}.
step 3. Annealing process:
    3.1 Add or remove N_{he} toward the current HEN.
    3.2 Obtain the TAC by optimizing the corresponding NLP model.
    3.3 Accept or reject the new structure based on the acceptance function.
    3.4 Updating the system temperature by multiplying the current temperature T with α.
step 4. Go back to step 3 when iterations is less than Max_{ite} , and return the current structure when reaching the maximum number of iterations.

To consider the TAC and TT simultaneously, we propose to follow the synthesis by utilizing SA, as shown in Fig 4.11. A random HEN will be generated in the beginning, but it ought to be free of loop. Then, the generated HEN will randomly add or remove the HEs and also make sure there are no loop presents. The newly obtained structure will be optimized by the NLP model, which is explained in detail in part 3.2.1. The new structure will update the current structure when TAC decreases, but it also can be

accepted by comparing the acceptance function with a random value in the range (0, 1). The acceptance step enlarges the chance to escape from the local optimal points of the algorithm. After updating the structure, the annealing temperature will decrease with a coefficient α. Then we check if the maximum iteration number is reached or not to continue the annealing process to try new structures; if yes then we terminate the iteration and return the current HEN as the optimized structure.

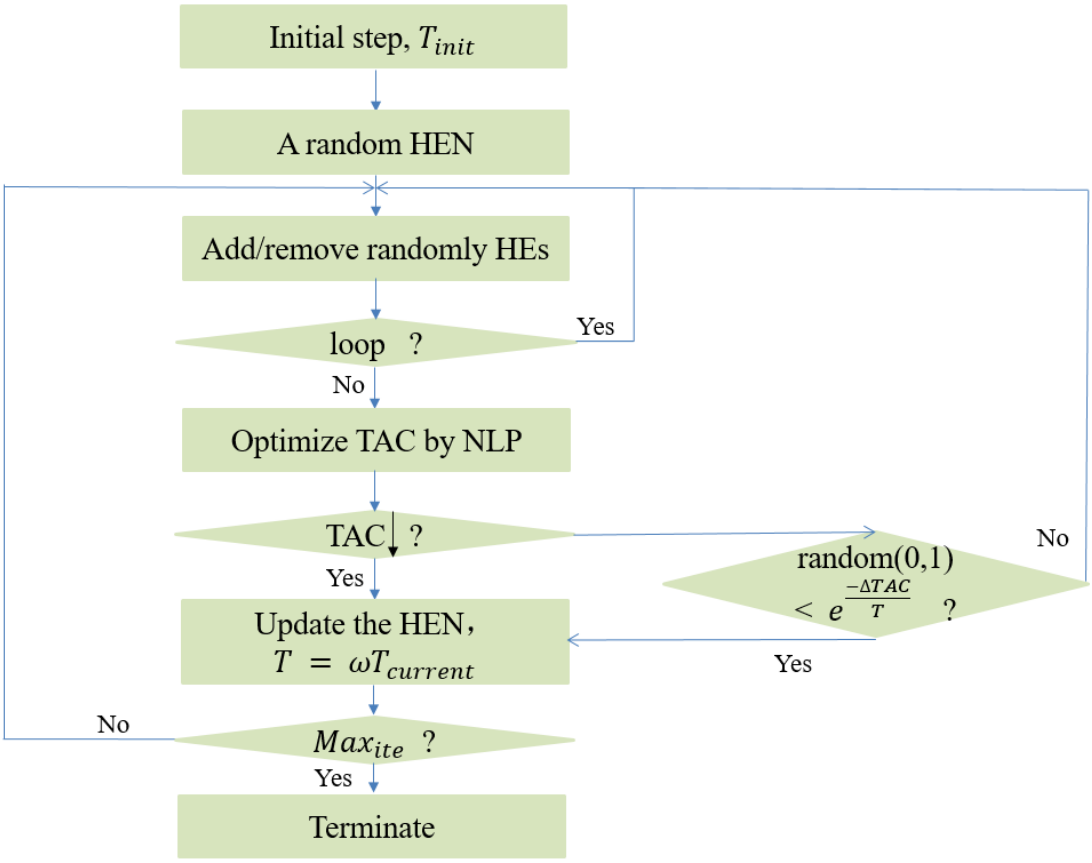

Fig 4.11. SA synthesis process

4.3.3 Comparison of synthesis strategies

Here, we are going to compare the suggested iterative strategy with SA through three medium-large case studies. We take the parameters setting for SA as in the work of (Aguitoni et al., 2019) shown in Table 4.6, since the range of case study scale and optimized TAC is close to the problem we plan to solve the followings. During the iteration, the number of HE to be added or removed in a random value between 1~3 as indicated by N_{he}. Max_{ite} is set to the same iteration time as IINLP approach requires for each case problem. The NLP model solving process is constrained within the 30s or ends with the first local optima point. The computer employed for the calculation is equipped with Intel Xeon (R) CPU 3.5GHz 32Gb, and the NLP models are solved by and Baron 19.3.24 (Kılınç and Sahinidis, 2018). Considering the SA might end with a different optimal result by each run, we repeat the SA synthesis process 3 times.

Table 4.6. Parameters for SA

T_{init}	10,000
N_{he}	1~3
α	0.9

Case 1

It is a typical single period synthesis problem in aromatic plants and consists of 9 process streams proposed by (Linnhoff and S.Ahmad, 1990) and has been widely studied in HEN synthesis works. We take the original data as the nominal working condition, increase the heat capacity flow and inlet temperature of hot streams to create a higher cooling condition, and finally, increase the heat capacity flow and decrease the inlet temperature of cold streams to obtain a higher heating condition. Hence, we have formed a three-period synthesis problem of which detailed parameters are provided in Table 4.7, and each operational period accounts for the same duration.

Table 4.7. Parameters for case 1

Streams	T_{in} ℃			T_{out} ℃	CP(kW/K)			h(kW/m²•K)
Period	1	2	3	All	1	2	3	All
H1	327	360	327	40	100	110	100	0.50
H2	220	242	220	160	160	176	160	0.40
H3	220	242	220	60	60	66	60	0.14
H4	160	176	160	45	400	440	400	0.30
C1	100	100	90	300	100	100	110	0.35
C2	35	35	31.5	164	70	70	77	0.70
C3	85	85	76.5	138	350	350	385	0.50
C4	60	60	54	170	60	60	66	0.14
C5	140	140	126	300	200	200	220	0.60

Area cost($) = 2000 + 70A, CHU(350-250 ℃) = 60 $/(kW•year), CCU(15 - 30 ℃) = 6 $/(kW•year), $\varepsilon = 1$, $\Delta T_{min} = 1K$
hhu = 0.5(kW/m²•K), hcu = 0.5(kW/m²•K)

Table 4.8. Comparison result of IINLP and SA of case 1

	Optimized TAC ($)	Difference-TAC
IINLP	2,986,794	0
SA1	3,025,190	1.28 %
SA2	3,725,680	24.74 %
SA3	3,080,000	3.12 %

The comparison of IINLP and SA optimized results are summarized as in Table 4.8. It takes about 11,300s for IINLP to terminate the optimization process. The optimized HEN provided by IINLP exhibits the lowest TAC. The optimized results of SA varied a lot in three rounds. The best one is very close to the result by IINLP with about 1.28% deviation. It also deserves to mention that the best TAC design found by SA2 is about 20% larger than SA1 and SA3. It means that the stochastic mechanism requires many iterations to confirm the best result. The optimized HEN structure by IINLP is depicted in Fig 4.12, along with operational parameters in Table 4.9. It gets 7 processes HEs, each stream ends up with a utility, and all the streams are connected with at least one HE. Bypasses are widely installed, and stream split exists in the 1st stage of H1 and C3, in which H1 was split into three branch streams, and C3 was split into two.

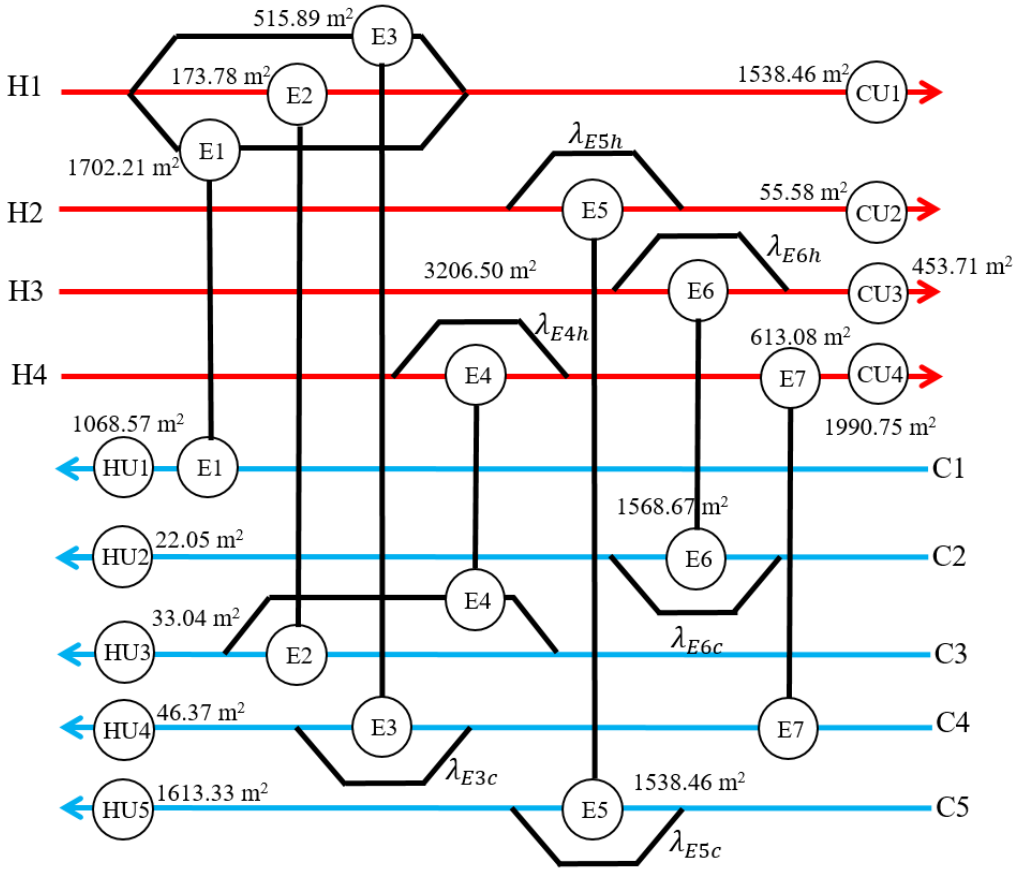

Fig 4.12. Optimized HEN with lowest TAC of case 1 (obtained by IINLP)

Table 4.9. Heat load and stream mass ratio of optimized HEN, case 1

HEs	P1			P2			P3		
	Q(kW)	FH	FC	Q(kW)	FH	FC	Q(kW)	FH	FC
E1	15615.13	0.748	1	19800	0.861	1	16083.51	0.682	1
E2	1406.37	0.058	0.023	43.45	0.0014	0	2973.94	0.119	0.067
E3	4457.58	0.194	1	3815.87	0.137	0.533	4750.67	0.199	1
E4	17143.63	1	0.977	18506.55	0.628	1	19392.19	1	0.933
E5	9600	1	1	12672	1	1	9600	0.809	0.706
E6	8834.62	1	1	9030	0.738	0.994	9289.83	1	1
E7	2142.42	1	1	2784.13	1	1	2219.66	1	1
CU1	7220.91	-	-	11540.68	-	-	4891.88	-	-
CU2	0	-	-	1760	-	-	0	-	-
CU3	765.38	-	-	2982	-	-	310.16	-	-
CU4	18713.95	-	-	27549.32	-	-	16388.15	-	-
HU1	4384.87	-	-	200	-	-	7016.49	-	-
HU2	195.38	-	-	0	-	-	912.66	-	-
HU3	0	-	-	0	-	-	1311.37	-	-
HU4	0	-	-	0	-	-	685.66	-	-
HU5	22400	-	-	19328	-	-	28680	-	-

FH: hot stream split ratio; FC: cold stream split ratio

The TAC evolution results found by the methods are given in Fig 4.13. IINLP keeps escaping the local optima points as the searching process goes on, and reached the final optimal result at about 9,500s. SA in three runs demonstrates different evolutionary processes. They both made significant progress at the beginning of the searching time. SA2 reached the final result at about 4,000s, and get no more progress afterward. SA1 and SA3 might start with a promising structure that enables them to escape from more local optimal points to have more progress as the searching process goes on.

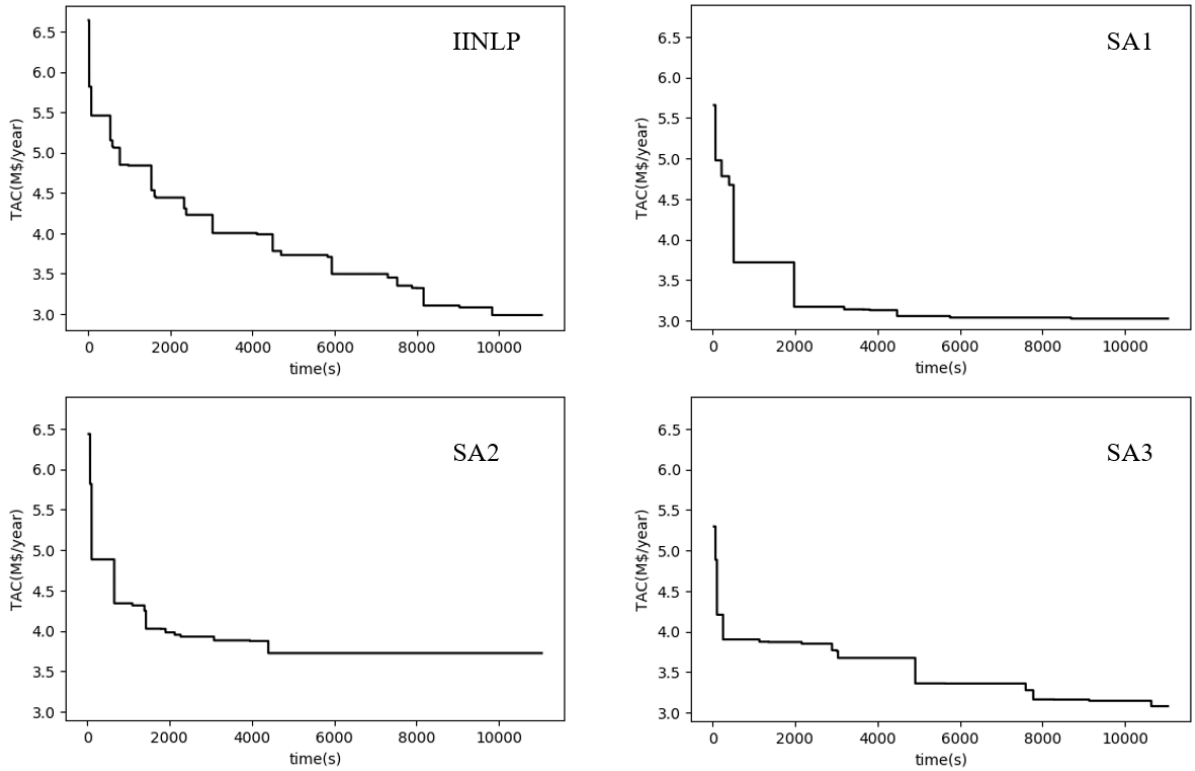

Fig 4.13. TAC evolution during the optimization of IINLP and SA (repeated 3 times) of case 1

Case 2

Case 2 is a single period synthesis problem that originated from the doctoral thesis (Ahmad, 1985), a widely studied 10 streams case with no fixed cost for HE units. Huang et al. (2012) suggested adding fixed cost (8,000$/year) to make it more realistic, and such strategy has also been adopted by (Pavão et al., 2016). Here, we take the same procedure as in case 1 to add maximum heating and maximum cooling operational periods to form a three-periods synthesis problem with detailed stream parameters provided in Table 4.10.

The comparison results are shown in Table 4.11. After searching for about 12,851s, the IINLP algorithm reached almost equivalent TAC design compared with the optimal results found by SA in three runs, and with about a slight advantage. The results generated by SA in three runs differ a little, SA3 found the optimal solution that is rather close to the result of IINLP, but SA1 and SA2 get 2.63%, 4.73% higher TAC design separately. The optimized HEN of IINLP is illustrated in Fig 4.14, and corresponding operation parameters are given in Table 4.12. In which, all streams are equipped with at least one process HE and end up with the utility, and only cold stream C4 get split streams. Bypasses are installed on both the hot and cold sides of E5.

Table 4.10. Parameters for case 2

Streams	T_{in} ℃			T_{out} ℃	CP(kW/K)			h(kW/m²•K)
Periods	1	2	3	All	1	2	3	All
H1	85	93.5	85	45	156.3	171.93	156.3	0.05
H2	120	132	120	40	50	55	50	0.05
H3	125	137.5	125	35	23.9	26.29	23.9	0.05
H4	56	61.6	56	46	1,250	1,375	1,250	0.05
H5	90	99	90	85	1,250	1,375	1,250	0.05
H6	225	247.5	225	75	50	55	50	0.05
C1	40	40	36	55	466.7	466.7	420.03	0.05
C2	55	55	49.5	65	600	600	660	0.05
C3	65	65	58.5	165	180	180	198	0.05
C4	10	10	9	170	81.3	81.3	89.43	0.05

Area cost($) = 8000 + 60A, CHU(200-199 ℃) = 100 $/(kW•year), CCU(15 - 25 ℃) = 15$/(kW•year), $\varepsilon = 1$, $\Delta T_{min} = 1K$
hhu = hcu = 0.05(kW/m²•K)

Table 4.11. Comparison result of IINLP and SA of case 2

	Optimized TAC ($)	Difference-TAC
INLP	7,621,837	0.00 %
SA1	7,822,234	2.63 %
SA2	7,982,709	4.73 %
SA3	7,624,355	0.03 %

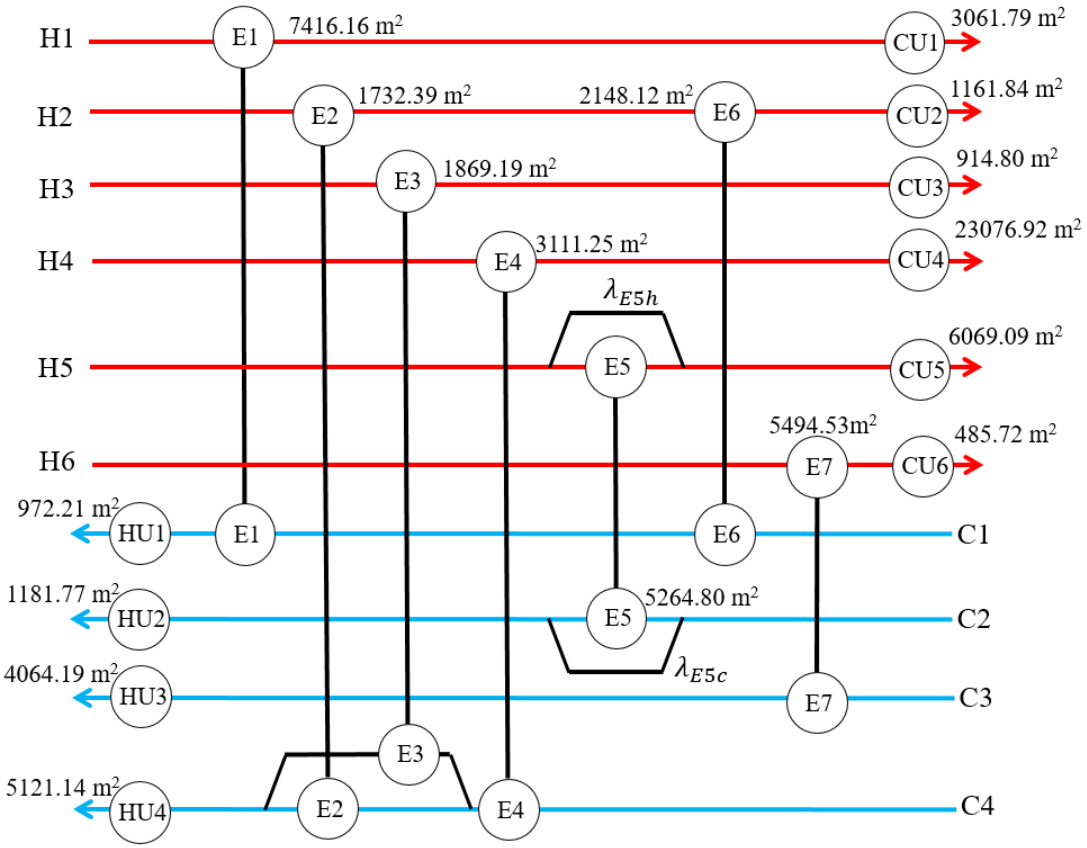

Fig 4.14. Optimized HEN with lowest TAC of case 2 (obtained by IINLP)

Table 4.12. Heat load and stream mass ratio of optimized HEN, case 2

HEs	P1			P2			P3		
	Q(kW)	FH	FC	Q(kW)	FH	FC	Q(kW)	FH	FC
E1	4222.78	1	1	5176.58	1	1	4673.65	1	1
E2	1807.08	1	0.502	2058.50	1	0.524	1909.87	1	0.511
E3	1560.17	1	0.498	1783.00	1	0.476	1615.82	1	0.489
E4	2271.31	1	1	2551.06	1	1	2405.48	1	1
E5	5264.80	1	1	6000	0.438	0.760	6165.81	1	1
E6	1410.33	1	1	1823.92	1	1	1476.03	1	1
E7	7174.01	1	1	8737.01	1	1	7500.00	1	1
CU1	2029.22	-	-	3162.03	-	-	1578.34	-	-
CU2	782.59	-	-	1177.57	-	-	614.10	-	-
CU3	590.83	-	-	911.73	-	-	535.18	-	-
CU4	10228.69	-	-	18898.94	-	-	10094.52	-	-
CU5	985.20	-	-	13250.00	-	-	84.19	-	-
CU6	325.99	-	-	750.49	-	-	0	-	-
HU1	1367.39	-	-	0	-	-	3604.34	-	-
HU2	735.20	-	-	0	-	-	4064.19	-	-
HU3	10825.99	-	-	9262.99	-	-	13587.00	-	-
HU4	7369.44	-	-	6615.44	-	-	8467.06	-	-

FH: hot stream split ratio; FC: cold stream split ratio

Checking the evolution of TAC over time depicted in Fig 4.15, IINLP takes considerable progress at the beginning of the searching process, and keeps finding lower TAC design with escaping quite a lot local optima points, and reaches the final design in about 11,500s. SA in three runs also illustrates quite different searching processes. SA1 shows similar processes as IINLP does but was unable to explore better results since 6,000s. SA2 made significant progress in the beginning, and almost get no better result until 10,000s. SA3 started with a relatively low TAC design structure, and ended up with an optimal TAC design close to the result by IINLP even without experiencing too much local optima points.

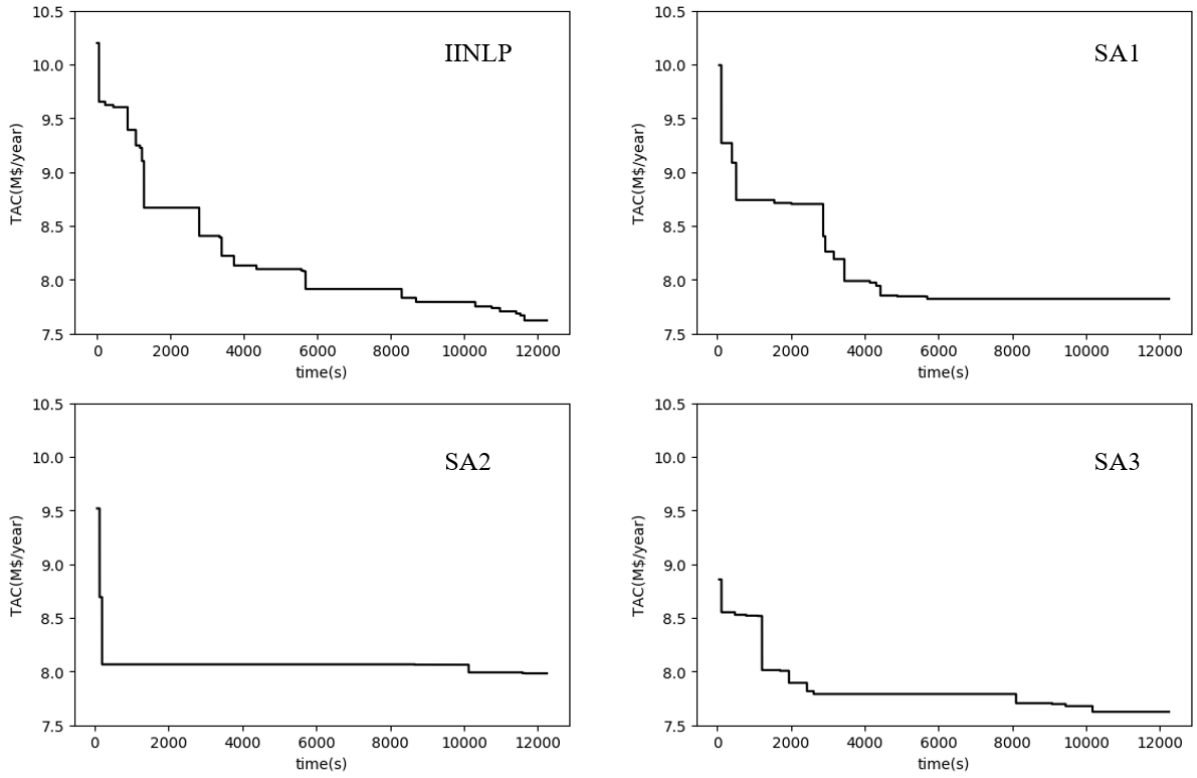

Fig 4.15. TAC evolution during the optimization of IINLP and SA (repeated 3 times) of case 2

Case 3

It is a large scale problem composed of 8 hot streams and 7 cold streams that originated from (Escobar et al., 2013b), and we transformed it into a three periods synthesis problem by keeping the original data as the nominal condition and adding maximum heating and maximum cooling periods with detailed parameters shown in Table 4.13.

The IINLP requires 20,228 s to terminate the searching process. The comparison of the optimized result is provided in Table 4.14. The IINLP locates a lower TAC (5.24%) design than the best SA result within the same iteration time. We require more searching time than case 1 and case 2 because of the increasing number of process streams, and the optimizing difficulty arises for each HEN.

The optimized HEN structure by IINLP is depicted as in Fig 4.16, except H4, H7, H8, C6, and C7 all the other streams get process HEs to recover heat. The temperature level of H1 is relatively high but still gets no process HE. This means that the model, in this case, might prefer lower number of units. Bypasses are placed on both sides of E2, E3, E4, and E5, and the stream split does not exist in the structure.

Table 4.13. Parameters for case 3

Streams		T_{in} ℃			T_{out} ℃			CP(kW/K)	h(kW/m^2•K)
Periods	1	2	3	All	1	2	3	All	
H1	180	198	180	75	30	33	30	2	
H2	280	308	280	120	60	66	60	1	
H3	180	198	180	75	30	33	30	2	
H4	140	154	140	40	30	33	30	1	
H5	220	242	220	120	50	55	50	1	
H6	180	198	180	55	35	38.5	35	2	
H7	200	220	200	60	30	33	30	0.4	

Streams		T_{in} °C		T_{out} °C		CP(kW/K)		h(kW/m²•K)
Periods	1	2	3	All	1	2	3	All
H8	120	132	120	40	100	110	100	0.5
C1	40	40	36	230	20	20	22	1
C2	100	100	90	220	60	60	66	1
C3	40	40	36	190	35	35	38.5	2
C4	50	50	45	190	30	30	33	2
C5	50	50	45	250	60	60	66	2
C6	90	90	81	190	50	50	55	1
C7	160	160	144	250	60	60	66	3

Area cost($) = 8000 + 500A$^{0.75}$, CHU(325 -325 °C) = 80 $/(kW•year), CCU(25 - 40 °C) = 10$/(kW•year), ε = 1, $\Delta T_{min} = 1K$, hhu = 1(kW/m²•K), hcu = 2(kW/m²•K)

Table 4.14. Comparison result of IINLP and SA of case 3

	Optimized TAC ($)	Difference-TAC
INLP	2,147,698	0
SA1	3,066,998	42.80 %
SA2	2,260,302	5.24 %
SA3	2,615,960	21.80 %

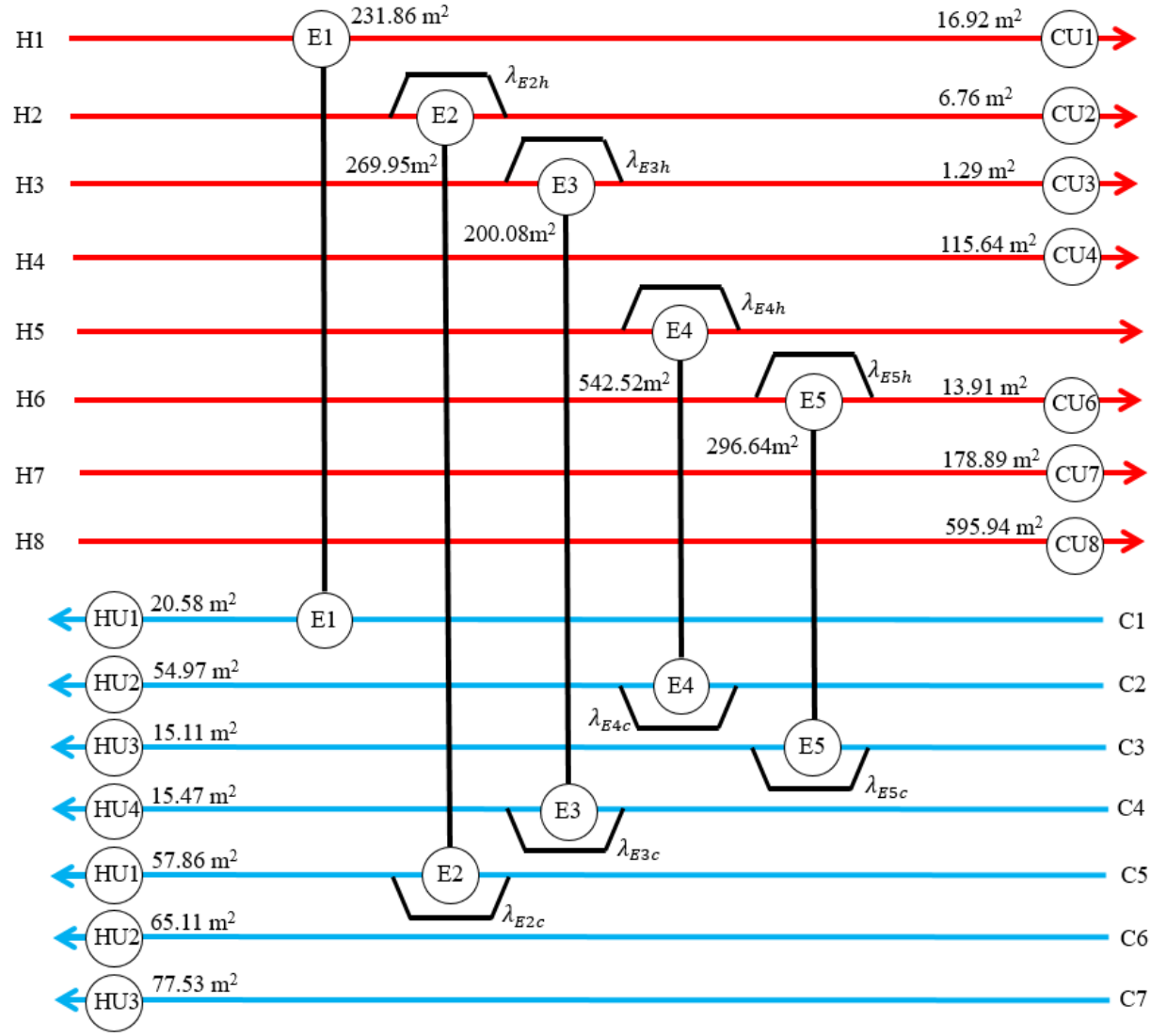

Fig 4.16. Optimized HEN with lowest TAC of case 3 (obtained by IINLP)

Table 4.15. Heat load and stream mass ratio of optimized HEN, case 3

HEs	P1			P2			P3		
	Q(kW)	FH	FC	Q(kW)	FH	FC	Q(kW)	FH	FC
E1	2725.22	1	1	3098.97	1	1	3021.80	1	1
E2	9600.00	0.857	0.968	12000.00	1	1	9600.00	0.798	0.926
E3	3150.00	0.973	0.881	4003.42	1	1	3150.00	0.818	0.914
E4	4896.82	1	1	5250	0.880	0.924	5000	1	1
E5	5000.00	0.907	0.938	6709.99	1	1	5000.00	0.806	0.859
E6	4375.00	1	0.996	5128.38	1	1	4375.00	0.919	0.953
CU1	424.78	-	-	960.03	-	-	128.20	-	-
CU2	0	-	-	408.00	-	-	0	-	-
CU3	0	-	-	55.58	-	-	0	-	-
CU4	3000.00	-	-	3762.00	-	-	3000.00	-	-
CU6	0	-	-	377.12	-	-	0	-	-
CU7	4200.00	-	-	5280.00	-	-	4200.00	-	-
CU8	8000.00	-	-	10120.00	-	-	8000.00	-	-
HU1	1074.78	-	-	701.03	-	-	1246.20	-	-
HU2	2200.00	-	-	490.00	-	-	3580.00	-	-
HU3	875.00	-	-	121.62	-	-	1554.00	-	-
HU4	1050.00	-	-	196.58	-	-	1635.00	-	-
HU5	2400.00	-	-	0	-	-	3930.00	-	-
HU6	5000.00	-	-	5000.00	-	-	5995.00	-	-
HU7	5400.00	-	-	5400.00	-	-	6996.00	-	-

FH: hot stream split ratio; FC: cold stream split ratio

The TAC evolutionary processes are given in Fig 4.17. IINLP reached the final optimal result gradually, as in the previous two cases, by experiencing many local optima points. SA1 starts with a relatively low TAC structure but made only two progressions during iterations. SA3 made three improvements, with each step moves larger than SA1, and reach the final result in about 9,000s. SA2 made relatively more progressions than the other two runs. The SA in three runs made fewer progressions than the above two cases, which might be caused by the number of streams in case3 (15 streams), SA generates easily a much more complicated HEN, and the model gets more difficulty converging within a given optimization time, thus can hardly locate better results.

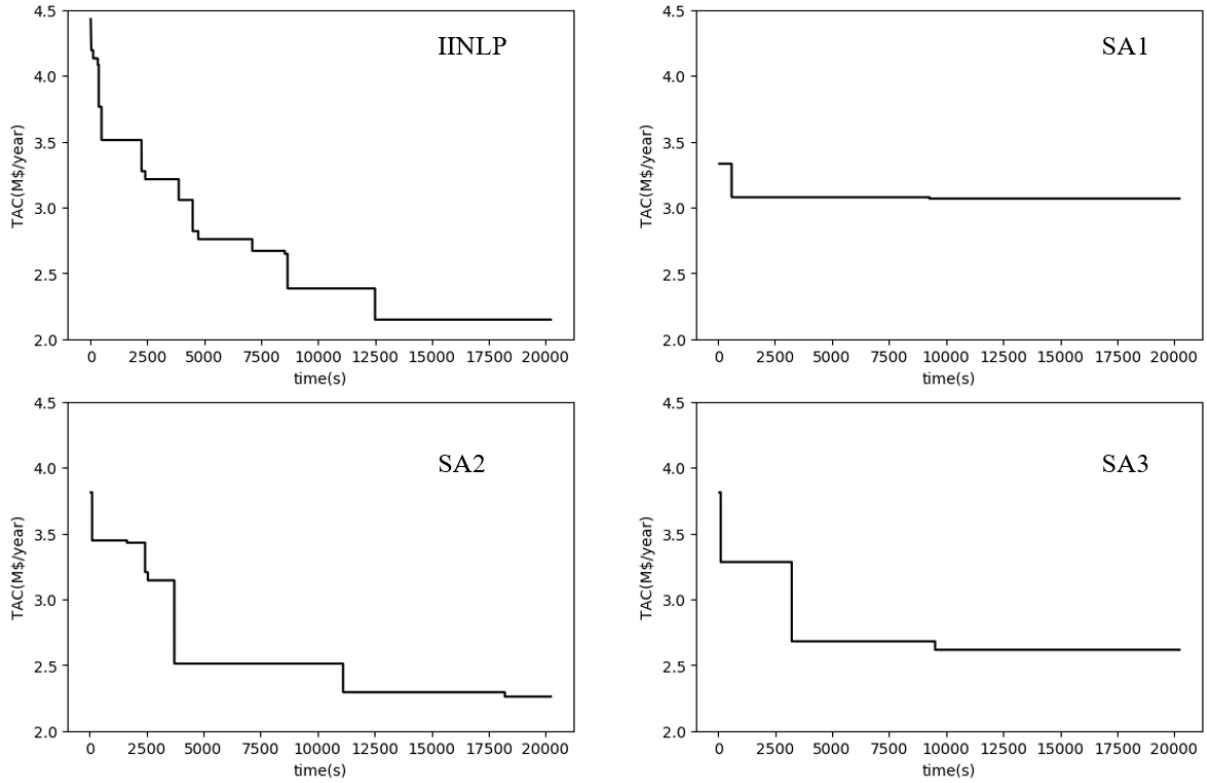

Fig 4.17. TAC evolution during the optimization of IINLP and SA (repeated 3 times) of case3

The proposed IINLP has been compared with SA through three medium-large HEN multi-period synthesis problems, IINLP has shown competitive searching ability. IINLP finds better solutions in all the three cases than SA (between 0.03 % and 42.80 % lower TAC). Even SA has run three times, which corresponds to about triple computational time. The performance difference of SA can be as vast as about 37 % in different runs, which confirmed the algorithm's stochastic characters, and the implementation always requires many runs to locate the best design.

4.4 TAC-TT trade-off result

We employ the same three case studies in the above part to study the TAC-TT trade-off result by following the synthesis methodology shown in Fig 4.10, together with the improved HEN dynamic model. All the three case studies get three operational periods, we choose to study the TT of all the hot streams when the system changes from period 3 to period1, there might be other operational changeovers, and the selection depends on the users or the operational requirements. The 0.1% deviation (of final stable value in K) is selected as the criteria to calculate the TT of the stream outlet temperature function when changing the operational period. The outlet temperature of all hot streams are taken as target variables, and the HEN TT takes the maximum TT among the sub-TT of all the hot streams. Two scenarios of iterations are used: IINLP and SA (3 times).

4.4.1 Case 1

The description of case 1 is given in part 4.3.3. Fig 4.18 shows the trade-off results between TAC and TT, the red dots stand for each optimized HEN, and the black curves depict the pseudo-Pareto-front of each trade-off result. The TT ranges from 150s to 4,500s for all methods of iterations. We also observe that a good TAC design can have a very high or very low TT, which explains why a trade-off result is useful to the designer to decide the best solution according to specific constraints on TT.

IINLP provides the best design (see part 4.3.3 for more information) with TT of about 1,500s. It is larger than the TT of the optimal TAC design by SA1 (about 1,000s), and also longer than the optimal TAC design of SA3 but almost the same time response as the optimal TAC design by SA2. On the other hand, the pseudo-Pareto-front of IINLP shows a significant reduction of TT while sacrificing a little the TAC. Even though it is still longer than the best optimal design in SA1, but IINLP gets an advantage over SA2 and SA3.

Putting all the pseudo-Pareto-fronts of various scenarios together as Fig 4.19 illustrates, it is easier to read the advantage of each run. In the region with lower TAC, IINLP provides competitive solutions than 3 rounds of SA (IINLP gives the lowest TAC design, but the TT is higher than the solution by SA with a slightly higher TAC). In the region with a fast TT requirement, IINLP can also propose solutions with lower TAC than SA in three runs. The dark dotted line combined all the points in the pseudo-Pareto-front of both IINLP and SA to reach an integrated pseudo-Pareto-front, and finally, 7 out of 11 points come from the IINLP result.

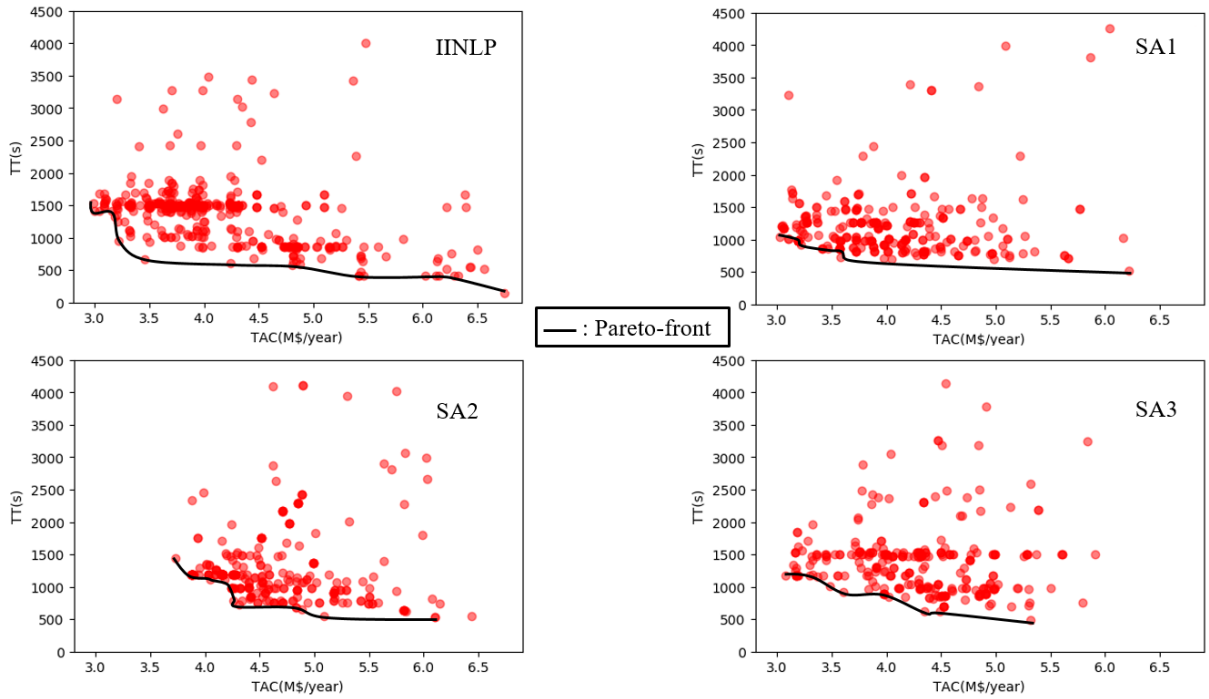

Fig 4.18. TAC-TT trade-off results of case 1

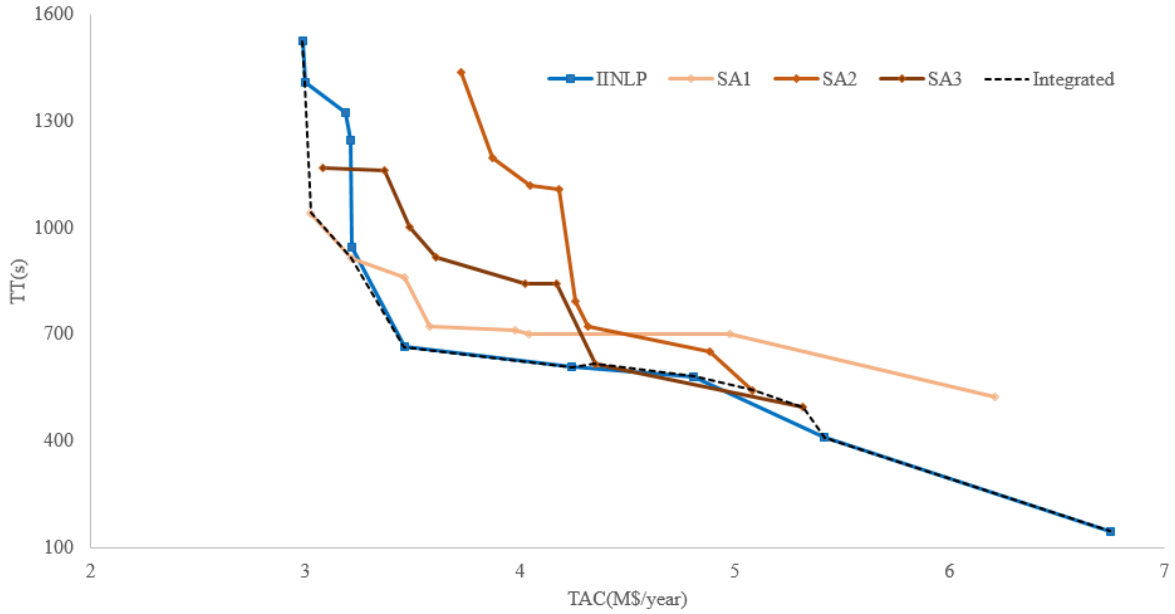

Fig 4.19. Pseudo-Pareto-fronts of various runs of case1

4.4.2 Case 2

The data of case 2 was presented in part 4.3.3. The TAC-TT result is provided in Fig 4.20. The TT ranges from 3,000s to 5,000s for various TT designs in all scenarios. Compared to case 1, TT is quite long in average, and the reason might be the heat transfer coefficients of the streams are about 10% compared to case 1 but required to transfer a similar level of heat, which leads to larger heat transfer area and correspondingly larger thermal inertia of metal wall that need longer time to change the operational period.

Comparing the optimal TAC designs of different iterations, SA1 requires the least TT, which is about 3,956s, SA2, and SA3 for about 4,492s and 4,757s separately, IINLP corresponds to about 4,313s. Putting all the pseudo-Pareto-fronts in Fig 4.20, the dark dotted line illustrates the integrated Pareto-front by combining all the points generated by both INLP and SA. Except for the most optimal point found by IINLP, most of the points in the integrated front come from the SA. It also deserves to mention that for the results provided by SA2, most of the HENs in the pseudo-Pareto-front are not competitive than the results given by IINLP (means the IINLP finds a design with lower TAC at the same level of TT).

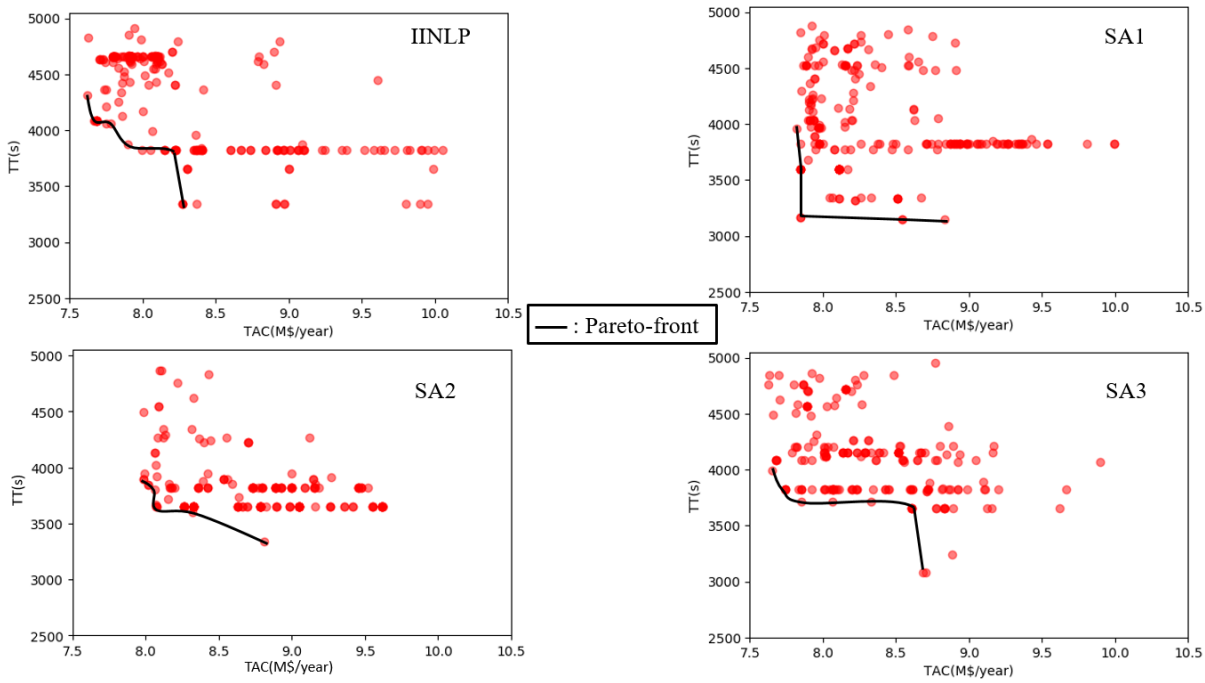

Fig 4.20. TAC-TT trade-off results of case 2

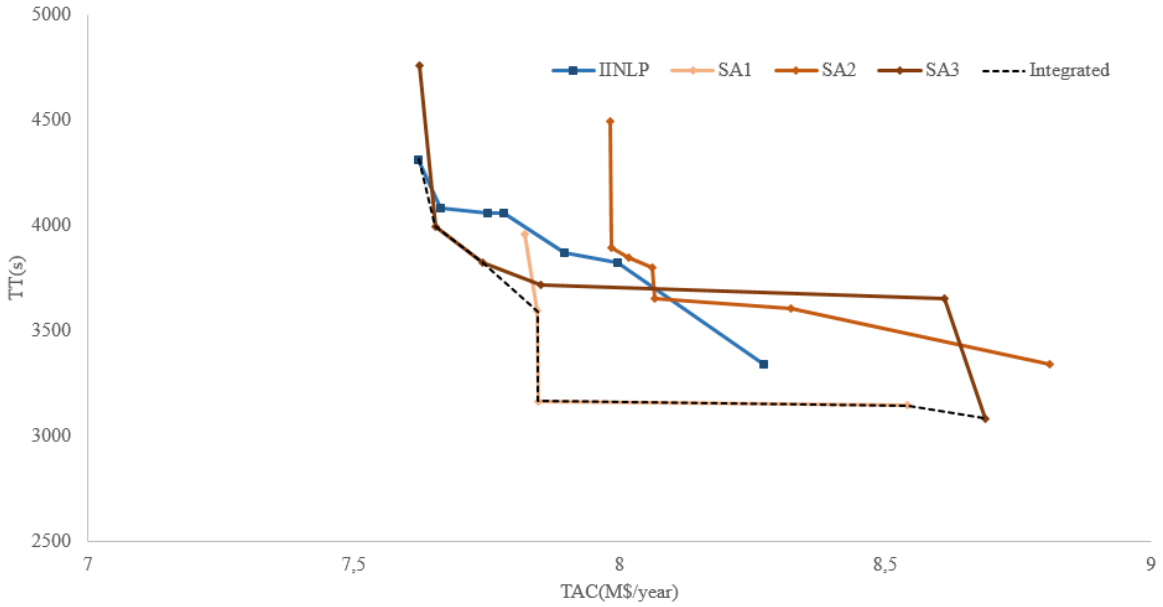

Fig 4.21. Pseudo-Pareto-fronts of various runs of case2

4.4.3 Case 3

A full description of case 3 was given in part 4.3.3. The trade-off result is provided in Fig 4.22 (a), the TT ranges from 100s to 4,500s. Since most of the designs locate within the range between 100s and 1,200s, and removing those HENs with rather long TT do not affect the result of the pseudo-Pareto-front for each iteration, we focus on the partial results are shown in Fig 4.22 (b). Comparing the best TAC optimal design in each Pareto-front, the optimal HEN found by INLP gets about 526s, and the SA in three runs is 511s, 909s, 629s individually. The relatively high heat transfer coefficient in this case study might be the main reason to have small heat transfer areas, thermal inertial, and correspondingly very low TTs.

Checking all the pseudo-Pareto-fronts in Fig 4.23 can help us better compare the IINLP and SA in this case study. It was evident that the optimal points found by IINLP dominate almost all the range of TACs, which is to say, for all the results found by SA, IINLP can provide a design with lower TAC and fast TT. We can observe that the pseudo-Pareto-fronts of SA in three runs are all in the right-upper region part of the pseudo-Pareto-front by IINLP, except limited points provided by SA to expand the integrated curve. Finally, IINLP contributed 10 out of 12 points in the integrated pseudo-Pareto-front.

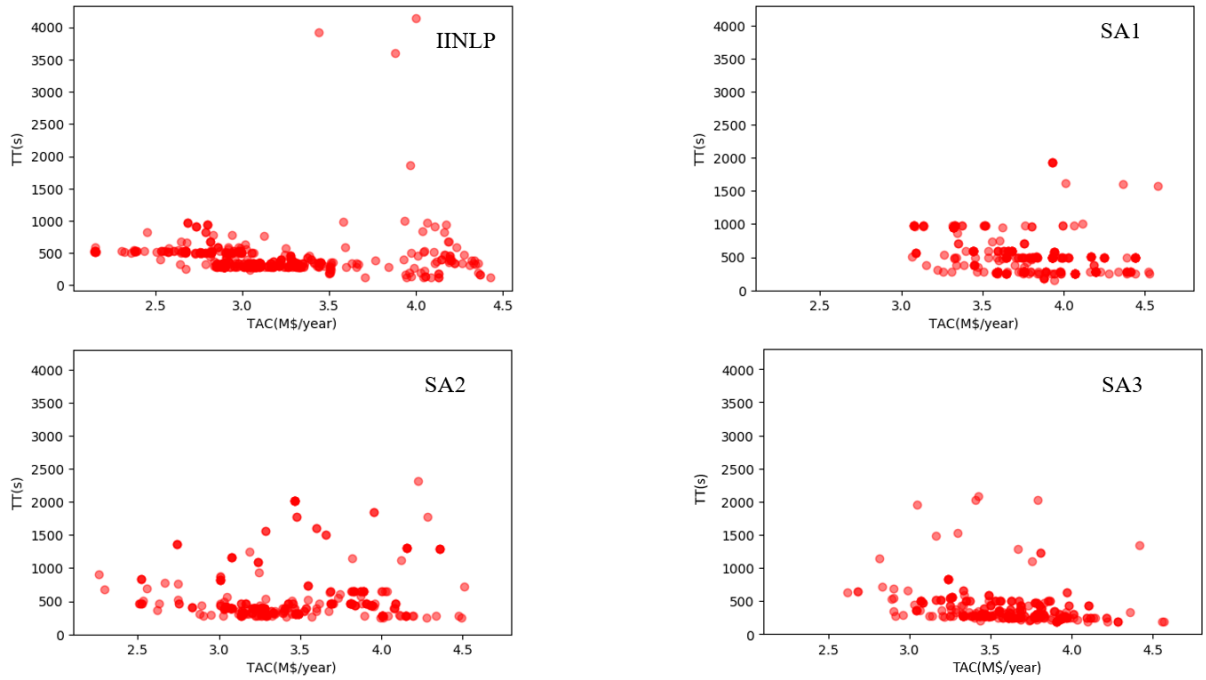

(a) Original results

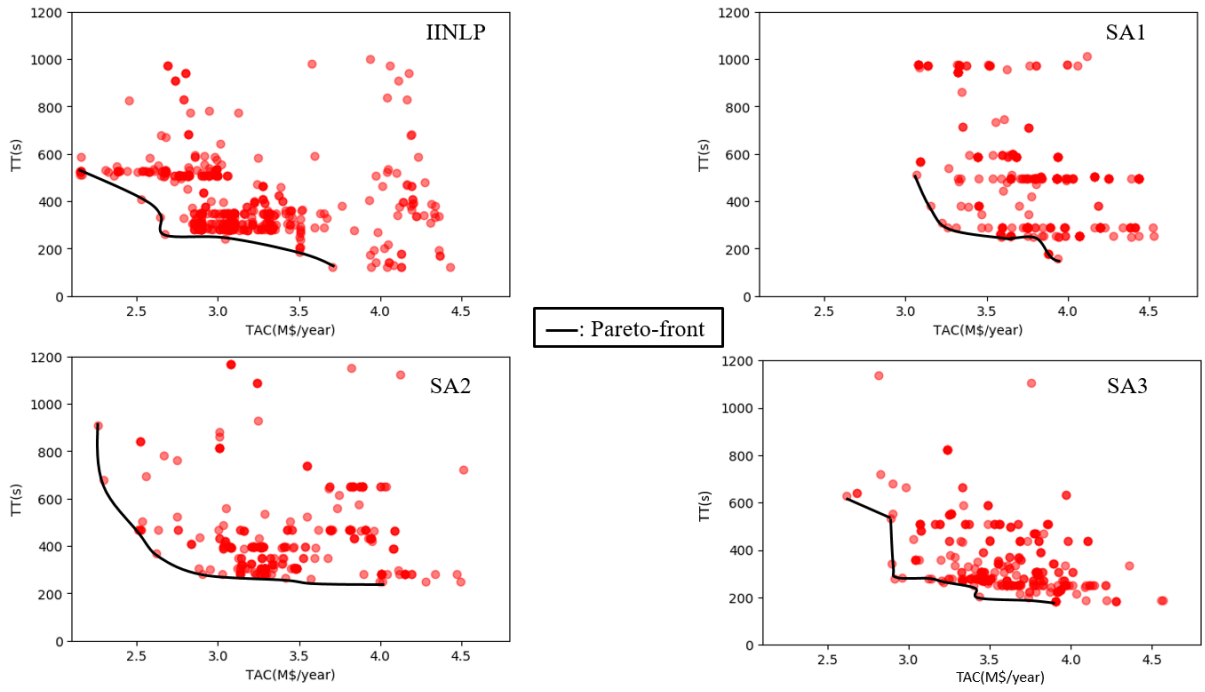

(b) Partially enlarged graphs

Fig 4.22. TAC-TT trade-off results of case 3

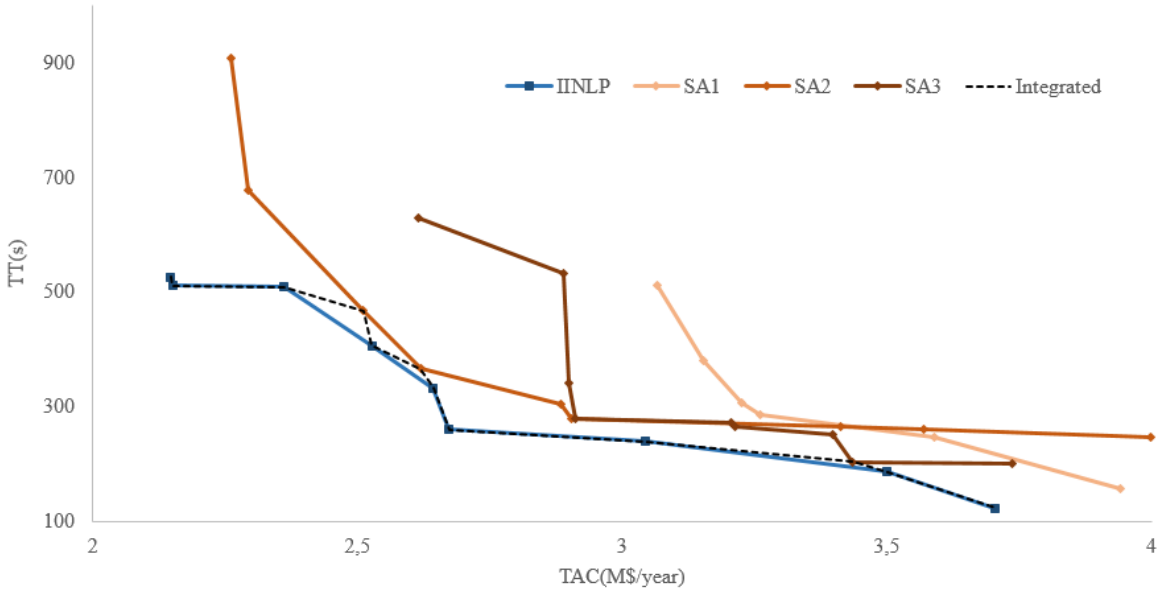

Fig 4.23. Pseudo-Pareto-fronts of various runs of case3

The time calculation discussed above does not include the calculation time of TT, which are 131s, 310s, 243s for case1, case2, and case3 of the IINLP method separately, and corresponding to less than 2% of the TAC searching time. There are two ways to implement the calculation in the code. The first one is to build an analytic solution for each HEN in all the period changeover conditions for each target stream and then apply it without iterating the calculation logic. The other way is to bring the numerical calculation into the logic and repeat it many times. We select the second because of the simple implementation of the code. The first way also requires considerable effort to build pure analytic solutions, but it will save time when applied in massive iterations. If the TT calculation time accounts for a considerable part in the whole iteration time, it can be improved by following the first approach. However, it is not the case in our context, and out of the thesis's scope to optimize this point.

Another point that needs to be taken care of is the potential TT deviation compared with the real result, as stated in part 3.3.4.2, which can be about 33 %, and it is a parameter-dependent problem. However, TT gets about 30 times difference for various designs in case 1, 66 % difference in case 2, and more than 40 times difference in case 3. Therefore, we believe the TT calculation model can help us differentiate those HENs are faster or slower. However, it is better to validate such a relation in the TT aspect by seeking real results, such as the numerical simulation way.

The above TAC-TT trade-off results of the three case studies exhibit the successful application of the improved method to design medium-large scale HEN multi-period problems. Compared with the SA, IINLP can find competitive results both in TAC and TT aspects. Through the three integrated pseudo-Pareto-front graphs above, IINLP and SA can only dominate in certain regions, neither of them can dominate another. The IINLP exhibits an average performance of SA in three runs.

4.5 Conclusion

This chapter improved two points of the preliminary method proposed in Chapter 3. The first one is to provide an improved dynamic model to directly obtain the HEN outlet temperature in the time domain without the concern of inverse Laplace transform. The second one is an improved iterative strategy to reduce the number of structures to evaluate. These two methods enable the proposed design methodology to be feasible in medium-large scale synthesis problems.

The dynamic model improvement aims to decompose the target temperature function into simple expressions in the Laplace domain so that their function in the time domain can be obtained directly by using the Laplace transform table. The basis to work out in such direction is that the temperature function expressions are the combinations of $\frac{b}{s+a}$ or $const$, the decomposition can be made before reaching the final complex function directly. The outlet temperature function consists of various pathways from the inlet sources to the target, and the decomposition can be carried out toward each pathway individually. Another advantage of the model is the capability to deal with various inlet change forms, such as the step, ramp, exponential or the combinations of them, etc.. An example with 24 pathways was taken to illustrate the decomposition for each pathway and obtain the function in time domain correspondingly. The improved dynamic model has been tested against a 10 streams HEN from the literature that faces inlet temperature change, mass flowrate change, and simultaneous change under the step signal and ramp signal conditions. The improved dynamic model has been compared with the simulation results by Dymola, which illustrates perfect coherence.

For the IINLP, it originated from the Pinch idea, that the optimizing process of HEN design keeps finding the new trade-off point between the heat load of process HEs and utilities. From the start of the search space, increase the heat load of HEs can help to decrease the TAC but it will stop to contribute when meeting the local optima, and then it might be needed to step back a bit to increase the heat load of utilities to restart the searching process by adding the HEs to recover more heat, the whole iteration stops when no more progress can be made. The strategy was validated against SA in three medium-large problems. Because of its stochastic mechanism, SA was applied three times, and the results have confirmed that the best-found solution can vary each run significantly. IINLP was able to find better TAC designs in all the three cases (lower TAC between 0.03 % and 42.8 %). Finally, we carried out the TT calculation with the new analytical model for those three cases to obtain the TAC-TT results. The improved dynamic model works successfully in three case studies. The TT results range from 150s to 4,500s in case1, 3,000s to 5,000s in case2, and 100s to 4,500s in case3. We compared the pseudo-Pareto-fronts of the IINLP and SA in three runs and reached the integrated pseudo-Pareto-front for all the three case studies, and found that IINLP contributes (7/11, 1/11, 10/12 in three cases individually). Neither of the IINLP or the SA can dominate the other one, and IINLP illustrates an average performance of SA in three runs. In general, the improved HEN multi-period synthesis method that considers time response can work successfully in medium-large scale problems.

Résumé du chapitre 5

La méthode améliorée du chapitre 4 a été appliquée dans un cas réel de l'industrie, qui est un système de préchauffage par distillation. Le problème se compose de six flux chauds, deux flux froids et deux périodes de travail. Nous avons supposé certains paramètres pour réaliser l'étude en raison du manque d'informations adéquates de la source. Les résultats ont montré que de nombreux modèles obtiennent une valeur TAC assez proche (écart de 1,83%), mais diffèrent assez largement (85,26%) dans l'aspect TT. La prise en compte de la réponse temporelle dans la phase de conception est plutôt utile. Même pour diverses conceptions proches des performances optimales du TAC, elles peuvent présenter une différence considérable dans l'aspect TT, ce qui pourrait considérablement retarder la période de transition du système entre les périodes d'exploitation.

Chapter 5 – Industrial Implementation in a Distillation Preheating Process

5.1 Description of the process

This chapter tests the developed methodology in a real industrial case problem that belongs to an oil refinery plant, presented in chapter 8 of the doctoral thesis (Payet, 2018). In her thesis, the HEN synthesis was carried out by Pinch technology to obtain the maximum energy recovery design, while in this thesis, we aim to provide a trade-off result between TAC and transition time (TT).

The atmospheric distillation preheating is an energy-intensive process in the refinery plants. The preheating process has already been equipped with a heat exchanger network to recover part of the products' heat. The configuration of the flow diagram is provided in Fig 5.1. Atmospheric distillation is the first operational unit for refinery processes. In this step, the crude oil was separated into different products according to their boiling point. These products are then cooled to the specification required in downstream unit operations. The crude oil must undergo a heating stage in the first part of the preheating train to reach the desalting process's temperature. During this operation, the crude oil is brought into contact with water to remove most of the salts. Then, the second step was followed before entering the oven, aiming to increase the crude oil's temperature to the inlet temperature of the distillation column and often close the boiling point. The preheated crude oil will be separated into five sections at the specific temperature, which are:

1. Distillate products (Top): it contains the most volatile fractions of crude oil, it is the basis of naphta and gasoline.
2. Kerosene: it is the basis of fuel in aviation and also termed as Jet A1.
3. Light diesel (LGO): it is used for diesel production after the treatment.
4. Medium diesel (MGO): these heavier gases are also used for diesel production.
5. Atmospheric residue (Residue): this heaviest part of crude oil corresponds to the predominant flow rate.

The three products in the middle of the column (Kerosene, MGO, LGO) are sent to different stripping columns. The bottom product will be supplied with steam to remove the light components, and the head vapors are then reinjected into the distillation column to reduce the partial pressure of the feed. The atmospheric distillation column has a pump-around system, in which part of the liquid stream is extracted from the column to be sent to the heat exchanger. This process acts as an internal condenser to guarantee continuous reflux. There are two lateral type withdrawals in this site: at the head of the column (TPA, Top Pump-Around) and in the middle of the column (MPA, Middle Pump-Around).

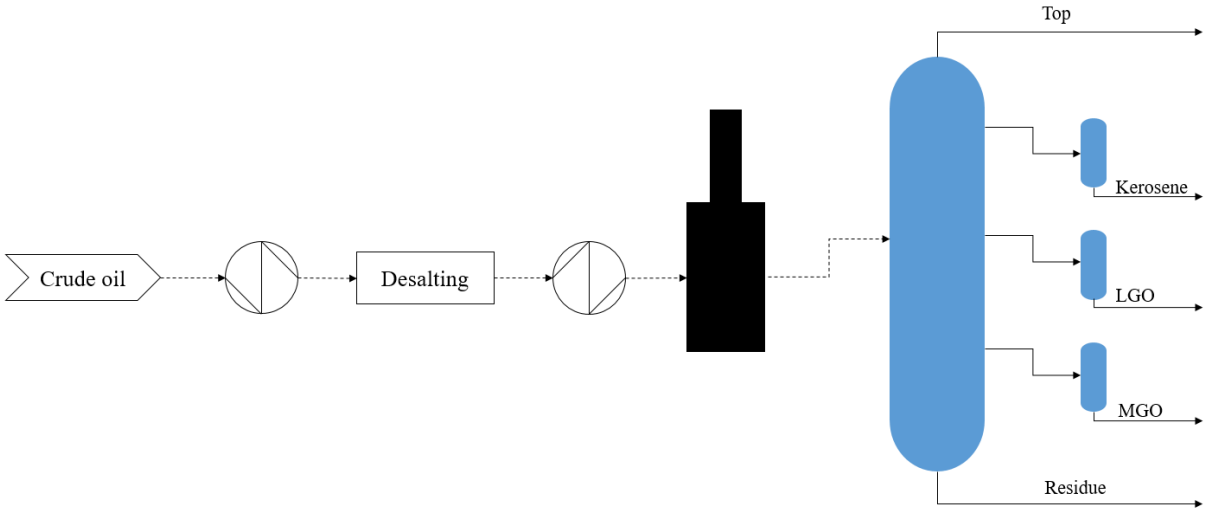

Fig 5.1. Flow diagram of the atmospheric distillation

The existing heat integration diagram is shown in Fig 5.2, in which Kerosene does not connect in the network, all the streams (TPA, LGO, MGO, MPA, and Residue) have been split into three streams. From the measurement obtained from the refinery, the preheating system has two operational periods. The transition time (TT) between them is about 2.5h to 3.5h, which corresponds to about 30% of the working period (Payet, 2018). The time response might be improved if a different design can be provided with our method. Thus, we will take this distillation preheating system as a case study to apply the improved method in Chapter 4 to carry out a grassroots design that can consider the TT between operational periods.

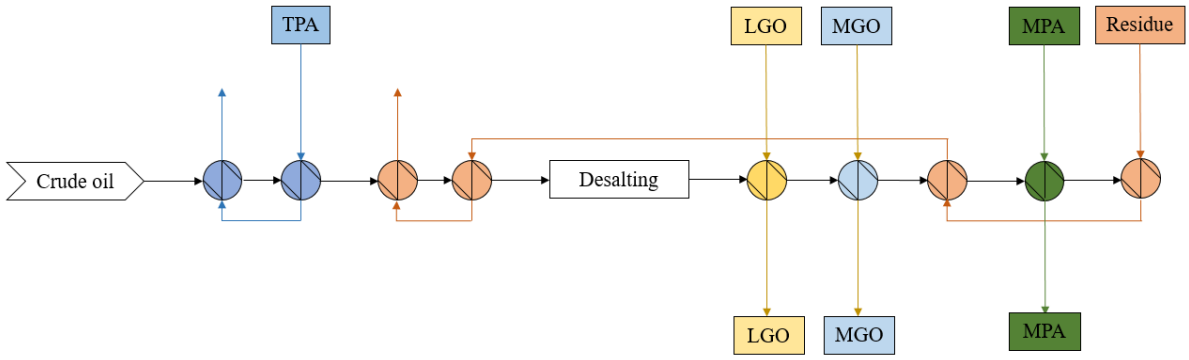

Fig 5.2. Scheme of the existing heat integration system

5.2 Formalizing the synthesis parameters

The parameters of the case problem are given in Table 5.1. It gets two operational periods, 6 hot streams, and 2 cold streams. This part aims to apply the synthesis method in previous chapters to carry out the design that considers the TAC and transition time trade-off results. Since the main parameters given in Table 8.6 and Table 8.7 in the thesis of Payet are not complete for carrying out the synthesis, we supply the other parameters either from other places in the document or assume a value. The heat transfer coefficient of all the streams and utilities is assumed to be 1 ($kW/m^2 \bullet K$). Moreover, we also assume that the two operational periods are evenly divided.

Table 5.1. The parameters of the distillation preheating system

Streams		Type	T_{in} ℃	T_{out} ℃	CP(kW/K)
Period 1					
TPA_A	H1	Hot	142.92	78.89	188.05
MPA_A	H2	Hot	279.76	213.12	74.38
RESI To4_A	H3	Hot	336.07	90.00	52.30
LGO_A	H4	Hot	248.63	40.00	17.43
MGO_A	H5	Hot	298.79	40.00	15.23
KERO_A	H6	Hot	188.01	40.00	26.03
FEEDI To2_A	C1	Cold	24.57	130.75	139.82
FEED3 To8_A	C2	Cold	128.62	339.00	197.35
Period 2					
TPA_A	H1	Hot	144.24	58.92	115.06
MPA_A	H2	Hot	289.41	224.84	78.80
RESI To4_A	H3	Hot	361.08	90.00	73.59
LGO_A	H4	Hot	254.32	40.00	18.36
MGO_A	H5	Hot	298.81	40.00	14.41
KERO_A	H6	Hot	193.26	40.00	19.53
FEEDI To2_A	C1	Cold	23.73	128.20	142.72
FEED3 To8_A	C2	Cold	126.38	369.00	198.16
	HU^{de}		390	375.14	-
	CU^{de}		32.62	50	-

Area cost($) [ch] = $300 + 5000A^{0.8}$, CHU= 300 $/(kW•year) [as], CCU= 50$/(kW•year) [as], $\varepsilon = 1$ [ch], $\Delta T_{min} = 6.14K$ [de]

as: the parameters not given and assumed a value;
ch: the parameters not given and checked from other chapters from the thesis;
de: the parameters not given and deduced from the thesis;

5.3 Study results and discussions

The case study here gets 8 streams, belongs to a medium size problem, and we need to apply the IINLP as proposed in Chapter 4. As the starting process of the solution, we select the number of stages of the HEN superstructure to be 3, since, in many large size synthesis problems, the optimized structure usually ends up with three stages (Escobar et al., 2013; Aguitoni et al., 2019). We choose to study the TT when HEN change from period 2 to period 1. The TT of the HEN takes the maximum TT of all the hot stream outlet temperatures, and the stream with the longest TT is termed as the dominant stream in the following. The calculation of TT takes 0.1% deviation (compared with the final stable value in K) as the criteria to locate the time to reach a stable status.

The iteration takes about 3,090s to complete the optimizing process and 255s to obtain the TT results for all the hot streams that transfer from period 2 to period 1. The progress of the best TAC as with the calculation time is provided in Fig 5.3. The HEN in the starting time gets zero processes HE, and the TAC decreases when adding process HEs, the final optimal result was found after about 20 local optimal points with about 45.83% progress of TAC. The lowest TAC design is provided in Fig 5.4, where bypasses are installed in E1, E2, and E3; the stream split happens for H5, C1, and C2. Except for H1, H2, and C1 only equipped with process HEs, all the rest streams end up with utilities.

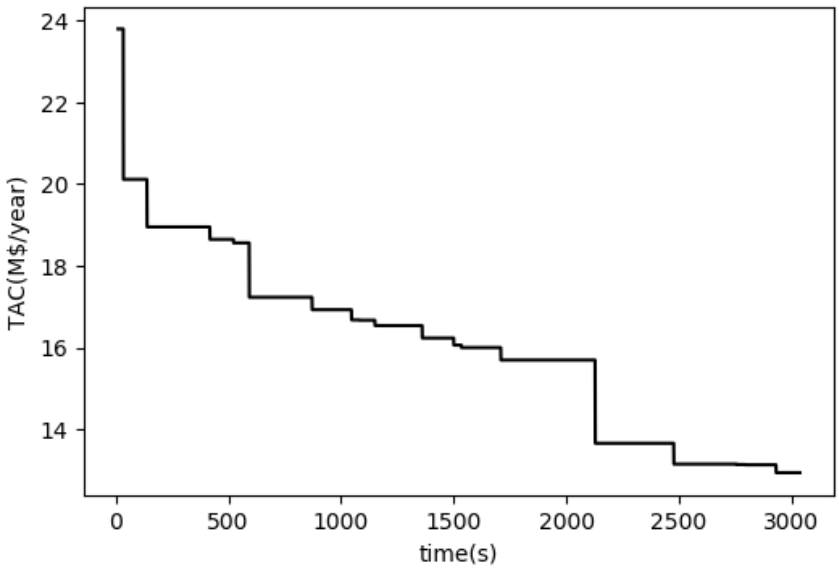

Fig 5.3. TAC evolution during the optimization of IINLP in the distillation preheating system

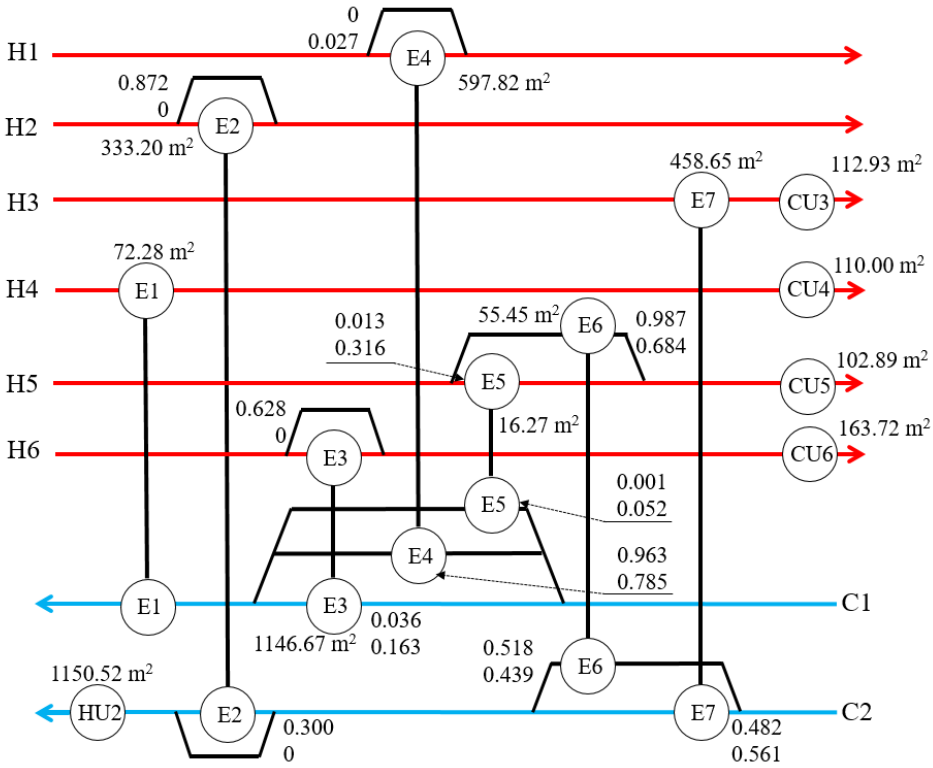

Fig 5.4. Optimal TAC design of the distillation preheating system

The TAC-TT trade-off results are depicted in Fig 5.5, in which the TT of various HEN design range from 290s to 2,660s, the lowest TAC design corresponds to the HEN with the longest TT. However, TT decreases very fast to about 400s when scarifying a little TAC. Moreover, there are also many HENs with different TAC but the same TT. In Fig 5.5, we select five HENs, in which HEN1, HEN2, HEN3, and HEN4 are in the Pareto-front, and HEN5 not. HEN1, HEN2, and HEN3 get rather close (1.83% deviation) TAC value but differ quite widely (85.26 %) in the TT aspect, HEN4 and HEN5 have a significant gap

(47.78 %) in TAC, but almost the same TT. HEN1 is also the optimal cost design, as shown in Fig 5.4, the other structures are given in Fig 5.6 to Fig 5.9.

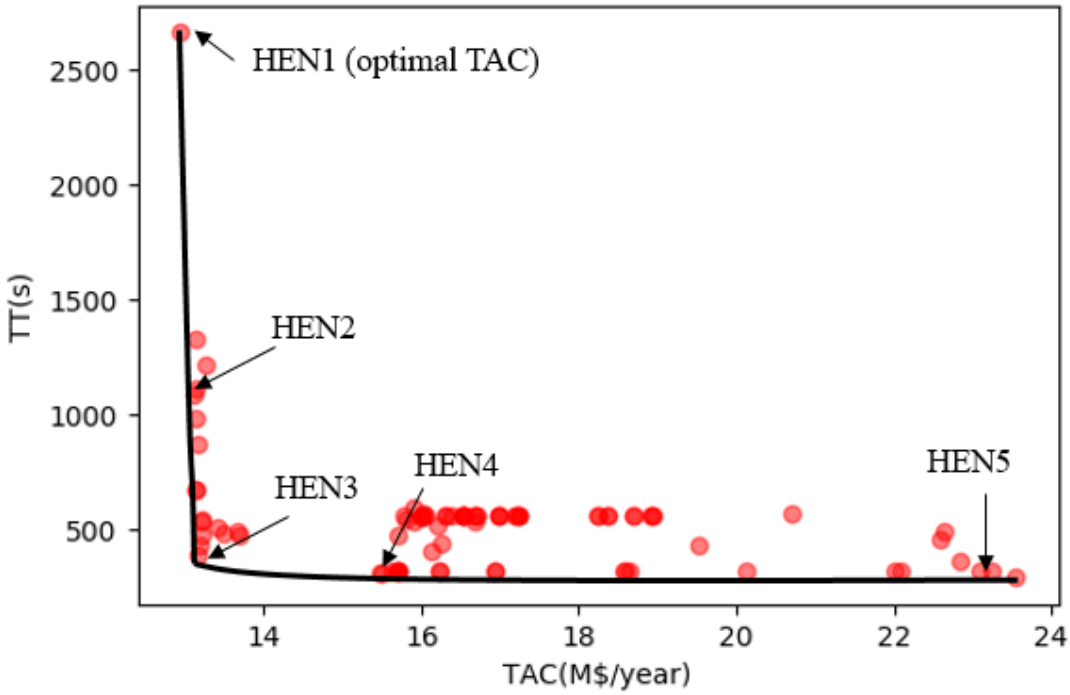

Fig 5.5. TAC-TT trade-off result of the distillation preheating system

Table 5.2. Summary of results of selected HENs in the Fig 5.5

	TAC (M$/year)	TAC-deviation (compared to the optimal one)	TT (s)	TT-deviation (compared to the fastest one)	Dominant stream
HEN1	12.935	0	2,660	817.24%	H5
HEN2	13.123	1.45%	1,085	274.14%	H6
HEN3	13.172	1.83%	392	35.17%	H3
HEN4	15.632	20.85%	316	8.97%	H5
HEN5	23.101	78.59%	316	8.97%	H5 & H6

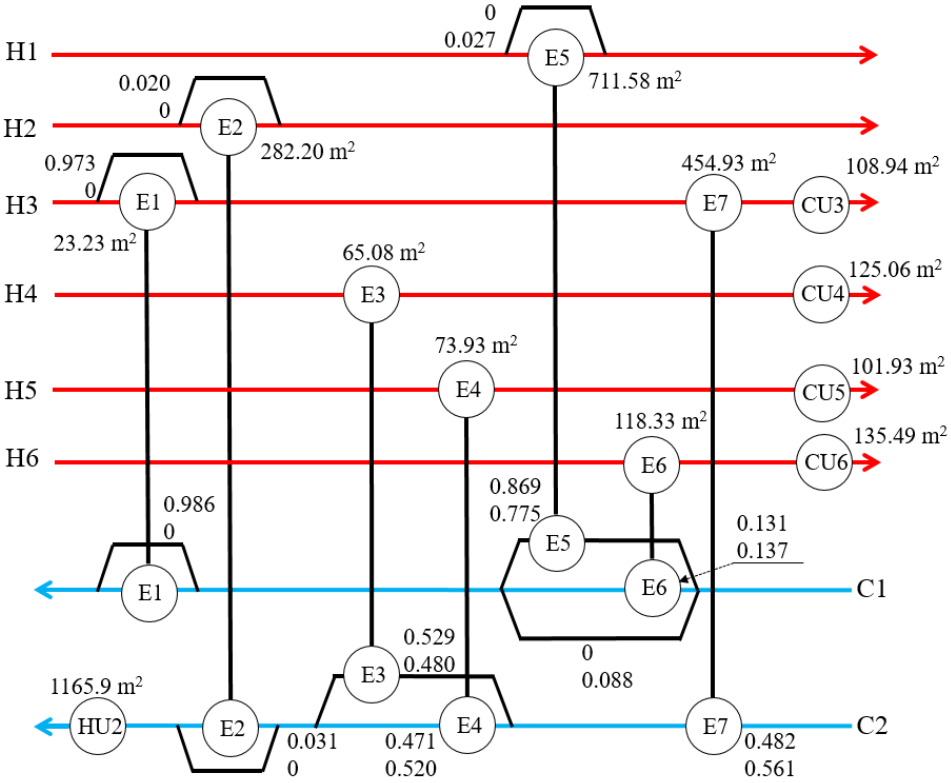

Fig 5.6. Configuration of HEN2 in Fig 5.5

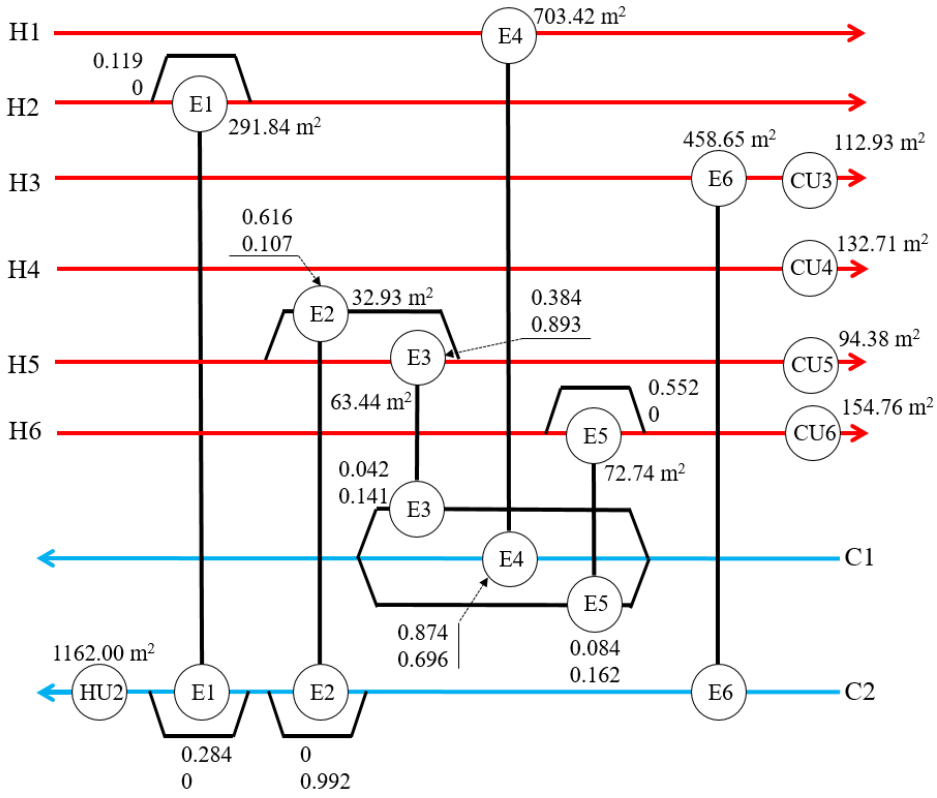

Fig 5.7. Configuration of HEN3 in Fig 5.5

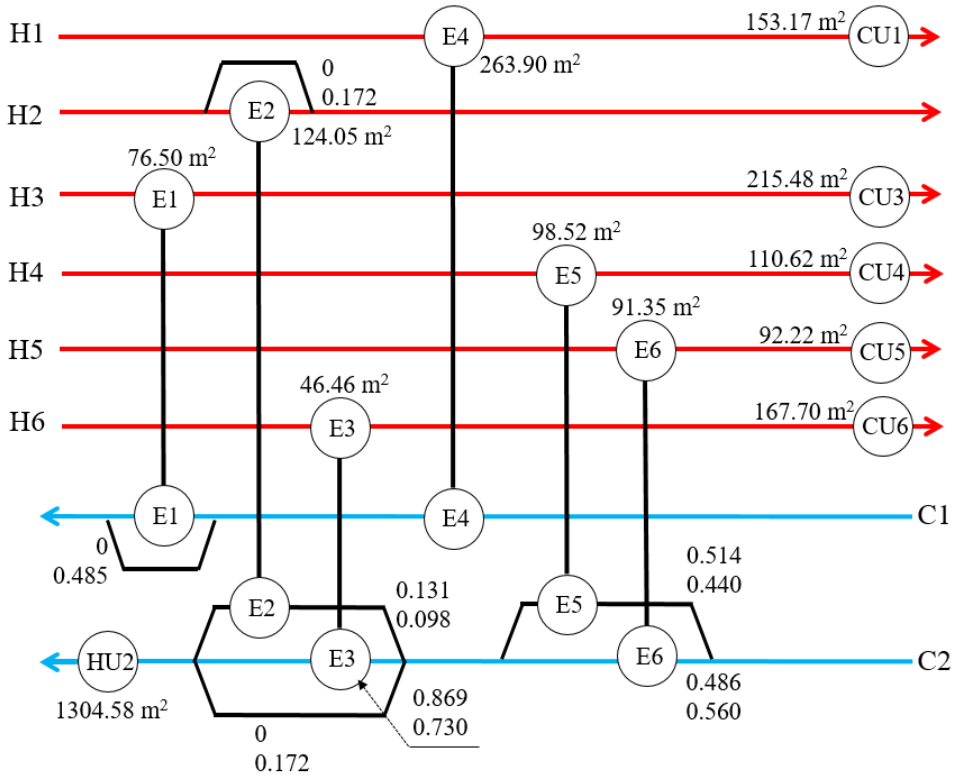

Fig 5.8. Configuration of HEN4 in Fig 5.5

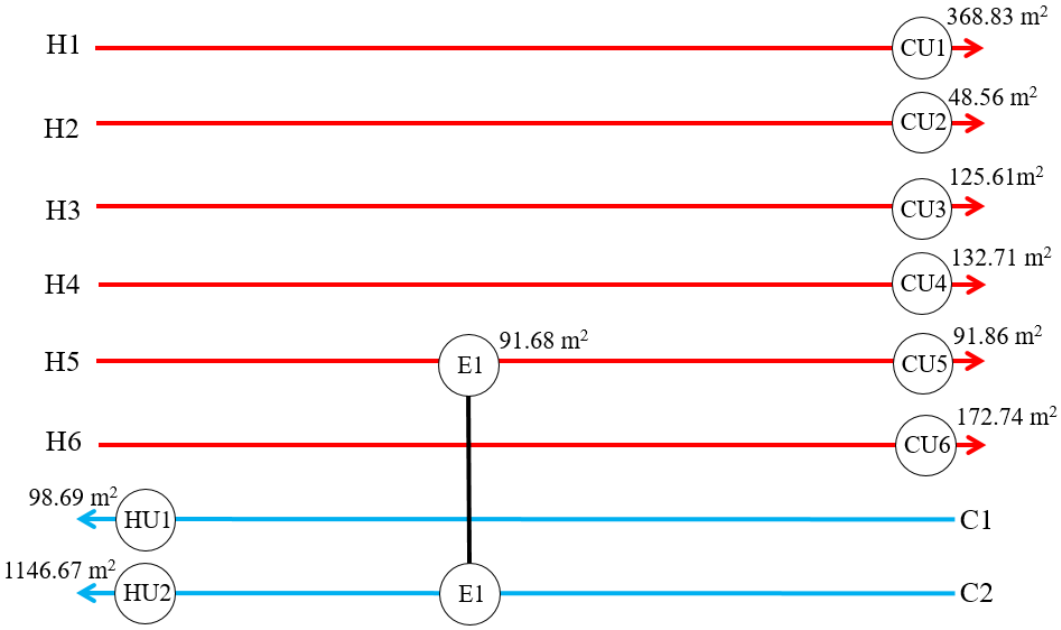

Fig 5.9. Configuration of HEN5 in Fig 5.5

The results of these five HENs are summarized in Table 5.2. HEN1 and HEN2 have the same number of process HEs and utilities, but the stream's connection brings the difference in TAC and TT results. In HEN1, only hot stream H5 gets parallel HEs in the branch stream among hot streams, and it dominates the TT of the structure when changing the operational period. HEN2 gets no hot stream to have parallel HEs, which makes it simpler than HEN1. That may explain why HEN2 is faster than HEN1.

We can observe that the outlet temperature of hot stream H3 in HEN2 can be affected by H6 through E6, E1, E7, and CU3, which is quite a long pathway compared to other streams. However, H3 does not dominate HEN2, and it might because the bypass ratio of E1 in period 1 is very high, which significantly weakens this pathway's impact. In HEN3, H3 dominates the time response of the network but not H5 that gets parallel HEs. HEN4 and HEN5 are all dominated by hot stream H5 and have almost the same TT even though HEN4 is more complicated than HEN5. The much more number of HEs in HEN4 makes it more cost-effective than HEN5. These observations confirm that we cannot easily judge the TT relation through a simple structure analysis based only on the number of HEs, the length of a pathway, or the number of branches. A dynamic model that calculates TT is necessary to compare different structures.

Reminds that the existing HEN requires about 2.5h to 3.5h to achieve the operational period transition, which differs significantly compared with the TT result predicted by our models. There are mainly two reasons that lead to the difference. The first one is that we do not use the same parameters to carry out the study due to the lack of information. The second one goes for the ignorance of the distillation column in the model calculation, which might account for the most important delay unit in real conditions.

The method's application in a real HEN problem indicates that the consideration of time response in the design stage is rather useful. Even for various designs close to the optimal TAC performance, they can have a considerable difference in the TT aspect, which might severely delay the system transition period between operational periods.

Résumé du chapitre 6

Ce chapitre récapitule les contributions de la thèse en discutant les mesures des performances dynamiques de HEN ainsi que les méthodes de synthèse de HEN et résume les principaux résultats des études de cas. À la fin, quelques perspectives ont été abordées pour faire des efforts potentiels en vue d'améliorer les méthodes proposées.

Chapter 6 – Conclusions & Perspectives

In this thesis, we pioneered to consider the time response in the heat exchanger network (HEN) design stage. In the beginning, we defined the transition time (TT) as the indicator to measure HEN's controllability in a dynamic performance aspect, and introduced the target of the thesis to explore a method that enables us to design a flexible, controllable and cost-effective HEN. The flexible aspect is to deal with multi-period synthesis. Controllability consideration is measured by the TT when HEN gets operational period changeover and set the total annualized cost (TAC) as the optimization target. Chapter 2 reviewed the achievement in HEN synthesis, enlarged the time-lines for the HEN synthesis, flexibility study, multi-period synthesis progress, and research about the controllability based on the previous review work. After reviewing relevant work, we found that such a problem has rarely been studied. We need to build the model from scratch.

We select to estimate the TT by building a dynamic model for HEN instead of the numerical simulation and experimental ways since the latter two are not appropriate to apply toward a massive number of structures in terms of potential time cost. The dynamic model requires the full information of a HEN (configuration, heat transfer area, mass flow ratio, etc.) to calculate the TT, and the calculation process cannot be formulated as expressions to be integrated into the HEN synthesis model. Therefore, the synthesis strategy requires to follow a sequential way, to iterate various structures gradually. Based on that, two levels of the methods have been provided. The preliminary method (BINLP) in chapter 3 deals with the small scale synthesis problem and the basic HEN dynamic model to obtain TT. The improved method (IINLP) in chapter 4 to cope with medium-large synthesis problems, and improved HEN dynamic model to calculate TT for more complex HENs.

- BINLP and basic HEN dynamic model in chapter 3

The HEN dynamic model takes the dynamic model of heat exchanger (HE) as the basis. However, the traditional dynamic model of HE is too heavy to reach the HEN outlet temperature, because they usually tried to explore the temperature distribution inside the HE that is not our primary concern. Here, we simplified the HE dynamic model by utilizing the arithmetic average temperature difference to describe the heat transfer process, and ignore the inside temperature information by considering the temperature of the metal wall to be uniform. The simplifications are correct when the size of HE is small, but it might also lead to bias in other cases, and the deviations in both static and dynamic aspects have been illustrated in the context. By implementing the Laplace transform, the HE's outlet temperature can be expressed by the combination of inlet streams, the thermal inertia of the metal wall, and other parameters of the HE. Together with the one-by-one iteration strategy to find the outlet temperature of HEs sequentially in a HEN, the outlet temperature of HEN can be reached. Then, HEN's outlet temperature in the time domain can be obtained after carrying out the inverse Laplace transform, and TT can be calculated correspondingly. The way to obtain the HEN's dynamic model has been validated by comparing the simulation results to guarantee the correctness of the idea, in which the model in the simulation platform follows the same governing equations of HE.

The synthesis process was to optimize a series of HENs, which became a group of nonlinear programming (NLP) problems. We started with the most basic strategy, which tries to iterate all the potential structures,

and it is acceptable in small case problems considering the potential structures are not that much. Moreover, we proposed to discard the isomorphic structures and the structures with a loop to avoid too many iterations. The strategy has been validated against the usual mixed-integer nonlinear programming (MINLP) way in four small scale problems both in single period and multi-period. The results show that the BINLP method can find much lower TAC designs than MINLP by following the same initial condition, even though the searching time is much longer.

Applying the BINLP approach and the HEN dynamic model in a four-stream three working periods case study, we found that TT results of various designs have a significant difference, ranging from 100s to 2,500s, the optimal TAC design requires about 703s. If there is a strict TT requirement, optimal TAC design might not be appropriate. Considering the potential bias caused by the dynamic model's assumptions, we selected three structures in the pseudo-Pareto-front of the TAC-TT results to obtain the real dynamic result in the simulation platform by discretizing the HE model into many small cells. Moreover, we found that the TT relationship predicted by the dynamic model still holds in the real result. Even though there is some evident bias between the dynamic model result and the real one, the dynamic model can help us to act as a convenient pre-selection tool in the design stage to consider the time response.

There are two reasons to limit the proposed method in chapter 3 only for small case synthesis problems. The first one is that the iterative strategy which is not efficient in medium-large scale problems since the potential structures will increase exponentially with the number of the streams. The second one is the limitation of the inverse Laplace transform process toward the HEN outlet temperature function because the process can easily fail to work when the function becomes complicated as HEN gets more and more streams and HEs. These two aspects are improved in chapter 4.

- IINLP and improved HEN dynamic model in chapter 4

To avoid the numerical difficulty when dealing with the inverse Laplace transform process to get the HEN outlet temperature in the time domain, we proposed to decompose the outlet temperature function in Laplace form into the combination of simple forms by analyzing each pathway's function individually. The inverse Laplace transform of those simple functions can be obtained easily by referring to the standard Laplace transform table. So, the HEN outlet temperature as a function of time can be reached analytically, and the HEN dynamic model becomes an analytical model. A four-stream HEN example has been employed to illustrate the procedure to obtain the pathway function, the decomposition process, and get the function in the time domain gradually. The analytic model has been applied to a 10-streams HEN problem where the inlet temperatures are assumed to change in the step and ramp signal separately. The comparison result with the numerical simulation model confirmed the correctness of the improved strategy. The analytical model can work in large scale problems without any burden.

In large scale HEN synthesis problems, the structure pre-selection procedures in the BINLP are not adequate since there will be massive potential structures, and the appropriate way is to choose a group of structures to test with a specific strategy. We suggest IINLP inspired by the HEN optimizing process's characters, which can be interpreted as the process to optimize the heat load distribution between the process HEs and utilities. The way to achieve such adjustment can be through the change of number of HEs in the HEN. From the start of the optimizing process, HE will be added one by one, each time keeping the HE that can have the lowest TAC. The adding process stops when no more progress can be

made, then to remove one HE in the current HEN by keeping the lowest TAC of the sub-HENs. Then, the adding process restarts, as well as the removing process, will follow. Until the remove and add process cannot make any progress in TAC, the iteration terminates. The IINLP has been validated against the simulated annealing (SA) algorithms in three medium-large cases (9-streams, 10-streams, and 15-streams) by comparing both TAC and TAC-TT trade-off results. Considering the SA's stochastic characters, we ran three times of SA for each case study, allowing the same calculation time as IINLP required in each case. Finally, IINLP can find lower TAC designs (1.28%, 0.03%, 5.24%) than SA in three runs for all three case studies. Moreover, the optimal TAC results provided by SA differ considerably between three runs, about 21% in case 1, 4% in case 2, and 37% in case 3. The TT of various HENs varied in vast ranges, it can be up to over 20 times in case 1 and case 3, and about 66 % in case 2. To compare the TAC-TT trade-off results, we provided the pseudo-Pareto-fronts of both IINLP and SAs separately and the integrated Pareto-fronts when combing all the iterations results of IINLP and SAs. IINLP demonstrates somewhat competitive results in case 1 and case 3, in which IINLP contributes more than 50% of the points in the integrated Pareto-fronts. In case 2, only the optimal TAC point by IINLP is more competitive than SA in three runs. It should be noted that SA was called three times, then the calculation time was three times longer than IINLP, and not all SA in different runs can perform well. The pseudo-Pareto-front of SA in the second run is almost in the right-upper region of IINLP in case 2, in which IINLP illustrates evident advantage. From the comparisons with SA, IINLP is believed to have an average performance of SA and free of the stochastic characters' concern, which means it does not need to run many times to confirm the best solution.

The improved synthesis method IINLP can run well for large scale problems, the preliminary one BINLP is only appropriate for small scale problems, but its implementation is convenient. The choice of one of these methods depends essentially on the size of the problem we want to solve.

The three case studies in chapter 4 originated from the single-period case problems in the literature by adding the maximum heating and maximum cooling operational periods, we tried to test the improved method in a real case that was put in chapter 5. It was a distillation preheating system of a refinery provided in a doctoral thesis, which composed of 6 hot streams, 2 cold streams, and two working periods. The IINLP and improved HEN model applied quite well in the case problem, in which various designs show the TT ranging from 290s to 2,660s. Moreover, many structures have similar TAC to the optimal TAC design, but the TT varies hugely. We selected five representative HENs to provide their optimized structures and found that we could not easily judge the TT relation through a simple structure analysis based only on the number of HEs, the length of the pathway, or the number of branches. A dynamic model that calculates TT is necessary to compare different structures in the design stage, allowing us to have a better design when taking the dynamic response into consideration.

Summarizing the thesis work, we identified the importance of studying TT in the design stage and pioneered to consider the TT in the HEN synthesis. Since the available controllability indicators are static criteria that are not enough, we developed new method to estimate TT and corresponding synthesis strategies that suit the different scales of problem. The methods run well and are validated against the numerical simulation. The preliminary method was tested in a four-stream case study, and the improved method was tested in three medium-large scale problems originating from the literature. Moreover, the improved method has also been applied to a real distillation preheating system. The proposed methods can be employed as a pre-selection tool when designing a cost-effective HEN under a constraint on TT.

The methods proposed in the thesis still have limitations, and they get the chance to be improved in the following perspectives:

- The HEN dynamic model or HE dynamic model can be improved in the way to increase the accuracy of the TT result. There are two potential ways, and the first one is to increase the number of cells to represent the HE dynamic model. The other is finding a new approach to replace the arithmetic mean temperature assumption to describe the heat transfer process better. Each way requires advanced math manipulations to make the problem solvable.
- The dynamic model can be extended to consider the time delay of the mass flow rate change and pipe residence, etc., to make the model much closer to the real operational condition.
- The HEN synthesis strategy aimed to optimize the TAC and consider TT as a kind of constraint. Multi-objective optimization can be explored to help reach the real Pareto-front result. Alternatively, based on the more in-depth understanding of the TT calculation process to derive equivalent indicators integrated into the synthesis model, simultaneous optimization can be achieved.

References

Aaltola, J., 2002. Simultaneous synthesis of flexible heat exchanger network. Appl. Therm. Eng. 22, 907–918.

Abikoye, B., Čuček, L., Isafiade, A.J., Kravanja, Z., 2019. Integrated design for direct and indirect solar thermal utilization in low temperature industrial operations. Energy 182, 381–396. https://doi.org/10.1016/j.energy.2019.05.205

Abuhalima, O., Sun, L., Chang, R., Luo, X., Zhao, Y., 2016. Synthesis of a multipass heat exchanger network based on life cycle energy saving. Appl. Therm. Eng. 100, 1189–1197. https://doi.org/10.1016/j.applthermaleng.2016.02.113

Adi, V.S.K., Chang, C.T., 2013. A mathematical programming formulation for temporal flexibility analysis. Comput. Chem. Eng. 57, 151–158. https://doi.org/10.1016/j.compchemeng.2013.04.001

Adi, V.S.K., Laxmidewi, R., Chang, C.T., 2016. An effective computation strategy for assessing operational flexibility of high-dimensional systems with complicated feasible regions. Chem. Eng. Sci. 147, 137–149. https://doi.org/10.1016/j.ces.2016.03.028

Adjiman, C.S., Androulakis, I.P., Floudas, C.A., 1997. Global optimization of MINLP problems in process synthesis and design. Comput. Chem. Eng. 21, S445–S450. https://doi.org/10.1016/s0098-1354(97)87542-4

Aguilera, N., Marchetti, J.L., 1998. Optimizing and controlling the operation of heat-exchanger networks. AIChE J. 44, 1090–1104. https://doi.org/10.1002/aic.690440508

Aguitoni, M.C., Pavão, L.V., Antonio da Silva Sá Ravagnani, M., 2019. Heat exchanger network synthesis combining Simulated Annealing and Differential Evolution. Energy 181, 654–664. https://doi.org/10.1016/j.energy.2019.05.211

Aguitoni, M.C., Pavão, L.V., Siqueira, P.H., Jiménez, L., Ravagnani, M.A. da S.S., 2018. Heat exchanger network synthesis using genetic algorithm and differential evolution. Comput. Chem. Eng. 117, 82–96. https://doi.org/10.1016/j.compchemeng.2018.06.005

Ahmad, M.I., Zhang, N., Jobson, M., Chen, L., 2012. Multi-period design of heat exchanger networks. Chem. Eng. Res. Des. 90, 1883–1895. https://doi.org/10.1016/j.cherd.2012.03.020

Ahmad, S., 1985. Heat exchanger networks : Cost tradeoffs in energy and capital. University of Manchester.

Ahmetović, E., Kravanja, Z., 2013. Simultaneous synthesis of process water and heat exchanger networks. Energy 57, 236–250. https://doi.org/10.1016/j.energy.2013.02.061

Akbari, A., Omidkhah, M.R., Hojjati, M.R., 2008. Heat exchanger network area targeting considering stream allocation to shell or tubes. Comput. Chem. Eng. 32, 3143–3152. https://doi.org/10.1016/j.compchemeng.2008.05.009

Akbarnia, M., Amidpour, M., Shadaram, A., 2009. A new approach in pinch technology considering piping costs in total cost targeting for heat exchanger network. Chem. Eng. Res. Des. 87, 357–365. https://doi.org/10.1016/j.cherd.2008.09.001

Allen, B., Savard-Goguen, M., Gosselin, L., 2009. Optimizing heat exchanger networks with genetic algorithms for designing each heat exchanger including condensers. Appl. Therm. Eng. 29, 3437–3444. https://doi.org/10.1016/j.applthermaleng.2009.06.006

Anantharaman, R., 2011. Energy Efficiency in Process Plants with emphasis on Heat Exchanger Networks. Norwegian University of Science and Technology.

Anantharaman, R., Nastad, I., Nygreen, B., Gundersen, T., 2010. The sequential framework for heat

exchanger network synthesis-The minimum number of units sub-problem. Comput. Chem. Eng. 34, 1822–1830. https://doi.org/10.1016/j.compchemeng.2009.12.002

Anastasovski, A., 2014. Enthalpy Table Algorithm for design of Heat Exchanger Network as optimal solution in Pinch technology. Appl. Therm. Eng. 73, 1113–1128. https://doi.org/10.1016/j.applthermaleng.2014.08.069

Angsutorn, N., Siemanond, K., Chuvaree, R., 2014. Heat exchanger network synthesis using MINLP Stage-wise model with pinch analysis and relaxation, in: Computer Aided Chemical Engineering. Elsevier B.V., pp. 139–144. https://doi.org/10.1016/B978-0-444-63456-6.50024-7

Arce, H., López, S.H., Perez, S.L., Rämä, M., Klobut, K., Febres, J.A., 2018. Models for fast modelling of district heating and cooling networks. Renew. Sustain. Energy Rev. 82, 1863–1873. https://doi.org/10.1016/j.rser.2017.06.109

Arteaga-Perez, L.E., Casas, Y., Peralta, L.M., Kafarov, V., Dewulf, J., Giunta, P., 2009. An auto-sustainable solid oxide fuel cell system fueled by bio-ethanol. Process simulation and heat exchanger network synthesis. Chem. Eng. J. 150, 242–251. https://doi.org/10.1016/j.cej.2009.02.032

Athier, G., Floquet, P., Pibouleau, L., Domenech, S., 1997. Synthesis of Heat-Exchanger Network by Simulated Annealing and NLP Procedures. AIChE J. 43, 3007–3020. https://doi.org/10.1002/aic.690431113

Azad, A.V., Ghaebi, H., Amidpour, M., 2011. Novel graphical approach as fouling pinch for increasing fouling formation period in heat exchanger network (HEN) state of the art. Energy Convers. Manag. 52, 117–124. https://doi.org/10.1016/j.enconman.2010.06.050

Bai, Y., Liu, L., Gu, S., Du, J., 2017. Synthesis of flexible heat exchanger networks considering fouling resistance. Chem. Eng. Trans. 61, 511–516. https://doi.org/10.3303/CET1761083

Bakošová, M., Oravec, J., 2014. Robust model predictive control for heat exchanger network. Appl. Therm. Eng. 73, 922–928. https://doi.org/10.1016/j.applthermaleng.2014.08.023

Bao, Z., Cui, G., Chen, J., Sun, T., Xiao, Y., 2018. A novel random walk algorithm with compulsive evolution combined with an optimum-protection strategy for heat exchanger network synthesis. Energy 152, 694–708. https://doi.org/10.1016/j.energy.2018.03.170

Björk, K.M., Westerlund, T., 2002. Global optimization of heat exchanger network synthesis problems with and without the isothermal mixing assumption. Comput. Chem. Eng. 26, 1581–1593. https://doi.org/10.1016/S0098-1354(02)00129-1

Bochenek, R., Je, A., 2001. Loop breaking in heat exchanger networks by mathematical programming. Appl. Therm. Eng. 21, 1429–1448.

Bogataj, M., Bagajewicz, M.J., 2008. Synthesis of non-isothermal heat integrated water networks in chemical processes. Comput. Chem. Eng. 32, 3130–3142. https://doi.org/10.1016/j.compchemeng.2008.05.006

Boyaci, C., Uztork, D., Akman, U., 1996. Dynamics and optimal control of flexible heat exchanger networks. Comput. chem. Engng 20, 775–780.

Bristol, E.H., 1966. On a new measure of interaction for multivariable process control. IEEE Trans. Automat. Contr. 11, 133–134. https://doi.org/10.1109/TAC.1966.1098266

Broeck, H. Ten, 1944. Economic Selection of Exchanger Sizes. Ind. Eng. Chem. 36, 64–67. https://doi.org/10.1021/ie50409a013

Bühler, F., 2018. Energy efficiency in the industry: A study of the methods, potentials and iteractons with the energy system. Université technique du Danemark. https://doi.org/10.1145/3300001.3300014

Bulasara, V.K., Uppaluri, R., Ghoshal, A.K., 2009. Revamp study of crude distillation unit heat exchanger network: Energy integration potential of delayed coking unit free hot streams. Appl. Therm. Eng. 29, 2271–2279. https://doi.org/10.1016/j.applthermaleng.2008.11.013

Chan, I., Alwi, S.R.W., Hassim, M.H., Ab, Z., Klemeš, M.J.J., 2014. Heat exchanger network design considering inherent safety. Energy Procedia 61, 2469–2473. https://doi.org/10.1016/j.egypro.2014.12.025

Chang, C., Chen, X., Wang, Y., Feng, X., 2017. Simultaneous synthesis of multi-plant heat exchanger networks using process streams across plants. Comput. Chem. Eng. 101, 95–109. https://doi.org/10.1016/j.compchemeng.2017.02.039

Chartrand, G., 1984. Introductory Graph Theory. Dover Publications Inc.

Chen, C., Hung, P., 2004. Simultaneous synthesis of flexible heat-exchange networks with uncertain source-stream temperatures and flow rates. Ind. Eng. Chem. Res. 43, 5916–5928. https://doi.org/10.1021/ie030701f

Chen, C.L., Chang, F.Y., Chao, T.H., Chen, H.C., Lee, J.Y., 2014. Heat-exchanger network synthesis involving organic rankine cycle for waste heat recovery. Ind. Eng. Chem. Res. 53, 16924–16936. https://doi.org/10.1021/ie500301s

Chen, J., Cui, G., Xiao, Y., 2018. An analytical solution to the dynamic behavior of heat exchanger networks. Int. J. Heat Mass Transf. 126, 466–478. https://doi.org/10.1016/j.ijheatmasstransfer.2018.05.041

Chen, J.J.J., 1987. Comments on improvements on a replacement for the logarithmic mean. Chem. Eng. Sci. 42, 2488–2489. https://doi.org/10.1016/0009-2509(87)80128-8

Chen, Q., Fu, R.H., Xu, Y.C., 2015. Electrical circuit analogy for heat transfer analysis and optimization in heat exchanger networks. Appl. Energy 139, 81–92. https://doi.org/10.1016/j.apenergy.2014.11.021

Chen, X., Li, Z., Yang, J., Shao, Z., Zhu, L., 2008. Nested tabu search (TS) and sequential quadratic programming (SQP) method, combined with adaptive model reformulation for heat exchanger network synthesis (HENS). Ind. Eng. Chem. Res. 47, 2320–2330. https://doi.org/10.1021/ie071245o

Chen, X., Wang, R.Z., Du, S., 2017. Heat integration of ammonia-water absorption refrigeration system through heat-exchanger network analysis. Energy 141, 1585–1599. https://doi.org/10.1016/j.energy.2017.11.100

Choomwattana, C., Chaianong, A., Kiatkittipong, W., Kongpanna, P., Quitain, A.T., Assabumrungrat, S., 2016. Process integration of dimethyl carbonate and ethylene glycol production from biomass and heat exchanger network design. Chem. Eng. Process. Process Intensif. 107, 80–93. https://doi.org/10.1016/j.cep.2016.06.001

Ciric, A.R., Floudas, C.A., 1991. Heat exchanger network synthesis without decomposition. Comput. Chem. Eng. 15, 385–396. https://doi.org/10.1016/0098-1354(91)87017-4

Cordella, L.P., Foggia, P., Sansone, C., Vento, M., 2001. An improved algorithm for matching large graphs, in: 3rd IAPR-TC15 Workshop on Graph-Based Representations in Pattern Recognition. pp. 149–159.

Craig, I.J.D., Thompson, A.M., Thompson, W.J., 1994. Practical Numerical Algorithms Why Laplace Transforms Are Difficult To Invert Numerically. Comput. Phys. 8, 648. https://doi.org/10.1063/1.4823347

Cullen, J.M., Allwood, J.M., Borgstein, E.H., 2011. Reducing energy demand: What are the practical limits? Environ. Sci. Technol. 45, 1711–1718. https://doi.org/10.1021/es102641n

Da Jiang and Chuei-Tin Chang, 2013. A new approach to generate flexible multiperiod heat exchanger network designs with timesharing mechanisms. Ind. Eng. Chem. Res. 52, 3794–3804. https://doi.org/10.1021/ie301075v

Dimitriads, V.D., Pistikopoulos, E.N., 1995. Flexibility Analysis of Dynamic Systems. Ind. Eng. Chem. Res. 34, 4451–4462. https://doi.org/10.1021/ie00039a036

Dolan, W.B., Cummings, P.T., LeVan, M.D., 1989. Process optimization via simulated annealing: Application to network design. AIChE J. 35, 725–736. https://doi.org/10.1002/aic.690350504

Dong, R., Yu, Y., Zhang, Z., 2014. Simultaneous optimization of integrated heat, mass and pressure exchange network using exergoeconomic method. Appl. Energy 136, 1098–1109. https://doi.org/10.1016/j.apenergy.2014.07.047

Dorigo, M., Di Caro, G., 1999. Ant colony optimization: A new meta-heuristic, in: Proceedings of the 1999 Congress on Evolutionary Computation, CEC 1999. IEEE Computer Society, pp. 1470–1477. https://doi.org/10.1109/CEC.1999.782657

Drobež, R., Pintarič, Z.N., Pahor, B., Kravanja, Z., 2012. Simultaneous synthesis of a biogas process and heat exchanger network. Appl. Therm. Eng. 43, 91–100. https://doi.org/10.1016/j.applthermaleng.2012.03.009

Erik A.Wolf, Sigurd Skogestad, M.H. and K.W.M., 1992. A procedure for controllability analysis, in: IFAC Workshop.

Escobar, M., O.Treirweiler, J., E.Grossmann, I., 2013a. Simultaneous Synthesis of Heat Exchanger Networks with Operability Considerations: Flexibility and Controllability. Comput. Chem. Eng. 14, 2335–2370. https://doi.org/10.1021/ie010389e

Escobar, M., Trierweiler, J.O., 2013. Optimal heat exchanger network synthesis: A case study comparison. Appl. Therm. Eng. 51, 801–826. https://doi.org/10.1016/j.applthermaleng.2012.10.022

Escobar, M., Trierweiler, J.O., 2011. Operational Controllability of Heat Exchanger Networks, IFAC Proceedings Volumes. IFAC. https://doi.org/10.3182/20100705-3-BE-2011.00017

Escobar, M., Trierweiler, J.O., Grossmann, I.E., 2013b. A heuristic Lagrangean approach for the synthesis of multiperiod heat exchanger networks. Appl. Therm. Eng. 63, 177–191. https://doi.org/10.1016/j.applthermaleng.2013.10.064

Faria, D.C., Young Kim, S., Bagajewicz, M.J., 2015. Global optimization of the stage-wise superstructure model for heat exchanger networks. Ind. Eng. Chem. Res. 54, 1595–1604. https://doi.org/10.1021/ie5032315

Floudas, C.A., Ciric, A.R., Grossmann, I.E., 1986. Automatic Synthesis of Optimum Heat Exchanger Network Configurations. AIChE J. 32, 276–290.

Floudas, C.A., Grossmann, I.E., 1987. Automatic generation of multiperiod heat exchanger network configurations. Comput. Chem. Eng. II, 123–142.

Floudas, C.A., Grossmann, I.E., 1986. Synthesis of flexible heat exchanger networks for multiperiod operation. Comput. Chem. Eng. 10, 153–168. https://doi.org/10.1016/0098-1354(86)85027-X

Francesconi, J.A., Oliva, D.G., Aguirre, P.A., 2017. Flexible heat exchanger network design of an ethanol processor for hydrogen production. A model-based multi-objective optimization approach. Int. J. Hydrogen Energy 42, 2736–2747. https://doi.org/10.1016/j.ijhydene.2016.10.156

Fricker, J., Maatouk, C., Zoughaib, A., 2013. Simulating load variations of an integrated process operating with heat pump in order to improve design and control strategies, in: 26th International Conference on Efficiency, Cost, Optimization, Simulation and Environmental Impact of Energy Systems.

Furman, K.C., Sahinidis, N. V., 2001. Computational complexity of heat exchanger network synthesis. Comput. Chem. Eng. 25, 1371–1390. https://doi.org/10.1016/S0098-1354(01)00681-0

Furman, K.C., Sahinidis, N. V, 2002. A Critical Review and Annotated Bibliography for Heat Exchanger Network Synthesis in the 20th Century. Ind. Eng. Chm. Res. 41, 2335–2370. https://doi.org/10.1021/ie010389e

Gabriel, K.J., El-Halwagi, M.M., Linke, P., 2016. Optimization across the Water-Energy Nexus for Integrating Heat, Power, and Water for Industrial Processes, Coupled with Hybrid Thermal-Membrane Desalination. Ind. Eng. Chem. Res. 55, 3442–3466. https://doi.org/10.1021/acs.iecr.5b03333

GIREI, S.A., 2015. Optimal design and operation of heat exchanger network. Cranfield University.

Grosdidier, P., 1990. Analysis of interaction direction with the singular value decomposition. Comput. Chem. Eng. 14, 687–689. https://doi.org/10.1016/0098-1354(90)87037-P

Grossmann, I.E., Floudas, C.A., 1987. Active constraint strategy for flexibility analysis in chemical processes. Comput. Chem. Eng. 11, 675–693. https://doi.org/10.1016/0098-1354(87)87011-4

Grossmann, I.E., Halemane, K.P., 1982. Decomposition strategy for designing flexible chemical plants. AIChE J. 28, 686–694. https://doi.org/10.1002/aic.690280422

Grossmann, I.E., Morari, M., 1983. Operability , Resiliency , and Flexibility : process design objectives for a changing world, in: Proceedings of Second International Conference on Foundations of Computer-Aided Process Design.

Grossmann, I.E., Sargent, R.W.H., 1978. Optimum design of chemical plants with uncertain parameters. AIChE J. 24, 1021–1028. https://doi.org/10.1002/aic.690240612

Gu, S., Liu, L., Zhang, L., Bai, Y., Du, J., 2019. Optimization-Based Framework for Designing Dynamic Flexible Heat Exchanger Networks. Ind. Eng. Chem. Res. 58, 6026–6041. https://doi.org/10.1021/acs.iecr.8b04121

Gundersen, T., Naess, L., 1988. The synthesis of cost optimal heat exchanger networks. An industrial review of the state of the art. Comput. Chem. Eng. 12, 503–530. https://doi.org/10.1016/0098-1354(88)87002-9

Gvozdenac, D., 2012. Analytical solution of dynamic response of heat exchanger, Heat Exchangers - Basics Design Applications. Dr. Jovan Mitrovic (Ed.), InTech. https://doi.org/10.5772/35944

Hanak, D.P., Biliyok, C., Yeung, H., Białecki, R., 2014. Heat integration and exergy analysis for a supercritical high-ash coal-fired power plant integrated with a post-combustion carbon capture process. Fuel 134, 126–139. https://doi.org/10.1016/j.fuel.2014.05.036

Hart, W.E., Watson, J.P., Woodruff, D.L., 2011. Pyomo: Modeling and solving mathematical programs in Python. Math. Program. Comput. 3, 219–260. https://doi.org/10.1007/s12532-011-0026-8

Hasan, M.M.F., Jayaraman, G., Karimi, I.A., 2010. Synthesis of heat exchanger networks with nonisothermal phase changes. AIChE J. 56, 930–945. https://doi.org/10.1002/aic

Hernández, S., Balcazar-Lopez, L., Sanchez-Marquez, J.., Gonzalez-Garcia, G., 2010. Controllability and operability analysis of heat exchanger networks including bypasses. Chem. Biochem. Eng. Q. 24, 23–28.

Hohmann, J., 1971. Optimum networks for heat exchanger. University of Southern California.

Huang, K.F., Al-mutairi, E.M., Karimi, I.A., 2012. Heat exchanger network synthesis using a stagewise superstructure with non-isothermal mixing. Chem. Eng. Sci. 73, 30–43. https://doi.org/10.1016/j.ces.2012.01.032

Huang, S.Y., Chang, C.T., 2012. An improved mathematical programming model for generating optimal heat-exchanger network (HEN) designs. Ind. Eng. Chem. Res. 51, 3508–3515. https://doi.org/10.1021/ie200865m

Huang, W., Fan, H., Qian, Y., Cheng, F., 2017. Assessment and computation of the delay tolerability for batch reactors under uncertainty. Chem. Eng. Res. Des. 124, 74–84. https://doi.org/10.1016/j.cherd.2017.06.010

Hwa, C.S., 1965. Mathematical Formulation and Optimization of Heat Exchanger Networks Using Separable Programming, in: AIChE- IChemE Symposium Series 4. New York, pp. 101–106.

IEA, 2017. Energy Technology Perspectives 2017 - Tracking Clean Energy Progress. https://doi.org/10.1787/energy_tech-2010-en

IEA, 2011. Clean energy progress report. https://doi.org/10.1038/477517a

Site. https://doi.org/10.1017/cbo9781107415416

Isafiade, A.J., Fraser, D.M., 2010. Interval based MINLP superstructure synthesis of heat exchanger networks for multi-period operations. Chem. Eng. Res. Des. 88, 1329–1341. https://doi.org/10.1016/j.cherd.2010.02.019

Isafiade, A.J., Short, M., 2017. Integrating renewables into multi-period heat exchanger network synthesis considering economics and environmental impact. Comput. Chem. Eng. 99, 51–65. https://doi.org/10.1016/j.compchemeng.2016.11.017

Isafiade, A.J., Short, M., 2016. Multi-Period Heat Exchanger Network Synthesis Involving Multiple Sources of Utilities and Environmental Impact, in: Computer Aided Chemical Engineering. Elsevier B.V., pp. 2067–2072. https://doi.org/10.1016/B978-0-444-63428-3.50349-0

Jezowski, J., 1994a. Heat exchanger network grassroot and retrofit design. The review of the state-of-the art: part II. Heat exchanger network synthesis by mathematical methods and approaches for retrofit design. Hungarian J. Ind. Chem. 22, 295–308.

Jezowski, J., 1994b. Heat exchanger network grassroot and retrofit design. The review of the state-of-the art: part I. Heat exchanger network targeting and insight based methods of synthesis. Hungarian J. Ind. Chem. 22, 279–294.

Jin, Z., Dong, Q., Liu, M., 2008. Heat exchanger network synthesis with detailed heat exchanger design. Chem. Eng. Technol. 31, 1046–1050. https://doi.org/10.1002/ceat.200800108

Jogwar, S.S., Baldea, M., Daoutidis, P., 2007. Dynamics and Control of Energy Integrated Networks: A Multi - Time Scale Perspective, in: AIChE Annual Meeting.

Johnson, D.B., 2005. Finding all the elementary circuits of a directed graph. SIAM J. Comput. 4, 77–84. https://doi.org/10.1137/0204007

Kang, L., Liu, Y., 2019. Synthesis of flexible heat exchanger networks: A review. Chinese J. Chem. Eng. 27, 1485–1497. https://doi.org/10.1016/j.cjche.2018.09.015

Kang, L., Liu, Y., 2018. Design of flexible multiperiod heat exchanger networks with debottlenecking in subperiods. Chem. Eng. Sci. 185, 116–126. https://doi.org/10.1016/j.ces.2018.04.017

Kang, L., Liu, Y., Liang, X., 2015. Multi-objective optimization of heat exchanger networks based on analysis of minimum temperature difference and accumulated CO2 emissions. Appl. Therm. Eng. 87, 736–748. https://doi.org/10.1016/j.applthermaleng.2015.05.047

Kang, L., Liu, Y., Wu, L., 2016. Synthesis of multi-period heat exchanger networks based on features of sub-period durations. Energy 116, 1302–1311. https://doi.org/10.1016/j.energy.2016.06.047

Kennedy, R., Eberhart, J., 1995. Particle swarm optimization, in: IEEE Conference Publication.

Khorasany, R.M., Fesanghary, M., 2009. A novel approach for synthesis of cost-optimal heat exchanger networks. Comput. Chem. Eng. 33, 1363–1370. https://doi.org/10.1016/j.compchemeng.2008.12.004

Kim, Jiyong, Kim, Jinkyung, Kim, Junghwan, Yoo, C.K., Moon, I., 2009. A simultaneous optimization approach for the design of wastewater and heat exchange networks based on cost estimation. J. Clean. Prod. 17, 162–171. https://doi.org/10.1016/j.jclepro.2008.04.005

Kirkpatrick, S., Gelatt, C.D., Vecchi, M.P., 1983. Optimization by simulated annealing. Science (80-.). 220, 671–680. https://doi.org/10.1126/science.220.4598.671

Kılınç, M.R., Sahinidis, N. V., 2018. Exploiting integrality in the global optimization of mixed-integer nonlinear programming problems with BARON. Optim. Methods Softw. 33, 540–562. https://doi.org/10.1080/10556788.2017.1350178

Knut W. Mathisen, 1994. Integrated design and control of heat exchanger networks. PhD Thesis. University of Trondheim The Norwegian Institute of Technology.

Knut W. Mathisen, S.S. and E.A.W., 1992. Bypass selection for control of heat exchanger networks, in: ESCAPE-1. pp. 24–28.

Knut W. Mathisen, S.S. and E.A.W., 1991. Controllability of heat exchanger networks, in: AlChE Annual Meeting.

Kuhlman, K.L., 2013. Review of inverse Laplace transform algorithms for Laplace-space numerical approaches. Numer. Algorithms 63, 339–355. https://doi.org/10.1007/s11075-012-9625-3

Lachi, M., El Wakil, N., Padet, J., 1997. The time constant of double pipe and one pass shell-and-tube heat exchangers in the case of varying fluid flow rates. Int. J. Heat Mass Transf. 40, 2067–2079. https://doi.org/10.1016/S0017-9310(96)00274-8

Lai, S.M., Wu, H., Hui, C.W., Hua, B., Zhang, G., 2011. Flexible heat exchanger network design for low-temperature heat utilization in oil refinery. Asia-Pacific J. Chem. Eng. 6, 713–733. https://doi.org/10.1002/apj.511

Leewongtanawit, B., Kim, J.K., 2008. Synthesis and optimisation of heat-integrated multiple-contaminant water systems. Chem. Eng. Process. Process Intensif. 47, 670–694. https://doi.org/10.1016/j.cep.2006.12.018

Leng, W., Abbas, A., Khalilpour, R., 2010. Pinch Analysis for Integration of Coal-fired Power Plants with Carbon Capture, in: 20th European Symposium on Computer Aided Process Engineering.

Lersbamrungsuk, V., Srinophakun, T., 2009. Structural Controllability Evaluation for Heat Exchanger Networks, in: Proceedings of the 7th Asian Control Conference. pp. 835–840.

Lewin, D.R., 1998. A generalized method for HEN synthesis using stochastic optimization - II. The synthesis of cost-optimal networks. Comput. Chem. Eng. 22, 1387–1405. https://doi.org/10.1016/S0098-1354(98)00221-X

Li, G., Luo, Y., Xia, Y., Hua, B., 2012. Improvement on the simultaneous optimization approach for heat exchanger network synthesis. Ind. Eng. Chem. Res. 51, 6455–6460. https://doi.org/10.1021/ie202271h

Li, J., Du, J., Zhao, Z., Yao, P., 2014. Structure and area optimization of flexible heat exchanger networks. Ind. Eng. Chem. Res. 53, 11779–11793. https://doi.org/10.1021/ie501278c

Lin, C.T., 1974. Structural Controllability. IEEE Trans. Automat. Contr. 19, 201–208. https://doi.org/10.1109/TAC.1974.1100557

Lin, M.H., Tsai, J.F., Yu, C.S., 2012. A review of deterministic optimization methods in engineering and management. Math. Probl. Eng. https://doi.org/10.1155/2012/756023

Lin, S.U.N., Xionglin, L.U.O., Benquan, H.O.U., Yujie, B.A.I., 2013. Bypass Selection for Control of Heat Exchanger Network. Chinese J. Chem. Eng. 21, 276–284.

Linnhoff, B., Flower, J.R., 1978. Synthesis of heat exchanger networks: I. Systematic generation of energy optimal networks. AIChE J. 24, 633–642. https://doi.org/10.1002/aic.690240411

Linnhoff, B., Hindmarsh, E., 1983. The pinch design method for heat exchanger networks. Chem. Eng. Sci. 38, 745–763. https://doi.org/10.1016/0009-2509(83)80185-7

Linnhoff, B., S.Ahmad, 1990. Cost optimum heat exchanger networks—1. Minimum energy and capital using simple models for capital cost. Comput. chem. Engng 14, 729–750.

Lira-Barragán, L.F., Ponce-Ortega, J.M., Serna-González, M., El-Halwagi, M.M., 2014. Optimum heat storage design for solar-driven absorption refrigerators integrated with heat exchanger networks. AIChE J. 60, 909–930. https://doi.org/10.1002/aic.14308

Liu, L., Bai, Y., Zhang, L., Gu, S., Du, J., 2019. Synthesis of Flexible Heat Exchanger Networks Considering Gradually Accumulated Deposit and Cleaning Management. Ind. Eng. Chem. Res. 58, 12124–12136. https://doi.org/10.1021/acs.iecr.9b01672

Liu, L.L., Du, J., Xiao, F., Chen, L., Yao, P.J., 2011. Direct heat exchanger network synthesis for batch process with cost targets. Appl. Therm. Eng. 31, 2665–2675. https://doi.org/10.1016/j.applthermaleng.2011.04.036

Liu, L.L., Fan, J., Chen, P.P., Du, J., Yang, F.L., 2015. Synthesis of heat exchanger networks considering fouling, aging, and cleaning. Ind. Eng. Chem. Res. 54, 296–306. https://doi.org/10.1021/ie5027524

Lou, H.H., Wang, J., 2013. A Method for Flexible Heat Exchanger Network Design under Severe Operation Uncertainty. Chem. Eng. Technol. 757–765. https://doi.org/10.1002/ceat.201200547

Lu, Y., Chen, J., 2012. Integration design of heat exchanger networks into membrane distillation systems to save energy. Ind. Eng. Chem. Res. 51, 6798–6810. https://doi.org/10.1021/ie2024245

Luo, X., Huang, X., El-Halwagi, M.M., Ponce-Ortega, J.M., Chen, Y., 2016. Simultaneous synthesis of utility system and heat exchanger network incorporating steam condensate and boiler feedwater. Energy 113, 875–893. https://doi.org/10.1016/j.energy.2016.07.109

Luo, X., Wen, Q.Y., Fieg, G., 2009. A hybrid genetic algorithm for synthesis of heat exchanger networks. Comput. Chem. Eng. 33, 1169–1181. https://doi.org/10.1016/j.compchemeng.2008.12.003

Luo, X., Xia, C., Sun, L., 2013. Margin design , online optimization , and control approach of a heat exchanger network with bypasses. Comput. Chem. Eng. 53, 102–121. https://doi.org/10.1016/j.compchemeng.2013.02.002

Lv, J., Jiang, X., He, G., Xiao, W., Li, S., Sengupta, D., El-Halwagi, M.M., 2017. Economic and system reliability optimization of heat exchanger networks using NSGA-II algorithm. Appl. Therm. Eng. 124, 716–724. https://doi.org/10.1016/j.applthermaleng.2017.05.154

Ma, X., Yao, P., Luo, X., ROETZEL, W., 2008. Synthesis of multi-stream heat exchanger network for multi-period operation with genetic/simulated annealing algorithms. Appl. Therm. Eng. 28, 809–823. https://doi.org/10.1016/j.applthermaleng.2007.07.015

Marselle, D.F., Morari, M., Rudd, D.F., 1982. Design of resilient processing plants-II Design and control of energy management systems. Chem. Eng. Sci. 37, 259–270. https://doi.org/10.1016/0009-2509(82)80160-7

Masoud, I.T., Abdel-Jabbar, N., Qasim, M., Chebbi, R., 2016. Methodological framework for economical and controllable design of heat exchanger networks: Steady-state analysis, dynamic simulation, and optimization. Appl. Therm. Eng. 104, 439–449. https://doi.org/10.1016/j.applthermaleng.2016.05.026

Masso, A.H., Rudd, D.F., 1969. The synthesis of system designs. II. Heuristic structuring. AIChE J. 15, 10–17. https://doi.org/10.1002/aic.690150108

Mathisen, K.W., Morari, M., 1994. Dynamic models for heat exchangers and heat exchanger networks. Comput. chem. Engng 18, 459–463. https://doi.org/10.1016/0098-1354(94)80075-8

McGalliard, R.L., Westerberg, A.W., 1972. Structural sensitivity analysis in design synthesis. Chem. Eng. J. 4, 127–138. https://doi.org/10.1016/0300-9467(72)80005-4

Metropolis, N., Rosenbluth, A.W., Rosenbluth, M.N., Teller, A.H., Teller, E., 1953. Equation of state calculations by fast computing machines. J. Chem. Phys. 21, 1087–1092. https://doi.org/10.1063/1.1699114

Miranda, C.B., Andrade, C.M.G., Ravagnani, M.A.S.S., 2017. Thermodynamically-Based Response Time as Controllability Indicator in Heat Exchanger Networks. Can. J. Chem. Eng. 95, 1305–1312.

Miranda, C B, Costa, C.B.B., Caballero, J.A., Ravagnani, M.A.S.S., 2016. Optimal synthesis of multiperiod heat exchanger networks : A sequential approach. Appl. Therm. Eng. 115, 1187–1202. https://doi.org/10.1016/j.applthermaleng.2016.10.003

Miranda, Camila B, Costa, C.B.B., Caballero, J.A., Ravagnani, M.A.S.S., 2016. Heat exchanger network optimization for multiple period operations. Ind. Eng. Chem. Res. 10301–10315. https://doi.org/10.1021/acs.iecr.6b01117

Morar, M., Agachi, P.S., 2010. Review: Important contributions in development and improvement of the heat integration techniques. Comput. Chem. Eng. 34, 1171–1179. https://doi.org/10.1016/j.compchemeng.2010.02.038

Navia, D., Prada, C. De, Gutierrez, G., Cubillos, F., 2010. Synthesis of Multiperiod Heat Exchanger Networks Comprising Different Heat Exchanger Types, in: 20th ESCAPE.

Nemet, A., KlemeŠ, J.J., Kravanja, Z., 2012. Minimisation of a heat exchanger networks' cost over its lifetime. Energy 45, 264–276. https://doi.org/10.1016/j.energy.2012.02.049

Nielsen, J.S., Hansen, M.W., Sten Bay Jørgensen, 1996. Heat Exchanger Network Modelling Framework for Optimal Design and Retrofitting. Comput. chem. Engng 20, S249–S254.

Nisenfeld, A.E., 1973. Process control: applying control computers to an integrated plant. Chem. Eng. Prog. 69, 45–48.

Novak Pintarič, Z., Kravanja, Z., 2015. A methodology for the synthesis of heat exchanger networks having large numbers of uncertain parameters. Energy 92, 373–382. https://doi.org/10.1016/j.energy.2015.02.106

Oliva, D.G., Francesconi, J.A., Mussati, M.C., Aguirre, P.A., 2011. Modeling, synthesis and optimization of heat exchanger networks. Application to fuel processing systems for PEM fuel cells. Int. J. Hydrogen Energy 36, 9098–9114. https://doi.org/10.1016/j.ijhydene.2011.04.097

Onishi, V.C., Ravagnani, M.A.S.S., Caballero, J.A., 2014. Simultaneous synthesis of heat exchanger networks with pressure recovery: Optimal integration between heat and work. AIChE J. 60, 893–908. https://doi.org/10.1002/aic.14314

Ozbilen, A., Dincer, I., Rosen, M.A., 2014. Development of new heat exchanger network designs for a four-step Cu-Cl cycle for hydrogen production. Energy 77, 338–351. https://doi.org/10.1016/j.energy.2014.08.051

Papalexandri, K.P., Pistikopoulos, E.N., 1994a. Synthesis and Retrofit Design of Operable Heat Exchanger Networks. 1. Flexibility and Structural Controllability Aspects. Ind. Eng. Chem. Res. 33, 1718–1737. https://doi.org/10.1021/ie00031a012

Papalexandri, K.P., Pistikopoulos, E.N., 1994b. Synthesis and Retrofit Design of Operable Heat

Exchanger Networks. 2. Dynamics and Control Structure Considerations. Ind. Eng. Chem. Res. 33, 1738–1755. https://doi.org/10.1021/ie00031a013

Papastratos, S., Isambert, A., Depeyre, D., 1993. Computerized optimum design and dynamic simulation of heat exchanger networks. Comput. Chem. Eng. 17, S329–S334. https://doi.org/10.1016/0098-1354(93)80247-K

Papoulias, S.A., Grossmann, I.E., 1983. A structural optimization approach in process synthesis—II: Heat recovery networks. Comput. Chem. Eng. 7, 707–721. https://doi.org/10.1016/0098-1354(83)85023-6

Paterson, W.R., 1984. A replacement for the logarithmic mean. Chem. Eng. Sci. 39, 1635–1636. https://doi.org/10.1016/0009-2509(84)80090-1

Pavão, L. V., Miranda, C.B., Costa, C.B.B., Ravagnani, M.A.S.S., 2018. Efficient multiperiod heat exchanger network synthesis using a meta-heuristic approach. Energy 142, 356–372. https://doi.org/10.1016/j.energy.2017.09.147

Pavão, L. V., Pozo, C., Costa, C.B.B., Ravagnani, M.A.S.S., Jiménez, L., 2017. Financial risks management of heat exchanger networks under uncertain utility costs via multi-objective optimization. Energy 139, 98–117. https://doi.org/10.1016/j.energy.2017.07.153

Pavão, L. V, Costa, C.B.B., Ravagnani, M.A. da S.S., Jiménez, L., 2016. Large-scale heat exchanger networks synthesis using simulated annealing and the novel rocket fireworks optimization. AIChE J. 63, 1582–1601. https://doi.org/10.1002/aic

Pavão, L. V, Costa, C.B.B., Ravagnani, M.A.S.S., Jiménez, L., 2017. Costs and environmental impacts multi-objective heat exchanger networks synthesis using a meta-heuristic approach. Appl. Energy 203, 304–320. https://doi.org/10.1016/j.apenergy.2017.06.015

Payet, L., 2018. Remodelage de réseaux d'échangeurs de chaleur : collecte de données avancée, diagnostic énergétique et flexibilité. Institut national polytechnique de Toulouse.

Pettersson, F., 2008. Heat exchanger network design using geometric mean temperature difference. Comput. Chem. Eng. 32, 1726–1734. https://doi.org/10.1016/j.compchemeng.2007.08.015

Pintarič, Z.N., Kravanja, Z., 2005. Identification of vertex and nonvertex critical points for large-scale approximate stochastic optimization. Comput. Aided Chem. Eng. 20, 91–96. https://doi.org/10.1016/S1570-7946(05)80137-3

Pintarič, Z.N., Kravanja, Z., 2004. A strategy for MINLP synthesis of flexible and operable processes. Comput. Chem. Eng. 28, 1105–1119. https://doi.org/10.1016/j.compchemeng.2003.09.010

Pistikopoulos, E.N., Mazzuchi, T.A., 1990. A novel flexibility analysis approach for processes with stochastic parameters. Comput. Chem. Eng. 14, 991–1000. https://doi.org/10.1016/0098-1354(90)87055-T

Ponce-Ortega, J.M., Serna-González, M., Jiménez-Gutiérrez, A., 2010. Synthesis of heat exchanger networks with optimal placement of multiple utilities. Ind. Eng. Chem. Res. 49, 2849–2856. https://doi.org/10.1021/ie901750a

Rathjens, M., Bohnenstädt, T., Fieg, G., Engel, O., 2016. Synthesis of heat exchanger networks taking into account cost and dynamic considerations. Procedia Eng. 157, 341–348. https://doi.org/10.1016/j.proeng.2016.08.375

Reynolds, W.C., Dolton, T.A., 1959. Use of integral methods in transient heat-transfer analysis. ASME 58-A-248.

Roetzel W., M.Li, X.Luo, 2002. Dynamic behaviour of heat exchangers. Adv. Comput. Methods Heat Transf. 20, 451–460.

Roetzel, W., Xuan, Y., 1992. Transient response of parallel and counterflow heat exchangers. Trans. ASME 114, 510–512.

Romie, F.E., 1999. Response of counterflow heat exchangers to step changes of flow rates. J. Heat Transfer 121, 746–748. https://doi.org/10.1115/1.2826046

Romie, F.E., 1984. Transient response of the counterflow heat exchanger. J. Heat Transfer 106, 620–626. https://doi.org/10.1115/1.3246725

Saboo, A.K., Morari, M., Woodcock, D.C., 1985. Design of resilient processing plants-VIII. A resilience index for heat exchanger networks. Chem. Eng. Sci. 40, 1553–1565. https://doi.org/10.1016/0009-2509(85)80097-X

Sadeli, E., Chang, C.T., 2012. Heuristic approach to incorporate timesharing schemes in multiperiod heat exchanger network designs. Ind. Eng. Chem. Res. 51, 7967–7987. https://doi.org/10.1021/ie202171g

Serna-González, M., Ponce-Ortega, J.M., Burgara-Montero, O., 2010. Total cost targeting for heat exchanger networks including pumping costs. Comput. Aided Chem. Eng. 28, 1135–1140. https://doi.org/10.1016/S1570-7946(10)28190-7

Shemfe, M.B., Fidalgo, B., Gu, S., 2016. Heat integration for bio-oil hydroprocessing coupled with aqueous phase steam reforming. Chem. Eng. Res. Des. 107, 73–80. https://doi.org/10.1016/j.cherd.2015.09.004

Short, M., Isafiade, A.J., Fraser, D.M., Kravanja, Z., 2016. Two-step hybrid approach for the synthesis of multi-period heat exchanger networks with detailed exchanger design. Appl. Therm. Eng. 105, 807–821. https://doi.org/10.1016/j.applthermaleng.2016.05.065

Silva, A.P., Ravagnani, M.A.S.S., Biscaia, E.C., 2008. Particle Swarm Optimisation in heat exchanger network synthesis including detailed equipment design. Comput. Aided Chem. Eng. 25, 713–718. https://doi.org/10.1016/S1570-7946(08)80124-1

Silva, A.P., Ravagnani, M.A.S.S., Biscaia, E.C., Caballero, J.A., 2010. Optimal heat exchanger network synthesis using particle swarm optimization. Optim. Eng. 11, 459–470. https://doi.org/10.1007/s11081-009-9089-z

Skogestad, S., 1996. A procedure for SISO controllability analysis—With application to design of pH neutralization processes. Comput. Chem. Eng. 20, 373–386.

Skogestad, S., Hovd, M., 1990. Use of frequency-dependent RGA for control structure selection. Proc. 1990 Am. Control Conf. (IEEE Cat. No.90CH2896-9), 23-25 May 1990 2133–2139.

Skogestad, S., Postlethwaite, I., 2005. Multivariable feedback control: analysis and design, John Wiley & Sons. https://doi.org/978-0-470-01167-6

Skogestad, S., Postlethwaite, I., 1996. Multivariable Feedback control analysis and design. WILEY.

Sun, L., Zha, X., Luo, X., 2018. Coordination between bypass control and economic optimization for heat exchanger network. Energy 160, 318–329. https://doi.org/10.1016/j.energy.2018.07.021

Sun, L., Zha, X.L., Luo, X.L., 2017. Coordination of bypass control and economic optimisation for heat exchanger network with stream splits. Chem. Eng. Trans. 61, 187–192. https://doi.org/10.3303/CET1761029

Swaney, R.E., Grossmann, I.E., 1985. An index for operational flexibility in chemical process design. Part I: Formulation and theory. AIChE J. 31, 621–630. https://doi.org/10.1002/aic.690310412

Tan, Y.L., Ng, D.K.S., El-Halwagi, M.M., Foo, D.C.Y., Samyudia, Y., 2014. Floating pinch method for utility targeting in heat exchanger network (HEN). Chem. Eng. Res. Des. 92, 119–126. https://doi.org/10.1016/j.cherd.2013.06.029

Tellez, R., Svrcek, W.Y., Young, B.R., 2006. Controllability of heat exchanger networks. Heat Transf. Eng. 38–49. https://doi.org/10.1080/01457630600672323

The European Commission: 2030 climate & energy framework | Climate Action, n.d. 2030 climate & energy framework | Climate Action [WWW Document]. URL https://ec.europa.eu/clima/policies/strategies/2030_en#tab-0-0 (accessed 6.21.20).

Verheyen, W., Zhang, N., 2006. Design of flexible heat exchanger network for multi-period operation. Chem. Eng. Sci. 61, 7730–7753. https://doi.org/10.1016/j.ces.2006.08.043

Wan Alwi, S.R., Manan, Z.A., 2016. Simultaneous energy targeting, placement of utilities with flue gas, and design of heat recovery networks. Appl. Energy 161, 605–610. https://doi.org/10.1016/j.apenergy.2015.06.013

Wan Alwi, S.R., Manan, Z.A., 2010. STEP-A new graphical tool for simultaneous targeting and design of a heat exchanger network. Chem. Eng. J. 162, 106–121. https://doi.org/10.1016/j.cej.2010.05.009

Wan Alwi, S.R., Manan, Z.A., Misman, M., Chuah, W.S., 2013. SePTA-A new numerical tool for simultaneous targeting and design of heat exchanger networks. Comput. Chem. Eng. 57, 30–47. https://doi.org/10.1016/j.compchemeng.2013.05.008

Wan Alwi, S.R., Manan, Z.A., Nam, S.K., 2012. A New Method To Determine The Optimum Heat Exchanger Network Approach Temperature, in: Computer Aided Chemical Engineering. Elsevier B.V., pp. 190–194. https://doi.org/10.1016/B978-0-444-59507-2.50030-5

Wang, Y., Wei, Y., Feng, X., Hoong, K., 2014. Synthesis of heat exchanger networks featuring batch streams. Appl. Energy 114, 30–44. https://doi.org/10.1016/j.apenergy.2013.09.040

Westerberg, A.W., Shah, J. V., 1978. Assuring a global optimum by the use of an upper bound on the lower (dual) bound. Comput. Chem. Eng. 2, 83–92. https://doi.org/10.1016/0098-1354(78)80012-X

Westphalen, D.L., Young, B.R., Svrcek, W.Y., 2003. A Controllability Index for Heat Exchanger Networks. Ind. Eng. Chem. Resour. 42, 4659–4667. https://doi.org/10.1021/ie020893z

Wu, H., Yan, F., Li, W., Zhang, J., 2015. Simultaneous Heat Exchanger Network Synthesis Involving Nonisothermal Mixing Streams with Temperature-Dependent Heat Capacity. Ind. Eng. Chem. Res. 54, 8979–8987. https://doi.org/10.1021/acs.iecr.5b01592

Xu, K., Smith, R., Zhang, N., 2017. Design and optimization of plate heat exchanger networks, in: Computer Aided Chemical Engineering. Elsevier B.V., pp. 1819–1824. https://doi.org/10.1016/B978-0-444-63965-3.50305-6

Yan, Q.Z., Yang, Y.H., Huang, Y.L., 2001. Cost-effective bypass design of highly controllable heat-exchanger networks. AIChE J. 47, 2253–2276. https://doi.org/10.1002/aic.690471012

Yang, A., Jin, S., Shen, W., Cui, P., Chien, I.L., Ren, J., 2019. Investigation of energy-saving azeotropic dividing wall column to achieve cleaner production via heat exchanger network and heat pump technique. J. Clean. Prod. 234, 410–422. https://doi.org/10.1016/j.jclepro.2019.06.224

Yang, M., Xiao, F., Liu, G., 2014. Heat exchanger network design considering the heat pump performance. Chem. Eng. Trans. 39, 1099–1104. https://doi.org/10.3303/CET1439184

Yang, P., Liu, L.L., Du, J., Li, J.L., Meng, Q.W., 2014. Heat exchanger network synthesis for batch processes by involving heat storages with cost targets. Appl. Therm. Eng. 70, 1276–1282. https://doi.org/10.1016/j.applthermaleng.2014.05.041

Yang, R., TRAN Cong-Toan, Assaad Zoughaib, 2020. Iterative non-linear programming (NLP) method for the heat exchanger network design, in: ECOS 2020, 33rd International Conference on Efficiency, Cost, Optimization, Simulation and Environmental Impact of Energy Systems. Osaka,

Japan.

Yang, R., TRAN Cong-Toan, Assaad Zoughaib, 2019. Fast bypass selection method during the heat exchanger network synthesis, in: 29th European Symposium on Computer Aided Chemical Engineering.

Yee, T.F., Grossmann, I.E., 1990. Simultaneous optimization models for heat integration - II. Heat exchanger network synthesis. Comput. Chem. Eng. 14, 1165–1184. https://doi.org/10.1016/0098-1354(90)85010-8

Yerramsetty, K.M., Murty, C.V.S., 2008. Synthesis of cost-optimal heat exchanger networks using differential evolution. Comput. Chem. Eng. 32, 1861–1876. https://doi.org/10.1016/j.compchemeng.2007.10.005

Yin, J., Jensen, M.K., 2003. Analytic model for transient heat exchanger response. Int. J. Heat Mass Transf. 46, 3255–3264. https://doi.org/10.1016/S0017-9310(03)00118-2

Yuan, X., Pibouleau, L., Domenech, S., 1989. Experiments in process synthesis via mixed-integer programming. Chem. Eng. Process. 25, 99–116. https://doi.org/10.1016/0255-2701(89)80035-2

Yuan, Z., Chen, B., Zhao, and J., 2011. An Overview on Controllability Analysis of Chemical Processes. AIChE J. 57, 1185–1201. https://doi.org/10.1002/aic

Zamora, J.M., Grossmann, I.E., 1998. A global MINLP optimization algorithm for the synthesis of heat exchanger networks with no stream splits. Comput. Chem. Eng. 22, 367–384. https://doi.org/10.1016/S0098-1354(96)00346-8

Zhang, C., Cui, G., Peng, F., 2016. A novel hybrid chaotic ant swarm algorithm for heat exchanger networks synthesis. Appl. Therm. Eng. 104, 707–719. https://doi.org/10.1016/j.applthermaleng.2016.05.103

Zhang, H., Cui, G., Xiao, Y., Chen, J., 2017. A novel simultaneous optimization model with efficient stream arrangement for heat exchanger network synthesis. Appl. Therm. Eng. 110, 1659–1673. https://doi.org/10.1016/j.applthermaleng.2016.09.045

Zhao, Y., Yu, B., Wang, B., Zhang, S., Xiao, Y., 2018. Heat integration and optimization of direct-fired supercritical CO2 power cycle coupled to coal gasification process. Appl. Therm. Eng. 130, 1022–1032. https://doi.org/10.1016/j.applthermaleng.2017.11.069

Appendix: Dymola simulation interface

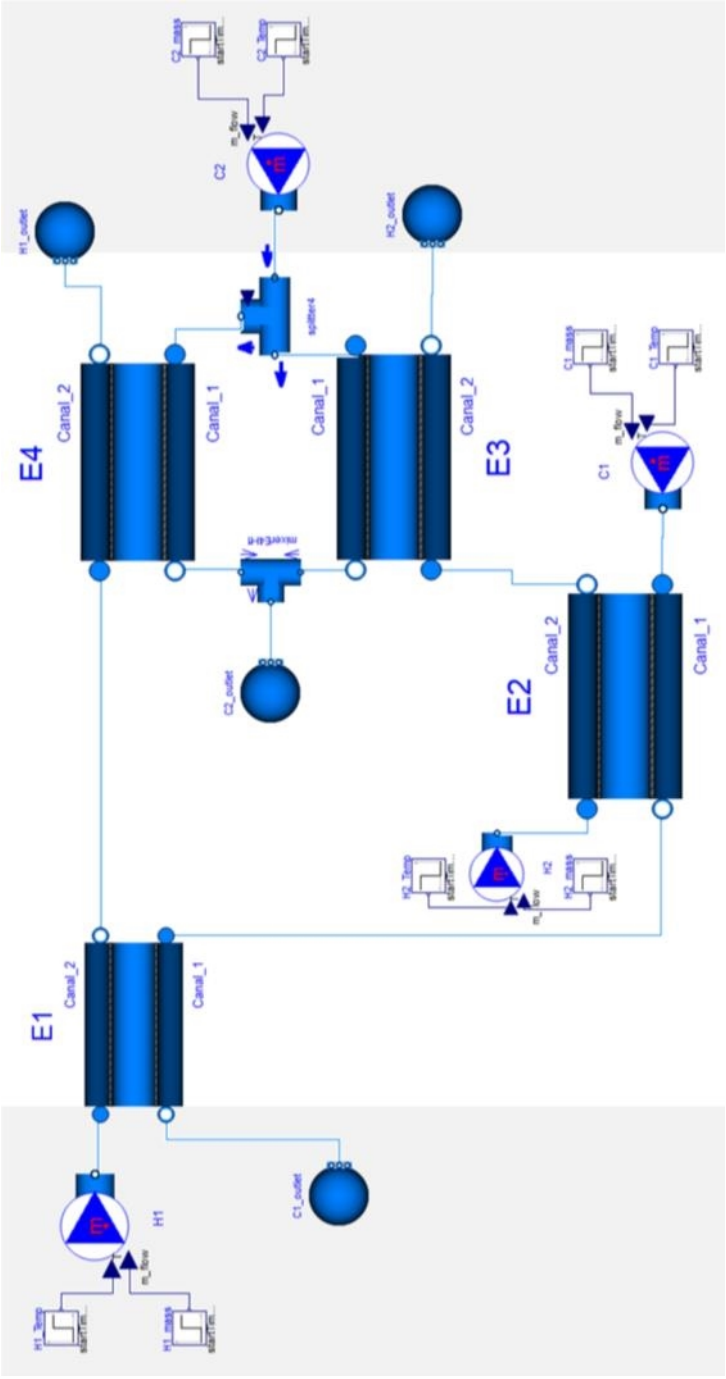

Fig A-1. Dymola simulation interface for part 3.3.4

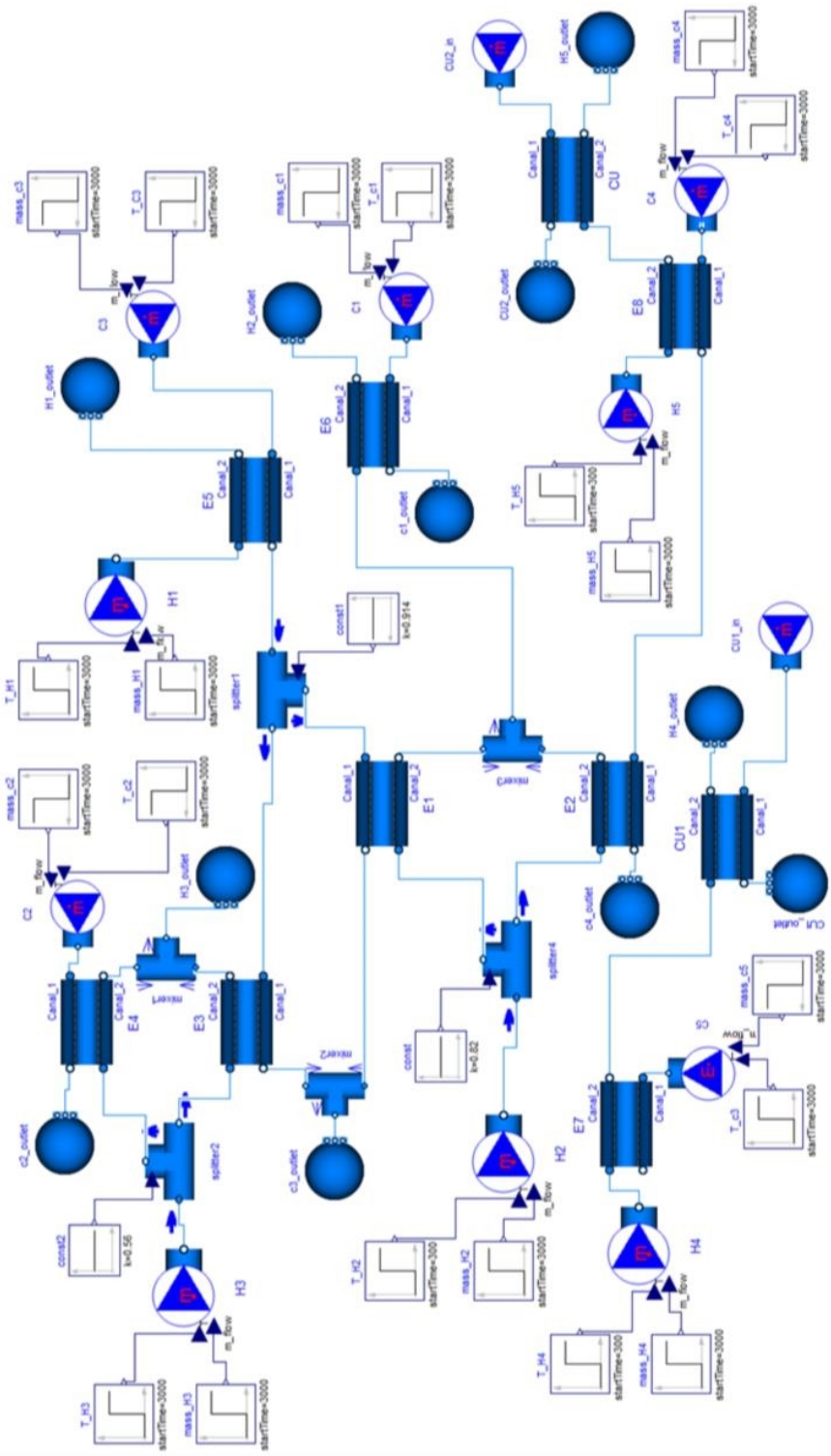

Fig. A-2. Dymola interface to validate the analytic model toward example in Fig 4.6 (the inlet parameters change with step or ramp signal, and the figure here just illustrates the step change condition)

RÉSUMÉ

Cette thèse a pour objectif de considérer les performances dynamiques d'un réseau d'échangeurs de chaleur (HEN) lors de sa conception. Nous définissons le temps de transition (TT) comme un indicateur pour mesurer les performances dynamiques lorsque le HEN subit des variations opérationelles. La thèse vise à résoudre deux problèmes: comment estimer le TT d'un HEN donné; et comment réaliser la conception pour optimiser le coût du HEN, ce qui nous permet d'obtenir un compromis entre le coût et le TT. En nous appuyant sur la transformation de Laplace, nous développons une formulation mathématique pour déterminer TT, et cela conduit à deux modèles dynamiques. Le modèle de base nécessite le processus de transformation inverse de Laplace. Le deuxième modèle, plus avancé, est basé sur des développements purement analytiques afin d'éviter la difficulté numérique de la transformation inverse de Laplace. Les méthodes de synthèse suivent l'approche séquentielle multi-période pour itérer différentes structures, puis le TT peut être calculé pour chaque HEN optimisé en coût. Nous proposons deux méthodes d'itération: BINLP pour le petit cas et IINLP pour les problèmes de moyenne à grande échelle. Les méthodes de synthèse et les modèles dynamiques HEN ont été appliqués avec succès dans cinq études de cas à travers différents chapitres, et nous constatons que le TT varie énormément selon les structures testés. Il est important de prendre en compte le temps de transition dans le problème de conception de HEN, et nos méthodes proposées peuvent servir d'outil de présélection pour aider à trier des HENen termes de coût et de performances dynamiques.

MOTS CLÉS

Réseau d'échangeurs de chaleur, synthèse, temps de réponse, optimisation, multi-période.

ABSTRACT

This thesis pioneers to consider the time response in the heat exchanger network (HEN) multi-period design problem. We define the transition time (TT) as an indicator to measure the dynamic performance when HEN gets an operational period changeover. The thesis aims to solve two problems: how to measure the TT of a given HEN; and how to carry out synthesis work to optimize the HEN cost, allowing us to obtain a trade-off between the cost and TT. Relying on the Laplace transform, we develop a mathematical formulation to reach TT, leading to two dynamic models. The basic one requires the inverse Laplace transform process during the calculation. The improved dynamic model follows the analytic way, and free of the concern of the numerical difficulty of the inverse Laplace transform. The synthesis methods follow the sequential approach to iterate various structures and then TT can be calculated for each cost-optimized HEN. We propose two iteration methods: BINLP for the small case and IINLP for medium-large scale problems. The synthesis methods and HEN dynamic models were applied successfully in five case studies through different chapters, and found that TT varied hugely for different designs in each case. It is important to consider the time response in the HEN design problem, and our proposed methods can act as a pre-selection tool to help sort out those designs in terms of the cost and dynamic performances.

KEYWORDS

Heat exchanger network, synthesis, time response, optimization, multi-period.